Title
Soft bioelectronics for self-powered neural tissue engineering

Author
Libanori, Alberto

Publication Date
2022

Peer reviewed|Thesis/dissertation

UNIVERSITY OF CALIFORNIA

Los Angeles

SOFT BIOELECTRONICS FOR SELF-POWERED NEURAL TISSUE ENGINEERING

A dissertation submitted in partial satisfaction of the

requirements for the degree Doctor of Philosophy

in Bioengineering

by

Alberto Libanori

2022

ABSTRACT OF THE DISSERTATION

Soft bioelectronics for self-powered neural tissue engineering

by

Alberto Libanori

Doctor of Philosophy in Bioengineering

University of California, Los Angeles, 2022

Professor Jun Chen, Chair

Soft bioelectronics have emerged as prominent solutions for diagnostic, energy producing and therapeutic solutions for *in vitro*, *in vivo*, and wearable applications, given their self-powered nature, low cost, flexibility, biocompatibility, miniaturized nature, and ability to use at scale. Through their use, electrical stimulation, a renowned modulator of biological activity and tissue regeneration, has re-emerged in a number of growing applicative fields, particularly in the field of neural engineering. In this work, we explore the use of soft bioelectronics for use in neural engineering applications. First we introduce the field of soft bioelectronics, including platform technologies employed, focusing on triboelectric and magnetoelastic generators and their working mechanism. We then debate their use in electrical stimulation for neural engineering. In the core chapters, we first discuss the development of an easy-to-fabricate magnetoelastic platform for *in vitro* electrical stimulation, including capabilities to scale using 3D printing, adaptation to 6, 12, 24, 48

and 96-well plates, and ability to address issues of wettability, size, third-party powering and biocompability, yielding electric output values of up to 10.52 mA and 9.5 mV. In the following chapter we carry out the first ever application of a magnetoelastic platform in cellular reprogramming and assess its efficacy in helping to promote fibroblast transdifferentiation into neurons using elicited electrical stimulation, increasing transdifferentiation efficiency (up to +104%), and enhancing neuron maturation (up to +251%), providing an easily devisable and scalable electrical stimulation device for research, and paving the way for future permeation of magnetoelastic generator-based implantable devices. Finally, we delve into the design of triboelectric nanogenerators for implantable *in vivo* use, by discussing a computational study of ultrasound-activated implantable triboelectric generators used in electrical stimulation for neural tissue repair in indications such as spinal cord injury, helping to pave the way for broader use of implanted soft bioelectronics. To conclude this work, some future considerations on electrical stimulation for the above research is provided, and a boarder outlook on the field of soft bioelectronic electrical stimulation for therapeutic applications is given, together with an essay on the permeation of soft bioelectronics in textile form for use in personalized healthcare.

The dissertation of Alberto Libanori is approved.

Nureddin Ashammakhi

Andrea Marie Kasko

Song Li

Hsian-Rong Tseng

Jun Chen, Committee Chair

University of California, Los Angeles,

2022

DEDICATION

Alla mia famiglia, che è la mia ancora.

To my friends, who are my encouragement.

And to that part of me, which keeps me going when things get tough.

"*Ethos anthropoi daimon*"

Heraclitus

TABLE OF CONTENTS

ABSTRACT OF THE DISSERTATION ii

DEDICATION iv

LIST OF FIGURES AND TABLES vii

ACKNOWLEDGMENTS x

VITA xi

CHAPTERS

1 INTRODUCTION 1

I. Soft bioelectronics 1

II. MEG and TENG 5

III. Soft bioelectronics for electrical stimulation 8

IV. Neuronal electrical stimulation for cell programming 14

V. Neuronal electrical stimulation for therapy and rehabilitation 20

2 MEG-BASED ELECTRICAL STIMULATION PLATFORM 26

I. Introduction 26

II. Magnetoelastic effect for biological applications 28

III. Fabrication of the MEG electrical stimulation platform 32

IV. 3D fabrication of the MEG electrical stimulation platform 38

V. Evaluation of the MEG electrical stimulation platform 40

VI. Conclusion 45

3 MEG-BASED NEURAL CELL PROGRAMMING 47

I. Introduction 47

II. MEG electrical stimulation enhances reprogramming efficiency 48

III. MEG electrical stimulation boosts maturation and ramification 52

IV. Conclusion 57

4 TENG BASED ULTRASOUND COMPUTATIONAL STUDY FOR NEURAL TISSUE ENGINEERING 60

I. Introduction 60

II. Theoretical background 63

III. Simulation rationale and mechanism 65

IV. Results and discussion 71

V. Conclusion 81

5 CONCLUSION AND PROSPECTIVE 84

I. Prospective for MEG electrical stimulation 84

II. Prospective for ultrasound TENG electrical stimulation 85

III. General future trends 86

6 REFERENCES 87

7 APPRENDIX 106

I. Future of soft bioelectronics: electrical stimulation for therapy

II. Future of soft bioelectronics: integration in everyday wear

LIST OF FIGURES AND TABLES

Figure 1. Milestone research timeline of platform technologies for smart healthcare soft bioelectronics.

Figure 2. Working principle of a triboelectric nanogenerator.

Figure 3. MEGs and their working principle.

Figure 4. Schematic illustration of the various applications of therapeutic electronic stimulation using soft bioelectronics.

Figure 5. Examples of soft bioelectronic generated electronic stimulation for cellular reprogramming.

Figure 6. Effect on neuronal transdifferentiation using soft bioelectronic generated electronic stimulation.

Figure 7. Soft bioelectronic electronic stimulation used for neural rehabilitation.

Figure 8. Soft bioelectronic electronic stimulation for motor function rehabilitation and use.

Figure 9. Magnetoelastic generator displays suitability for biological applications.

Figure 10. The MEG electrical stimulation platform is simple to fabricate and provides a resilient *in vitro* tool.

Figure 11. ITO glass functionalization to enhance cell adhesion.

Figure 12. Fibroblast anchoring.

Figure 13. An alternative set up of the MEG electronic stimulation platform.

Figure 14. 3D printing capabilities of an MEG electronic stimulation platform.

Figure 15. The MEG electrical stimulation platform's output can be tailored to required experimental conditions.

Figure 16. Perforation of the MEG electronic stimulation platform.

Figure 17. Maximum air pressure tolerance.

Figure 18. The MEG electrical stimulation platform enhances efficiency and maturation of fibroblast transdifferentiation to induced neurons.

Figure 19. MEG electrical stimulation protocols.

Figure 20. Effect of MEG electrical stimulation on transdifferentiation.

Figure 21. Effect of MEG electrical stimulation effect on neuronal maturation**.**

Figure 22. Visual effect of MEG electrical stimulation on mature neurons, with Synapsin staining.

Figure 23. Visual effect of MEG electrical stimulation on mature neurons, with MAP2 staining.

Figure 24. Schematic representation of an ultrasound implantable ultrasound-activated-TENG.

Figure 25: The illustration of the computational model utilized in our simulation.

Figure 26. Simulation of acoustic pressure distribution with and without a triboelectric layer.

Figure 27. The meshing of the simulation model.

Figure 28. Surface displacement of triboelectric layer induced by ultrasound irradiation.

Figure 29. The equipotential map of the displacement with different number of isopotential lines.

Figure 30. The effects of various materials properties on the area displacement of triboelectric nylon layer.

Figure 31. Physical ultrasound irradiation parameters and their effect on triboelectric layer energy transduction.

Figure 32. Further imaging of computational studies.

Table 1: Summary of experimental simulation values used.

ACKNOWLEDGMENTS

I would like to acknowledge, first and foremost, my family, for their support, patience, understanding and steadfast presence. They are my strength and stay.

My most special thanks to Dr Jennifer Soto for her patience and guidance and to Dr Weili Deng for his support, Dr Yang Song, to Dr Jana Zarubova, to Trinny Tat and to Jing Xu, for all teaching me so very much. To Dr Sahar Andalib, for her help. I would also like to acknowledge my present lab mates for their support.

A special mention and thanks to Dan McClory for his trust, support, and mentorship.

My comrades and friends Tyler Hoffman, Peyton Tebon, Melina Mastrodimos, and again Trinny Tat. You have represented my family during this adventure have helped me become a better scientist and a more rounded individual.

Utmost gratitude to my Doctoral Committee, specifically Prof. Andrea Marie Kasko for her guidance throughout turbulent times, Prof. Nureddin Ashammakhi, for being a mentor, a fine scientist, and a friend, Prof. Hsian-Rong Tseng for his support and macro vision on my research and person, and to Prof. Song Li, for his empathy, scientific guidance, support, and patience. Finally, to Prof. Jun Chen, for his dedication, care, steering, guidance, and contagious passion for scientific research.

I humbly owe this outcome to all of you.

VITA

ACADEMIC CURRICULUM

EDUCATION:

2011-2012 University of Cambridge, UK**.** MPhil (*Cantab*) in Bioscience Enterprise

2007-2010 University of St Andrews, UK. BSc (Hons) in Biomolecular Sciences

PUBLICATIONS: ***First or co-first authorship**

***Libanori A**, Soto J, Song Y, Zarubova J, Tat T, Xu J, Yue S, Jonas S, Li S, Chen J. Biocompatible and self-powered magnetoelastic generator platform for *in vitro* electrical stimulation (manuscript in submission).

Deng W, ***Libanori A**, Xiao X, Fang J, Zhao X, Zhou Y, Chen G, Li S, Chen J. Computational investigation of ultrasound induced electricity generation via a triboelectric nanogenerator. *Nano Energy.* 2022 Jan 1;91:106656.

***Libanori A**, Chen G, Zhao X, Zhao Y, Chen J. Smart textiles for personalised healthcare. *Nature Electronics* (manuscript accepted, in print).

Deng W, ***Libanori A**, Zhou Y, Chen G, Yang W, Chen J. Piezoelectric nanogenerators for personalized healthcare. *Chemical Society Reviews* (manuscript accepted, in print).

Conta G, ***Libanori A**, Tat T, Chen G, Chen J. Triboelectric nanogenerators for therapeutic electrical stimulation. *Advanced Materials*. 2021 Jul;33(26):2007502.

Tat T, **Libanori A**, Au C, Yau A, Chen J. Advances in triboelectric nanogenerators for biomedical sensing. *Biosensors and Bioelectronics*. 2021 Jan 1;171:112714.

Liu B, **Libanori A**, Zhou Y, Xiao X, Xie G, Zhao X, Su Y, Wang S, Yuan Z, Duan Z, Liang J. Simultaneous Biomechanical and Biochemical Monitoring for Self-Powered Breath Analysis. *ACS Applied Materials & Interfaces*. 2022 Jan 25.

Zou Y, **Libanori A**, Xu J, Nashalian A, Chen J. Triboelectric nanogenerator enabled smart shoes for wearable electricity generation. *Research.* 2020 Nov 9;2020.

Xu S, **Libanori A**, Luo G, Chen J. Engineering bandgap of CsPbI3 over 1.7 eV with enhanced stability and transport properties. *Iscience*. 2021 Mar 19;24(3):102235.

Yang X, Tat T, **Libanori A**, Cheng J, Xuan X, Liu N, Yang X, Zhou J, Nashalian A, Chen J. Single-atom catalysts with bimetallic centers for high-performance electrochemical CO2 reduction. *Materials Today*. 2021 May 1;45:54-61.

Zhu J, Zhou X, **Libanori A**, Sun W. Microneedle-based bioassays. *Nanoscale Advances*. 2020;2(10):4295-304.

Xiao X, Chen G, **Libanori A**, Chen J. Wearable triboelectric nanogenerators for therapeutics. *Trends in Chemistry*. 2021 Apr 1;3(4):279-90.

Zhou Z, Weng L, Tat T, **Libanori A**, Lin Z, Ge L, Yang J, Chen J. Smart insole for robust wearable biomechanical energy harvesting in harsh environments. *ACS nano.* 2020 Oct 12;14(10):14126-33.

Tan S, Zhang S, Deng Y, **Libanori A**, Zhou Y, Yang J, Tat T, Yang L. In-situ-grown silver–polymer framework with coordination complexes for functional artificial tissues, *Nature Chemistry* (manuscript in revision)

Qu M, Wang C, Zhou X, **Libanori A**, Jiang X, Xu W, Zhu S, Chen Q, Sun W, Khademhosseini A. Multi-Dimensional Printing for Bone Tissue Engineering. *Advanced Healthcare Materials.* 2021 Jun;10(11):2001986.

Chu D, Zhao X, Xiao B, **Libanori A**, Zhou Y, Tan L, Ma H, Pang H, Wang X, Jiang Y, Chen J. Nickel/cobalt molybdate hollow rods induced by structure and defect engineering as exceptional electrode materials for hybrid supercapacitor. *Chemistry–A European Journal.* 2021 Jun 4;27(32):8337-43.

Li Y, Xing L, Yu D, **Libanori A**, Yang K, Sun J, Nashalian A, Zhu Z, Ma Z, Zhai Y, Chen J. Hollow IrCo Nanoparticles for High-Performance Overall Water Splitting in an Acidic Medium. *ACS Applied Nano Materials*. 2020 Dec 8;3(12):11916-22.

Xiao X, Xiao X, Nashalian A, **Libanori A**, Fang Y, Li X, Chen J. Triboelectric nanogenerators for self-powered wound healing. *Advanced Healthcare Materials*. 2021 Oct;10(20):2100975.

Zhang B, Chun F, Chen G, Yang T, **Libanori A**, Chen K, Conta G, Xiong D, Yan C, Yang W, Chen J. Water-evaporation-induced intermolecular force for nano-wrinkled polymeric membrane. *Cell Reports Physical Science*. 2021 Jun 23;2(6):100441.

Liu H, Wang C, Chen G, Liao Y, Mao M, Cheng T, **Libanori A**, Xiao X, Hu X, Liu K, Chen J. Moisture assisted photo-engineered textiles for visible and self-adaptive infrared dual camouflage. *Nano Energy*. 2022 Mar 1;93:106855.

Haghniaz R, Rabbani A, Vajhadin F, Khan T, Kousar R, Khan AR, Montazerian H, Iqbal J, **Libanori A**, Kim HJ, Wahid F. Anti-bacterial and wound healing-promoting effects of zinc ferrite nanoparticles. *Journal of Nanobiotechnology*. 2021 Dec;19(1):1-5.

Kiaee G, Dimitrakakis N, Sharifzadeh S, Kim HJ, Avery RK, Moghaddam KM, Haghiniaz R, Yalcintas EP, Barros N, Karamikamkar S, **Libanori A**, Khademhosseini A .Laponite-based Nanomaterials For Drug Delivery. *Advanced Healthcare Materials*. 2022 Jan 6:2102054.

CHAPTER 1

INTRODUCTION

I. Soft bioelectronics

The permeation of novel diagnostic, therapeutic and energy producing devices is being bolstered by the emergence of novel platform technologies in the form of soft bioelectronics. These miniaturizable technologies have enabled a shift in the way in which not only can biomonitoring be decentralized using self-powering devices, but also made *in situ* therapeutic intervention, such as in the form of electrical stimulation, a much more accessible and scalable reality.

Soft bioelectronics – or electronic devices which are not bulky or rigid in morphology – have emerged with prominence in recent years, due to their conformable nature, their ability to be utilized as both wearable, on body and implantable devices, and their positioning as inexpensive solutions for biomonitoring. Furthermore, soft bioelectronics, which are able to connect to the internet of things and provide personalized healthcare, can help with therapeutic, diagnostic, combined theranostic and energy producing applications.

Since the introduction of soft bioelectronics in healthcare and biological applications[1–6], many signal-to-function associative platform technologies have been developed (**Figure 1**). These include. ***Electroluminescent Platforms.*** Light reflection and refraction provide useful biometric diagnostic information when interacting with tissues[7], whilst on a therapeutic front, light-emitting soft bioelectronics have also shown many applications[8–12]. ***Piezoresistive Platforms.*** Piezoresistive semiconductors change electrical resistivity when exposed to mechanical stress. This mechanism has been

harnessed for highly sensitive biomechanical sensing[13]. Chemical interactions[14] and temperature changes[15] have also been exploited for personalised biomolecular analysis and body temperature monitoring.

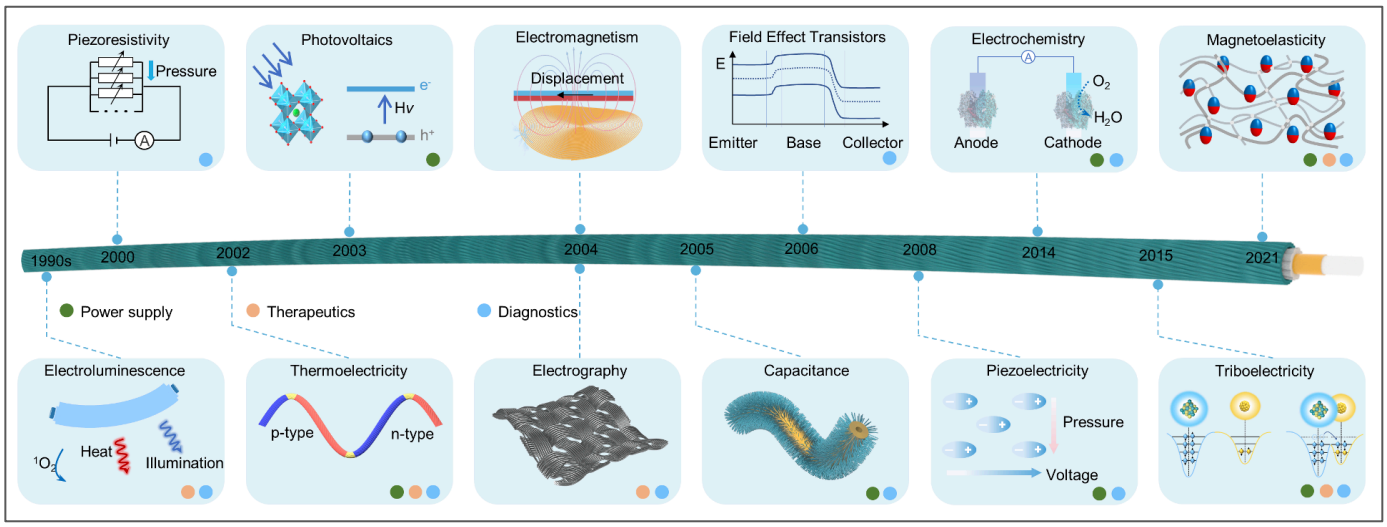

Figure 1. Milestone research timeline of platform technologies for smart healthcare soft bioelectronics. Embedding electronics into soft bioelectronics began in the 1990s and was in turn applied to the field of healthcare. Nanoelectronics and material science platform technology developments saw the introduction of a plethora of diagnostic, therapeutic and energizing applications. A timeline and summary of such technology platform developments and applications to the healthcare field is presented.

Thermoelectric Platforms Thermoelectric generators can convert heat changes into electricity using the thermoelectric effect[16]. These soft bioelectronics thermoelectric generators have been explored to leverage body heat and generate electricity for healthcare applications[17]. ***Photovoltaic Platforms.*** Solar cells can convert sunlight directly into electricity[18]. Integrating photovoltaic technologies within soft bioelectronics has provided powering capabilities for diagnostic and therapeutic devices within personalised healthcare settings[19]. ***Electrographic Platforms.*** Electrographic platforms can help in the diagnosis of heart and neurological conditions[20]. Their soft bioelectronics

integration has been shown to provide highly flexible, comfortable, and long-lasting personalised healthcare platforms[21]. ***Capacitive Platforms.*** Textile capacitors exploit capacitance changes brought about by human motion[22] . In view of their high sensitivity, fast response time, and high stability, they have been frequently used in diagnostic devices[23]. Soft bioelectronics supercapacitors can moreover serve as an energy storage unit to power biomedical sensors or therapeutic devices[24]. ***Electromagnetic Platforms***. Electromagnetic generators (EMGs) have been explored to convert human motion into electricity[25] and have been frequently used to harvest biomechanical energy[26]. ***Transistor Platforms.*** Transistors represent one of the building blocks of healthcare electronics[27]. Soft bioelectronics-based organic field-effect transistors and electrochemical transistors have been widely used for biomarker sensing[28], vital signs monitoring[29] and biomolecular analysis[30]. Moreover, soft bioelectronics transistors can be used to construct on-body circuits[31] to acquire data, and compute clinical interventions directly *in situ*. ***Piezoelectric Platforms.*** Piezoelectric nanogenerators (PENG) rely on the piezoelectric effect to generate electricity and detect biomechanical motion via mechanical deformation[32]. Soft bioelectronics-based PENGs possess high pressure sensitivity[33] and their easy implementation and self-powering capabilities have made them a more modern smart soft bioelectronics platform technology used in healthcare applications (sensing[34], electrical stimulation[35], and energy harvesting[36]). ***Electrochemical Platforms*** Electrochemical platforms have been explored to rely on the conversion of chemical energy to electricity, via known redox reactions[37]. Such platforms have shown the ability to leverage on ordinary perspiration, harnessing it as a renewable biofuel[38], as well as a bioanalytically relevant metabolite source for clinical insight.

Triboelectric Platforms. Triboelectric nanogenerators (TENG) convert mechanical motions into electricity, using contact electrification and electrostatic induction coupling[39–41]. TENGs effectively convert biomechanical movements to high voltage and low current signals[41]. Such performance, and a vast array of available biocompatible triboelectric materials, have led to TENGs integration in smart healthcare soft bioelectronics for use in diagnostic[42], therapeutic[43] and power supplying applications[44–46]. ***Magnetoelastic Platforms.*** Very recently, mechanically induced giant magnetoelastic effect in soft system has been discovered and developed in stand-alone systems, namely, magnetoelastic generators (MEGs)[47]. This technology has shown promise in vital sign monitoring and diagnosis, as well as in biomechanical energy harvesting for healthcare device powering.

Triboelectric platforms and magnetoelastic platforms have emerged with particular relevance as soft bioelectronic platform technologies. For the purpose of this thesis, we have chosen to explore their application for neural engineering, focusing specifically on their use in therapeutic electrical stimulation. Specifically, we will be delving into magnetoelastic platforms for self-powered electrical stimulation for *in vitro* applications, looking at both fabrication methodologies (**Chapter 2**), application to cellular reprogramming (**Chapter 3**), and finally we will carry out a computational investigation for next generation triboelectric generators activated using ultrasound, for implantable applications in neuronal engineering and therapy (**Chapter 4**).

II. TENGs and MEGs

TENGs. TENGs were developed in the Zhong Lin Wan lab in 2012 to harvest passive energy sources for a myriad of applications[39]. Through their *modus operandi*, TENGs convert external mechanical energy into electricity by a conjunction of the triboelectric effect and electrostatic induction. Over the last decade, their application has focused greatly on biomedical applications, given their small size, self-powering nature, use of inexpensive materials, and versatility in energy harvesting and biomechanical detection on the human body. Indeed, simple pressure-inducing motions (including any type of joint motion) can provide TENGs with enough mechanical energy to elicit an electrical output.

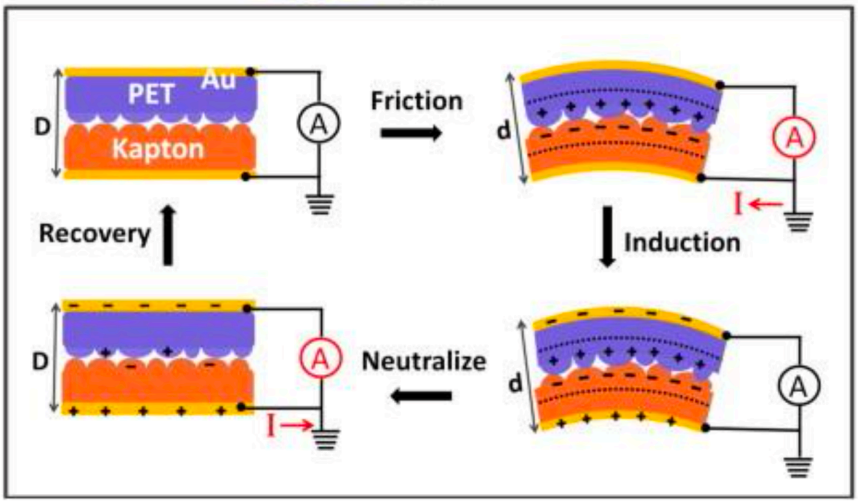

Figure 2. Working principle of a triboelectric nanogenerator. PET and Kapton, at opposite triboelectric scale level, are fractioned in a vertical contact mode separation approach to yield an induced current brought about by coupling the triboelectric effect, contact electrification, and potential charge discharge[39]. Adapted with permission[39], Copyright 2012, Elsevier

Within a TENG, an electric potential is generated *via* the triboelectric effect between two surface material layers which exhibit opposite tribopolarity in an inner circuit, and upon application of a mechanical pressure. To neutralize this electric potential, in the

outer part of the circuit, electrons are driven between the back sides of the TENG, generating an electric output (**Figure 2**).

TENG functionalities have been developed to rest on a set of clear working models, namely vertical contact separation mode, lateral sliding mode, single electrode mode, and freestanding mode. In this thesis we will explore the use of TENGs for neural engineering, as described in Chapter 4.

***MEGs*.** Very recently, in 2021, the Chen lab developed MEGs by discovering and subsequently harnessing the giant magnetoelastic effect in soft systems[47]. By dispersing magnetizable nanoparticles in a soft polymeric matrix, MEGs have been devised to detect mechanical deformation *via* means of coupling mechanical, magnetic and magnetomechanical variations to elicit an electric output. Over the last few months, this technology has been applied to the fields of biomonitoring, energy harvesting, smart textiles and ultra-high-power generation for small scaled soft bioelectronics and is set to pave the way in a number of novel applications where TENGs and other self-powered soft bioelectronics could not go.

Indeed, MEGs set themselves apart from other predecessor and fellow self-powered technologies because of their innate soft polymeric nature (and thus bioconformability), one-body design, and capability to work in wetted conditions, including underwater. These key differences from older platform technologies are furthermore highlighted as MEGs biomechanical-to-electrical energy conversion mechanism does not present low inherent current density and high internal impedance, unlike TENGs and PENGs, whose energy conversion mechanisms stem from capacitive power generation

principles reliant on the manipulation of the electric dipoles at the constitutive materials' interfaces.

The working mechanism of MEGs obeys the following sequence: magnetizable nanomagnets dispersed in a soft polymer matrix can be aligned to a commonly shared magnetic flux, using simple impulse magnetization, as nanomagnets are free to rotate in a cured matrix, and able to align. Upon mechanical deformation of the polymer matrix, the magnetic flux of their system is perturbed, leading to a change in magnetic flux density. By coupling the above layer (a magnetoelastic coupling layer) with a conductive layer, electromagnetic induction can be produced in a nearby conductor, yielding high current and low voltage outputs for use in diagnostics, therapeutic and energy producing applications (**Figure 3**).

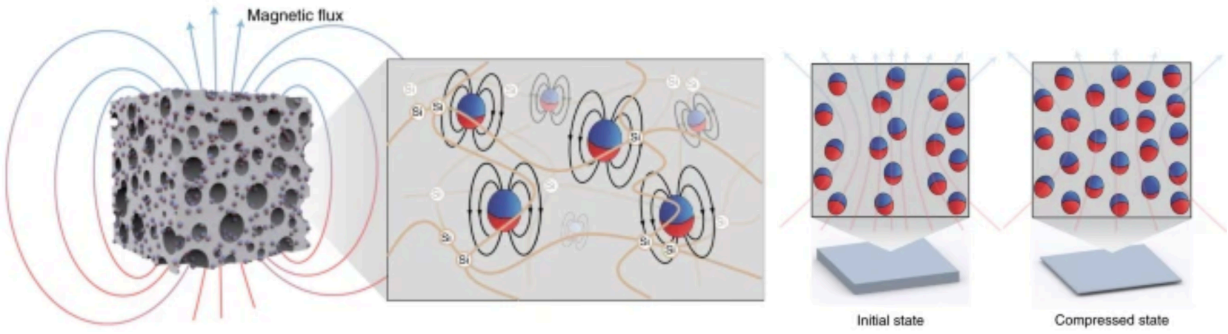

Figure 3. MEGs and their working principle. Left. Sketch of a polymer soft system generating a magnetic flux. Inset: sketch of the internal structure showing micromagnets (red and blue spheres) dispersed in a polymer silicone matrix (orange lines). **Right**. Illustration of the magnetic dipole alignment changing the magnetic flux density of the soft system in the initial state and the compressed state based on a wavy chain model. Red and blue spheres represent micromagnets[47]. Adapted with permission[47], Copyright 2021, Springer Nature.

III. Soft bioelectronics for electrical stimulation

Owing to the ever-growing prominence of devices within the Internet of Things (IoTs) paradigm, and increasing demands for personalized healthcare, implantable (in body), and surface (on body) bioelectronics — collectively known as in and on body (IOB) bioelectronics — are set to become key players in the future of healthcare[48–50]. With the advent of 5G wireless networks, the use of IOB bioelectronics is expected to dramatically increase. The National Intelligence Council predicts that most of our everyday objects will be interconnected to the IoT ecosystem by 2025[51]. Although most IOB bioelectronics are focused on sensing[52–55], there is a growing trend to develop minimally invasive therapeutic devices focused, for instance, on the application of electrical stimulation (ES)[56]. Electrical impulses are at the basis of cognitive and skeletal functions for human beings, constituting a fundamental messaging vehicle within the human nervous system[57]. Leveraging on the existence of natural electrical impulses, external ES can be employed as a natural alternative to addressing medical disorders[58] where synthetically derived small molecules and biotherapeutics fall short[59]. Electrical impulses have been shown to enhance tissue regeneration processes and aid with therapy in unmet medical needs, including bone fractures[60–62], skin wounds[63–65], obesity (satiation)[66–69], cancer[70,71], muscular dystrophy[72–74], soft tissue damage[75–77], hair loss[78–80], and bladder control dysfunction[81,82]. IOB bioelectronics can provide localized ES with tailored benefits. Considering the large number of pathologies that can be addressed through ES, attaining a self-sustainable bioelectronic system capable of delivering therapeutic ES can provide an invaluable tool to the continued development of personalized healthcare within an IoT ecosystem. The recent development of the triboelectric nanogenerator (TENG) has

sparked a lot of interest in generating body area networks capable of sensing as well as treating various conditions considering TENGs can provide self-powered and bioconformable alternatives to conventional ES approaches. Current wearable devices capable of emitting therapeutic ES come in various morphologies that are heterogeneous in nature and varying in form, depending on the sought intervention. Indeed TENG has been the leading nanogenerator and soft bioelectronic employed for ES. For instance, within regenerative medicine applications, including wound healing, tissue and bone regeneration, devices administering ES are generally composed of an electronic skin-like structure[83–86]. Conversely, devices creating a mind–body neural interface to help address problems such as obesity (satiation) and bladder-related conditions, generally retain a neural dust platform carefully wrapped around the peripheral nerve of interest[87–90]. Although not directly used as a therapeutic agent, ES is also known to aid with drug delivery and is generally integrated in devices composed of stretchable elastomers which contain therapeutic depots of drug loaded nanoparticles[91–93]. Finally, solutions employing ES to target cellular engineering applications, such as cellular excitation and cancer therapy, retain a relatively simple structure comprising a power source connected to an organic light emitting diode element[94–96].

In spite of recent advances of IOB bioelectronic ES's use in the medical field, important limitations still persist. Primarily, external power sources are still necessary, usually leading to both impractical and uncomfortable solutions[97–99]. Moreover, most of these devices utilize batteries, which contain toxic chemicals that pose both cellular and physiological health risks, rendering battery-powered devices a temporary and often non-implantable solution. To overcome this limitation, researchers have developed wearable

technologies capable of generating their own electrical energy, bypassing the need for battery use[100–103]. Moreover, by operating on a high voltage and current supply, these devices also pose heat-related complications. Finally, many of these devices are often bulky in nature and unsuitable for everyday use given the lack of cohesiveness between their various subparts, and the generally unsuitably high Young's Modulus of the materials employed[104]. In order to make these devices more suitable for everyday use, using biomimicking materials capable of bending with the various motions of the human body would present obvious advantages.

With the invention of the TENG, wearable bioelectronics are evolving to become ever more suited to the human body. TENGs are able to harness the coupling effect of contact electrification[105] and electrostatic induction between two thin films, and harness electricity from a myriad of natural biomechanical movements. The TENG has emerged as a fundamentally new and efficient technology to convert human biomechanical movements into electricity *via* its innate modus operandi. When the TENG's triboelectric layers, which are made of materials on the opposite sides of the triboelectric series, cycle between biomechanical motion induced contact and separation, an alternating current between the two electrodes is generated, inducing an electrical current that can be employed for a plethora of biomedical applications. As of now, within the biomedical field, TENG-generated electricity has been utilized to power wearable devices, enable the sensing of physiological functions such as heart rate, and treat various diseases and conditions through therapeutic ES. There are four different types of TENG working modes including vertical contact separation[106], in-plane sliding[107], single electrode[108], and freestanding[109], which give further leeway to utilizing TENG devices for IOB therapeutic applications due

to the ability of TENG devices to harness electricity from a wide variety of biomechanical motions. TENGs' versatility renders them optimal self-powered biomedical sensors, providing sensing insight *via* means of signal-to-function association. This versatility can be easily manifested by employing a TENG-coupled microprocessor that extrapolates biological information such as heart rate and blood pressure. The electricity produced by these different types of TENG devices can not only be used to deduce biological information as a sensor, but it can also be utilized as a therapeutic device, applying ES to different parts of the body *via* electrodes. Implantable versions are also being developed by embedding standard TENGs in protective pouches composed of hydrophobic materials that serve as a barrier, shielding the device from the unfavorable conditions in the human body[110]. These protective measures are also necessary to protect TENG devices from environmental conditions when utilized for IOB applications.

Owing to their unique working mechanism and a wide range of available material choices, TENG devices' characteristic flexible, bioconformable, soft, and lightweight properties make them a perfect candidate for IOB bioelectronics, especially considering long-term durability and resistance to fatigue. Capturing electricity from physiological movements ranging from blood circulation to ambulatory motion can allow for ubiquitous IOB use of TENG devices. In addition, TENG technology can be easily integrated with common manufacturing techniques, which, in conjunction with the use of low-cost materials, make TENG devices a scalable and affordable option. Through the conjunction of triboelectrification and electrostatic induction between a broad range of flexible materials, including silk, wool, and cotton, as well as rigid materials, including various commonly manufactured synthetic compounds, TENG devices can be rendered soft or rigid.

However, in the space of IOB TENG use, there has been specific effort focused on developing body conforming soft TENG devices due to their increased wearability. The soft and flexible nature of certain TENG devices is not their only strong suit; operating TENG devices emit reduced heat, considering the low current output they generate. This, moreover, enables TENG devices to remain biocompatible while still achieving high voltage outputs. In addition, TENG devices provide a self-sustainable power source, which overall permits for the integration of the power source into the device itself, yielding a product that is more compact, comfortable, and bioconformable. Using soft bioelectronics devices as a source of ES for therapy can provide a platform solution to a number of unmet medical needs (**Figure 4**) including regenerative medicine, neural engineering, rehabilitation engineering, and pharmaceutical engineering.

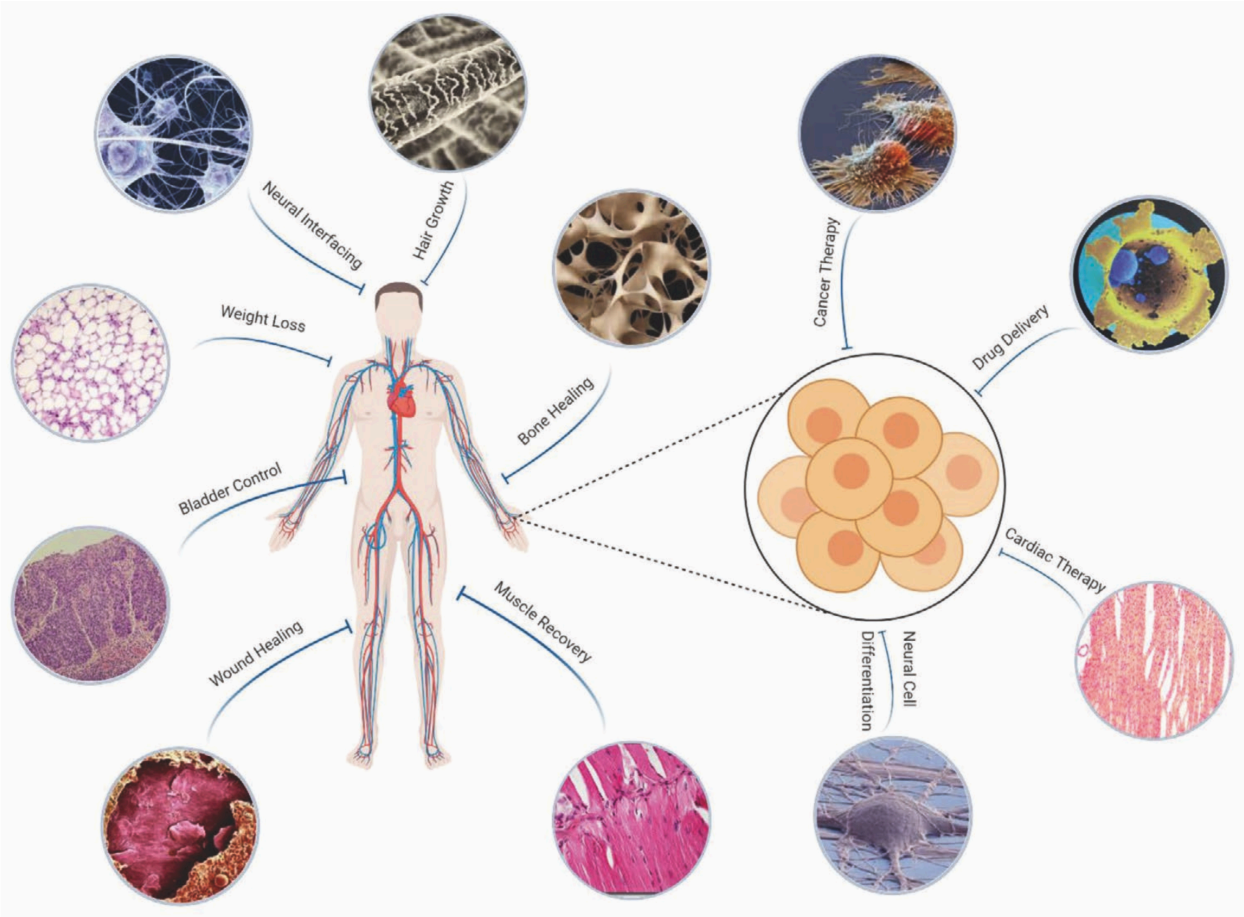

Figure 4. Schematic illustration of the various applications of therapeutic electrical stimulation using soft bioelectronics. Applications ranging from physiological applications such as bladder control to cellular applications such as cancer therapy[111]. Reproduced with permission[111], Copyright 2021, Wiley-VCH.

The mechanistic reasons behind ES's beneficial effect on a number of regenerative and proliferative processes are still subject to investigation and are subjective in each ES application and field. However, there is the general understanding that ES aids at the tissue level by increasing capillary perfusion and blood flow, thus optimizing site oxygenation and healing, as well as at the cellular level by means of electric field creation, which encourages fibroblast activity, granulation, and cellular alignment[112]. We will explore this in more depth later in the thesis.

IV. Neuronal electrical stimulation for cell programming

Neurons are cells that function as transmitters of information between the brain and the various parts of the human body, allowing amongst other things, for the human body to optimize its interaction with the external environment it is found in, all while maintaining epigenetic homeostasis. Neurogenesis generally occurs in the developmental stages of embryo though neuronal cell differentiation is a critical process contributing to the correct functioning of the nervous system[113,114]. Neuronal cell differentiation is the process by which a neuronal cell is derived from another cell, whether this cell be a stem cell, or another type of cell depends on the process by which the neural differentiation is conducted. The most well-known process to achieve this, is stem cell differentiation, in which unspecialized stem cells are known to be able to differentiate into a number of cell types. Neural stem cell differentiation is the process by which unspecialized stem cells differentiate into neuronal cells, including neurons, astrocytes, oligodendrocytes, or other types of neuronal cells, through the introduction of, for instance, specific physicochemical factors into the microenvironment of the stem cells[113]. In addition to this process, direct cell conversion also exists, which is a more recently discovered, and complex process by which fully differentiated mature cells are converted into specialized cell types, e.g. neuronal cells[114]. Direct cell conversion is a unique process capable of converting virtually any cell type into the desired cell type through a differentiation process that does not include a pluripotent state. To date, the large body of work on soft bioelectronic use for this field has involved TENGs. Indeed, this background is of relevance as TENG-ES has been studied to assess its effects on neural cell differentiation, covered below:

Stem Cell Differentiation. In several studies researching the effectiveness of TENG-ES on stem cell differentiation into neuronal cells, mesenchymal stem cells (MSC) were utilized as an easily sourced starting cell line, which could be isolated relatively easily. MSCs do not immediately differentiate into neuronal cells as they require external factors to induce differentiation, such as growth factors, extracellular matrix components, and even electrical signals. Thus, the application of TENG-ES to assess MSC differentiation was studied. Using a suitable neural scaffold, such as poly(3,4-ethylenedioxythiophene), or PEDOT, is a known method with which to aid the process of stem cell differentiation. PEDOT, specifically, is the most promising scaffold used in this sense, up to now. However, PEDOT presents biocompatibility issues as it has trouble degrading *in vitro*. In order to address this issue, the carboxylic acid portion of graphene oxide nanosheets (rGO) can be incorporated into PEDOT's structure. This hybridization between the rGO-PEDOT microfibers was utilized in a study conducted by Guo et al., and allowed the researchers to develop a neural scaffold that was both biocompatible and highly conductive, due to the presence of rGO microfibers and PEDOT nanoparticle, respectively[115]. The crosslinking nature of the interaction between the rGO microfibers and the PEDOT nanoparticles allowed for increased protein adsorption, which accelerated the process of stem cell differentiation[115,116]. By itself, the rGO-PEDOT hybrid neural scaffold supports stem cell differentiation into neuronal cells, but it does not necessarily accelerate the process. TENG-ES was utilized as this external promoting factor since ES has been shown to have a significant effect on the process of stem cell differentiation into neuronal cells[117–119]. In order to determine how TENG-ES affects the process of stem cell differentiation, Guo et al. studied four experimental groups: two

control groups of rGO and 15% rGO-PEDOT microfibers without exposure to TENG-ES, and two stimulation groups of rGO and 15% rGO-PEDOT microfibers with exposure to TENG-ES. As shown in **Figure 5 (top)**, through the DAPI stained images, after 21 days of treatment the ES groups showed a much larger distribution and density of cells[115]. In order to determine how many of these cells were neuronal cells, the groups were also stained to visualize the existence of two neural markers (Tuj1 for neuronal cells, and GFAP for glial cells). The ES groups showed a much larger degree of Tuj1 expression, however, more noticeably, the 15% rGO-PEDOT groups yielded a significantly higher degree of Tuj1 expression compared to their unhybridized counterpart.

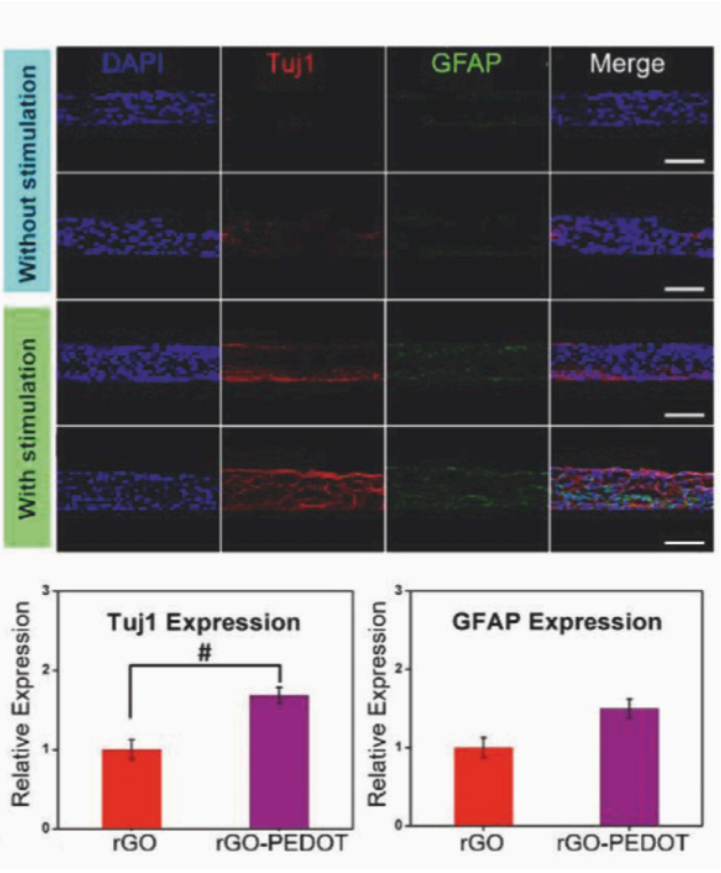

Figure 5. Examples of soft bioelectronic generated electrical stimulation for cellular reprogramming (**Top**) Immunostaining with DAP1, Tuj1, and GFAP with and without TENG-ES (scale bars: 100 μm). (**Bottom**) qPCR analysis of cell expression levels of Tuj1 and GFAP with and without

hybridization of rGO and PEDOT microfibers[115]. Adapted with permission[115], Copyright 2018, American Chemical Society.

These results show that the hybridization of rGO microfibers and PEDOT nanoparticles serves as an excellent scaffold to support neural stem cell differentiation when combined with TENG-ES therapy, due to the highly conductive nature of the PEDOT nanoparticles. As can be seen by **Figure 5 (bottom)**, the combination of the 15% rGO-PEDOT neural scaffold with TENG-ES served as the most effective tool for stem cell differentiation into neuronal cells, as it resulted in the highest expression of neural marker cells such as Tuj1 and GFAP. The use of an rGO-PEDOT neural scaffold induces stem cell differentiation into neuronal cells due to the conductive nature of the PEDOT nanoparticles and the biocompatible nature of the rGO microfibers. However, the implementation of this hybridized neural scaffold with TENG-ES is shown to be the most effective therapeutic application to accelerate stem cell differentiation into neuronal cells. This research is encouraging as it can seemingly lead to developments in IOB bioelectronic technology capable of inducing nerve regeneration. Utilizing TENG for ES in this case is of added benefit given the capability to organize the architecture of the device in such a manner that could be used to uniformly stimulate batches of stem cells for specific differentiation pathways.

Direct Cell Conversion: Direct cell conversion is a process in which any mature, or somatic cell is directly converted into another somatic cell type. This process occurs through the introduced expression of certain genes which code for cell type-specific transcription factors. For neural engineering applications, these cell type-specific transcription factors enhance the production of neuronal cell factors, which subsequently promote the process of converting the original mature cell into a neuronal cell[114,120]. Direct

cell conversion can convert any cell type into the desired cell type. However, some cell types such as fibroblasts, are easier to transform[114]. Thus, to test whether or not TENG-ES promotes this process of direct cell conversion into neuronal cells, mouse fibroblasts were used. The process of direct cell conversion to neuronal cells requires the introduction of neuronal genes into the sample. Normally the process of direct cell conversion would occur at a slow rate, but through the use of TENG-ES this process can be sped up and rendered more efficient[120]. In a study conducted by Jin et al., TENG-ES was found to closely mimic innate natural electric cues that control and stimulate the process of direct cell conversion, allowing TENG-ES to promote the direct differentiation process. In order to determine the efficiency of TENG-ES's ability to induce direct cell conversion of fibroblasts to neuronal cells, the fibroblasts were separated into two separate cultures with and without exposure to TENG-ES, and subsequently stained for neuronal marker class III beta-tubulin (Tuj1) starting on the ninth day of culture. **Figure 6** shows the increased concentration of Tuj1 in the TENG-ES group compared to the other control groups. It was on this ninth day of the application of TENG-ES to the system that the cells that were originally fibroblasts started to take a more elongated shape, similar to that of a neuron.

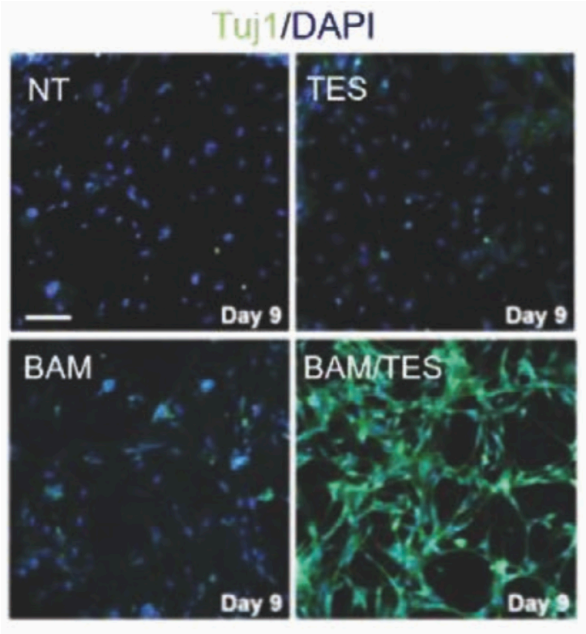

Figure 6. Effect on neuronal transdifferentiation using soft bioelectronic generated electrical stimulation. Expression of Tuj1 gene after 9 days of culture with various forms of stimulation (scale bar: 100 μm)[120]. Reproduced with permission[120], Copyright 2016, Wiley-VCH.

The conversion efficiency, which was calculated as the percentage ratio of Tuj1 positive cells to total cells, was 8.85%, compared to a mere 0.13% in the group lacking exposure to TENG-ES. In addition, during the 12th-14th days the conversion efficiency of the TENG-ES group was 14.17% whereas the control group had a conversion efficiency of only 6.41%[120]. This significant increase in the conversion efficiency correlates to an increase in the number of neural-like cells within the sample, with significant indication that TENG-ES promotes direct cell conversion of fibroblasts into neuronal cells.

In addition, the continued use of TENG-ES through days 14-18 yielded induced neuronal cells with a more complex neural morphology. Following the maturation of the cells until the 30th day yielded neuronal cells with highly mature neural phenotype markers, evidence of synaptic connections. Throughout this entire process, the group of cells that

were subjected to TENG-ES yielded significantly higher conversion efficiency rates and more evidence of neuronal cell morphologies.

V. Neuronal electrical stimulation for therapy and rehabilitation

Utilizing external ES can be beneficial in therapeutic applications, as ES can effectively mimic native electrical impulses in the body. TENG-based neural interfacing of a particular nerve to control specific motor functions can potentially be utilized to treat various diseases and conditions. For this reason, soft bioelectronics such as TENGs were used to this end. TENG-based neural interfacing with a particular nerve has been studied in the hopes to restore muscle function in patients with peripheral nerve injury. However, since current research in this field is still in its infant stage, a large portion of research has focused on the treatment of foot drop *via* TENG-ES of the sciatic nerve, albeit simplistic, a linear and low-barrier research approach in attempting to prove TENG's efficacy in restoring lost or hindered function due to peripheral nerve damage[121,122]. Neural interfacing is achieved through the combination of a stimulator, the TENG, and a neural interface, in this case a flexible sling interface that wraps around the nerve to ensure efficient and safe nerve stimulation. The neural interface can either interact with the central nervous system (CNS), composed of the brain and spinal cord, or the peripheral nervous system (PNS), composed of all the peripheral nerves within the rest of the nervous system. However, due to the stark anatomical differences between the two nervous systems, the mode of neural interfacing utilized must be compatible with the anatomical features of that particular neural structure. Currently, a majority of the studies regarding TENG-based neural interfacing are focused on PNS neural interfacing through

the use of a flexible neural sling that wraps around the nerve of interest[123]. This is a generally safe mode of neural interfacing as it essentially stimulates that entire section of the nerve so there is a healthy balance between invasiveness and selectivity. On the other hand, other modes of neural interfacing such as intraneural multichannel microelectrodes offer optimal selectivity in neural fiber activation at the expense of a high degree of invasiveness and potential glial scarring[124]. However, Lee et al. developed a novel TENG device capable of attaining a high degree of selectivity without a corresponding increase in invasiveness. Using an array structure of neural electrodes, each individual pixel in the array could be individually activated to electrically stimulate the nerve of interest[121]. A major hurdle preventing effective neural interfacing with the CNS is that electrical signals tend to spread out within brain tissue, thus without a proper mode of application, neural interfacing with the CNS presents issues of low selectivity, and could lead to major neural damage in the brain[125–127]. Consequently, current studies are generally focused on neural interfacing with the PNS. It is conceivable to see, however, how such a microscaled technology as TENGs could be applied to the CNS upon development of proper neural interfacing mechanisms adapted to the anatomy of the CNS. This is something we will explore in Chapter 4. As mentioned, the bulk of TENG-based neural interfacing research is based on the treatment of foot drop *via* neural interfacing of a section of the sciatic nerve. Normal foot motion is characterized by dorsiflexion and plantar flexion of the muscles in the foot during each phase of gait. However in patients with foot drop, certain motions such as excessive foot inversion and toe flexion yield the typical phenotypic result associated with the dropping of the forefoot. Thus, in order to treat foot drop, the TENG-based neural interfacing system must be able

to prevent these detrimental motions of excessive foot inversion and toe flexion, as well as control the flexion of various muscles within the foot[128].

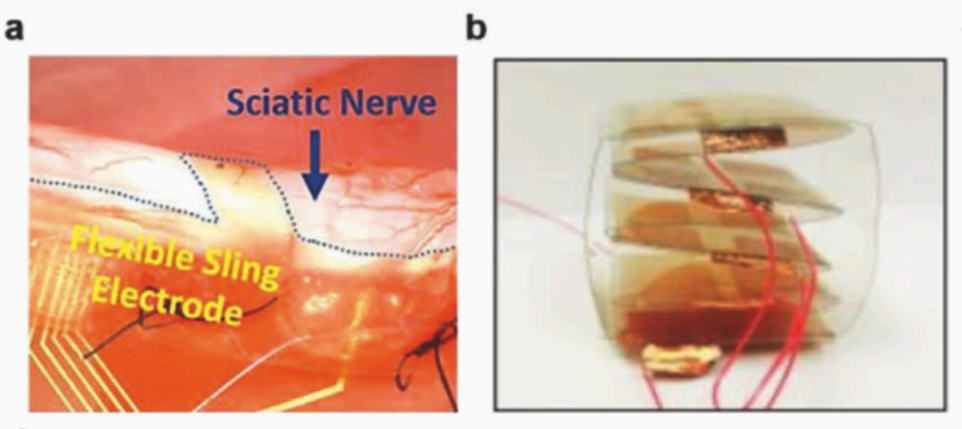

Figure 7. Soft bioelectronic electrical stimulation used for neural rehabilitation. (a) Implanted flexible sling electrode on rat sciatic nerve[122]. Reproduced with permission[122], Copyright 2017, Elsevier. (b) Layered TENG device composed of Cu and PDMS triboelectric layers. PDMS = polydimethylsiloxane.[121]. Reproduced with permission[121], Copyright 2018, IOPscience.

Only a particular set of nerves needs to be stimulated in each phase of gait. In order to achieve this, a flexible sling neural interface is utilized as its selectiveness is sufficient enough to stimulate only the desired nerves, thus enabling certain ankle motions, while avoiding undesired ones. The way in which the flexible sling neural interface is able to achieve this level of selectiveness is through its unique structure. As shown in **Figure 7a**, Lee et al., devised a study in which the flexible sling interface was wrapped around the sciatic nerve with six electrodes on its central bridge, and two more ring electrodes surrounding the nerve on a neighboring bridge[121]. This bridge system enables the flexible sling interface to wrap around the nerve with optimal surface level contact that does not apply too much pressure, a factor that could potentially damage the nerve. In addition,

the flexible nature of the sling interface allows it to integrate with a variety of sizes of nerves, making it an effective tool for TENG-ES neural interfacing. The flexible sling interface is used in conjunction with the stacked TENG shown in **Figure 7b**. The stacked TENG generates an electrical current, which is then passed through the flexible neural interface in order to stimulate a section of the sciatic nerve affecting the movement of a particular muscle. Due to the unique structure and the sheer number of electrodes on the flexible sling interface, this device was able to transmit the TENG-ES to stimulate the nerve of choice in two configurations: transverse and longitudinal polar. It was found that the transverse configuration could effectively function at only 0.4 mA while the longitudinal polar configuration could effectively function only at a much higher current of 2.4 mA[121]. The higher current associated with the longitudinal polar configuration generates more heat, which can have detrimental effects on the nerve, as well as delaminate the electrodes in the flexible sling interface. In addition, the transverse configuration yielded compound muscle action potentials (CMAPs) with a significantly higher amplitude than those of the longitudinal polar configuration. Thus, the transverse configuration is shown to be both the safer and more effective option for the application of TENG-ES to the sciatic nerve, for the treatment of foot drop. In order to test the selectivity of the flexible sling interface, the CMAPs of the gastrocnemius medialis (GM) and tibialis anterior (TA) muscles were measured in response to TENG-ES of a specific portion of the sciatic nerve.

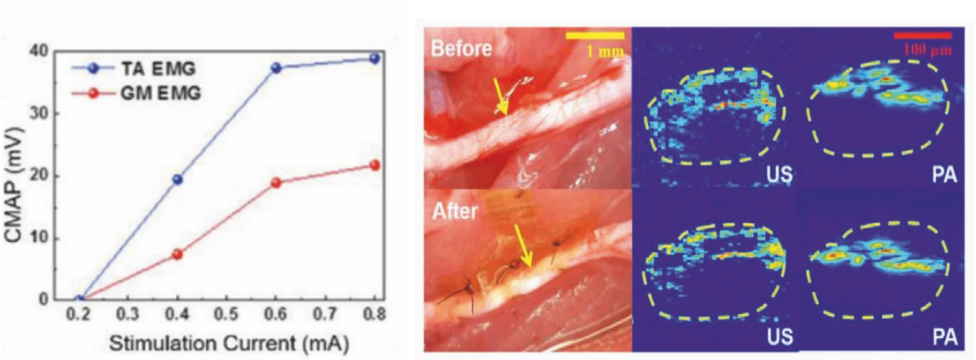

Figure 8. Soft bioelectronic electrical stimulations for motor function rehabilitation and use. (**left**) TA and GM EMG signals. (**right**) Photos of sciatic nerve before and after implantation of sling electrode in addition to photoacoustic measurements to assess hemodynamics. Reproduced with permission[121]. Adapted with permission[121], Copyright 2017, Elsevier.

As shown in **Figure 8 (left)**, the TA muscles were more effectively stimulated compared to the GM muscle. Thus, the researchers determined that the existing system did not have a high enough degree of selectivity. In order to increase the selectivity of the system and test whether or not the TENG system was capable of generating enough electricity to induce full muscle contraction, the researchers wrapped a pair of Pt/Ir wires around a section of the sciatic nerve interfacing with the flexible neural sling interface. With the addition of the Pt/Ir wires, the TA muscle underwent full contraction and completed the dorsiflexion movement necessary in treating foot drop[121]. Thus, the TENG device seemed able to generate enough charge to control the contraction of the TA muscle when implemented with a flexible neural interface and a mode of increasing the selectivity of the system. Neural interfacing with peripheral nerves through ES is a delicate process that can have a number of unwanted side effects. It is critical to test whether or not this neural interfacing has any effect on the nerves' other functions and processes, including their hemodynamics profile. Functional photoacoustic microscopy (fPAM) was utilized to determine the effect of TENG-ES on the sciatic nerve's hemodynamics. As shown in

Figure 8 (right), fPAM images show no change in the blood flow within the sciatic nerve before and after the implantation of the flexible sling interface. Indeed, TENG-ES neural interfacing with the sciatic nerve seemed to indicate no detrimental effect on the hemodynamics of the sciatic nerve[121]. Through the combination of the TENG, used as a stimulator, and a flexible sling interface, used as a neural interface, complete contraction of the TA muscle was achieved by the researchers, effectively counteracting foot drop. The use of TENGs in the modulation of motor function through neural interfacing is a relatively new field, and although at the moment one of the only applications of TENGs in neural interfacing is the treatment of foot drop, many new applications beyond this are likely to emerge in the coming years.

CHAPTER 2

MAGNETOELASTIC GENERATOR-BASED ELECTRICAL STIMULATION PLATFORM

Developing biocompatible electrically stimulating platforms for tissue engineering purposes is limited by external power dependency, wetting resistance requirements, micro scale size need, and suitable flexibility. The giant magnetoelastic effect in soft systems can be harnessed to overcome these shortcomings, providing a versatile platform which allows tunable electrical stimulation for biological applications. Here, we develop a one-design, easy to build self-powered magnetoelastic generator platform for *in vitro* electrical stimulation, activated using simple air pressure (100 - 400 kPa). The platform yielded current values of up to 10.52 mA and 9.5 mV, with simple fabrication in standard well plates, and biocompatible surface tissue culture growth, and showed easily integrated capabilities for 3D printing and production at scale. The platform could be adapted to 6, 12, 24, 48 and 96-well plates and sterilized using commonplace techniques including autoclaving and ethanol wetting. This platform represents the foundation for a low cost and scalable electrical stimulation for *in vitro* use.

I. Introduction

The role of electrical stimulation (ES) in biological systems is well established[129] and has been extensively exploited in pre-clinical research[130] as well as an innumerable number of therapeutic solutions[131–133]. With the importance of physical stimuli (including electrical stimulation) becoming ever more apparent in processes including morphogenesis[134],

tissue regeneration[135] and cellular differentiation[136,137], developing an easily implementable and adaptable electrical simulation platform for *in vitro* studies represents a highly desired tool. Furthermore, *in vitro* validation of such a type of platform represents a necessary step towards any novel technology's eventual *in vivo* adoption.

Recent focus has been placed on exploiting novel platform technologies to substitute commercially available solutions which are costly, difficult to adapt, and could potentially lead to dangerous live current exposures. Nanogenerators, including those harnessing the triboelectric and piezoelectric effect, have been explored as alternatives for use as ES platforms[111,138]. Although these technologies provide self-powered solutions which are easy to fabricate and require inexpensive materials, they also often lack biocompatibility, biocomformability, and cannot be operated in wetted environments, factors which have hampered their adoption into research settings. Furthermore, these biomechanical-to-electrical energy conversion platform technologies present particularly low inherent current density and high internal impedance, stemming from their capacitive power generation principles reliant on the manipulation of the electric dipoles at the materials' interfaces[139,140].

A novel platform technology has become available with the recent discovery of the giant magnetoelastic effect in soft systems[47], exploiting magnetoelastic and electromagnetic induction coupling, able to produce electricity *via* the use of a magnetoelastic generator (MEG). This platform technology, which has been validated as an effective biomonitoring and energy harvesting tool[141], can be easily modified to elicit and obtain desired current and voltage outputs. Indeed, aside boosted current outputs, the inherent waterproof encapsulation and soft polymeric nature of the MEG position it as

an ideal candidate for the development of an ES platform[142]. MEGs are made with inexpensive materials[143] which are readily available, and can be applicable and fabricated directly onto existing tissue culture platforms. Considering the layered and adaptable nature of the MEG platform itself, biocompatible materials such as polydimethylsiloxane (PDMS) can be employed during fabrication to render these stand-alone ES platforms tissue compliant and biocompatible.

From an operational perspective, MEGs are inherently self-powered and can be activated using simple mechanical motion including (bio)mechanical stimuli, a concept upon which we built to enable their activation through simple air pressure use. Considering the pervasive presence of air pressure appliances in labs across the world, we devised a platform exploiting this simple modus operandi, and investigated MEG ES in genetic engineering applications.

An important factor when devising any tool which may be used in large scale, is ensuring the ease of fabrication and production. To ensure this, we further devised a 3D printing protocol using readily available commercial 3D printers, to demonstrate the scalable manufacturing of the MEG ES platform for 6, 12, 48 and 96-well plates.

II. Magnetoelastic effect for biological applications

Finding novel ways to readily generate electricity is paramount to the development of next generation ES platforms. Although the magnetoelastic effect has been recognized since the late 19th century, its application in miniaturized and soft systems has been limited by a number of factors including: the rigid nature of the ferromagnetic materials traditionally employed (such as Fe1-xCox, TbxDy1-xFe2 (Terfenol-D)[144], and GaxFe1-x

(Galfenol))[145,146], the need for an applied external magnetic field to the system, and the very large applied pressure – megapascal range[144] – required to generate the effect. The giant magnetoelastic effect has been recently discovered in soft systems[47], bypassing the need for external fields, as well as reducing pressure requirements by orders of magnitude, and becoming tolerable for biological use (**Figure 9**).

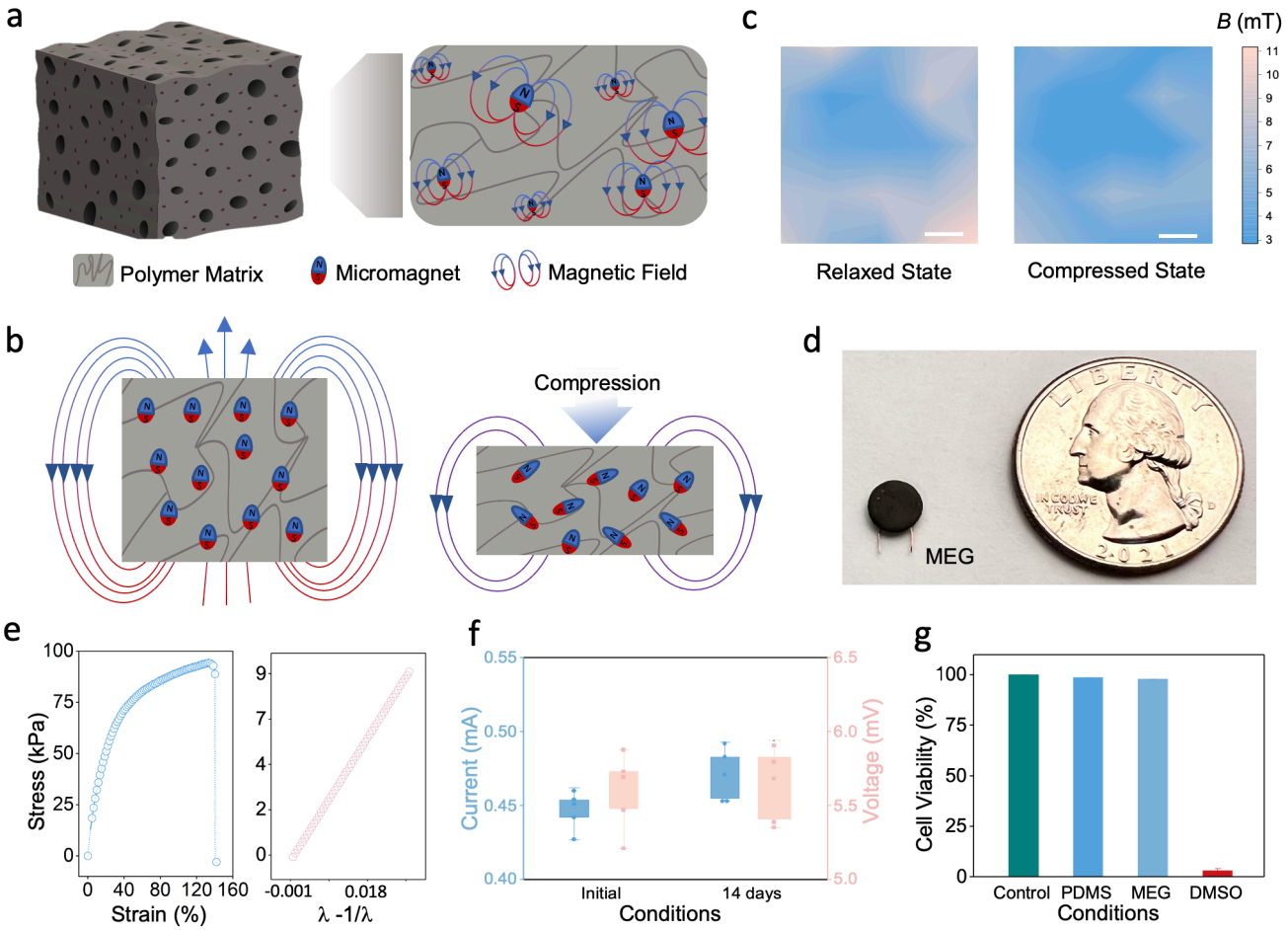

Figure 9. Magnetoelastic generator displays suitability for biological applications. (a) Schematic representation of nanoparticles dispersed in a polymer matrix. (b) Wavy chain model and magnetic field variations brough about by the compression of a magnetoelastic layer. (c) Vertical magnetic flux density (□B⊥) of the soft system on the South Pole surface, and its variation from a relaxed (0 N) state to a compressive (20 N) force state. Scale bar 0.5cm. (d) A photograph of a miniaturized MEG placed alongside a US quarter dollar coin, for comparison. (e) Stress and strain curve of the soft system, and Young's modulus calculation using a neo-Hookean model. (f) MEG current and voltage outputs prior and subsequent to, water submersion for 14 days. Box plots represent mean + standard deviation values, n=5. (g) Cell viability of mouse fibroblasts cultured atop PDMS and the soft MEG, shown in contrast to positive and negative (DMSO) controls, respectively,

as determined using a PrestoBlue assay. Bar graphs show mean + standard deviation of the results (n=4). DMSO, dimethyl sulfoxide.

In order to form such a device, neodymium boron (NdFeB) nanoparticles can be homogeneously dispersed in a liquid silicon rubber solution, and subsequently magnetized for intra-structural dipole alignment post curing, yielding a soft system (**Figure 9a**) which can be easily deformed using minimal, and biologically tolerable force. The physical disturbance of the system from a relaxed to a deformed state (whether compressed or stretched) (**Figure 9b**), has been shown to lead to a change in the magnetic dipole alignment of the nanomagnets, modifying the magnetic flux density of the soft system (**Figure 9c**).

Magnetic flux density changes can be exploited to yield an electromotive force – electricity, produced by a non-electrical source – when coupled with an electrical conductor. Encouragingly, magnetic fields can permeate wetted environments without any significant intensity decrease[147], making them suitable for use in wetted environments ubiquitously found in biological systems and biological applications. MEGs, combining giant magnetomechanical coupling (MC) layers and magnetic electrical induction (MI) layers, are thus able to act as electricity generators which can be used for ES in miniaturized systems (**Figure 9d**). Furthermore, beyond their inherent energy transducing (self-powering) and bioconformable encapsulation, MEGs can be operated with physiologically tolerable pressure values - Young's modulus of 446.42 kPa and ultimate strain of 140.28% (**Figure 9e**) - can withstand prolonged exposure in wetted environments without compromise in functionality (**Figure 9f**) and can be made using biocompatible materials (**Figure 9g**), helping their nifty integration into biological systems and research laboratory tools. As a novel platform technology, MEGs have demonstrated

suitability for biomonitoring applications[142], therapeutic applications, and energy generation[141]. Their easily devisable architecture has been revised to fit various declinations, including integration in textile form[143], and use in film form. With our study, we set out to explore MEG use as an ES platform by integrating it in existing research tools in the form of tissue culture well plates. Mechanical deformation induced by air pressure was then harnessed to alter the inner magnetic dipole-dipole interaction of MEG, leading to a change of its magnetic field. Said change was then exploited to generate electricity via electromagnetic induction, for *in vitro* exploitation.

In order to address the above a number of experiments were carried out. Biological suitability of MEG: Magnetic flux density measurement were recorded as follows: Uniaxial stress (20 N) was applied onto a magnetoelastic film of size 25 mm by 25 mm, and the vertical component of the magnetic field was measured using the axial probe of a digital Gauss meter (TD8620, Tunkia). The stress-strain curves were determined by stretching a magnetoelastic film of 15mm (w) x 3mm (h) x 23mm (l) using a dynamic mechanical analyzer (Instron 5564, stretching rate of 5mm/s). The Young's modulus was calculated by fitting the experimental curves with a neo-Hookean model. A magnetized magnetoelastic layer (83 wt%) showed a Young's modulus of 446.42 kPa and an ultimate strain of 140.28%. For water performance testing, a MI-MC layer of non PDMS-encapsulated MEG was soaked in water for 14 days with its current and voltage output tested pre and post soaking. For biocompatibility testing, mouse fibroblasts expanded in fibroblast medium consisting of DMEM basal medium (Gibco, 11965), 10% fetal bovine serum (Gibco, 26140079) and 1% penicillin/streptomycin (Gibco, 15140122) were seeded and grown on PSMD, a silicone (Cu/NdFeB-Ecoflex) based MC-MI ("MEG") layer,

and in tissue culture well controls, and cultured in an incubator at 37 °C and 5% CO2. After 24 hours, cell viability was assayed using PrestoBlue Cell Viability Reagent (Invitrogen, A13261) according to the manufacturer's protocol. Cells were incubated with 10% PrestoBlue reagent for 2 hours and results were normalized to the control samples (for which we used fibroblasts seeded in the tissue culture plate). DMSO was used as negative control. Absorbance reading were recorded using an Enspire nanoplate reader (PerkinElmer, Massachusetts, USA).

III. Fabrication of the MEG electrical stimulation platform

The MEG ES platform we fabricated (**Figure 10**) consists of a multilayered system including a MI layer encapsulated within an MC layer, a biocompatible PDMS layer, and an indium-titanium oxide coated glass (ITO glass) (**Figure 10a**), fabricated, and encased in a commercially available tissue culture well plate.

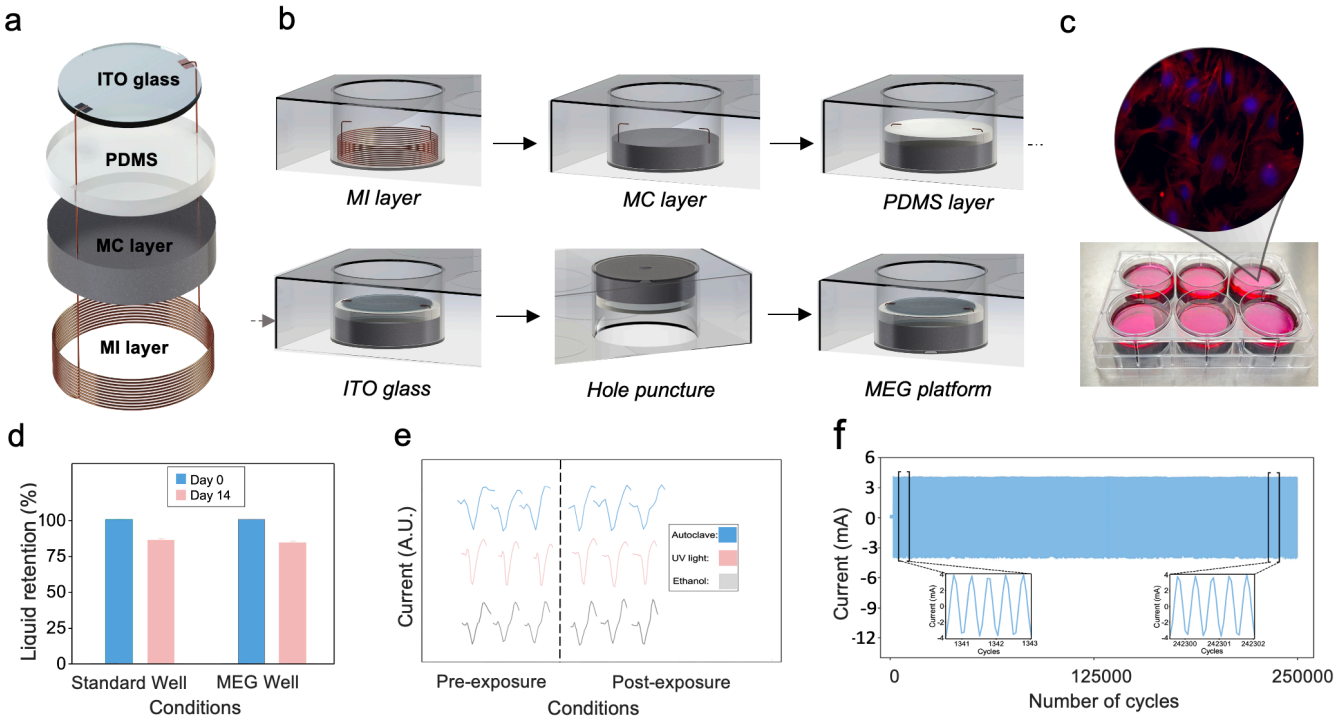

Figure 10. The MEG electrical stimulation platform is simple to fabricate and provides a resilient *in vitro* tool. (a) Exploded schematic view of the MEG ES platform. Figure 2. The MEG ES platform is simple to fabricate and provides a resilient *in vitro* tool. (a) Exploded schematic view of the MEG ES platform. (b) A schematic representation of the fabrication process *in situ* a commercially available tissue culture well plate. (c) The as-fabricated MEG electrical platform with fibroblasts seeded onto its ITO glass surface, in DMEM media, and an immunofluorescent image of the seeded fibroblasts with clear nuclear (DAPI - blue) and cytoskeletal (phalloidin –red) staining. (d) Liquid retention in an MEG ES well as compared to a control standard tissue culture well confirms the absence of absorption or leakage in the MEG ES platform. (e) Commonplace sterilization techniques do not affect the electrical output of as-fabricated MEG ES platforms. (f) Durability testing of the MEG ES platform to assess long-term performance and output current effect. The performance of the MEG is virtually unaffected after extensive cycling.

To fabricate our ES platform, we utilized commercially available non-tissue culture well plates, into which the platform was sequentially constructed (**Figure 10b**). To begin, the initial MI layer was fabricated: copper (Cu) wires were used as the MI layer and prepared. Subsequent to the MI layer fabrication, the MC layer was prepared by pouring uncured silicone rubber matrix that had been previously mixed with non-magnetized NdFeB nanoparticles, into the MI-containing tissue well plates, and then cured in a heat oven at 60˚C. Once the MI-MC layered MEG was fully cured, the MC layers was magnetized. Later, uncured PDMS was poured into the well plates to provide an optimal biocompatible layer and hermetically seal the MEG platform, overall preventing its dislodgment during platform activation (air pressure use) and left to cure. Mid-curing, an ITO glass cut to the required tissue culture well size, was deposited above and partially into the layer to enable fixing into the MEG ES platform, allowing space for the MI electrode wires to exit and connect (at the ITO glass' antipodes), and further cured at 60˚C for 3 hours in an oven to complete the curing process (**Figure 10b**). Prior to application, the ITO glass was functionalized using plasma to reduce its hydrophobicity (**Figure 11**), optimizing wettability and cell adhesion.

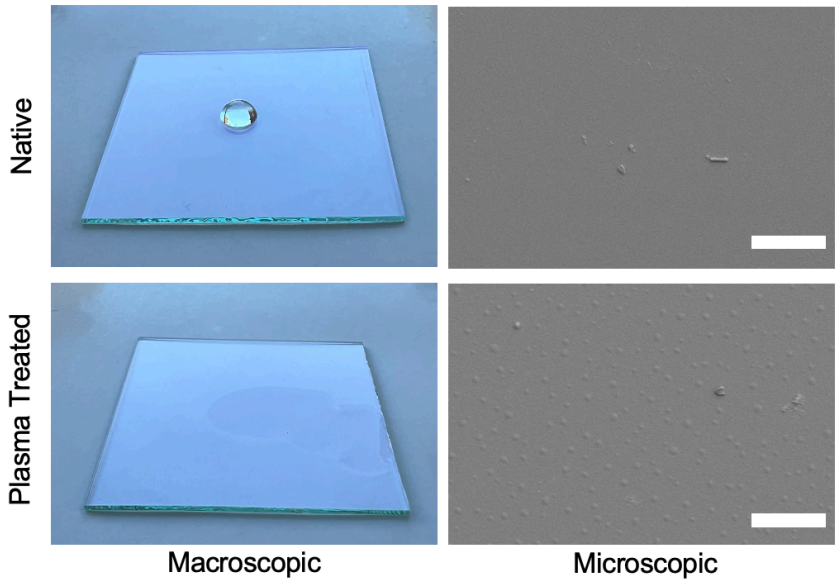

Figure 11: ITO glass functionalization to enhance cell adhesion. Macroscopic and microscopic views of ITO glass pre- and post- a 5-minute plasma treatment protocol. Hydrophobicity loss of the ITO glass is demonstrated by the change of surface dispersion of a drop of water at the macro level, and by the formation of a functionalized surface at the microscopic level (SEM microscopy). Scale bar = 10 µm. SEM = Scanning electron microscopy. SEM photos taken using a Zeiss, supra 40VP microscope.

This step could also be carried out once the MEG ES platform was fully cured and prepared, and with the ITO glass integrated, without affecting the functionality and structural integrity of the MEG ES platform. Finally, small 3 mm diameter holes were carefully drilled in the bottom of each tissue culture well plate, so as to permit subsequent air pressure activation.

The as-fabricated MEG ES platform could be subsequently used for cell seeding, permitting cell culturing experiments (**Figure 10c**). In order to assess the resilience and resistance of the MEG ES platform to the exposure to various experimental conditions, we tested hermetic capabilities and leakage prevention within the platform (**Figure 10d**), and subsequently assessed the MEG ES performance after a number of commonplace sterilization techniques, including autoclaving, UV irradiation, and ethanol wetting. No tangible output decrease was noted in the MEG ES platform after any of the physical

exposure (**Figure 10e**). This is encouraging as NdFeB's Curie Temperature for conservation of magnetic properties is 300˚C, well above the autoclaving ~150˚C steam conditions. Finally, as the platform might be utilized for long term ES experiments, its resistance to repeated cycling was tested, showing output retention after 250,000 cycles (**Figure 9f**).

The PDMS layer provides a biocompatible environment on top of which tissue culture media can be deposited and helps form a further hermetic seal around the platform, preventing tissue culture media leakage. Atop the biocompatible layer, the ITO glass, connected to the MI layer's electrode wires, allows for cell seeding and direct ES to the biological sample. ITO glass was chosen as its suitability had been previously reported26 with regards to cell toxicity and cell anchoring (**Figure 12**).

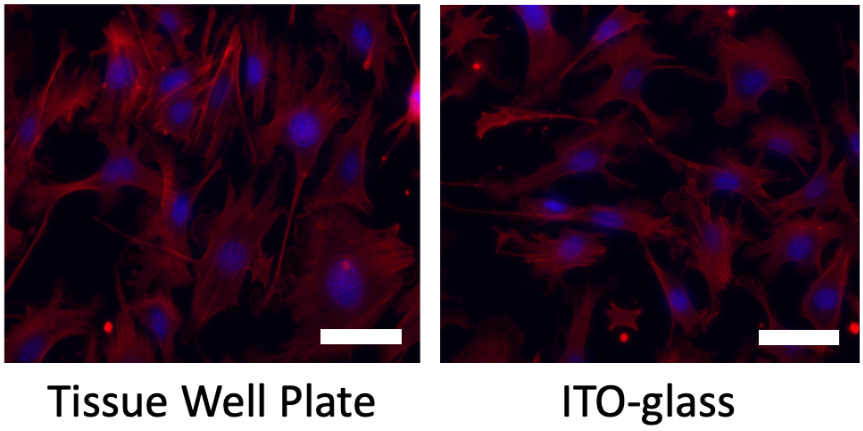

Figure 12: Fibroblast anchoring. Fibroblast anchoring on standard tissue-well plates *vs* plasma-treated ITO glass. Clear morphology and cellular anchoring visible via phalloidin- and DAPI-staining with no observable difference. Scale bar = 50 μm.

Furthermore, although other, more flexible ITO-coated polymers are available for use, their ITO coating process is laborious and requires specialized machinery[148,149]. In addition, electrically stimulated samples often need to be visualized under fluorescence microscopy, and the use of glass helps as ITO glass can be commercially sourced, easily cut into desired shapes, stained, and mounted for post-experimental analysis. An alternative set up of the MEG ES platform was devised to allow parallel ES of various samples using one single external MEG, particularly useful for samples that need to be observed using standard bifocal microscopy during the course of the experimentation (**Figure 13**).

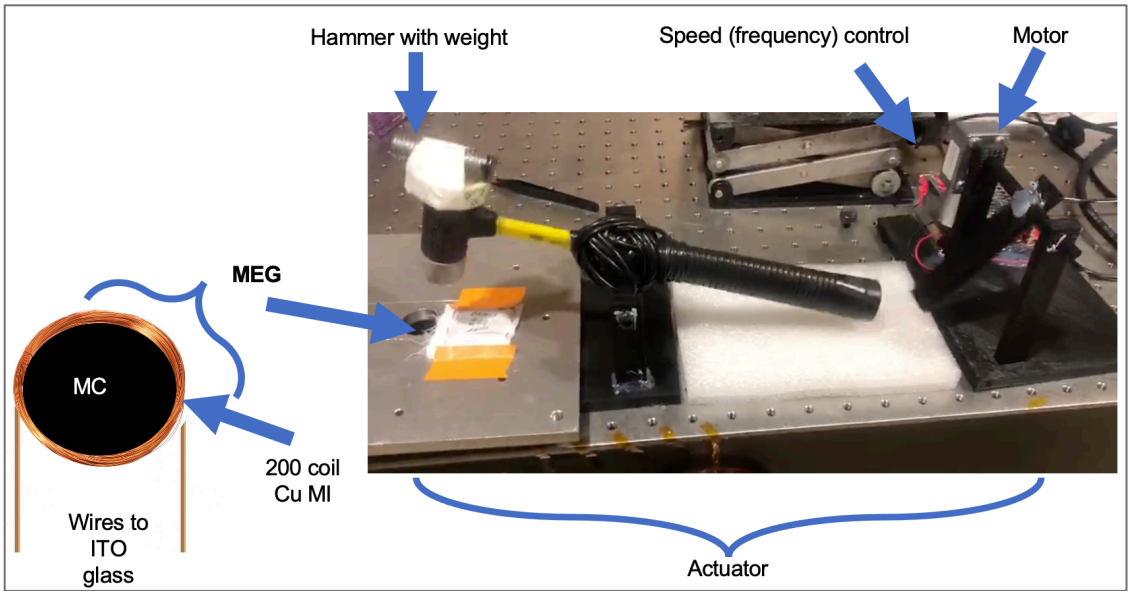

Figure 13: An alternative set up of the MEG electrical stimulation platform. A mechanical actuator in the form of a rotating motor cyclically hits a weighted hammer which falls on the associated MEG under its own weight. The speed (and thus frequency) of the actuator can be modified according to experimental need. A schematic of the fabric-enveloped MEG is also shown. This particular set up (MC: 83% NdFeB, 4 mm thick, 25 mm diameter; MI: 200 Cu coils; Hammer weight: 250g) could yield up to 3 mA and be connected in series or parallel to ITO glass samples for use in ES protocols.

In order to assess the above, a number of experiments were carried out. Manual fabrication of MEG ES platform: This process was repeated for each of the wells in the 6-tissue culture wells plates (Falcon™ Polystyrene Nanoplates, ThermoFisher), in parallel. MI layer preparation: Cu wire (Enameled Cu Wire, 28 AWG, 28SNSP, Remington Industries) was spun in various coil turns (50, 100, 200 and 400) using a 25 mm diameter acrylic rod (TAP Plastics) and placed in the middle of a 6-well tissue culture plate, with the Cu wire extremities made to stand vertical at opposite ends, 15 mm in height. MC layer preparation: Standard MC layers were prepared by thoroughly mixing an uncured silicone rubber matrix with non-magnetized NdFeB nanoparticles poured directly onto the MI layer, with the Cu wire extremities made to stand vertical at opposite ends and then cured in an oven. Specifically, Ecoflex 00-30-part A, part B and NdFeB nanoparticles (MQFP-B-20076-088, Neo Magnequench) were blended thoroughly using a stirring rod. The weight ratio of Ecoflex 00-30-part A and part B was kept at 1:1 for all MC layers. NdFeB Nanomagnets with weight concentrations of 43%, 53%, 63%, 73% and 83% were used to fabricate different MC layers for optimizing the mechanical, magnetic and magnetomechanical properties of the soft system. For the characterization tests, varying amounts of MC layers were poured to yield different thickness MC layers (2, 4, 6, and 8 mm). All the mixtures were cured at 60 °C in an oven (ThermoFisher) for 3 hours, with the MI layer Cu wire extremities made to stand out of the solution. The non-magnetized soft system was magnetized by applying a magnetic pulse (~2.655 T) using an impulse magnetizer (IM-10-30, ASC Scientific) to import stable remnant magnetization.

This process could be done on cured MI-MC layers removed from the tissue culture well plate or on the totality of the tissue culture well plate using a larger impulse

magnetizer (Magnet-Physik, M-Series) and applying the same magnetic pulse (~2.655 T). PDMS layer preparation: A thin PDMS layer (mixing ratio of 20:1, ~1 mm, Dow SYLGARD™ 184, Ellesworth Adhesives) was used to confine the MI-MC layer, avoid possible leakage, seal the platform, and improve the surface's biocompatibility, with the Cu wire extremities made to stand out of the curing solution. ITO layer preparation:

A 1.1 mm thick flat-ITO film glass (10.1 Ohm/sq, Geomatec), previously plasma treated for 5 minutes (Plasma Prep II, 2SPI), was cut to a 25 mm diameter circle using a circular glass cutter compass, and placed atop the curing the PDMS layer, mid curing (1 hour into the total 2-hour curing process) at 60˚C in an oven (ThermoFisher). Finally the Cu wire extremities were cut to ~4 mm above the ITO glass, with the insulation removed by carefully cleaning the tips using a metal blade. The Cu wires were each bent atop the ITO glass and fixed in place using 3 mm-long pieces of 5 mm strong adhesive tape (Kaisiking). The finalized device was placed at 60˚C to finishing curing. A 3 mm diameter hole was drilled carefully at the bottom of each tissue culture well plate using an electric drill (DeWalt).

IV. 3D fabrication of the MEG electrical stimulation platform

Important factors which help assess likelihood of permeation of any new technology are its reproducibility and ability to fabricate at scale. To determine whether this was the case for the MEG ES platform, we tested out 3D printing capabilities, demonstrating rapid 3D printing directly *in situ* 6, 12, 24, 48 and 96 well plates. The fabrication of such a platform required less than a day of preparation (the only time limiting step being the MC and

PDMS layers curing) and was carried out using heated plates found incorporate in the 3D printer (**Figure 14**). More information is provided below.

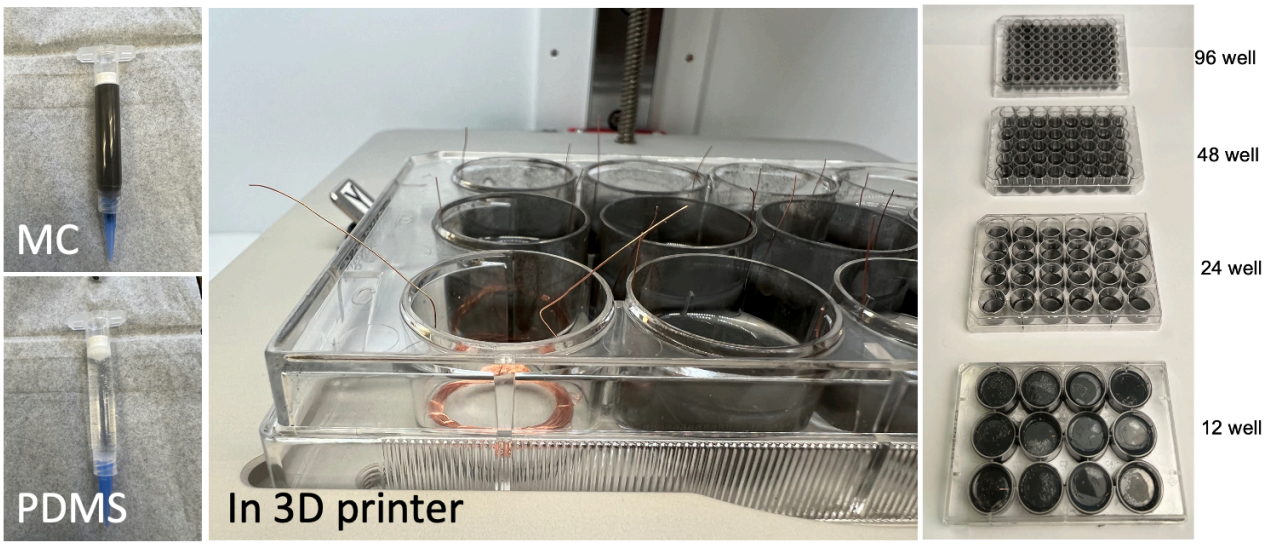

Figure 14: 3D printing capabilities of an MEG electrical stimulation platform. 3D printing capabilities of the MEG ES platform using a commercially available 3D printer. Simple MC and PDMS ink use and deposition using a 3D printer. 3D printed 12 well to 96 well plate MEG ES platforms, directly *in situ.*

In order to assess the above, a number of experiments were carried out. 3D printing of MEG ES platform: Certain aspects of the MEG ES platform could be automated. The fabrication of MC layer and PDMS layer was automated using a pneumatic extrusion-based 3D printer (BioX, Cellink, Gothenburg, Sweden) into each well of 6, 12, 24, 48 and 96 well tissue culture well plate (Falcon™ Polystyrene Nanoplates, ThermoFisher). A computer-assisted design (CAD) software (Fusion360, Autodesk) was used to create the 3D cylindrical model of 40 mm, 20 mm, 5 mm and 3 mm, respective to 12, 24, 48 and 96 well plates. Cylinder models were a constant of 6 mm in height to 3D print silicone-based ink in a concentric lattice structure. MC layer: After mixing an uncured EcoFlex with non-magnetized NdFeB nanoparticles, the mixture was degassed under vacuum for 20 min,

and carefully loaded into a 3D printer cartridge (3 ml cartridge, Cellink). 3D printer print bed was preheated to 65ºC, and the MC layer was printed at a rate of 10 mm/s with 15k Pa of air pressure, through 20 gauge tapered plastic nozzle. PDMS layer: After the printing of MC layer, well plates were left on the heated print bed at 65ºC for 30 min to allow MC layer to briefly cure. The PDMS layer (mixing ratio of 20:1, Dow SYLGARD™ 184, Ellesworth Adhesives) was then 3D printed with extrusion speed and pressure of 10mm/s and 10kPa, respectively, to form a 1.5 mm layer, to confine the MI-MC layer.

V. Evaluation of the MEG electrical stimulation platform

To evaluate the effectiveness and adaptability of an MEG ES platform, we set out to test a number of parameters and determine how the architecture of the various components of the platform itself affected current and voltage output (**Figure 15**). When the MC layer becomes deformed *via* air pressure, biomechanical-to-magnetoelastic energy conversion occurs, followed by concomitant magnetic induction in the MI layer, bringing about magnetic-to-electrical conversion, and a correlated electric output (**Figure 15a**). We began by assessing how varying the number of coils in the MI layer affected output performance, noticing a notable increase in both current and voltage output proportional to the increase in MI coil number (**Figure 15b**).

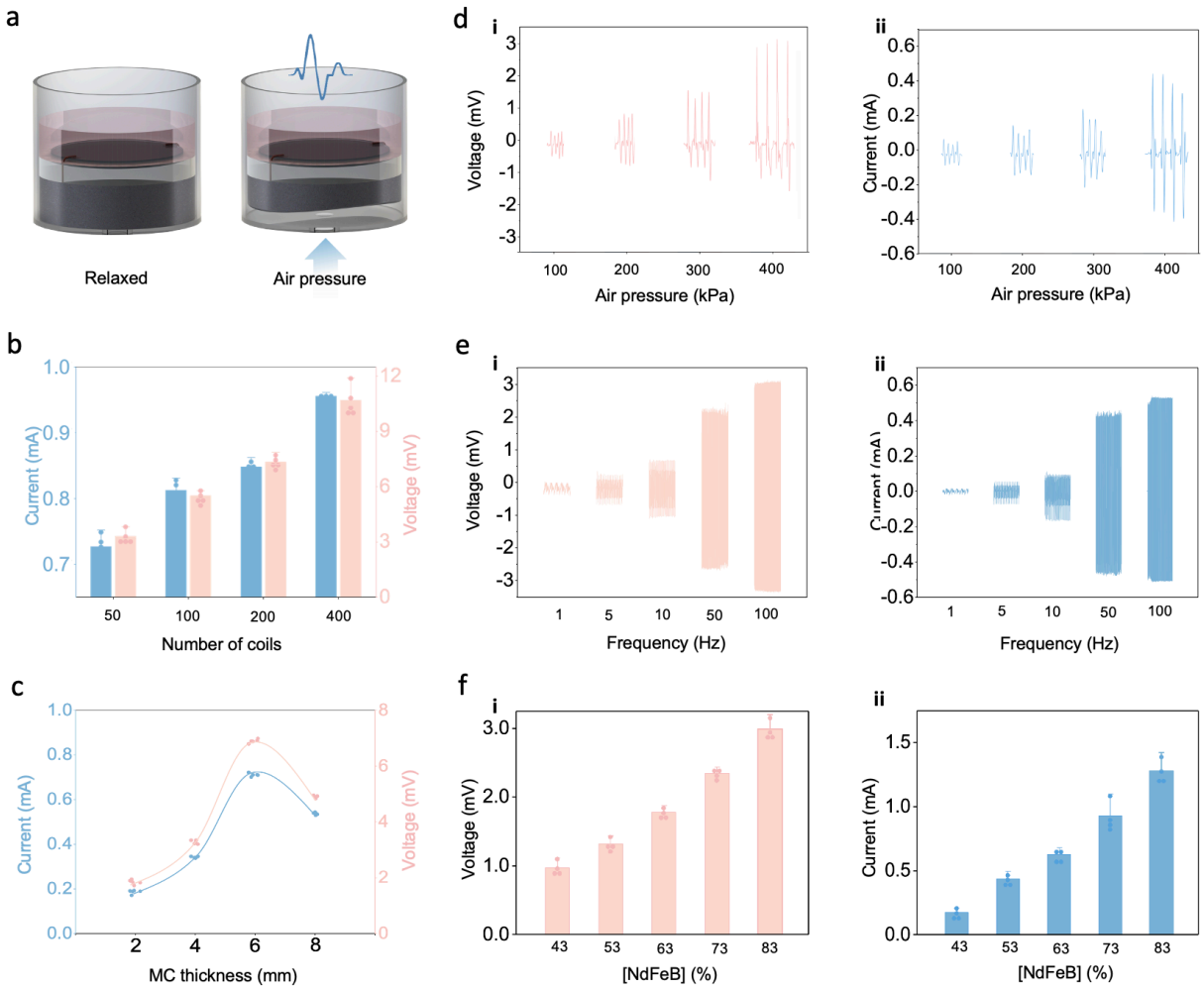

Figure 15. The MEG electrical stimulation platform's output can be tailored to required experimental conditions. (a) The working mechanism and principle of the MEG ES platform, reliant on air pressure-deformation and activation of the MI-MC layer to yield an electric output. (b) Output current and voltage of the MEG ES platform can be adjusted by varying the number of MI layer coils. Bar graphs show mean + standard deviation of the results (n=5). (c) MC-layer thickness is positively correlated to current and voltage output until thickness-induced hampering of the MI-MC layer compression. Curves indicate general trend and elastic limit. (d) Effect of air pressure intensity on (i) voltage and (ii) current output of the MEG ES platform. (e) The MEG ES platform enables the use of different frequency parameters to yield specific (i) voltage and (ii) current values. (f) (i) Voltage and (ii) current dependance on [NdFeB] concentration in the MC layer.

Subsequently, we tested the effects of modifying the MC layer. First, we altered the thickness of the MC layer, by pouring varying amounts of the uncured MC mixture into the well, thus obtaining MC layers of different thickness (2 mm, 4 mm, 6 mm, and 8 mm) (**Figure 15c**). Here, the results showed an increase in output with subsequent

peaking of voltage and current at 0.71 mA and 6.92 mV (6 mm), owed to the increased rigidity of the MC layer, and thus proportional decrease in magnetoelastic performance of the layer. Subsequently, we analyzed the effect on electric output brought about by varying the air pressure magnitude on the MEG ES platform, using the punctured holes on its bottom (**Figure 15d**). Considering frequency is one of the testing parameters explored in electrical stimulation, we assessed the voltage and current output performance by exposing the MEG ES platform to various stimulation frequencies. We observed an increase in electric output, peaking at 6.02 mV and 0.9 mA at 100 Hz stimulations. (**Figure 15e**). Finally we assessed how modifying the nanomagnet concentration (43%, 53%, 63%, 73% and 83%) of the MEG's MC layer, affected output, noticing a correlated increase in both current and voltage output (**Figure 15f**).

Modifying the MI layer was shown to be an easily implementable intervention to help modify and tune the MEG ES platform's desired output. However, the optimal MC weight concentration of NdFeB was shown to be 83%, yielding the most effective ratio in balancing elastomer plasticity and electricity generation, overall optimizing mechanical, magnetic, and magnetomechanical properties of the soft system upon air pressure stimulation. In line with maintaining apt magnetomechanical properties in the MEG ES platform's soft system, the most effective output thickness for the MC layer in a standard 6-well tissue culture sized MEG ES well plate, was shown to be 6 mm. Finally, much like for the MI layer, air pressure modification was also shown to be an easily implementable intervention to help modify and tune the MEG ES platform's desired output (**Figure 16**).

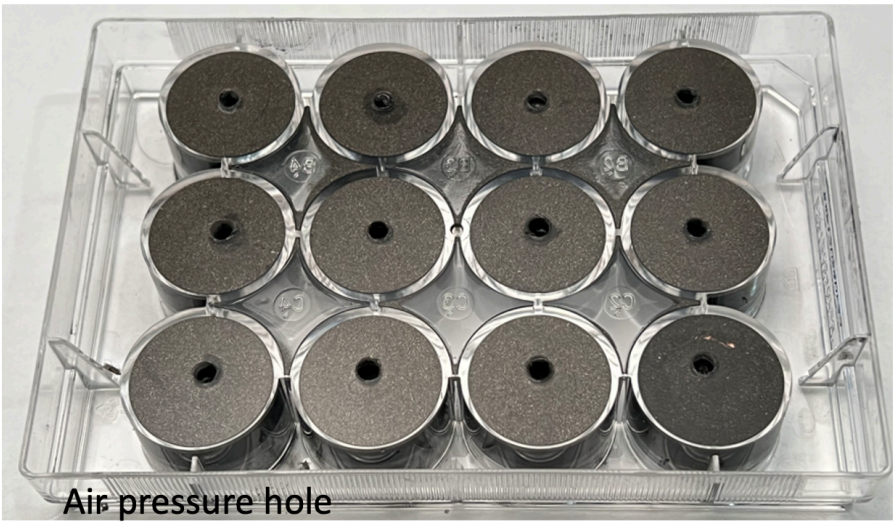

Figure 16. Perforation of the MEG electrical stimulation platform. Clear perforation on the bottom side of a 12-well tissue culture plate onto which the MEG ES platform was fabricated. Air pressure holes allow for MEG ES activation using simple air pressure actuation.

However, we noticed that for a standard 6-well tissue culture sized MEG ES well plate, the maximum air pressure prior to device failure and/or dislodgment from the well was 800 kPa (**Figure 17**). It seemed thus advisable to utilize lower air pressure values for MEG ES platform activation in order to help preserve its mechanical integrity, especially in long term ES protocols.

Tissue Culture Type	MI (coils)	MC thickness (mm)	PDMS thickness (mm)	ITO-glass thickness (mm)	Aperture for Air Pressure (mm)	Pressure MAX (kPa) *
6-well plate	150	6	15	1.1	3	**800**
12-well plate	75	5	15	1.1	3	**650**
24-well plate	35	4	15	1.1	25	**320**
48-well plate	20	3	15	1.1	15	**250**
96-well plate	10	2.5	15	1.1	15	**200**

Figure 17: Maximum air pressure tolerance. Varying air pressure limits for different MEG ES platforms. *Key values.

Various methodologies were implemented to bring about the afore MEG ES fabrication and testing. Performance of the MEG ES platform: For liquid retention testing, an MEG ES well plate, and a non-tissue culture well plate (Standard), were each filled with 5 ml DMEM media and left to rest at room temperature until day 14, with the liquid then collected from each sample and measured again. Sterilization protocol testing of the MEG electrical platform was carried out with pre- and post-testing, as follows: 30 min UV exposure resistance was tested using a biosafety cabinet fume hood UV-C germicidal lamp (LabGard ES Nu-540, Class II, NuAire), ethanol resistance was tested by filling each of the as-fabricated MEG well with 5ml of ethyl alcohol (HistoPrepTM 70% denatured, Fisherbrand), and leaving to soak for 1 week. Autoclaving resistance was tested by exposing a complete MEG ES platform to the autoclaving process (2840EL-D, Tuttnauer, glass setting, steam at 134˚C, 340 kPa). For performance cycling and frequency testing of the MEG, a pulse generator (comprising a coupled arbitrary function generator (Tektronix afg1062), linear power amplifier (Labworks, PA-138) and electrodynamic transducer (Labworks, ET-127)) was used at 25 Hz (for 10,000 seconds – 250,000 cycles) and varying (1, 5, 10, 50, 100 Hz) values, respectively. Voltage signals of the MEG ES platform were measured using a Stanford low-noise voltage preamplifier (SR560), whilst current signals were measured using a Stanford low-noise current preamplifier (SR570). For air pressure testing, an air pressure gauge (PSL15-160, PneumaticPlus) was connected to a compressed air outlet (UCLA Bioengineering line) and openings for 100, 200, 300 and 400 kPa outputs were devised for pulsed release.

VI. Conclusion

With this research we explored the first application and use on soft magnetoelastic effect for tissue engineering purposes, devising an electrical stimulating platform which is inexpensive, easy to fabricate, and which can be replicated at scale using 3D printing, and incorporated in existing research tools (tissue culture plates). We demonstrated a self-powering platform which could be adapted for both air pressure as well as mechanical activation. To our knowledge, this is the first time a self-powered ES platform could be directly integrated and built within existing tissue culture research tools, providing a biocompatible, bioconformable soft system which could be used for *in vitro* electric stimulation. We further demonstrated easy adaptability of the platform to yield specific current and voltage outputs, as required per and during experimental protocols, and demonstrated easy integration in sterilization and sanitization processes, without losing functionality despite exposure to UV irradiation, ethanol soaking, and even autoclaving.

3D printing of the platform was also shown to be a possibility. Since the thickness of MC layer is proportionate to electricity generation, controlling the consistency in thickness within all wells of the same plate is an important factor. Automating the process with a 3D printer allowed precise control of layer height in every plate, so as to allow for the air pressure stimulus to induce equal current output in all wells, increasing the consistency and repeatability of cell experiments. 3D printing also allowed us to save a recipe of the printing set up, meaning the platform could be consistently re-fabricated, drastically increasing throughput. Manufacturing the device in a 3D printer can also help with sterility, reduce contamination likelihood, and allow direct cell seeding within the printing chamber, which is UV-sterilized and equipped with HEPA filtered laminar air flow. Furthermore, the

use of conductive carbohydrate glasses, which can print like thermoplastic, means that conductive ITO glass-like coverslips could also be printed *in situ*, allowing a one-stop fabrication approach.

Overall, the nifty integration of ITO glass enables for samples to be analyzed using immunofluorescent staining without disrupting standard analytical processes broadly implemented across the research community. Considering the above, and in view of the potential of MEG-based platforms, this study was carried out also to bridge the development and journey towards its *in vivo* validation and application. We look forward to this platform and technology being applied to more research avenues and regenerative medicine applications, including co-stimulation such as mechanoelectrical stimulation, useful in the upkeep of transdifferentiated somatic cell types such as induced neurons, which we will explore in the next chapter.

CHAPTER 3

MAGNETOELASTIC GENERATOR BASED NEURONAL CELL PROGRAMMING

Soft bioelectronics have been employed in a number of cellular reprogramming protocols, though a number of shortcomings including, lack of biocompatibility and limited working capabilities under wetted conditions have hampered their applicative use in a large number of fields. With previous work we have demonstrated how magnetoelastic generators could *de facto* be built and incorporated directly into readily available tissue culture well plates and we set out to test its capabilities in *in vitro* transdifferentiation, and specifically by focusing on fibroblast into neuron transdifferentiation. This application was chosen as neurons represent a somatic cell type whose use is highly significant in the study and treatment of neuronal disorders, and for which the use of electrical stimulation is a known modulator[1]. We assessed the platform's efficacy in promoting fibroblast transdifferentiation into neurons (+104%), and enhancing neuron maturation (+251%), providing an easily devisable and scalable electrical stimulation device for research, and paving the way for future permeation of magnetoelastic generator-based implantable devices. Furthermore, we provide suggestions for future exploration of this platform.

I. Introduction

Electrical stimulation (ES) platforms have been widely used in a plethora of biotech and clinical experimental applications. To allow for their progression from the bench to the bedside, platform technologies need to be first assessed and characterized in laboratory

settings. To help pave this platform technology's development, and actively bridge this gap, we applied the MEG ES platform to assess its effect on the direct conversion of fibroblast into induced neurons.

The direct transdifferentiation of fibroblasts into neurons represents an effective way to obtain neuronal cells to use in fundamental, as well as applied clinical research. These studies have traditionally seen the use of *ex vivo* neuronal cultures, which present a number of drawbacks including sample sourcing, poor experimental design and issues demonstrating statistical significance[152]. Furthermore, *ex vivo* neuronal cultures' application in drug screening remains limited considering the inability to scale[153]. Besides this, although direct somatic transdifferentiation from fibroblasts to induced neurons exists, efficiency still remains low[154].

ES has been shown to help with somatic cell transdifferentiation, including promoting neuron induction, though for these experiments, reliance has focused on externally powered devices[120]. In the few instances where self-powered devices were used, these were always decoupled from the experimental set up, and presented the core problems described in our introduction. The introduction of a stand-alone, easily fabricated, and self-powered MEG ES platform was therefore put forward to help provide a versatile platform for simple electrical research at scale, demonstrated in an extremely relevant applicative scenario.

II. MEG electrical stimulation and neuron transdifferentiation efficiency

We set out to assess the biological effect of MEG ES on virally transduced fibroblasts[155] with and without exposure to MEG ES (**Figure 18**). Given the heterogeneity of ES

parameters used in previous studies for fibroblast transdifferentiation into induced neurons, we first assessed ES tolerance range for adult mouse ear fibroblasts employed in our protocol (**Figure 18**), and exposed the cells to nA, µA and mA range currents for varying intervals, determining a suitable, non-toxic values in the nA range, with maximum exposure in the 30min range, and 1Hz impulse frequency.

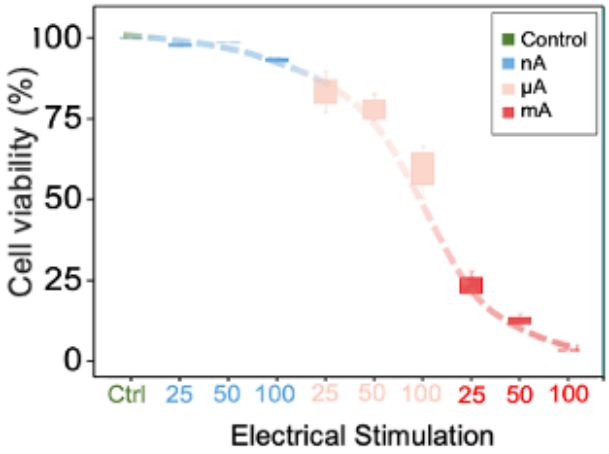

Figure 18. The MEG electrical stimulation platform enhances efficiency and maturation of fibroblast transdifferentiation to induced neurons. (a) Cell viability as a function of varying current MEG ES values, in the nano, micro, and milli Ampere ranges. Bar graph shows mean ± SD (n=5).

In order to carry out the MEG ES viability assays: Fibroblasts were plated and allowed to attach overnight. The following day, cells were treated to nA (25, 50, 100 nA), µA (25, 50, 100 µA), and mA (25, 50, 100 mA) values for 30 min, at 1 Hz frequency, using an alternative MEG ES platform (**Figure 13**). The modified MEG platform yielded 2 mA current, with its output adjusted to the testing regime using an Ohm resistance box (Resistance Decade Box 380400, Extech Instruments). Cells were left to grow for 24 hours, after which cell viability was assayed using PrestoBlue Cell Viability Reagent (Invitrogen, A13261) according to the manufacturer's protocol. Cells were incubated with the PrestoBlue Reagent for 2 hours. Results were normalized to control (i.e., no

stimulation) samples. The 1 mA value test was subsequently repeated whilst being visualized in time lapse under a Zeiss Axio Observer Z1 inverted fluorescence microscope, with images being taken every minute, for 30 minutes, to show cell detachment and subsequent death, corroborating the PrestoBlue reagent results.

Subsequently, we set out to carry out various MEG ES protocols during the transdifferentiation process (**Figure 19**).

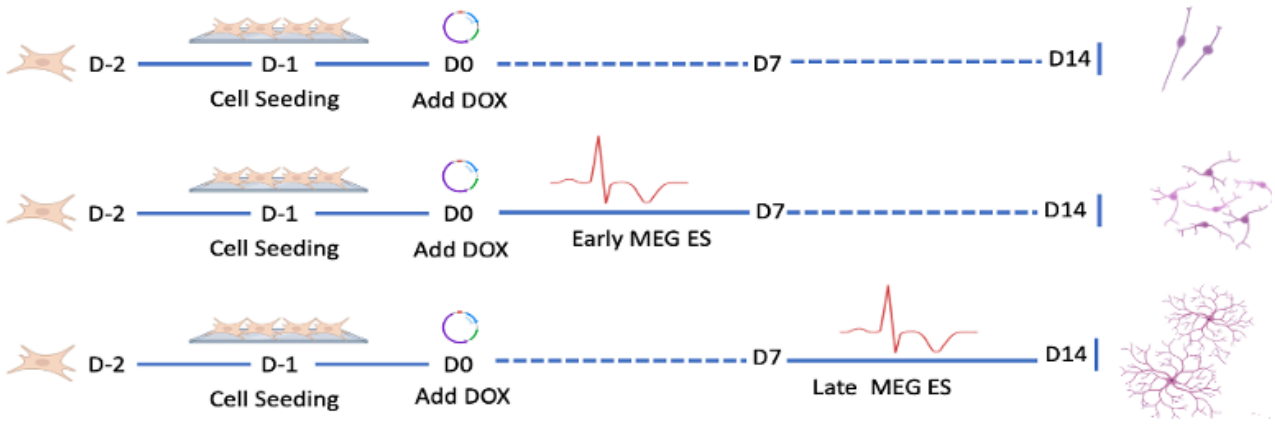

Figure 19. MEG electrical stimulation protocols. Schematic representation of the various protocols implemented to assess MEG electrical stimulation's effect on transdifferentiation. D = day, ES = electrical stimulation, Dox = doxycycline. Yielded neuron relative morphology and number, schematically shown.

Using a 6-well plate MEG ES platform fabricated in the forestated fashion, we first gelatin-coated the plasma treated ITO glass, and subsequently seeded adult mouse ear fibroblasts transduced with doxycycline (Dox)-inducible lentiviral vectors, containing the three reprogramming factors Brn2, Ascl1, and Mytl1 (BAM). The following day Dox was added (marked as day 0) to induce BAM expression and begin the transdifferentiation process, with cells being cultured in serum-free N2B27 medium for the remainder of the experiment. We devised MEG ES platforms to output 50 nA – confirmed using a low-noise current preamplifier – and first examined the effect of MEG ES on

transdifferentiation efficiency, which we defined as the percentage of neuronal beta-tubulin III (Tubb3+) induced neurons at day 14. To do so, we pulsed the transduced fibroblasts with 1 Hz frequency, 50 nA current ES for 1 min and 5 min, respectively, at 48-hour intervals, for a duration of 7 days, starting day 1, and left cultures to grow until day 14 (**Figure 19**). The experiment revealed a 104% increase in transdifferentiation efficiency (number of Tubb3+ cells) with 1 min stimulation (2.77% to 5.64%) and a 46% increase in transdifferentiation efficiency (number of Tubb3+ cells) with 5 min stimulation (2.77 % to 4.05%) (**Figure 20**), reinforcing the idea that early-stage MEG ES platform helps increase neuron yield. From a quantitative perspective, very statistically significant differences were noted in the transdifferentiation efficiency of early-stage electrically stimulated samples, versus control. Furthermore, the results seem to indicate that the duration of ES was important in enhancing direct conversion in early-stage stimulations, but not in late-stage ES (**Figure 20**) a factor likely ascribed to the key timing in activation of transcription factors involved in the transdifferentiation process.

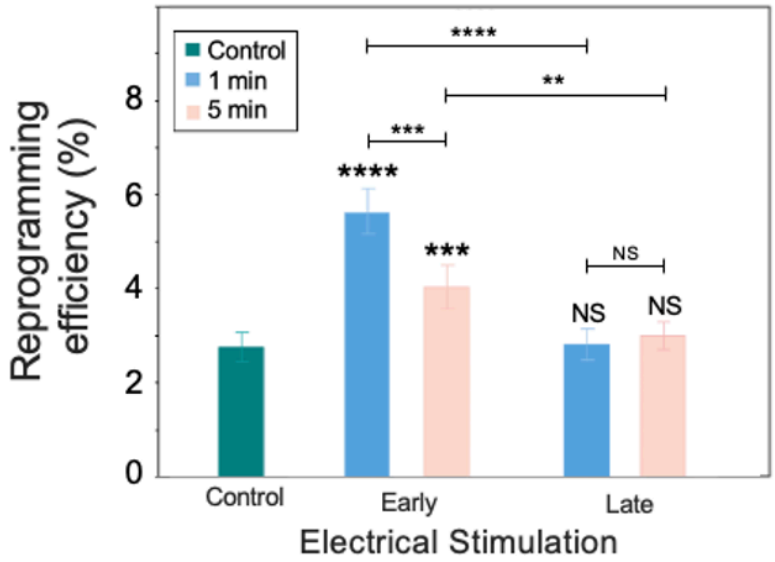

Figure 20. Effect of MEG electrical stimulation on transdifferentiation. Transdifferentiation efficiency of fibroblast transdifferentiation into induced neurons in varying ES protocols (based on

Tubulin Beta 3 Class III+ (Tubb3+) cells on day 14 relative to the number of fibroblast cells initially seeded), Bar graph shows mean ± SD (n=5), **p ≤ 0.01, ***p ≤0.001 **** p≤0.0001, NS = not significant. Significance was determined by a one-way ANOVA and Tukey's multiple comparison test.

III. MEG electrical stimulation boosts maturation and neuritic ramification

Secondly, we examined the effect of MEG ES on neuronal maturation, characterized using immunocytochemical staining and analysis. To understand whether MEG ES had any maturation effect when applied during later stage transdifferentiation (on already formed induced neurons), we performed 1 min and 5 min, 50 nA 1 Hz MEG electrical stimulation, with 48-hour intervals, on samples from day 8 to day 14 of the protocol (**Figure 19**). While the samples did not show an increase in transdifferentiation efficiency into induced neurons, we observed a marked increase in Tubb3+ cells expressing neuronal maturity markers Synapsin, and microtubule associated protein 2 (MAP2). Specifically, samples which had undergone late-stage MEG ES in the form of 5 min stimulations, showed a 218% increase (from 22.5% to 71.5%) in Tubb3+/Synapsin+ neurons (**Figure 21 – left**), and a 251% increase (from 20.5% to 72%) in Tubb3+/MAP2+ neurons, when compared to the control (**Figure 21 – right**).

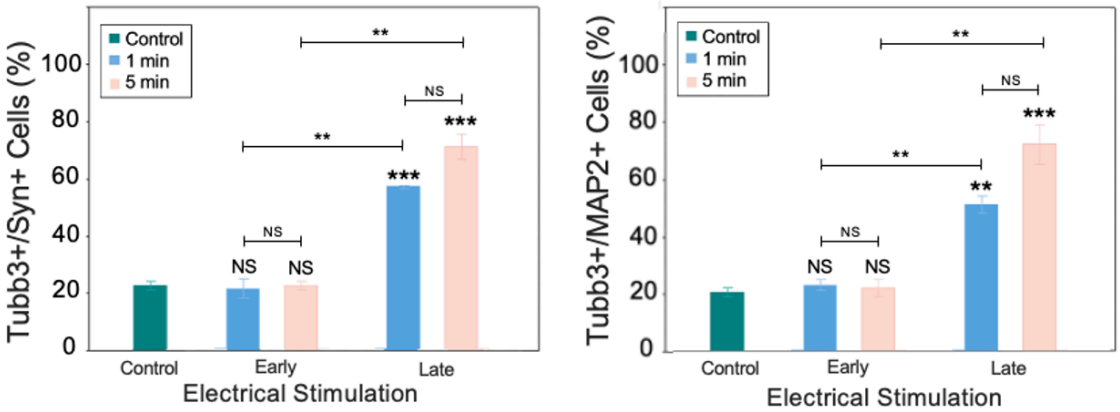

Figure 21. Effect of MEG electrical stimulation effect on neuronal maturation. (Left) Quantification of mature neurons (based on Tubb3+ and Synapsin+ cells on day 14 relative to the number of Tubb3+ cells). Bar graph shows mean ± SD (n=2), **p ≤ 0.01, ***p ≤0.001, NS = not significant. Significance was determined by a one-way ANOVA and Tukey's multiple comparison test.

(**Right**) Quantification of mature neurons (based on Tubb3+ and microtubule associated protein 2 (MAP2+) cells on day 14 relative to the number of Tubb3+ cells). Bar graph shows mean ± SD (n=2), **p ≤ 0.01, ***p ≤0.001, NS = not significant. Significance was determined by a one-way ANOVA and Tukey's multiple comparison test.

Lower MEG ES duration of 1 min, showed a more modest, yet significant increase of 156% (from 22.5% to 57.5%), and 173% (from 20.5% to 56%) in Tubb3+/Synapsin+ and Tubb3+/MAP2+ neurons, respectively, when compared to the control.

For the fibroblast isolation, culturing and reprogramming, lentiviral production and transduction: Dox-inducible lentiviral vectors for Tet-O-FUW-Brn2, Tet-O-FUW-Ascl1, Tet-O-FUW-Myt1l, and FUW-rtTA plasmids were used to transduce fibroblasts for ectopic expression of Brn2, Ascl1, Myt1L, and rtTA (Dox-binding inducible promoter). Lentivirus was produced by using established calcium phosphate transfection methods, and Lenti-X Concentrator (Clontech, 631 232) was utilized to concentrate viral particles according to the manufacturer's protocol. Stable virus was aliquoted and stored at −80 °C. Fibroblasts were incubated with the virus for 24 hours before being seeded onto gelatin-coated ITO glass.

Fibroblast isolation, culture and transdifferentiation: Fibroblasts were isolated from ear tissue of one-month old adult C57BL/6, and expanded using fibroblast medium: DMEM (Gibco, 11965), 10% fetal bovine serum (FBS; Gibco 26140079), and 1% penicillin/streptomycin (GIBCO, 15140122). For all experiments, passage-2 cells were used. Fibroblasts were transduced with lentivirus-containing BAM constructs and the following day seeded onto ITO glass (10.1 Ohm/sq, Geometec) coated with 0.1 mg mL−1 gelatin (30 mins) at a density of 7000 cells per glass slide, with the ITO glass having previously been plasma treated for 5 min (Plasma Prep II, 2SPI). The following day (i.e.,

day 0), the medium was replaced with MEF medium containing Dox (2 ng mL−1, Sigma) to initiate the expression of the transgenes and thus, transdifferentiation. Twenty-four hours later (i.e., day 1), cells were cultured in N2B27 medium: DMEM/F12 (Gibco, 11 320 033), N-2 supplement (Gibco, 17 502 048), B-27 supplement (Gibco, 17 504 044), 1% penicillin/streptomycin, and Dox (2ngmL−1), and half medium changes were performed every 2 days. MEG electrical stimulation: For the early-stage MEG ES study, using an ad hoc MEG ES platform yielding 50 nA, we pulsed the transduced fibroblasts with 1 Hz frequency, 50 nA current ES for 1 min and 5 min, at 48-hour intervals, for a duration of 7 days, starting day 1, and left cultures to grow until day 14. For the late-stage MEG ES study stage, we pulsed the transduced fibroblasts with 1 Hz frequency, 50 nA current ES for 1 min and 5 min, at 48-hour intervals, for a duration of 7 days, starting day 8 until day 14. On day 14, cells were fixed and stained for Tubb3 to determine the transdifferentiation efficiency, whilst other samples were also stained for Synapsin and MAP2 to determine maturation stage. Induced neuronal cells were identified based on positive Tubb3 staining and neuronal morphology (defined as Tubb3+/DAPI+, with the presence of at least two or more neurites filopodia-like protrusions which exceeded the diameter of the cell body). The transdifferentiation efficiency was determined as the percentage of Tubb3+ cells on day 14 relative to the number of the fibroblast cells initially seeded at 24 hours.

With regards to the results, samples which had been electrically stimulated only in the early stage of the transdifferentiation process (day 1- day 7), did not show a higher percentage of mature neuronal markers when compared to the control, corroborating evidence from previous studies that electrical stimulation's influence on transdifferentiation and maturity is distinct, depending on when it is applied[156–158].

Interestingly, though late-stage ES enhances maturation of neurons, its duration seemed to be less important in determining degree of neuronal maturation (**Figure 21**). This could likely be ascribed to somatic / neuronal maturation being a less time-sensitive process than that of transdifferentiation of transcription factors involved in the transdifferentiation process.

One further important difference which became apparent when visualizing induced neurons which had been exposed to late-stage MEG ES under fluorescent microscopy was the stark difference in interconnectivity between control samples and those that had undergone ES and those who did not. Induced neurons observed in control samples showed less articulate morphologies, with far fewer and far less intrinsic neuritic ramifications, unlike for those encountered in electrically stimulated samples (**Figure 22**).

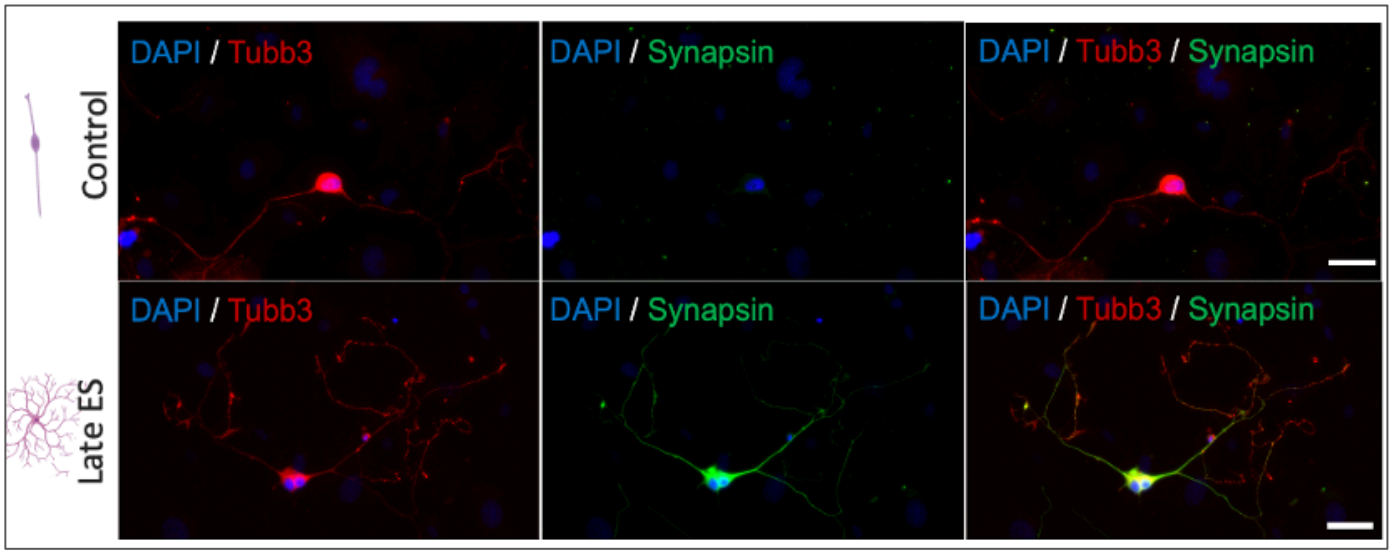

Figure 22. Visual effect of MEG electrical stimulation on mature neurons, with Synapsin staining. Immunofluorescent images showing induced neurons without and with late MEG ES, on Day 14, and stained with mature neuronal marker Synapsin, highlight neurite abundance and ramification. Yielded neuron relative morphology and number, schematically shown. Scale bar = 50 μm.

Clustering of induced neurons was also much more pronounced in electrically stimulated samples (**Figure 23**), with highly inter-networked neuronal systems comprising as many as tens of Tubb3+/Synapsin+ and Tubb3+/MAP2+ neurons, all interconnected.

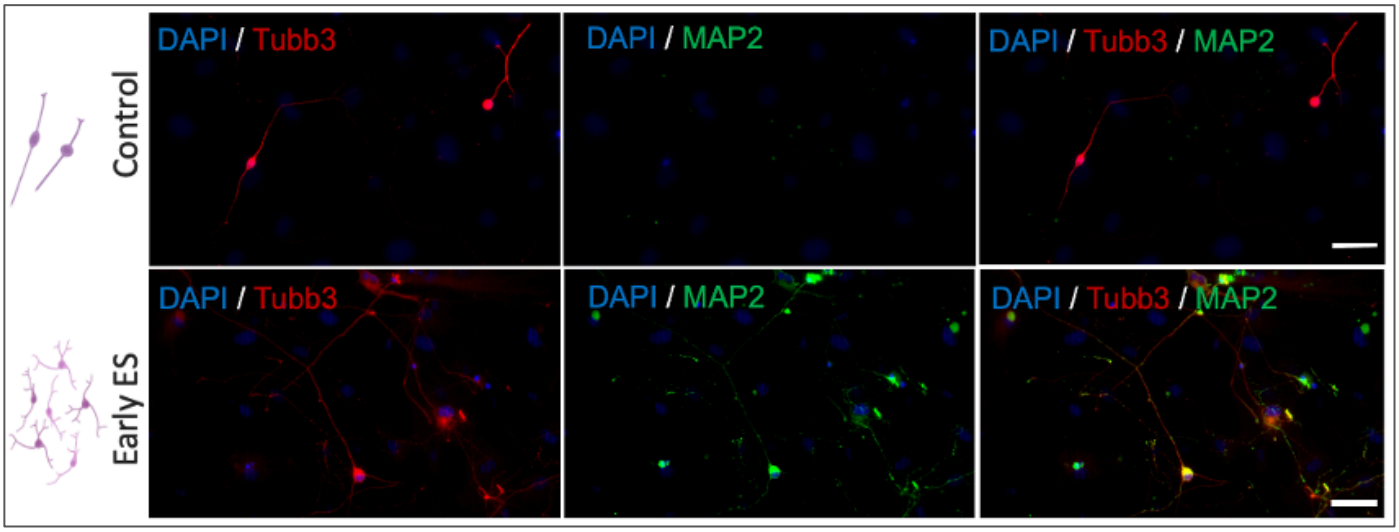

Figure 23. Visual effect of MEG electrical stimulation on mature neurons, with MAP2 staining. (g) Immunofluorescent images showing induced neurons without and with early MEG ES, on Day 14, and stained with mature neuronal marker microtubule associated protein 2 (MAP2) highlight increased efficiency with promoted induced neuron density and interconnection. Yielded neuron relative morphology and number, schematically shown. Scale bar = 75 μm.

In order to achieve the desired Immunofluorescent staining and characterization of neurons and mature neurons: All samples collected for immunofluorescence staining at the indicated time points were washed once with PBS and fixed in 4% paraformaldehyde for 10 min. Samples were then washed three times with PBS for 5 min each and permeabilized using 0.5% Triton X-100 for 10 min. The ITO glass with fixed cells were dismounted from the MEG ES platform and, after three subsequent PBS washes, blocked with 5% normal donkey serum (NDS; Jackson Immunoresearch, 017000121) in PBS for 1 hour. Samples were incubated with primary antibodies (Tubb3; 1:1000, Biolegend #802001, MAP2; 1:300, Biolegend #801801, Synapsin; 1:400, Abcam #ab254349) in

antibody dilution buffer (5% NDS in PBS) overnight at 4 °C followed by three PBS washes and a 1-hour incubation with Alexa Fluor 488- and/or Alexa Fluor 546-conjugated secondary antibodies (Molecular Probes). Nuclei were stained with DAPI (1:1000, Molecular Probes, Eugene, OR) in PBS for 10 min. For F-actin staining, cytoskeletons were stained using Phalloidin (1:200, Phalloidin-iFluor™ 514 Conjugate, AAT Bioquest). Epifluorescence images were collected using a Zeiss Axio Observer Z1 inverted fluorescence microscope and analyzed using ImageJ. Induced neurons were confirmed as such by nucleic DAPI+ and cellular Tubb3+ staining association, as well as the presence of at least two or more neurites (filopodia-like protrusions which exceeded the diameter of the cell body), mature neurons were confirmed as such by DAPI+/Tubb3+/Synapsin+ and DAPI+/Tubb3+/MAP2+ staining association.

To assess overall data relevance we performed statistical analysis of cell-based experiments: All data were presented as mean ± one standard deviation (SD). Comparisons among values for groups were performed using a one-way analysis of variance (ANOVA) followed by a Tukey's post-hoc test. For all cases, significance level α = 0.05 was set with a 95% confidence to detect a significant difference, and p-values less than 0.05 were considered statistically significant. GraphPad Prism 8.0.2 software was used for all statistical evaluations. For cell viability assay, n=5, where all experimental groups were compared with (normalized by) untreated control.

IV. Conclusion

We applied the MEG ES platform in a highly relevant tissue engineering practice, highlighting how, when used in concomitance with viral delivery of delivery of genes

encoding neuronal BAM transcription factors, the use of our platform could help increase transdifferentiation efficiency up to 104%, when compared gene delivery alone, and enhance the presence of mature neurons up to 251%, when again compared to gene delivery alone. Furthermore, the MEG ES platform demonstrated capabilities to help form well-developed neurite networks and intraneuronal connectivity. These results corroborate previous studies which highlighted a role for ES in promoting both transdifferentiation efficiency[1], and neuronal maturation[158]. Mechanistically, although not fully understood, it is thought that ES activates N-type Ca^{2+}channels during the early stages of transdifferentiation, inducing neuronal gene expression induction, and thus improving conversion efficiency. Similarly, on induced neurons, ES is thought to lead to an increase in Ca^{2+} mobility, and indirect protein kinase C activation, in turn promoting the phosphorylation of extracellular signal-regulated kinase 1/2 (ERK1/2). This latter cascade is fundamental in cellular differentiation and its increased activation has been linked to neurite growth[156]. Interestingly, in preliminary studies, we observed that when MEG ES was applied continuously to samples (from day 1 to day 18), there was an overall detrimental effect on cell sample survival, indicating that excessive frequency of ES was counterproductive. Similarly, excessively high MEG ES protocols lead to cellular detachment from the ITO glass surface and subsequent metabolic death. The above study reinforced the idea and use of an MEG ES platform for *in vitro* use, as exemplified by its application in promoting transdifferentiation efficiency of fibroblast to induced neuron protocols, in addition to inducing a more mature neuronal phenotype when compared to samples which did not receive MEG electrical stimulation. Considering the above, and in view of the potential of MEG-based platforms, this study was carried out

also to bridge the development and journey towards its *in vivo* validation and application. We look forward to this platform and technology being applied to more research avenues and regenerative medicine applications, including co-stimulation (such as mechanoelectrical stimulation), highly valuable for the maintenance and functionality of transdifferentiated somatic cell types such as induced cardiomyocytes.

CHAPTER 4

ULTRASOUND COMPUTATIONAL PRELIMINARY STUDY FOR FUTURE CELL PROGRAMMING

The efficient conversion of ultrasound into electrical energy remains a highly desirable wireless powering solution, with potentially profound ramifications in energy transfer across virtually all industrial fields, especially for implantable medical devices. Triboelectric nanogenerators have been shown to effectively carry out ultrasound energy transduction, though efficiency remains poor. Here, we devise a computational model to investigate the optimal triboelectric nanogenerator irradiation conditions, including frequency, probe distance, size, and design, as represented by irradiated triboelectric surface area displacement. Our investigation may set the foundations for the establishment of a standardized protocol for efficient ultrasound mechanical energy harvesting. This holds considerable significance and could be paramount in designing an ever-growing number of applicative solutions in wireless energy transfer, providing a scalable, cost effective and time saving solution in the development of implantable medical devices[159].

I. Introduction

Triboelectric nanogenerators (TENGs)[39,160–163], have emerged favorably as next generation implantable medical devices (IMDs) driven by their self-powering, microscaled, and morphologically fitting flexible nature[1,164–166]. Their application in human health, moreover, has been growing in view of the many biocompatible,

biodegradable and drug-wetted biomaterials available for their manufacture, and considering TENGs' extensive validation in biosensing[167,168], therapeutics[169,170], and third-party device powering applications[171,172]. Recently, pioneering work has further opened novel research avenues by demonstrating wireless activation of TENGs using ultrasound waves[173–175], de facto opening a novel field of TENG research focused around implantable ultrasound-activated (IUA) TENGs. Given ultrasound's capabilities to penetrate human tissue with minimal side effects[176], there has been a surge in attempts to use and harness ultrasound as a power source, both for IMDs[177], as well as for direct interventional therapy[178,179].

To date however, poor energy conversion efficiency and the presence of bulky transducers have slowed the development of effective ultrasound powered IMDs[180]. IUA-TENGs have now seemingly provided an effective wireless energy transfer platform with which to intervene transdermally and bridge that developmental gap.

The clinical significance of IUA-TENG use is considerable. IUA- TENGs have the potential to provide an interventional platform for direct, ad hoc, regenerative medicine and tissue engineering solutions in a myriad of clinical applications (**Figure 24**).

Their simple use is now set to enable immediate ultrasound-to-electricity energy conversion via means of an easily administered ultrasound irradiation. Considering previous experimental validation, IUA-TENGs have the potential to help deliver therapeutic drugs or electrical stimulation, or be used to activate and power implanted third party devices[111,181]. Specifically, pharmacological interventions such as drug-load release[182], and enhancement of regenerative process (**Figure 24a**) including those occurring in wound healing[183], cellular reprogramming and transdifferentiation[120], have

all been demonstrated using TENGs, and could thus benefit greatly from this novel research avenue. Alongside the scientific rationale, the need for a novel class of next-generation powered devices is warranted by IMDs' $100 billion market's 7.1% compound annual growth rate, as well as the desire to push IMDs into novel therapeutic avenues[184].

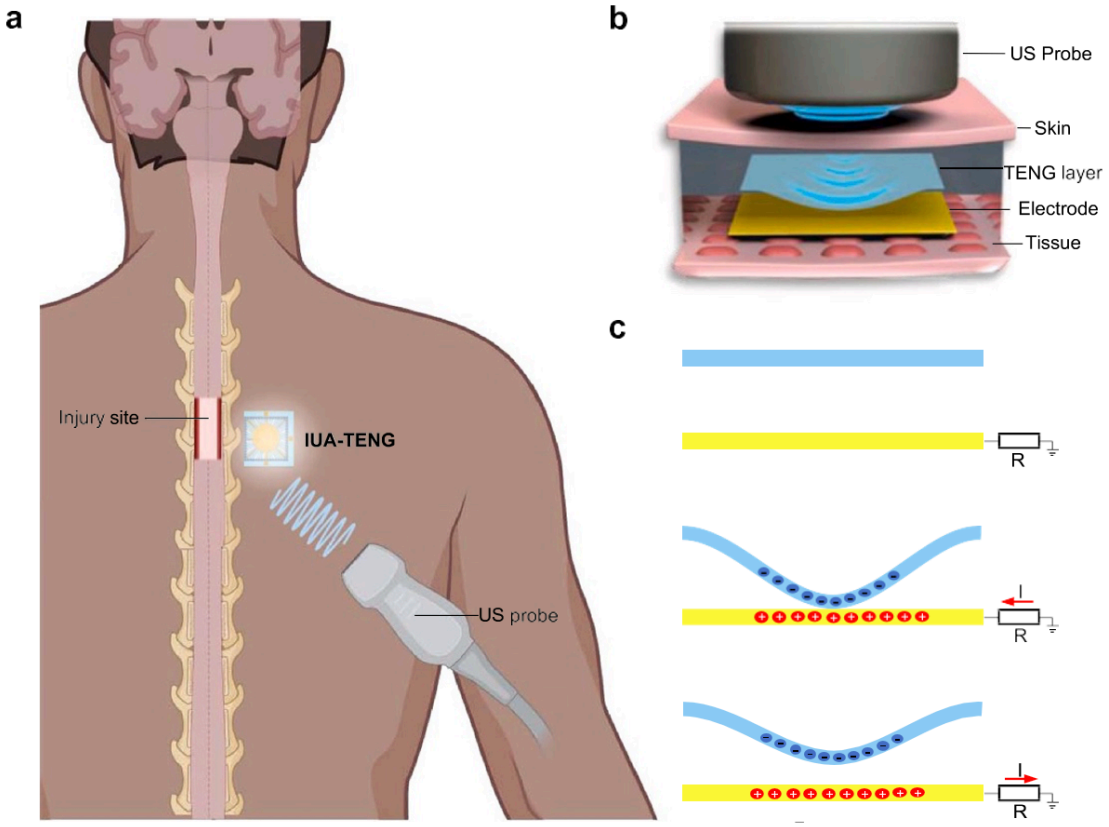

Figure 24. Schematic representation of an implantable ultrasound activated TENG. (a) Ultrasound probe irradiating the implanted TENG to help in neuroregeneration processes, such as spinal cord injury healing. (b) Illustration of up-close ultrasound activation of the TENG. (c) Representation of mechanical ultrasound wave conversion to electricity *via* the TENG single electrode working mode. The triboelectric layer (in blue) oscillates vertically as it is hit by ultrasound waves, leading to the contact electrification of the electrode layer below (yellow), discharging a current (I) cyclically. Circuitry equivalence is shown next to the representation, where R is resistance, and the red arrow represents current direction[159].

Indeed, developing energy transmitting solutions to help provide cost-effective, safe and non-invasive alternatives to legacy battery approaches is a key component to achieve this goal. IUA-TENGs could not only enable the improvement of existing powered

devices – which require periodical battery replacement, can leak toxic chemicals within the body, and present user wearability comfort issues – but can also help provide energy sources with which IMDs can connect into the growing healthcare Internet of Medical Things (IoMT) ecosystems. Much like next generation wearables, interconnectability of IMDs to existing healthcare infrastructure can bring about continuous device and patient health monitoring and highlight eventual functionality issues with the IMDs themselves. Enabling such energy-consuming operations however warrants microscaled IMDs which rely on novel powering solutions.

Despite the aforementioned potential, ultrasound-to-electricity conversion efficiency remains limited, and novel IUA-TENG design approaches are needed to provide the groundwork for this field and enable transition to industry and the clinic. In order to optimize the efficiency of IUA-TENGs, there lies the need for theoretical guidance in improving transducing efficiency of IUA-TENGs and improve energy conversion output. Such insight could be applied to developing high efficiency IUA- TENGs, which can be readily optimized and validated *in silico*, prior to implementing time consuming and costly manufacturing protocols. Moreover it could also help leverage the use of artificial intelligence for evermore optimized triboelectric structures and designs, and overall IUA-TENG IMDs.

II. Theoretical background

TENGs produce electricity by leveraging on their innate working mechanism of contact electrification and electrostatic induction, directly converting mechanical energy into electricity[185–187], with their triboelectric layer in effect able to function as a transducer of

mechanical energy[188,189]. Long-standing experimental studies have demonstrated that the efficiency of a TENG is dependent on the materials employed, working mechanism used, presence of impurities, and reduction of charge loss[190]. Once those physical TENG parameters have been determined however, on a theoretical front, a TENG's electrical output maximum is directly proportional to its ability to induce the largest possible charge in its electrode, through a triboelectric (from the Greek "tribos" or rubbing) effect. Indeed, TENG's innate ability to convert mechanical energy into electricity reaches theoretical peak with a complete displacement, and involvement, of the triboelectric layer. Ultrasound waves, acting as a form of mechanical energy, can bring about the micro displacement of TENGs' triboelectric layer, *via* the formation of nodes and antinodes on the material's surface in a free vibration mode, helping to wirelessly induce a triboelectric layer displacement and resulting electron movement.

The energy flow of ultrasound waves, their passage through a dense (transdermal equivalent) medium, their resonance interaction with the triboelectric layer, and their subsequent induced generation of a charge on the TENG, are processes which need to be optimized to ensure maximum energy conversion efficiency. In order to maximize the vibrational induction of the triboelectric layer using the ultrasound irradiation as a physical inductor, acoustic resonance of the layer itself must be achieved. Such an outcome is not only dependent on ultrasound source frequency, but also on its source (probe) size, distance from the targeted triboelectric layer, and positioning with its regard. In the specific, the mathematical relationship between the voltage generated by the ultrasound irradiation of the triboelectric layer can be described[178] as:

$$\Delta V = \frac{\sigma . d(t)}{\varepsilon}$$

Where ΔV is the voltage generated by the triboelectric layer, σ is the triboelectric charge density, *d(t)* is the displacement between the triboelectric layer and the electrode, and ε is the permittivity. Indeed, in electric stimulation, the high voltage, low current output, innate to TENGs, render their power output optimal for applications in human health. To enhance our understanding of this, we set out to model ultrasound interaction with a TENG's triboelectric layer, leveraging on computational and theoretical modelling to accrue a theoretical understanding of the relationship between ultrasound wave and acoustic TENG layer output (**Figure 24b**). The theoretical reasoning stands that triboelectric layer displacement, of any type, whether mechanical or acoustic, will yield the same discharge, assuming the area size and displacement gradient are large enough.

III. Simulation rationale and mechanism

Using COMSOL Multiphysic® as the simulation software, we aimed to investigate the optimized irradiation parameters of the IUA-TENGs. Our goal was to ultimately help with the functional development of IUA-TENGs and delineate a theoretical and *in silico* guideline to help optimize the IUA-TENGs design prior to fabrication, overall providing IMD-suited and structurally lean solutions. Since their invention, TENGs have been engineered to operate in four optimized (and now standardized) working modes: vertical contact mode, single-electrode mode, lateral sliding mode, and freestanding triboelectric layer mode. In our study, we opted for a single-electrode mode simulation (**Figure 24c**).

Of the four TENG working modes, the single-electrode mode presents the most miniaturized mechanistic approach when harnessing the triboelectric effect, a great asset when devising minimally invasive IMDs. Moreover, given the absence of a second dielectric material within the TENG (unlike in the remaining three working modes), the surface charge of the triboelectric layer employed in a single-electrode mode can be maximized, avoiding charge backflow exiting to the other dielectric layer. Considering the clinical size implications and the paramount importance of surface charge density linked to an increased triboelectric output, we thus found the single-electrode mode TENG to be the most compelling simulation candidate. Indeed, although such a modality yields a decreased output performance compared to its sibling working modes, it enables considerable miniaturization of a fully functional IUA-TENG.

Building on this decision, and considering that in an IUA-TENG setup, the triboelectric layer is the only component to be detached from the circuitry system, we decided to carry out our computational simulations on a standalone single layer of triboelectric layer. We modeled a 30 × 30 mm nylon triboelectric layer, a realistic implantable sized TENG device equivalent, and utilized water as a simulated medium to mimic the body fluid environment that would be encountered by the ultrasound upon transdermal passage in an IMD scenario. (**Figure 25**).

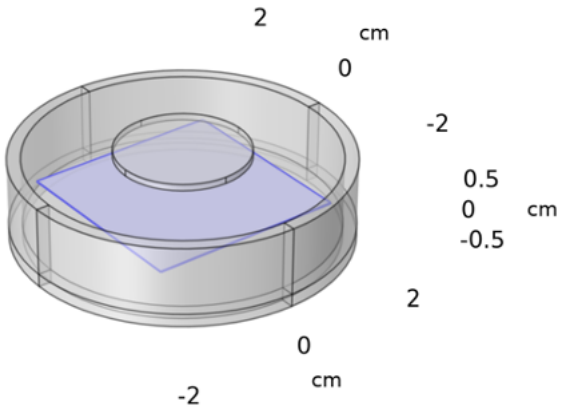

Figure 25: The illustration of the computational model utilized in our simulation. Segmentation and sizing of the working computation model[159].

On the material front, we tested a number of materials including nylon, to fulfill the logical rationale of our computational analysis. Nylon was ultimately chosen from our preliminary studies considering that material pairing of “polyamide-to-metal” has been previously shown to hold the greatest surface charge density subsequent to a triboelectric charge transfer, reaching Coulomb values of up to 3 × 10− 3 C/m^2. These materials are at diametrically opposite ends of the triboelectric scale[191,192]. Moreover, nylon is one of the most commonly used triboelectric materials in bioengineering applications, and, considering it has been utilized as a biocompatible material in a number of regulatory-approved medical devices, and has seen extensive validation as a triboelectric layer in many engineered TENGs, we chose it as a prime candidate for our theoretical investigation.

Using COMSOL, we sought to investigate the absorption of an ultrasound acoustic wave by a modeled nylon TENG layer with various thickness, followed by an analysis of

how ultrasound frequency, as well as ultrasound probe diameter, distance, and medium, affects the responses of the nylon TENG layer.

The COMSOL environment parameters tested are summarized in **Table 1**. Subsequently, we carried out material simulations to investigate how theoretical Poisson's ratio and material density alter the ultrasound absorbance and responses of the nylon layer.

Parameters	Fixed Values	Varying Values
TENG layer Material	Nylon	TENG layer Thickness: 50–350 μm
Immediate Environment	Air	Ultrasound Frequencies: 20–1000 kHz
Irradiation Medium	Water	Ultrasound Probe Distance: 1–9 mm
Environment Size	80 μm	Ultrasound Probe Diameter: 2–30 mm
Medium Size	5 cm	Ultrasound Probe Displacement: − 15–15 mm

Table 1: **Summary of experimental simulation values used**. A number of fixed experimental values and conditions were used to investigate IUA-TENG optimization using COMSOL Multiphysics, these are reported in the Table[159].

On the other hand, we also simulated a maintained thin air layer above the surface of nylon layer, necessary to ensure a fully dry environment for the triboelectric effect to occur.

The employed COMSOL software utilizes a default "Pressure Acoustics" feature which models harmonic sound waves in the water domain using the Helmholtz equation for sound pressure, detailed in the following equation:

$$\nabla \cdot \left(-\frac{1}{\rho_c}\nabla p\right) - \frac{\omega^2 p}{\rho_c c^2} = 0$$

Here the acoustic pressure is a harmonic quantity defined as $p=p_0e^{i\omega t}$, where p is the pressure (SI unit: N/m^2), ρ_c is the density (kg/m^3), ω is the angular frequency (SI unit: rad/s), and c is the speed of sound (SI unit: m/s). In order to calculate the harmonic stresses and strains in the model for a frequency-response analysis and thus determine the vibration of the computationally tested triboelectric layer, we used COMSOL's default "Linear Elastic Material Model" feature as found under the Solid Mechanics interface. The represented material data were all taken directly from the built-in database of COMSOL.

The computational 3D simulation model we designed for testing of IUA TENG energy transduction was devised using the "Acoustic-Solid Interaction" and "Frequency Domain" Multiphysics coupling sets. For our study we wished to represent a relatively miniaturized scenario, to mimic realistic implantable equivalents. Consequently, a cylinder with a diameter of 50 mm and a height of 125 mm was set up within a simulated water domain to simulate human tissue equivalence, considering dermal and epidermal soft tissue is in a majority part constituted of water. Further to this, in the spirit of real-life equivalence simulation, a square film with a side length of 30 mm and adjustable thickness (ranging between 50-350 μm – shown as a blue square) was combined with a fixed film and was used to simulate the triboelectric layers and device, immersed in water (tissue equivalent) domain. Indeed the COMSOL interface's closest medium to real life scenario was water. The frequency of ultrasound was varied from 20 kHz to 900 kHz, and probe diameter (shown as a circle) was changed from 3 mm to 30 mm.

From a methodology perspective, COMSOL software based on finite element method was applied to build the computational model of IUA-TENG and investigate optimal ultrasound irradiation conditions. In order to simulate the applicative scenario of IUA-TENG more realistically, a 3D model was created using the “Acoustic-Solid Interaction” and “Frequency Domain” Multiphysics coupling. This coupling involved two physics interfaces: the “Solid Mechanics” and the “Pressure Acoustics, Frequency Domain”. The software was also used to define an “Acoustic-Structure Boundary” coupling feature. A cylinder with a diameter of 50 mm and a height of 12.5 mm was set up as a water domain to mimic human tissue. A square film with a side length of 30 mm and adjustable thickness combined with a fixed film, was used to simulate the TENG layer, and computationally immersed in the aforementioned water domain. Ultrasound with a typical frequency of 20 kHz and acoustic pressure of 1 MPa was emitted downward from the top of the water domain. The harmonic acoustic pressure in the water on the surface of the TENG acted as a boundary load to ensure pressure continuity. The coupling between the fluid domain (pressure waves) and the solid domain, was carried out in an automatic fashion by the “Acoustic-Structure Boundary” coupling feature. Four cylindrical, perfectly matched layers (PMLs), and one rounded PML – placed around the whole cylinder – were finally used to absorb the outgoing ultrasound waves. On this basis, the designed model was able to calculate harmonic displacements and correlated TENG film layer mechanical stress, subsequently calculating surface area displacements that represented triboelectric energy conversion efficiency.

IV. Results and discussion

As mentioned, we initially assessed and confirmed the absorption of ultrasound by the nylon triboelectric layer and modeled the acoustic pressure distribution with and without a triboelectric layer (**Figure 26**).

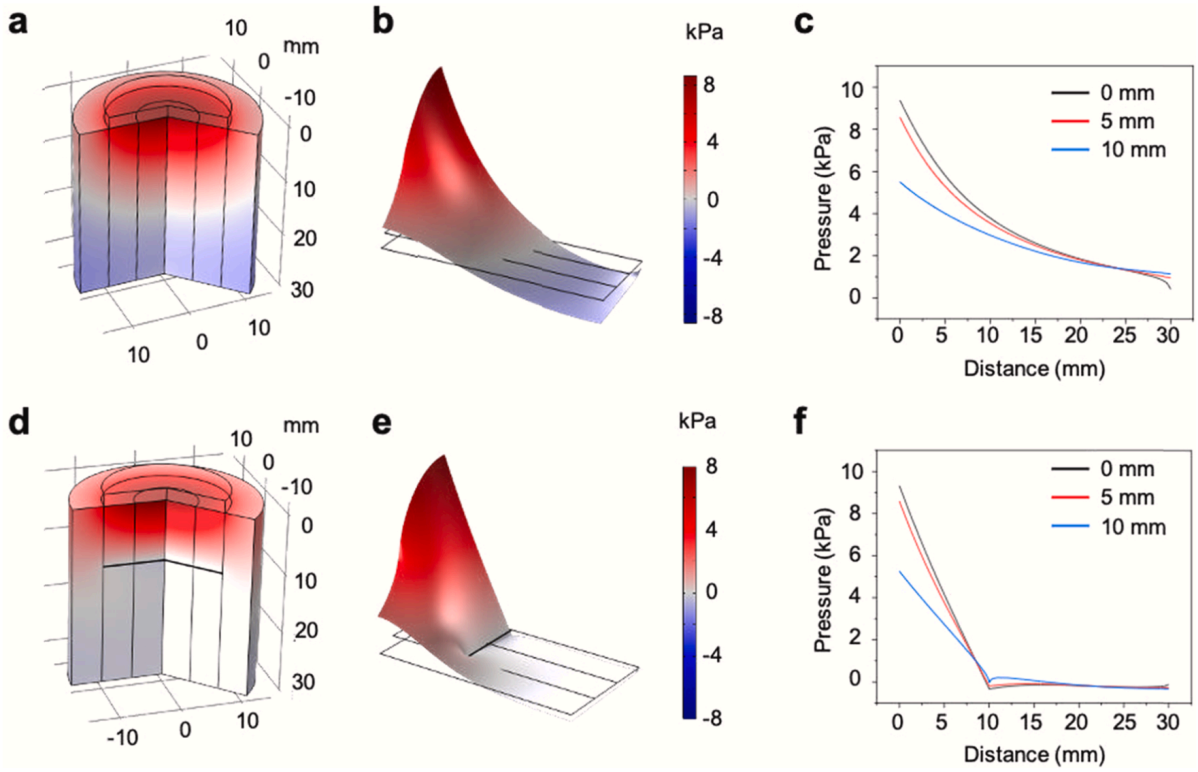

Figure 26. Simulation of acoustic pressure distribution with and without a triboelectric layer. 3D simulation results of acoustic pressure distribution without (a) and with (d) the triboelectric layer. 2D simulation results of acoustic pressure distribution without (b) and with (e) a triboelectric layer. Color gradient scale illustrates ranging pressure (Pa) values. Acoustic pressure distribution without (c) and with (f) the triboelectric layer in the Z-direction, at different distances from the center of the probe. Presence of the triboelectric layer confirms clear absorption of acoustic pressure wave[159].

This was done to ensure an effective blockage of the ultrasound wave propagation and thus subsequent energy absorption by the impeding nylon layer. From the simulation results of acoustic field distribution without (**Figure 26a-b**) and with (**Figure 26d-e**) the

triboelectric layer, evident acoustic pressure differences can be noticed. Further quantifications of Z-direction sound pressure at various distances from the probe's center (**Figure 26c)** highlight a marked sharp decay in sound pressure at the triboelectric layer level (**Figure 26f**) and consequent ultrasound energy absorption by the triboelectric layer. Once this was validated, we simulated ultrasound mechanical wave excitation of the triboelectric layer (**Figure 28**).

A 3D model with a diameter of 50 mm and a height of 12.5 mm was set up comprising a water domain, to closely mimic human tissue. A square film with a side length of 30 mm and adjustable thickness was used to simulate the triboelectric layer. By slicing the model mesh and imposing multi-physics field coupling calculations (**Figure 27**), a typical 3D simulation result was obtained.

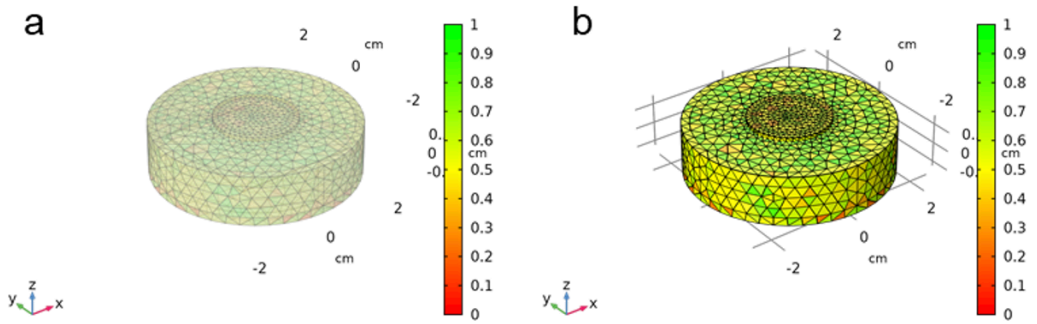

Figure 27. The meshing of the simulation model. (a) Perspective view, (b) Non-perspective view [159].

In order to best represent acoustic propagation and rheology within the domain as it would occur in uniform cutaneous human tissues with an IUA-TENG, we made sure to simulate the most uniform and efficient propagation mesh. Using COMSOL, all domains within our computational 3D simulation model were meshed in the form of a Free

Tetrahedral, and the element sizes were controlled to fit within the fluid domain, corresponding to 6 elements per wavelength (**Figure 28a**).

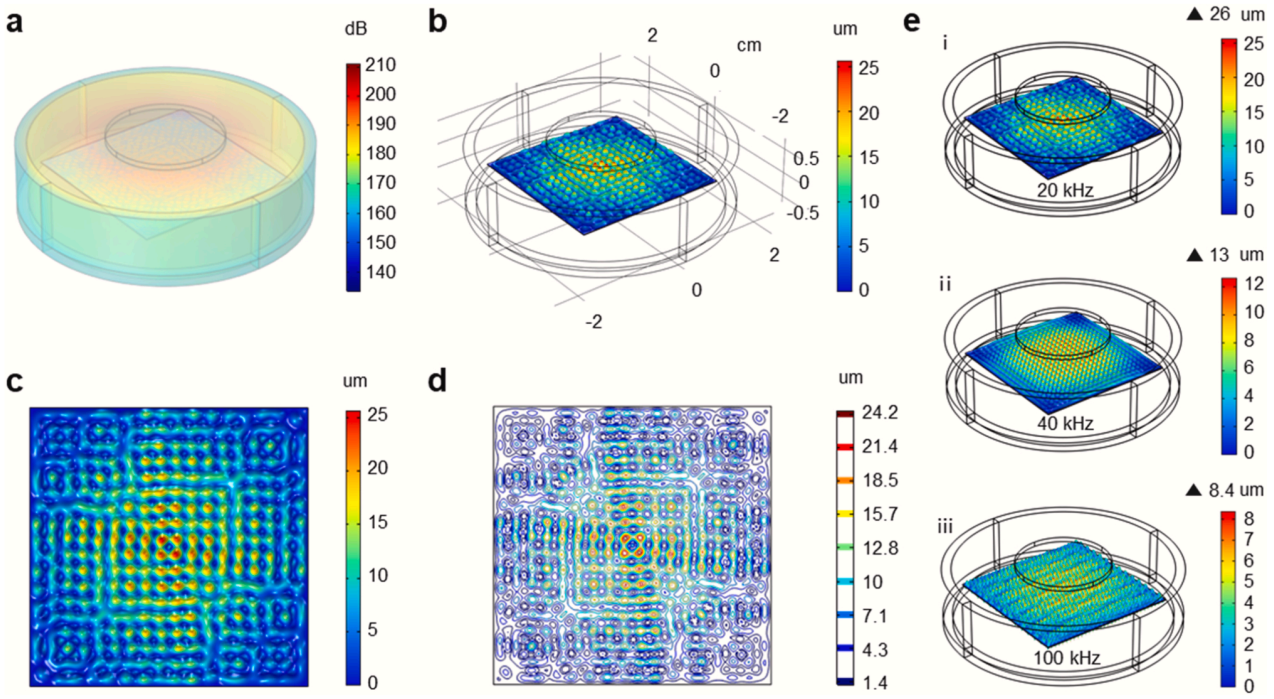

Figure 28. Surface displacement of triboelectric layer induced by ultrasound irradiation. (a) 3D simulation results of acoustic pressure distribution from an ultrasound probe irradiating a squared triboelectric layer within a COMSOL simulation space. The 3D (b) and 2D (c) view of displacement of the triboelectric layer under ultrasound probe irradiation. (c) Resultant node and anti-nodes on the triboelectric layer, visible as ripples. (d) 2D equipotential plane of the triboelectric layer displacement. (e) Notably different triboelectric layer displacement outcome shown in 3D according to ultrasound irradiation frequency. 20 kHz clearly shown to elicit the biggest node/antinode displacement. (The clear circle above the nylon layer represents the ultrasound probe, whilst the white framework represents the COMSOL observed simulation space)[159].

Here the sound pressure distribution from the ultrasound probe irradiated the square triboelectric layer. Further examination of the triboelectric layer state after ultrasound stimulation revealed multimodal vibration patterns, known to mechanistically facilitate the contact and separation mode of single-electrode TENGs (**Figure 28b**). TENG output is positively correlated to the size of the functional material contact area. The TENG (and IUA-TENG) electrical output can be subsequently inferred by quantifying the triboelectric

layer contact area size, as observed in the 2D view (**Figure 28c**). Encouragingly, to further simplify the calculation, the contact area size can also be calculated by assessing the displacement of triboelectric layer in a 2D equipotential map (**Figure 28d**). In detail, it can be said that when the displacement of the film exceeds a certain value, the area of the corresponding two-dimensional equipotential line is the contact area at the microscopic scale. Further, by means of statistical calculation, all contact areas (in other words the electrical output of TENG), can be obtained. More closely, the 2D equipotential map can be altered according to the distance between the triboelectric layer and the electrode (**Figure 29**). Depending on the ultrasonic irradiation frequency, the 3D results show significant alterations in triboelectric layer displacement (**Figure 28e**). Obviously, the maximum displacement of the membrane gradually decreases with the increase of frequency under the same conditions, though the resonance points of vibration gradually increase.

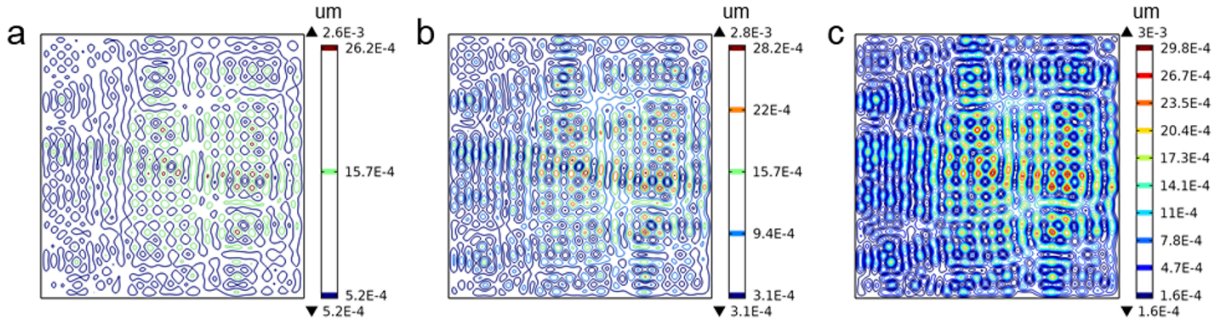

Figure 29 The equipotential map of the displacement with different number of isopotential lines. Namely: (a) three, (b) five, and (c) ten[159].

The key factor in effective energy transduction from ultrasound waves to the IUA-TENG's triboelectric lies is assessing the physical displacement of the layer as it resonates and

vibrates. Considering the node/anti-node interference and acoustic propagation, the layer's vibration is heterogenous across the surface area, depending on irradiation frequency, distance and intensity. In our preliminary studies we investigated the number of isopotential lines to integrate within the simulation model in order to achieve a more precise sense of total triboelectric area displacement (**Figure 29**).

A range of parameters were tested out to readily ascertain a rapid visual validation of triboelectric nylon layer micro-displacement in the form of node and anti-nodes formation. Considering such physical manifestations are the precursors and prerequisites to an effective ultrasound energy transduction via means of the tribmarginoelectric layer, it was important for us to assess the presence of this phenomenon. Once this validation was complete, we set out to assess how physical parameters of the nylon triboelectric layer would affect the eventual ultrasound acoustic propagation and transduction (**Figure 30**), including Poisson's ratio (**Figure 30a**), density (**Figure 30b**), Young's modulus (**Figure 30c**), thickness (**Figure 30d**), ultrasound frequency (**Figure 30e**), and material stress (**Figure 30f).**

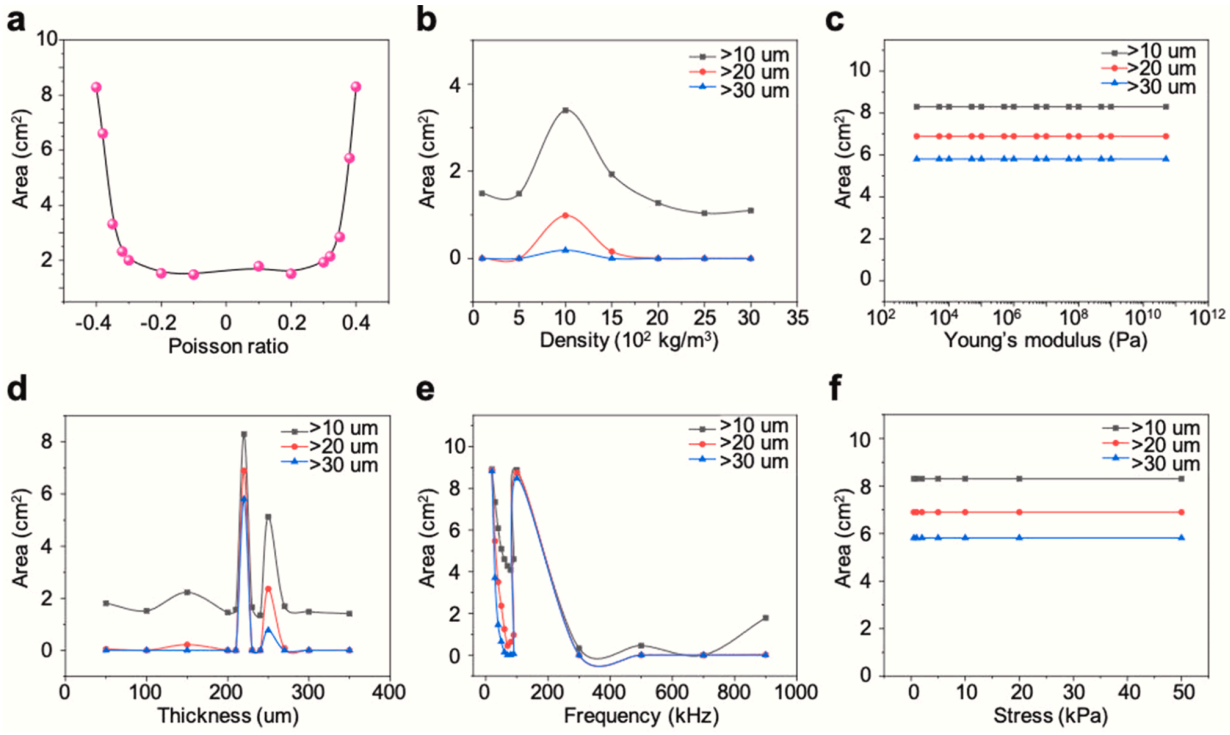

Figure 30. The effects of various materials properties on the area displacement of triboelectric nylon layer. Various triboelectric nylon layer's Poisson ratio (a), density (b), Young's modulus (c), thickness (d), ultrasound irradiation frequency (e), and stress profiles (f), were tested to assess their effect on triboelectric layer area displacement subsequent to ultrasound irradiation. Triboelectric layer displacements are grouped in > 10 μm (black line), > 20 μm (red line), and > 30 μm (blue line). The total (maximum theoretically displaceable) triboelectric nylon layer's surface area is 9 cm^2 [159].

The Poisson's ratio is a measure of the Poisson effect, the deformation of a material in directions perpendicular to the direction of loading. The value of Poisson's ratio is the negative of the ratio of transverse strain to axial strain, whilst the density of a substance is defined as its mass per unit volume ($\rho = m/v$). The Young's modulus is the ratio of stress to strain. From the results, it can be seen that there is a large displacement of the triboelectric layer at the Poisson's ratio of ± 0.4, and the displacement tends to increase and then decrease with the increase of density, with an optimal displacement output at 1000 kg/m^3. As mentioned, we chose to model a triboelectric nylon layer, and started by assessing optimal layer thickness, modeling variants of 50–350 μm *vs* standardized (20

kHz) ultrasound frequency vibration. Having identified an ideal thickness of 220 μm, we then tested frequency ranges to identify which optimal resonance frequency would yield the best vibrating effect on the layer. The testing ultrasound frequencies ranged from 20 kHz to 1000 kHz. We observed the best resonance peaks (layer displacement) at 20 kHz and 120 kHz. The former value was chosen as preferred considering its lower energy impact on tissue, with ultrasound probe-to-nylon layer distances subsequently trialed to identify the optimal irradiation parameters. It was noted that both Young's modulus and material stress have little effect on the displacement of the triboelectric layer, at least insofar as the tested range was concerned. This is surprising. One potential explanation we attribute to this is the low thickness/XY dimension ratio.

of the triboelectric layer at the Poisson's ratio of ± 0.4, and the displacement tends to increase and then decrease with the increase of density, with an optimal displacement output at 1000 kg/m^3. As mentioned, we chose to model a triboelectric nylon layer, and started by assessing optimal layer thickness, modeling variants of 50–350 μm *vs* standardized (20 kHz) ultrasound frequency vibration. Having identified an ideal thickness of 220 μm, we then tested frequency ranges to identify which optimal resonance frequency would yield the best vibrating effect on the layer. The testing ultrasound frequencies ranged from 20 kHz to 1000 kHz. We observed the best resonance peaks (layer displacement) at 20 kHz and 120 kHz. The former value was chosen as preferred considering its lower energy impact on tissue, with ultrasound probe-to-nylon layer distances subsequently trialed to identify the optimal irradiation parameters. It was noted that both Young's modulus and material stress have little effect on the displacement of the triboelectric layer, at least insofar as the tested range was concerned. This is

surprising. One potential explanation we attribute to this is the low thickness/XY dimension ratio.

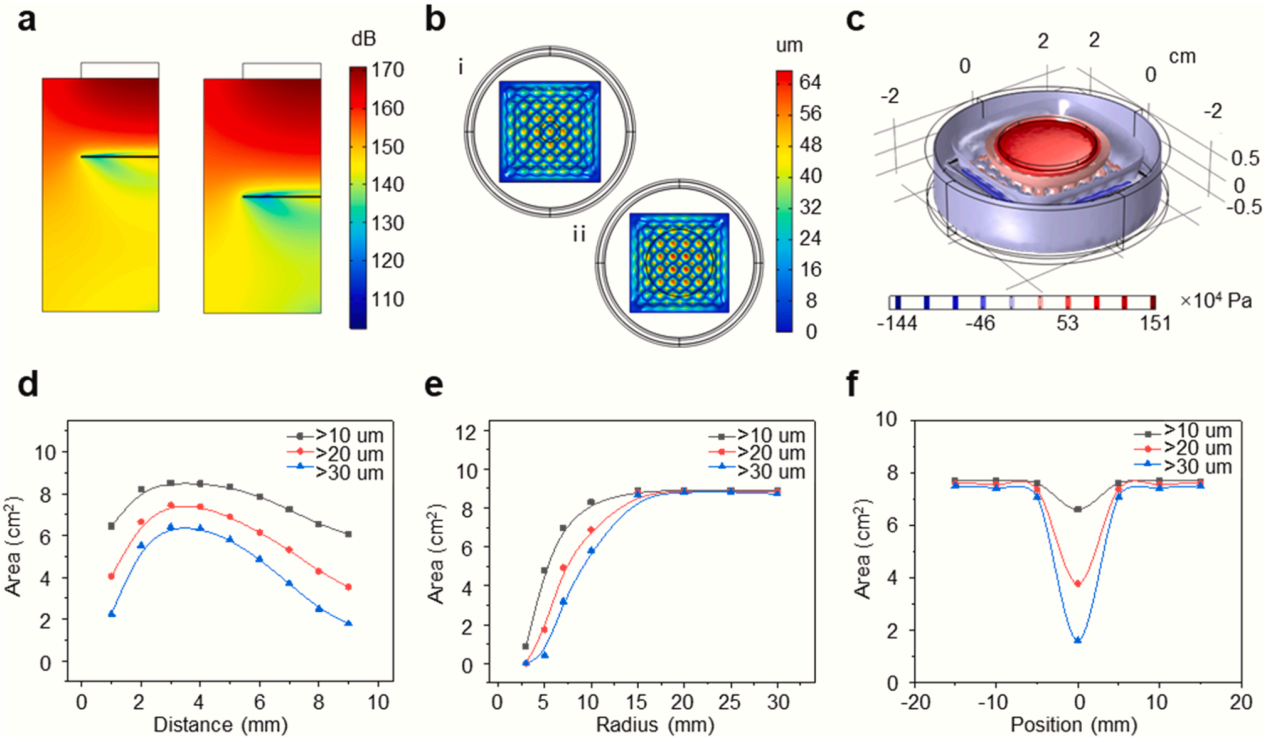

Figure 31. **Physical ultrasound irradiation parameters and their effect on triboelectric layer energy transduction.** 2D simulation results of distance-dependent acoustic pressure (dB) distribution of an ultrasound irradiated triboelectric layer (a). 3D simulation results of displacement of the triboelectric layer (b) at 2 mm (i) and 4 mm (ii) probe distance, and 3D simulation result of the ultrasound field itself (c). Vibrational displacement area varies with ultrasound probe distance (d), ultrasound probe radius (e), and ultrasound probe position (f). Please note an atypical dip in area displacement in (f) upon ultrasound irradiation directly from above the triboelectric layer, likely associated with ultrasound wave phase cancellation. Triboelectric layer displacements are grouped in2> 10 μm (black line), > 20 μm (red line), and > 30 μm (blue line). The total (maximum theoretically displaceable) triboelectric nylon layer's surface area is 9 cm^2 [159].

Once the physical parameters of the triboelectric nylon layer were determined and optimized, the simulation focus was shifted to investigating how ultrasound vibration could affect micro-displacement of the triboelectric layer, and thus the energy transduction efficiency (**Figure 31**). The 2D simulation results of distance-dependent, sound pressure distribution in the ultrasound irradiated triboelectric layer, show clear distance-dependent

effects on sound field propagation (**Figure 31a**). We ran simulations testing ultrasound probe-triboelectric nylon layer distances ranging from 1 to 9 mm, with 3 mm yielding optimal performance (**Figure 31d**). In practical terms, this was reassuring, as it remained a realistic real-life implementation, with an envisioned IUA-TENG IMD application that could be positioned just below the surface of most areas of the skin on the body. Later we altered the ultrasound probe diameter from 2 to 30 mm in size (**Figure 31b**), identifying the 20 mm sized ultrasound probe yielding the largest layer displacement (**Figure 31e**). Finally, we tested for ultrasound probe positioning with regards to the triboelectric nylon layer, testing 0 mm to + 15 mm displacements (to its North), and 0 mm to − 15 mm displacements (to its South) (**Figure 31c**), observing the most uniform nylon layer resonance when the probe was just to the side whilst directly above the device (or at +/- 5 mm displacement respectively) (**Figure 31f**).

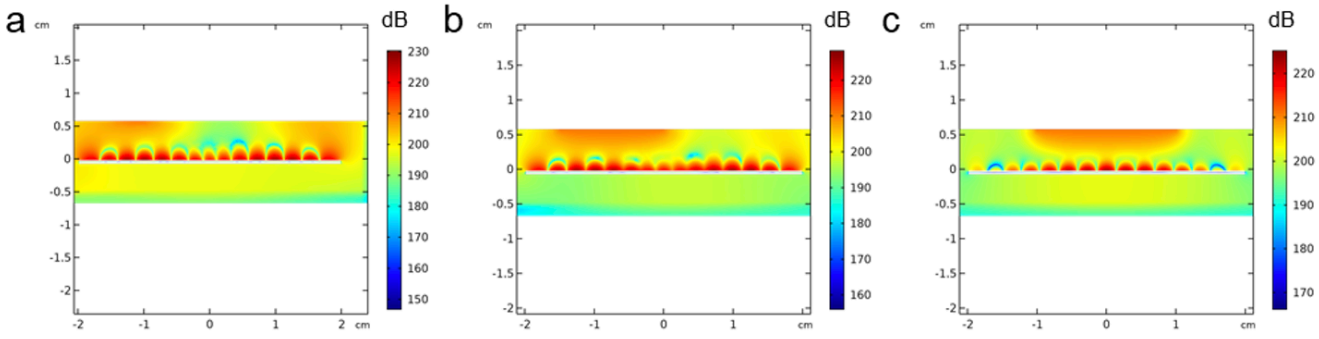

Figure 32. Further imaging of computational studies. The sound pressure level of the model with different positions of ultrasound probe center at (a) -150 mm, (b) -50 mm, (c) 0 cm[159].

Acoustic pressure level assessment is essential to assess both correct running of the computational 3D simulation model, and to assess energy transduction modulation. Within this, demonstrating that IUA-TENG's transduction capabilities were contingent to

an optimized acoustic probe positioning from the implanted device, was essential. To this end, we ran preliminary simulations to demonstrate variation in line with different acoustic probe positioning, at fixed decibel levels (**Figure 32**).

In these simulations, we were able to obtain up to 8.49 cm^2 triboelectric area displacement when simulating the irradiation of a 220 μm triboelectric layer with 20 kHz ultrasound frequency at 3 mm ultrasound probe distance. This equaled a free vibration of > 90% of the total nylon triboelectric surface available. Considering that in a real-life scenario, there would need to be some type of anchoring of the triboelectric nylon layer to keep it in place, and that thus not all of the surface would be available to vibrate freely, we can assume that with these optimized simulated parameters we can achieve almost complete energy efficiency transformation from ultrasound mechanical waves to triboelectric layer vibration and contact electrification / triboelectric effect. Moreover, the observed displacement of the triboelectric layer reached up to > 30 μm, though this would not have an effect on the current output of the TENG device, but merely on the voltage output[193]. Mechanistically, in the single-electrode mode simulation we computed, only one electrode serves as the triboelectric layer whilst the other electrode acts as an electric potential reference. Upon cyclical displacement brought about by the ultrasound, the latter comes into contact with the electrode and a negative charge on its internal membrane is generated. This surface charge transfer occurs due to the triboelectric effect and overall decreases the electrode's potential energy, leading to an intermittent current which is correspondent to the frequency of cyclical contact separation.

V. Conclusion

Developing a microscaled, remotely chargeable, and powered IMD device holds considerable scientific significance. Within the IMD market, nearly 25% of concerned products are classified as active implantable devices. Given the bulky, temporary and morphologically unsuitable nature of existing IMDs, growing efforts are needed to improve existing devices, as well as develop novel technological approaches which can allow for more tailored IMD therapies, as well as reach into previously untapped clinical applications. IUA-TENGs allow for the exploitation of a highly validated therapeutic approach to tissue engineering and regenerative medicine, for a larger number of more delicate and microscaled tissue types, paving the way for novel interventional applications still out of our grasp. In addition, the development of IUA-TENGs can help establish a novel scientific platform for the future of IMDs, one which is also able to leverage on the interconnectability with the IoMTs and the growing 5G network, in a forward-looking paradigm and new era of personalized medicine and clinical interventions.

There are a number of highly innovative approaches to this research. To our knowledge this is the first attempt at utilizing detailed computational modeling to optimize ultrasound energy conversion parameters for an implantable TENG. By leveraging on such an approach, we are hoping to set the foundations for creating a standardized "TENG device modeling protocol" for future use in IUA-TENGs. Indeed, there are a number of ways in which harnessed ultrasound energy can be utilized depending on the final therapeutic application sought. Within the context of this translational research, we have developed a methodical approach, combining computational design and material

science analysis, to yield a fully comprehensive strategy to developing the next generation IMD. By employing a fully rounded bioengineering approach, we chose not to bypass any of the essential requirements which touch upon IMD IUA-TENG development, but merely enrich it.

This study was able to rapidly provide direct guidance into optimal triboelectric irradiation protocols and physical parameters, helping bypass time consuming operations. Overall, we achieved our goal of readily assessing, and at a low cost and timed effort, the optimal ultrasound probe size, positioning, distancing, as well as triboelectric layer thickness in an IUA-TENG that utilizes a polyamide-metal single-electrode mode, features both commonly found in previously developed TENG solutions, and solutions also well suited to an IMD role. Ultrasound acoustic simulations moreover suggested ideal ultrasound probe irradiation requires a minimum surface diameter equal at least to the size of the IUA-TENG triboelectric layer, and that transdermal ultrasound irradiation onto the IUA-TENG should not be done directly perpendicular to the IMD. Such practice indeed risks leading to ultrasound phase wave cancellation and a minimized transduction of energy. Overall, we hope that this computational simulation setup will provide a substantial added value compared to “ex novo” practical experimental design.

Ultrasound waves have had a profound role in clinical care over the last 80 years, enabling a myriad of fundamental medical diagnostic and interventional imaging procedures and providing useful therapeutic solutions for many medical conditions[194,195]. TENGs’ innate ability to convert mechanical energy into electricity *via* the conjunction of triboelectrification and electrostatic induction, with recent expansion into ultrasound irradiation, is paving a new future in IMD powering and activation. Optimization of the

ultrasound wave interaction with the TENG layer is essential to yield a high-performance energy conversion IUA-TENG. By resting on *in silico* simulation, we have validated a cheaper, more rapid, and easily tunable investigational method to integrate alongside the arsenal of tools used in IUA-TENG development, especially considering this novel platform will be able to yield wireless powering solution much more simple and effective than current capacitive and radio-frequency wireless powering alternatives, which moreover yield inefficient transfers and cytotoxic heat production.

CHAPTER 5

CONCLUSION AND PERSPECTIVE

I. Prospective for MEG electrical stimulation

With the above work we have demonstrated how a new family of soft bioelectronics, MEGs, can enable simple, inexpensive, and rapid access to a new field of self-powered electrical stimulation devices, specifically for easy integration in use in *in vitro* and *in vivo* applications, owing to their innate properties. To advance on this field, a number of areas could be explored.

On the fabrication front, prospective work could focus on developing the fabrication and development of self-powered MEG ES platforms on different media and using different techniques, such as soft lithography, stereolithography, electrospinning and direct 3D printing with cellular incorporation. The ability to devise MEGs using simple polymeric-nanomagnet systems and conductive induction layers (which can take the form of liquid metals), in one body system stand-alone devices has enormous benefits. Considering the pivotal role of electrical stimulation in so very many biological processes, miniaturizing and developing such platforms can not only provide an integrating self-powered platform, but also a way to delve into the molecular effect of ES.

On the ES applicative front, there are innumerate avenues in which the MEG ES platform could be trialed. For instance, current MEG ES platform could be tested on other known transdifferentiation, reprogramming and cellular engineering protocols with diverse cell lines and to different ends. Furthermore, the co-coupling of MEG ES and other mechanostimulation ought also to be trialed. Considering the miniaturizability of the MEG

ES layers (MC-MI layer system specifically), we anticipate air pressure-driven self-powered electromechanical stimulation. Owing to the inherent magnetic flux changes of MEG actuators, it could also be of interest to investigate magnetobiological implications and effect on cellular systems *in vitro*.

One of the key components and landmarks of this MEG ES research was the first applicative use of such generators directly for cell reprogramming, and in constant close contact with biological matter. This important step however is a stepping-stone towards the *in vivo* application of MEG ES devices. The use of *in vivo* electrical stimulation is covered in the Appendix (Section I), and the application of MEG ES into these fields, and specifically within implantable devices, is up for grabs for many researchers seeking to use a new and biocompatible ES device for many theranostic applications.

II. Prospective for ultrasound TENG electrical stimulation

The use of TENG for ES is very well documented, but its use *via* "*ad hoc"* ultrasound irradiation is a relatively novel development, with lagging and low energy transduction efficiency. With our work, we hope to set the foundation to help bolster this novel field in a potentiated manner and provide an engineering tool that may help in the design and actuation of novel implantable TENG devices.

To expand on this work, we envisage focusing on the development of an ever growingly more sophisticated computational simulation method which takes into consideration TENGS of different constitutive materials, architectures, and outputs. Specifically, implanted TENG are used for a number of applications, including direct ES therapy, third-party device powering, and other electrically induced implanted effect, such

as drug release (more information is provided in the Appendix - Section I). Optimization of US irradiation using bespoke computational simulation and design of implantable TENG can help achieve desired irradiation conditions for specific electrical output. We anticipate future studies coupling *in silico* computational design with *in vitro* and *in vivo* validation, and adaptation of the simulation to transcutaneous irradiation in and across various parts of the body which represent different physical media.

III. General future trends

The permeation of soft bioelectronics is an unstoppable phenomenon. Whether for diagnostic, therapeutic, coupled theranonstic, or energy producing applications, soft bioelectronics are set to hold an increasingly large space in our daily lives, especially in the fields of diagnosis and biomonitoring. The development of autonomous body area wide soft bioelectronic networks is moreover set to allow the implementation of intelligent closed loop systems for personalized healthcare.

MEG, still at its infancy is likely to become a major player in the field, given its superior performance, and biological and physiological suitability, and we invite researchers to help foster this novel platform technology for future use. An in-depth exploration of the future of soft bioelectronics is provided in depth in the Appendix (Section II) of this work.

REFERENCES

1. Chen, G., Li, Y., Bick, M. & Chen, J. Smart Textiles for Electricity Generation. *Chem. Rev.* **120**, 3668–3720 (2020).
2. Alberghini, M. Sustainable polyethylene fabrics with engineered moisture transport for passive cooling. *Nat. Sustain* **4**, 715–724 (2021).
3. Sundaram, S. Learning the signatures of the human grasp using a scalable tactile glove. *Nature* **569**, 698–702 (2019).
4. Post, E. R., Orth, M., Russo, P. R. & Gershenfeld, N. E-broidery: Design and fabrication of textile-based computing. *IBM Syst. J* **39**, 840–860 (2000).
5. Carpi, F. & Rossi, D. D. Electroactive polymer-based devices for e-textiles in biomedicine. *IEEE Trans. Inf. Technol. Biomed* **9**, 295–318 (2005).
6. Catrysse, M. Towards the integration of textile sensors in a wireless monitoring suit. *Sensors and Actuators A: Physical* **114**, 302–311 (2004).
7. Grillet, A. Optical fiber sensors embedded into medical textiles for healthcare monitoring. *IEEE Sens. J* **8**, 1215–1222 (2008).
8. Lyu, S., He, Y., Yao, Y., Zhang, M. & Wang, Y. Photothermal clothing for thermally preserving pipeline transportation of crude oil. *Adv. Funct. Mater* **29**, 1900703 (2019).
9. Mordon, S. The conventional protocol vs. A protocol including illumination with a fabric-based biophotonic device (the phosistos protocol) in photodynamic therapy for actinic keratosis: A randomized, controlled, noninferiority clinical study. *Br. J. Dermatol* **182**, 76–84 (2020).
10. Shen, J., Chui, C. & Tao, X. Luminous fabric devices for wearable low-level light therapy. *Biomed. Opt. Express* **4**, 2925–2937 (2013).

11. Park, S. One-step optogenetics with multifunctional flexible polymer fibers. *Nat. Neurosci* **20**, 612–619 (2017).
12. Zhang, Z. A colour-tunable, weavable fibre-shaped polymer light-emitting electrochemical cell. *Nat. Photonics* **9**, 233–238 (2015).
13. Liu, M. Large-area all-textile pressure sensors for monitoring human motion and physiological signals. *Adv. Mater* **29**, 1703700 (2017).
14. Cho, S.-Y. Continuous meter-scale synthesis of weavable tunicate cellulose/carbon nanotube fibers for high-performance wearable sensors. *ACS Nano* **13**, 9332–9341 (2019).
15. Wu, R. Silk composite electronic textile sensor for high space precision 2D combo temperature–pressure sensing. *Small* **15**, 1901558 (2019).
16. Ding, T. Scalable thermoelectric fibers for multifunctional textile-electronics. *Nat. Commun* **11**, 6006 (2020).
17. Sun, T. Stretchable fabric generates electric power from woven thermoelectric fibers. *Nat. Commun* **11**, 572 (2020).
18. Jeong, E. G., Jeon, Y., Cho, S. H. & Choi, K. C. Textile-based washable polymer solar cells for optoelectronic modules: Toward self-powered smart clothing. *Energy Environ. Sci* **12**, 1878–1889 (2019).
19. Zhang, N. A wearable all-solid photovoltaic textile. *Adv. Mater* **28**, 263–269 (2016).
20. Matsuhisa, N. Printable elastic conductors with a high conductivity for electronic textile applications. *Nat. Commun* **6**, 7461 (2015).
21. Jin, H. Enhancing the performance of stretchable conductors for e-textiles by controlled ink permeation. *Adv. Mater* **29**, 1605848 (2017).

22. Lee, J. Conductive fiber-based ultrasensitive textile pressure sensor for wearable electronics. *Adv. Mater* **27**, 2433–2439 (2015).
23. Li, R. Supercapacitive iontronic nanofabric sensing. *Adv. Mater* **29**, 1700253 (2017).
24. Dalton, A. B. Super-tough carbon-nanotube fibres. *Nature* **423**, 703–703 (2003).
25. Etches, J., Bond, I. & Mellor, P. *The manufacturing of magnetically-active fiber-reinforced composites for use in power generation*. (SPIE, 2004).
26. Lee, H. & Roh, J.-S. Wearable electromagnetic energy-harvesting textiles based on human walking. *Text. Res. J* **89**, 2532–2541 (2019).
27. Li, H. Chemical and biomolecule sensing with organic field-effect transistors. *Chem. Rev* **119**, 3–35 (2019).
28. Kim, S. J. A new architecture for fibrous organic transistors based on a double-stranded assembly of electrode microfibers for electronic textile applications. *Adv. Mater* **31**, 1900564 (2019).
29. Shi, W., Guo, Y. & Liu, Y. When flexible organic field-effect transistors meet biomimetics: A prospective view of the internet of things. *Adv. Mater* **32**, 1901493 (2020).
30. Yang, A. Fabric organic electrochemical transistors for biosensors. *Adv. Mater* **30**, 1800051 (2018).
31. Hamedi, M., Forchheimer, R. & Inganäs, O. Towards woven logic from organic electronic fibres. *Nat. Mater* **6**, 357–362 (2007).
32. Egusa, S. Multimaterial piezoelectric fibres. *Nat. Mater* **9**, 643–648 (2010).
33. Qin, Y., Wang, X. & Wang, Z. L. Microfibre–nanowire hybrid structure for energy scavenging. *Nature* **451**, 809–813 (2008).

34. Su, Y. Muscle fibers inspired high-performance piezoelectric textiles for wearable physiological monitoring. *Adv. Funct. Mater* **31**, 2010962 (2021).
35. Azimi, B. Electrospinning piezoelectric fibers for biocompatible devices. *Adv. Healthc. Mater* **9**, 1901287 (2020).
36. Soin, N. Novel “3-D spacer” all fibre piezoelectric textiles for energy harvesting applications. *Energy Environ. Sci* **7**, 1670–1679 (2014).
37. Kwon, C. H. High-power biofuel cell textiles from woven biscrolled carbon nanotube yarns. *Nat. Commun* **5**, 3928 (2014).
38. Lv, J. Sweat-based wearable energy harvesting-storage hybrid textile devices. *Energy Environ. Sci* **11**, 3431–3442 (2018).
39. Fan, F.-R., Tian, Z.-Q. & Lin Wang, Z. Flexible triboelectric generator. *Nano Energy* **1**, 328–334 (2012).
40. Chen, J. & Wang, Z. L. Reviving vibration energy harvesting and self-powered sensing by a triboelectric nanogenerator. *Joule* **1**, 480–521 (2017).
41. Chen, G., Au, C. & Chen, J. Textile triboelectric nanogenerators for wearable pulse wave monitoring. *Trends Biotechnol* **39**, 1078–1092 (2021).
42. Zhou, Z. Single-layered ultra-soft washable smart textiles for all-around ballistocardiograph, respiration, and posture monitoring during sleep. *Biosens. Bioelectron* **155**, 112064 (2020).
43. He, T. Self-sustainable wearable textile nano-energy nano-system (NENS) for next-generation healthcare applications. *Adv. Sci* **6**, 1901437 (2019).
44. Jung, S., Lee, J., Hyeon, T., Lee, M. & Kim, D.-H. Fabric-based integrated energy devices for wearable activity monitors. *Adv. Mater* **26**, 6329–6334 (2014).

45. Chen, C. 3D double-faced interlock fabric triboelectric nanogenerator for bio-motion energy harvesting and as self-powered stretching and 3d tactile sensors. *Mater. Today* **32**, 84–93 (2020).
46. Zhong, J. Fiber-based generator for wearable electronics and mobile medication. *ACS Nano* **8**, 6273–6280 (2014).
47. Zhou, Y. Giant magnetoelastic effect in soft systems for bioelectronics. *Nat. Mater* **20**, 1300 (2021).
48. Firouzi, F. *et al. Future Gener. Comput. Syst* **78**, 583 (2018).
49. Kelati, A. & H. Tenhunen. in *Proc. of the 2018 IEEE/ACM Int. Conf. on Connected Health: Applications, Systems and Engineering Technolo* 7–8 (IEEE, 2018).
50. Mirtaheri, E. & Li, C.-Z. Wearable biomedical devices: State of the art, challenges, and future perspectives. *Electrochem. Soc. Interface* **28**, 71–74 (2019).
51. Misra, G., Kumar, V., Agarwal, A. & Agarwal, K. *Am. J. Electr. Electron. Eng* **4**, 23 (2016).
52. Kim, J., Campbell, A. S., Ávila, B. E.-F. & Wang, J. Wearable biosensors for healthcare monitoring. *Nat. Biotechnol* **37**, 389–406 (2019).
53. Bandodkar, A. J. & Wang, J. Non-invasive wearable electrochemical sensors: a review. *Trends Biotechnol.* **32**, 363–371 (2014).
54. Stoppa, M. & Chiolerio, A. Wearable electronics and smart textiles: a critical review. *Sensors (Basel)* **14**, 11957–11992 (2014).
55. Tamsin, M. Int. *J. Sci* **13**, 697 (2015).
56. Mahmud, M. A. P., Huda, N., Farjana, S. H., Asadnia, M. & Lang, C. Adv. *Energy Mater* **8**, 1701210 (2018).

57. Rattay, F. The basic mechanism for the electrical stimulation of the nervous system. *Neuroscience* **89**, 335–346 (1999).

58. Ranck, J. B., Jr. Which elements are excited in electrical stimulation of mammalian central nervous system: a review. *Brain Res.* **98**, 417–440 (1975).

59. Imberti, R. & Amatu, A. Drug delivery to the central nervous system. *Eur. J. Histochem.* **54**, (2010).

60. M. Doblaré, M. J. G., J. M. GarcÍa. *Eng. Fract. Mech* **71**, (2004).

61. Ghiasi, M. S., Chen, J., Vaziri, A., Rodriguez, E. K. & Nazarian, A. Bone fracture healing in mechanobiological modeling: A review of principles and methods. *Bone Rep.* **6**, 87–100 (2017).

62. Sabet, F. A., Raeisi Najafi, A., Hamed, E. & Jasiuk, I. Modelling of bone fracture and strength at different length scales: a review. *Interface Focus* **6**, 20150055 (2016).

63. Pastar, I. *et al.* Epithelialization in wound healing: A comprehensive review. *Adv. Wound Care (New Rochelle)* **3**, 445–464 (2014).

64. Portou, M. J., Baker, D., Abraham, D. & Tsui, J. The innate immune system, toll-like receptors and dermal wound healing: A review. *Vascul. Pharmacol.* **71**, 31–36 (2015).

65. Tremblay, A. & Doucet, E. Obesity: a disease or a biological adaptation? *Obes. Rev.* **1**, 27–35 (2000).

66. Ahima, R. S. Digging deeper into obesity. *J. Clin. Invest.* **121**, 2076–2079 (2011).

67. Assimacopoulos-Jeannet, F., Jeanrenaud, B., & Clin. Endocrin.

68. Ramachandrappa, S. & Farooqi, I. S. Genetic approaches to understanding human obesity. *J. Clin. Invest.* **121**, 2080–2086 (2011).

69. Altekruse, S. F. *et al. SEER Cancer Statistics Review* (1975).

70. Deandrea, S., Montanari, M., Moja, L., Apolone, G. & Oncol, A. (2008).

71. Beuken-van Everdingen, M. H. J. *et al. Ann. Oncol* **18**, 1437 (2007).

72. Karagan, N. J. Intellectual functioning in Duchenne muscular dystrophy: A review. *Psychol. Bull.* **86**, 250–259 (1979).

73. Snow, W. M., Anderson, J. E., Jakobson, L. S., & Neurosci. Biobehav. *Rev* **37**, 743 (2013).

74. Verhaart, I. E. C. & Aartsma-Rus, A. *Nat. Rev. Neurol* **15**, 373 (2019).

75. Peake, J. M., Neubauer, O., Della Gatta, P. A. & Nosaka, K. Muscle damage and inflammation during recovery from exercise. *J. Appl. Physiol.* **122**, 559–570 (2017).

76. Neher, M. D., Weckbach, S., Flierl, M. A., Huber-Lang, M. S. & Stahel, P. F. *J. Biomed. Sci* **18**, 90 (2011).

77. Ibrahim, D. A., Swenson, A., Sassoon, A., Fernando, N. D., & Clin. Orthop. *Relat. Res* **475**, 560 (2017).

78. Gupta, M., Mysore, V. & Cutan, J. Aesthet. *Surg* **9**, 3 (2016).

79. Almohanna, H. M., Ahmed, A. A., Tsatalis, J. P. & Tosti, A. *Dermatol. Ther* **9**, 51 (2019).

80. Fabbrocini, G. *et al.* Female pattern hair loss: A clinical, pathophysiologic, and therapeutic review. *Int. J. Womens Dermatol.* **4**, 203–211 (2018).

81. Grape, H. H., Dedering, A. & Jonasson, A. F. Retest reliability of surface electromyography on the pelvic floor muscles. *Neurourol. Urodyn.* **28**, 395–399 (2009).

82. Suskind, A. M. The aging overactive bladder: A review of aging-related changes from the brain to the bladder. *Curr. Bladder Dysfunct. Rep.* **12**, 42–47 (2017).

83. Gerritsen, M., Lutterman, J. A. & Jansen, J. A. Wound healing around bone-anchored percutaneous devices in experimental diabetes mellitus. *J. Biomed. Mater. Res.* **53**, 702–709 (2000).

84. Kloth, L. C. Electrical stimulation technologies for wound healing. *Adv. Wound Care (New Rochelle)* **3**, 81–90 (2014).

85. Mollon, B., da Silva, V., Busse, J. W., Einhorn, T. A. & Bhandari, M. Electrical stimulation for long-bone fracture-healing: a meta-analysis of randomized controlled trials. *J. Bone Joint Surg. Am.* **90**, 2322–2330 (2008).

86. Victoria, G., Petrisor, B., Drew, B. & Dick, D. Bone stimulation for fracture healing: What's all the fuss? *Indian J. Orthop.* **43**, 117–120 (2009).

87. D'Argent, J. Gastric electrical stimulation as therapy of morbid obesity: preliminary results from the French study. *Obes. Surg.* **12 Suppl 1**, 21S-25S (2002).

88. Bielefeldt, K. Adverse events of gastric electrical stimulators recorded in the Manufacturer and User Device Experience (MAUDE) Registry. *Auton. Neurosci.* **202**, 40–44 (2017).

89. van Balken, M. R., Vergunst, H. & Bemelmans, B. L. H. The use of electrical devices for the treatment of bladder dysfunction: a review of methods. *J. Urol.* **172**, 846–851 (2004).

90. Reddy, S., He, L. & Ramakrishana, S. Miniaturized-electroneurostimulators and self-powered/rechargeable implanted devices for electrical-stimulation therapy. *Biomed. Signal Process. Control* **41**, 255–263 (2018).

91. Cho, Y., Shi, R., Ivanisevic, A. & Borgens, R. B. *Nanotechnology* **20**, 275102 (2009).

92. Razzacki, S. Z., Thwar, P. K., Yang, M., Ugaz, V. M. & Burns, M. A. Adv. *Drug Delivery Rev* **56**, 185 (2004).

93. Entezami, A. A. & Massoumi, B. Iran. *Polym. J* **15**, 13 (2006).

94. Smith, T. J. & Marineo, G. Treatment of postherpetic pain with Scrambler therapy, a patient-specific neurocutaneous electrical stimulation device. *Am. J. Hosp. Palliat. Care* **35**, 812–813 (2018).

95. Borges, M. R. *et al.* Transcutaneous electrical nerve stimulation is superior than placebo and control for postoperative pain relief. *Pain Manag.* **10**, 235–246 (2020).

96. Searle, R. D., Bennett, M. I., Johnson, M. I., Callin, S. & Radford, H. Transcutaneous electrical nerve stimulation (TENS) for cancer bone pain. *J. Pain Symptom Manage.* **37**, 424–428 (2009).

97. Bhogal, N., Grindon, C., Combes, R. & Balls, M. Toxicity testing: creating a revolution based on new technologies. *Trends Biotechnol.* **23**, 299–307 (2005).

98. Otsubo, Y. *et al.* Binary test battery with KeratinoSens™ and h-CLAT as part of a bottom-up approach for skin sensitization hazard prediction. *Regul. Toxicol. Pharmacol.* **88**, 118–124 (2017).

99. Osborne, R. & Perkins, M. A. An approach for development of alternative test methods based on mechanisms of skin irritation. *Food Chem. Toxicol.* **32**, 133–142 (1994).

100. Choi, S. *et al. Nat. Nanotechnol* **13**, 1048 (2018).

101. Khan, Y. *et al.* vol. 28 4373 (2016).

102. Kudo, H. *et al.* vol. 22 558 (2006).

103. Drury, R. L. Wearable biosensor systems and resilience: a perfect storm in health care? *Front. Psychol.* **5**, 853 (2014).

104. Liu, S.-C., Tomizuka, M. & Ulsoy, G. Strategic issues in sensors and smart structures. *Struct. Contr. Health Monit.* **13**, 946–957 (2006).

105. Weng, W. *et al.* A route toward smart system integration: From fiber design to device construction. *Adv. Mater.* **32**, e1902301 (2020).

106. Jin, C., Kia, D. S., Jones, M. & Towfighian, S. On the contact behavior of micro-/nano-structured interface used in vertical-contact-mode triboelectric nanogenerators. *Nano Energy* **27**, 68–77 (2016).

107. Niu, S. *et al.* Theoretical investigation and structural optimization of single-electrode triboelectric nanogenerators. *Adv. Funct. Mater.* **24**, 3332–3340 (2014).

108. Yang, Y. *et al.* Single-electrode-based sliding triboelectric nanogenerator for self-powered displacement vector sensor system. *ACS Nano* **7**, 7342–7351 (2013).

109. Yi, F. *et al.* Stretchable-rubber-based triboelectric nanogenerator and its application as self-powered body motion sensors. *Adv. Funct. Mater.* **25**, 3688–3696 (2015).

110. Jiang, W. *et al.* Fully bioabsorbable natural-materials-based triboelectric nanogenerators. *Adv. Mater.* **30**, 1801895 (2018).

111. Conta, G., Libanori, A., Tat, T., Chen, G. & Chen, J. Triboelectric Nanogenerators for Therapeutic Electrical Stimulation. *Advanced Materials* **33**, 2007502 (2021).

112. Hunckler, J., Mel, A. & Healthcare, J. M. vol. 10 179 (2017).

113. Vieira, M. S. *et al. Biotechnol. Adv* 36, (2018).

114. Pfisterer, U. *et al.* Small molecules increase direct neural conversion of human fibroblasts. *Sci. Rep.* **6**, (2016).

115. Guo, W. *et al.* Self-powered electrical stimulation for enhancing neural differentiation of mesenchymal stem cells on graphene–poly(3,4-ethylenedioxythiophene) hybrid microfibers. *ACS Nano* **10**, 5086–5095 (2016).

116. Aydin, T., Gurcan, C., Taheri, H. & Yilmazer, A. Stem Cells, Bio-Materials and Tissue Engineering. *Cell Biology and Translational Medicine* **3**, 129–142 (2018).

117. Du, J. *et al. Biomaterials* **181**, 347 (2018).

118. Zhu, W. *et al. Nanomedicine* **14**, 2485 (2018).

119. Damaraju, S. M. *et al. Biomaterials* **149**, 51 (2017).

120. Jin, Y. *et al.* Triboelectric Nanogenerator Accelerates Highly Efficient Nonviral Direct Conversion and In Vivo Reprogramming of Fibroblasts to Functional Neuronal Cells. *Advanced Materials* **28**, 7365–7374 (2016).

121. Lee, S., Wang, H., Thakor, N. V., Yen, S. C. & Lee, C. *J. Phys. Conf. Ser* **1052**, 012007 (2018).

122. Lee S. *et al. Nano Energy* **33**, 1 (2017).

123. Pisanello, M. *et al.* The three-dimensional signal collection field for fiber photometry in brain tissue. *Front. Neurosci.* **13**, 82 (2019).

124. Jiman, A. A. *et al.* Multi-channel intraneural vagus nerve recordings with a novel high-density carbon fiber microelectrode array. *Sci. Rep.* **10**, 15501 (2020).

125. Navarro, X. *et al.* Nerv. *Syst* **10**, 229 (2005).

126. Sahyouni, R. *et al. Neurosurg. Rev* **42**, 227 (2019).

127. Mora Lopez, C. Unraveling the brain with high-density CMOS neural probes: Tackling the challenges of neural interfacing. *IEEE solid-state circuits mag.* **11**, 43–50 (2019).

128. Miller, L. *et al. Arch. Phys. Med. Rehabil* **98**, 1435 (2017).

129. Tyler, S. E. B. Nature's Electric Potential: A Systematic Review of the Role of Bioelectricity in Wound Healing and Regenerative Processes in Animals, Humans, and Plants. *Frontiers in Physiology* **8**, (2017).

130. Balint, R., Cassidy, N. J. & Cartmell, S. H. Electrical Stimulation: A Novel Tool for Tissue Engineering. *Tissue Engineering Part B: Reviews* **19**, 48–57 (2013).

131. Zhang, J. & Chen, J. D. Z. Systematic review: applications and future of gastric electrical stimulation. *Alimentary Pharmacology & Therapeutics* **24**, 991–1002 (2006).

132. Bestmann, S. & Walsh, V. Transcranial electrical stimulation. *Current Biology* **27**, R1258–R1262 (2017).

133. Carmel, J. B. & Martin, J. H. Motor cortex electrical stimulation augments sprouting of the corticospinal tract and promotes recovery of motor function. *Front. Integr. Neurosci.* **8**, (2014).

134. McCaig, C. D., Rajnicek, A. M., Song, B. & Zhao, M. Controlling cell behavior electrically: current views and future potential. *Physiol Rev* **85**, 943–978 (2005).

135. Sullivan, K. G., Emmons-Bell, M. & Levin, M. Physiological inputs regulate species-specific anatomy during embryogenesis and regeneration. *Commun Integr Biol* **9**, e1192733 (2016).

136. Sun, L.-Y. *et al.* Effect of pulsed electromagnetic field on the proliferation and differentiation potential of human bone marrow mesenchymal stem cells. *Bioelectromagnetics* **30**, 251–260 (2009).

137. Sun, L.-Y., Hsieh, D.-K., Lin, P.-C., Chiu, H.-T. & Chiou, T.-W. Pulsed electromagnetic fields accelerate proliferation and osteogenic gene expression in

human bone marrow mesenchymal stem cells during osteogenic differentiation. *Bioelectromagnetics* **31**, 209–219 (2010).

138. Deng, W. *et al.* Piezoelectric Nanogenerators for Personalized Healthcare. *Chemical Society Review*.

139. Zi, Y., Basset, P. & Chen, J. Triboelectric nanogenerator—Progress and perspectives. *EcoMat* **3**, e12129 (2021).

140. Gu, L. *et al.* Enhancing the current density of a piezoelectric nanogenerator using a three-dimensional intercalation electrode. *Nat Commun* **11**, 1030 (2020).

141. Chen, G. *et al.* Wearable Ultrahigh Current Power Source Based on Giant Magnetoelastic Effect in Soft Elastomer System. *ACS Nano* **15**, 20582–20589 (2021).

142. Zhao, X. *et al.* Soft fibers with magnetoelasticity for wearable electronics. *Nat Commun* **12**, 6755 (2021).

143. Chen, G. *et al.* Discovering giant magnetoelasticity in soft matter for electronic textiles. *Matter* **4**, 3725–3740 (2021).

144. Davino, D., Giustiniani, A. & Visone, C. The piezo-magnetic parameters of Terfenol-D: An experimental viewpoint. *Physica B, Condensed Matter* **407**, 1427–1432 (2012).

145. Datta, S., Atulasimha, J., Mudivarthi, C. & Flatau, A. B. Stress and magnetic field-dependent Young's modulus in single crystal iron–gallium alloys. *Journal of Magnetism and Magnetic Materials* **322**, 2135–2144 (2010).

146. Jen, S. U., Lo, Y. & Pai, L. Temperature dependence of mechanical properties of the Fe 81 Ga 19 (Galfenol) alloy. *Journal of Physics D: Applied Physics* **49**, 145004 (2016).

147. Braibant, S., Giacomelli, G. & Spurio, M. *Particles and Fundamental Interactions: An Introduction to Particle Physics*. (Springer Science & Business Media, 2011).

148. Boehme, M. & Charton, C. Properties of ITO on PET film in dependence on the coating conditions and thermal processing. *Surface and Coatings Technology* **200**, 932–935 (2005).

149. Løveng Sunde, T. O. *et al.* Transparent and conducting ITO thin films by spin coating of an aqueous precursor solution. *Journal of Materials Chemistry* **22**, 15740–15749 (2012).

150. Michelson, N. J., Eles, J. R., Vazquez, A. L., Ludwig, K. A. & Kozai, T. D. Y. Calcium activation of cortical neurons by continuous electrical stimulation: Frequency dependence, temporal fidelity, and activation density. *J Neurosci Res* **97**, 620–638 (2019).

151. Brocker, D. T. & Grill, W. M. Principles of electrical stimulation of neural tissue. *Handb Clin Neurol* **116**, 3–18 (2013).

152. Lossi, L. & Merighi, A. The Use of ex Vivo Rodent Platforms in Neuroscience Translational Research With Attention to the 3Rs Philosophy. *Front Vet Sci* **5**, 164 (2018).

153. Azzarelli, R., Oleari, R., Lettieri, A., Andre', V. & Cariboni, A. In Vitro, Ex Vivo and In Vivo Techniques to Study Neuronal Migration in the Developing Cerebral Cortex. *Brain Sci* **7**, 48 (2017).

154. Xu, Z. *et al.* How to reprogram human fibroblasts to neurons. *Cell & Bioscience* **10**, 116 (2020).

155. Song, Y. *et al.* Asymmetric Cell Division of Fibroblasts is An Early Deterministic Step to Generate Elite Cells during Cell Reprogramming. *Adv. Sci.* **8**, 2003516 (2021).

156. Chang, Y.-J., Hsu, C.-M., Lin, C.-H., Lu, M. S.-C. & Chen, L. Electrical stimulation promotes nerve growth factor-induced neurite outgrowth and signaling. *Biochimica et Biophysica Acta (BBA) - General Subjects* **1830**, 4130–4136 (2013).

157. Brosenitsch, T. A. & Katz, D. M. Physiological Patterns of Electrical Stimulation Can Induce Neuronal Gene Expression by Activating N-Type Calcium Channels. *J. Neurosci.* **21**, 2571–2579 (2001).

158. Calcium Signaling in Neurons: Molecular Mechanisms and Cellular Consequences. https://www.science.org/doi/abs/10.1126/science.7716515.

159. Deng, W. *et al.* Computational investigation of ultrasound induced electricity generation via a triboelectric nanogenerator. *Nano Energy* **91**, 106656 (2022).

160. Wang, Z. L. Entropy theory of distributed energy for internet of things. *Nano Energy* **58**, 669–672 (2019).

161. Wang, Z. L. On the first principle theory of nanogenerators from Maxwell's equations. *Nano Energy* **68**, 104272 (2020).

162. Wang, Z. L. Nanogenerators, self-powered systems, blue energy, piezotronics and piezo-phototronics – A recall on the original thoughts for coining these fields. *Nano Energy* **54**, 477–483 (2018).

163. Zhao, X., Askari, H. & Chen, J. Nanogenerators for smart cities in the era of 5G and Internet of Things. *Joule* **5**, 1391–1431 (2021).

164. Lai, S.-N. *et al.* Ultrasensitivity of self-powered wireless triboelectric vibration sensor for operating in underwater environment based on surface functionalization of rice husks. *Nano Energy* **60**, 715–723 (2019).

165. Zhu, G., Peng, B., Chen, J., Jing, Q. & Lin Wang, Z. Triboelectric nanogenerators as a new energy technology: From fundamentals, devices, to applications. *Nano Energy* **14**, 126–138 (2015).

166. Xiao, X., Chen, G., Libanori, A. & Chen, J. Wearable Triboelectric Nanogenerators for Therapeutics. *Trends in Chemistry* **3**, 279–290 (2021).

167. Tat, T., Libanori, A., Au, C., Yau, A. & Chen, J. Advances in triboelectric nanogenerators for biomedical sensing. *Biosensors and Bioelectronics* **171**, 112714 (2021).

168. Zhou, Z. *et al.* Sign-to-speech translation using machine-learning-assisted stretchable sensor arrays. *Nat Electron* **3**, 571–578 (2020).

169. Zhang, S. *et al.* Leveraging triboelectric nanogenerators for bioengineering. *Matter* **4**, 845–887 (2021).

170. Wang, J. *et al.* Investigation of Low-Current Direct Stimulation for Rehabilitation Treatment Related to Muscle Function Loss Using Self-Powered TENG System. *Advanced Science* **6**, 1900149 (2019).

171. Zheng, Q. *et al.* In Vivo Powering of Pacemaker by Breathing-Driven Implanted Triboelectric Nanogenerator. *Advanced Materials* **26**, 5851–5856 (2014).

172. Yan, C. *et al.* A linear-to-rotary hybrid nanogenerator for high-performance wearable biomechanical energy harvesting. *Nano Energy* **67**, 104235 (2020).

173. Zhao, H. *et al.* Dual-Tube Helmholtz Resonator-Based Triboelectric Nanogenerator for Highly Efficient Harvesting of Acoustic Energy. *Advanced Energy Materials* **9**, 1902824 (2019).

174. Xi, Y. *et al.* High efficient harvesting of underwater ultrasonic wave energy by triboelectric nanogenerator. *Nano Energy* **38**, 101–108 (2017).

175. Chen, C. *et al.* Micro triboelectric ultrasonic device for acoustic energy transfer and signal communication. *Nat Commun* **11**, 4143 (2020).

176. Miller, D. L. *et al.* Overview of Therapeutic Ultrasound Applications and Safety Considerations. *Journal of Ultrasound in Medicine* **31**, 623–634 (2012).

177. Mazzilli, F., Thoppay, P. E., Praplan, V. & Dehollain, C. Ultrasound energy harvesting system for deep implanted-medical-devices (IMDs). in *2012 IEEE International Symposium on Circuits and Systems (ISCAS)* 2865–2868 (2012). doi:10.1109/ISCAS.2012.6271911.

178. Hinchet, R. *et al.* Transcutaneous ultrasound energy harvesting using capacitive triboelectric technology. *Science* (2019) doi:10.1126/science.aan3997.

179. Ultrasound-Induced Wireless Energy Harvesting for Potential Retinal Electrical Stimulation Application - Jiang - 2019 - Advanced Functional Materials - Wiley Online Library. https://onlinelibrary.wiley.com/doi/full/10.1002/adfm.201902522?casa_token=fyFV0sBVVKcAAAAA%3AnAKOZsG-a7VnIuMKcbvSNP-UeFeBlEIJW-dvmM9jJ6dPc26hAs3qIc25OqZPm7DLK699KVkDfBweTUA.

180. Hannan, M. A., Mutashar, S., Samad, S. A. & Hussain, A. Energy harvesting for the implantable biomedical devices: issues and challenges. *BioMedical Engineering OnLine* **13**, 79 (2014).

181. Xiao, X. *et al.* Triboelectric Nanogenerators for Self-Powered Wound Healing. *Advanced Healthcare Materials* **10**, 2100975 (2021).

182. Liu, G. *et al.* Flexible Drug Release Device Powered by Triboelectric Nanogenerator. *Advanced Functional Materials* **30**, 1909886 (2020).

183. Parandeh, S. *et al.* Advances in Triboelectric Nanogenerators for Self-Powered Regenerative Medicine. *Advanced Functional Materials* **31**, 2105169 (2021).

184. Hassija, V., Chamola, V., Bajpai, B. C., Naren & Zeadally, S. Security issues in implantable medical devices: Fact or fiction? *Sustainable Cities and Society* **66**, 102552 (2021).

185. Wang, Z. L., Lin, L., Chen, J., Niu, S. & Zi, Y. *Triboelectric Nanogenerators*. (Springer International Publishing, 2016). doi:10.1007/978-3-319-40039-6.

186. Zheng, M. *et al.* Cd(OH)2@ZnO nanowires thin-film transistor and UV photodetector with a floating ionic gate tuned by a triboelectric nanogenerator. *Nano Energy* **73**, 104808 (2020).

187. Zhang, W. *et al.* A general charge compensation strategy for calibrating the voltage of a triboelectric nanogenerator measured by a capacitive circuit. *Nano Energy* **86**, 106056 (2021).

188. Zhou, Y., Deng, W., Xu, J. & Chen, J. Engineering Materials at the Nanoscale for Triboelectric Nanogenerators. *Cell Reports Physical Science* **1**, 100142 (2020).

189. Zhang, W. *et al.* Measuring the actual voltage of a triboelectric nanogenerator using the non-grounded method. *Nano Energy* **77**, 105108 (2020).

190. Xu, J., Zou, Y., Nashalian, A. & Chen, J. Leverage Surface Chemistry for High-Performance Triboelectric Nanogenerators. *Frontiers in Chemistry* **8**, (2020).

191. Zou, H. *et al.* Quantifying and understanding the triboelectric series of inorganic non-metallic materials. *Nat Commun* **11**, 2093 (2020).

192. Zou, H. *et al.* Quantifying the triboelectric series. *Nat Commun* **10**, 1427 (2019).

193. Wang, Z. L., Chen, J. & Lin, L. Progress in triboelectric nanogenerators as a new energy technology and self-powered sensors. *Energy Environ. Sci.* **8**, 2250–2282 (2015).

194. Duck, F. A., Baker, A. C. & Starritt, H. C. *Ultrasound in Medicine*. (CRC Press, 2020).

195. Carovac, A., Smajlovic, F. & Junuzovic, D. Application of Ultrasound in Medicine. *Acta Inform Med* **19**, 168 (2011).

APPENDIX

I. Future of soft bioelectronics: electrical stimulation for therapy

This section is summarized in the following published article which we have written, and which follows next page.

Conta G, ***Libanori A**, Tat T, Chen G, Chen J. Triboelectric nanogenerators for therapeutic electrical stimulation. *Advanced Materials*. 2021 Jul;33(26):2007502.

ADVANCED MATERIALS
www.advmat.de

Triboelectric Nanogenerators for Therapeutic Electrical Stimulation

*Giorgio Conta, Alberto Libanori, Trinny Tat, Guorui Chen, and Jun Chen**

Current solutions developed for the purpose of in and on body (IOB) electrical stimulation (ES) lack autonomous qualities necessary for comfortable, practical, and self-dependent use. Consequently, recent focus has been placed on developing self-powered IOB therapeutic devices capable of generating therapeutic ES for human use. With the recent invention of the triboelectric nanogenerator (TENG), harnessing passive human biomechanical energy to develop self-powered systems has allowed for the introduction of novel therapeutic ES solutions. TENGs are especially effective at providing ES for IOB therapeutic systems given their bioconformability, low cost, simple manufacturability, and self-powering capabilities. Due to the key role of naturally induced electrical signals in many physiological functions, TENG-induced ES holds promise to provide a novel paradigm in therapeutic interventions. The aim here is to detail research on IOB TENG devices applied for ES-based therapy in the fields of regenerative medicine, neurology, rehabilitation, and pharmaceutical engineering. Furthermore, considering TENG-produced ES can be measured for sensing applications, this technology is paving the way to provide a fully autonomous personalized healthcare system, capable of IOB energy generation, sensing, and therapeutic intervention. Considering these grounds, it seems highly relevant to review TENG-ES research and applications, as they could constitute the foundation and future of personalized healthcare.

1. Introduction

Owing to the ever-growing prominence of devices within the Internet of Things (IoTs) paradigm, and increasing demands for personalized healthcare, implantable (in body), and surface (on body) bioelectronics—collectively known as in and on body (IOB) bioelectronics—are set to become key players in the future of healthcare.[1–3] With the advent of 5G wireless networks, the use of IOB bioelectronics is expected to dramatically increase. The National Intelligence Council predicts that most of our everyday objects will be interconnected to the IoT ecosystem by 2025.[4] Although most IOB bioelectronics are focused on sensing,[5–8] there is a growing trend to develop minimally invasive therapeutic devices focused, for instance, on the application of electrical stimulation (ES).[9] Electrical impulses are at the basis of cognitive and skeletal functions for human beings, constituting a fundamental messaging vehicle within the human nervous system.[10] Leveraging on the existence of natural electrical impulses, external ES can be employed as a natural alternative to addressing medical disorders[11] where synthetically derived small molecules and biotherapeutics fall short.[12]

Electrical impulses have been shown to enhance tissue regeneration processes and aid with therapy in unmet medical needs, including bone fractures,[13–15] skin wounds,[16–18] obesity (satiation),[19–22] cancer,[23–25] muscular dystrophy,[26–28] soft tissue damage,[29–31] hair loss,[32–36] and bladder control dysfunction.[37–39] IOB bioelectronics can provide localized ES with tailored benefits. Considering the large number of pathologies that can be addressed through ES, attaining a self-sustainable bioelectronic system capable of delivering therapeutic ES can provide an invaluable tool to the continued development of personalized healthcare within an IoT ecosystem.

The recent development of the triboelectric nanogenerator (TENG) has sparked a lot of interest in generating body area networks capable of sensing as well as treating various conditions considering TENGs can provide self-powered and bioconformable alternatives to conventional ES approaches. Current wearable devices capable of emitting therapeutic ES come in various morphologies that are heterogeneous in nature and varying in form, depending on the sought intervention. For instance, within regenerative medicine applications, including wound healing, tissue and bone regeneration, the devices administering ES are generally composed of an electronic skin-like structure.[40–49] Conversely, devices creating a mind–body neural interface to help address problems such as obesity (satiation) and bladder-related conditions, generally retain a neural dust platform carefully wrapped around the peripheral nerve of interest.[50–58] Although not directly used as a therapeutic agent, ES is also known to aid with drug delivery and is generally integrated in devices composed of stretchable elastomers which contain therapeutic depots of drug loaded nanoparticles.[59–68] Finally, solutions employing ES to target cellular engineering applications, such as cellular excitation and cancer therapy, retain a relatively simple structure comprising a power source

G. Conta, A. Libanori, T. Tat, G. Chen, Prof. J. Chen
Department of Bioengineering
University of California, Los Angeles
Los Angeles, CA 90095, USA
E-mail: jun.chen@ucla.edu

The ORCID identification number(s) for the author(s) of this article can be found under https://doi.org/10.1002/adma.202007502.

DOI: 10.1002/adma.202007502

connected to an organic light emitting diode element.[69–77] Unlike the above examples, certain therapeutic ES applications including muscle recovery[78] and hair growth[79] present limited wearable bioelectronics options, suggesting that, even though various approaches are known within the current literature, it is difficult to highlight significant commonalities in their engineering designs.

In spite of recent advances of IOB bioelectronic ES's use in the medical field, important limitations still persist. Primarily, external power sources are still necessary, usually leading to both impractical and uncomfortable solutions.[80–83] Moreover, most of these devices utilize batteries, which contain toxic chemicals that pose both cellular and physiological health risks, rendering battery-powered devices a temporary and often non-implantable solution. To overcome this limitation, researchers have developed wearable technologies capable of generating their own electrical energy, bypassing the need for battery use.[84–92] Moreover, by operating on a high voltage and current supply, these devices also pose heat-related complications.[93,94] Finally, many of these devices are often bulky in nature and unsuitable for everyday use given the lack of cohesiveness between their various subparts, and the generally unsuitably high Young's Modulus of the materials employed.[95–97] In order to make these devices more suitable for everyday use, using biomimicking materials[98–106] capable of bending with the various motions of the human body would present obvious advantages.

With the relatively recent invention of the TENG,[107–118] wearable bioelectronics are evolving to become ever more suited to the human body. TENGs are able to harness the coupling effect of contact electrification[119–121] and electrostatic induction [122,123] between two thin films, and harness electricity from a myriad of natural biomechanical movements. The TENG has emerged as a fundamentally new and efficient technology to convert human biomechanical movements into electricity via its innate modus operandi. When the TENG's triboelectric layers, which are made of materials on the opposite sides of the triboelectric series, cycle between biomechanical motion induced contact and separation, an alternating current between the two electrodes is generated, inducing an electrical current that can be employed for a plethora of biomedical applications. As of now, within the biomedical field, TENG-generated electricity has been utilized to power wearable devices, enable the sensing of physiological functions such as heart rate, and treat various diseases and conditions through therapeutic ES.[124–136] There are many different types of TENG working modes including vertical contact separation,[137,138] in-plane sliding,[139,140] single electrode,[141–144] and freestanding,[145–148] which give further leeway to utilizing TENG devices for IOB therapeutic applications due to the ability of TENG devices to harness electricity from a wide variety of biomechanical motions. TENGs' versatility renders them optimal self-powered biomedical sensors,[149–155] providing sensing insight via means of signal-to-function association. This versatility can be easily manifested by employing a TENG-coupled microprocessor that extrapolates biological information such as heart rate[156,157] and blood pressure.[158] The electricity produced by these different types of TENG devices can not only be used to deduce biological information as a sensor, but it can also be utilized as a therapeutic device applying ES to different parts of the body via electrodes. Implantable versions are also being developed by embedding standard TENGs in protective pouches composed of hydrophobic materials that serve as a barrier, shielding the device from the unfavorable conditions in the human body.[159–161] These protective measures are also necessary to protect TENG devices from environmental conditions when utilized for IOB applications.[162–165]

Owing to their unique working mechanism and a wide range of available material choices, TENG devices' characteristic flexible, bioconformable, soft, and lightweight properties make them a perfect candidate for IOB bioelectronics, especially considering long-term durability and resistance to fatigue. Capturing electricity from physiological movements ranging from blood circulation to ambulatory motion can allow for ubiquitous IOB use of TENG devices. In addition, TENG technology can be easily integrated with common manufacturing techniques, which, in conjunction with the use of low-cost materials, make TENG devices a scalable and affordable option.[166,167]

Through the conjunction of triboelectrification and electrostatic induction between a broad range of flexible materials, including silk, wool, and cotton, as well as rigid materials, including various commonly manufactured synthetic compounds, TENG devices can be rendered soft or rigid. However, in the space of IOB TENG use, there has been specific effort focused on developing body-conforming soft TENG devices due to their increased wearability.[168–170] The soft and flexible nature of certain TENG devices is not their only strong suit; operating TENG devices emit reduced heat, considering the low current output they generate. This, moreover, enables TENG devices to remain biocompatible while still achieving high voltage outputs.[171–174] In addition, TENG devices provide a self-sustainable power source, which overall permits for the integration of the power source into the device itself, yielding a product that is more compact, comfortable, and bioconformable. Using TENG devices as a source of ES for therapy can provide a platform solution to a number of unmet medical needs (**Figure 1**) including regenerative medicine, neural engineering, rehabilitation engineering, and pharmaceutical engineering. Regenerative medicine includes the subfields of orthopedic engineering,[175–177] wound healing,[178–180] and hair growth.[181] The field of neural engineering comprises the modulation of motor function,[182–186] neuronal cell differentiation,[187,188] as well as weight,[189] and bladder control.[190,191] Rehabilitation engineering comprises interventions in muscle recovery[192–194] and cardiac therapy.[195] Finally, in pharmaceutical engineering, we review how different forms of drug delivery can be supported by TENG-ES,[196–201] including cancer therapies.[202] Remarkably, the TENG provides a unified solution to diverse health problems.

Here, we present an overall depiction of research on IOB TENGs and their various therapeutic ES-based applications. The following sections will cover research applications of TENGs in regenerative medicine, neural engineering, rehabilitation engineering, and pharmaceutical engineering. In order to achieve a broader understanding and present an all-inclusive scope of the field, we will cover the biological effects and significance of each application of

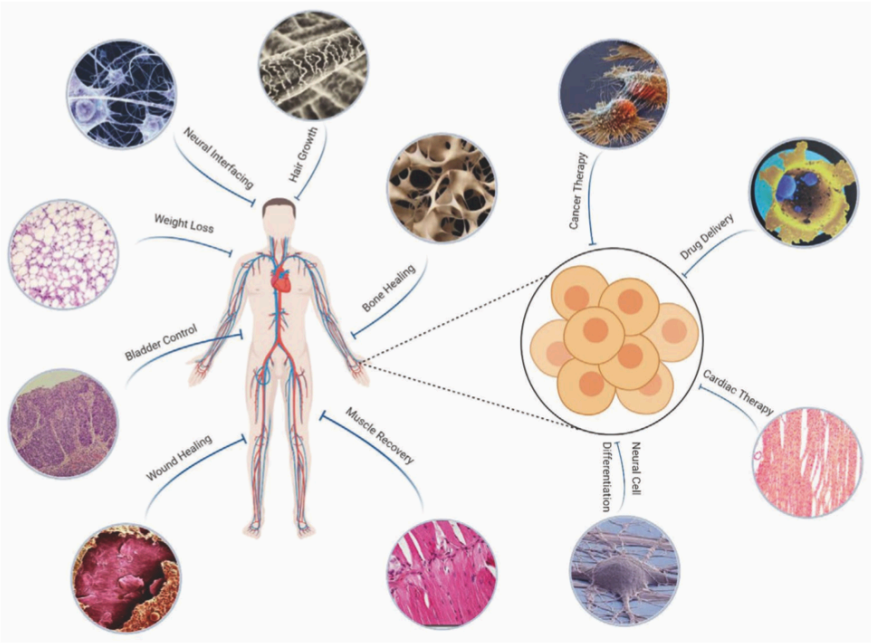

Figure 1. Schematic illustration of the various applications of therapeutic TENG-ES, ranging from physiological applications such as bladder control to cellular applications such as cancer therapy.

these TENGs. Finally, we will discuss the overall challenges and next steps for the future of IOB TENGs for ES, in order to highlight the technology's potential to change the course and development of personalized healthcare for the better. The mechanistic reasons behind ES's beneficial effect on a number of regenerative and proliferative processes are still subject to investigation, and are subjective in each ES application and field. However, there is the general understanding that ES aids at the tissue level by increasing capillary perfusion and blood flow, thus optimizing site oxygenation and healing, as well as at the cellular level by means of electric field creation, which encourages fibroblast activity, granulation, and cellular alignment.[203]

2. Regenerative Medicine

Regenerative medicine is the study of replacing or regenerating parts of the body at the cellular, tissue, or organ level, by enhancing and leveraging on the body's existing regenerative capabilities.[204] This field of study is becoming of vital importance in our ever-aging population as advancing medical standards are increasing the average global lifespan. Indeed, leaders of the field have predicted that due to progress of medicinal technology there is a more than 50% probability that by 2030 the national female life expectancy will surpass the 90-year-old mark, and similar trends are predicted for male life expectancy in the coming years, thus creating a need to help regenerate aged tissues and organs.[205] Effectively harnessing regenerative medicine technologies would drastically contribute to improving the quality of life in our aging population,[206] and there is a concentrated effort by researchers to use therapeutic ES in this aspect.[207,208] The presence of an electric potential difference has been identified in regenerative processes involving bones,[209] the skin,[210] hair follicles,[211] and other tissue types.[212] It has been long assumed that applying external ES induces a positive effect on these processes, with numerous studies demonstrating that ES can promote cellular proliferation and differentiation, two processes critical to tissue regeneration.[175–181]

Rather than rely on large extracorporeal devices to apply a constant supply of ES, the advent of TENG technology can allow for continuous ES treatment without the need for third party intervention, including travelling to a physician or point of care, all due to TENG's self-sufficient nature. In the past three years, TENG devices have been developed for applications to numerous areas within the field of regenerative medicine, including orthopedic engineering,[175–177] wound healing,[178–180] and hair growth[181] as an effective tool to solve health problems that affect the world's population.

2.1. Orthopedic Engineering

There are a number of diseases that affect the functioning of bones, of which osteoporosis represents a large socioeconomic affliction, characterized by the degradation of bones into brittle and easily fractured states.[213,214] Osteoporosis and other bone-targeting diseases greatly decrease the quality of life as well as the life expectancy of many, considering that osteoporosis alone results in fractures responsible for nearly 500 000 hospitalizations and a direct expenditure of $12 to 18 BN in the

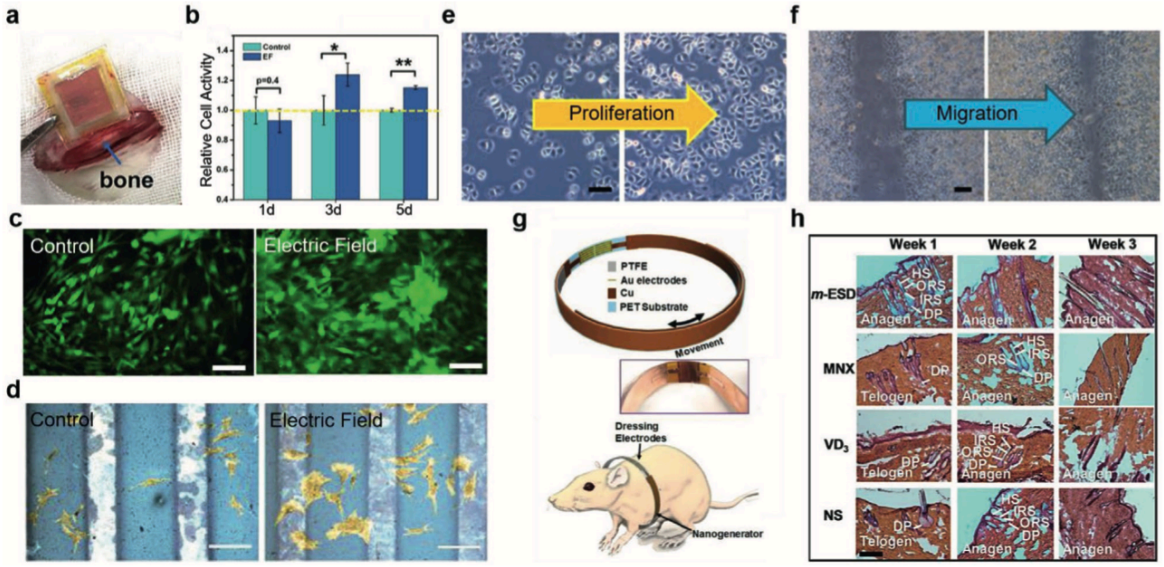

Figure 2. a–h) TENG-ES therapeutic devices for regenerative medicine applications including bone healing (a–d), wound healing (e–g), and hair growth (h). a) Flexible TENG device composed of Al and PTFE triboelectric layers implanted near the femur. b) MTT analysis comparing proliferation of preosteoblasts with and without exposure to TENG-ES. c) Optical fluorescence images of preosteoblasts with and without exposure to an electric field. d) Extracellular ALP levels in preosteoblasts with and without exposure to TENG-ES (scale bars: 200 μm). a–d) Reproduced with permission.[175] Copyright 2019, Elsevier. e) Proliferation (scale bars: 100 μm) and f) migration of fibroblasts exposed to TENG-ES (scale bars: 200 μm). e,f) Reproduced with permission.[178] Copyright 2019, Elsevier. g) Device structure, material usage, and in vivo testing setup of effect of TENG-ES on wound healing in rat models. Reproduced with permission.[179] Copyright 2019, American Chemical Society. h) H&E staining of epidermal cells showing various hair growth stages at different times from various treatments including TENG-ES. Reproduced with permission.[181] Copyright 2019, American Chemical Society.

US.[215] In order to address this issue, researchers have developed various TENG devices capable of providing constant therapeutic ES, which have been shown to promote osteogenesis and bone tissue regeneration both in vitro and in vivo.[175–177] Seemingly, these TENG devices could be applied to osteoporotic patients to help regenerate their bone tissue and enhance their quality of life.

There are three processes that must occur for correct bone tissue regeneration: osteoblast differentiation, attachment, and proliferation, all of which TENG-ES has been shown to promote.[175–177] Tian et al. conducted a study comprising three primary experiments aimed at studying the effect of TENG-ES on osteoblast differentiation, attachment, and proliferation.[175] In order to track the different stages of osteoblast differentiation during ES, a specific line of preosteoblasts often found in mice, MC3T3-E1 cells, were specifically tracked as they only become functional once they have undergone differentiation into osteoblasts. Furthermore, Tian et al. utilized alkaline phosphatase (ALP), an early marker for osteoblast differentiation, to determine the degree of osteoblast differentiation resulting from exposure to ES. When assessing the levels of osteoblast attachment due to ES, Tian et al. used phalloidin and 4′,6-diamidino-2-phenylindole (DAPI) to stain the cytoskeleton and nucleus, respectively, which shed light on the adhesion effectiveness of the MC3T3-E1 cells. The researchers utilized 3-(4,5-dimethylthiazol-2-yl)-2,5-diphenyltetrazolium bromide for (MTT) assay with the purpose of assessing osteoblast proliferation, as the resulting dissolved crystals represented viable proliferated cells. With these three experiments, the positive effects that TENG-ES had on osteoblast differentiation, attachment, proliferation, and consequently bone tissue regeneration, could be readily observed.

In order to provide a local and specific intervention, a TENG device aimed at bone regeneration via means of ES, ought to be implanted at the site of the bone fracture (**Figure 2**a). Due to the humid and hostile environment within the human body, the implantable TENG requires protection from external factors, as its working mechanism depends on complete absence of water and humid conditions. Several types of protective coverings have been developed to this effect, including biocompatible materials that allow for long-term tolerance of implanted devices. These protective coverings slightly reduce the power output of the TENG. However, with the TENG being implanted so close to the site of the bone fracture, TENGs have been shown to produce ample ES that promotes the processes associated with bone tissue growth.[175] Utilizing a miniaturized TENG for ES is surely an added benefit given its localizability in close proximity to the fracture site.

Tracking osteoblast differentiation is a critical process in determining the effect of TENG-ES on bone tissue growth, but recent studies have failed to establish an effective methodology with which to quantify the differentiation potential of osteoblasts with and without exposure to TENG-ES. In the previously mentioned study conducted by Tian et al. preosteoblasts were utilized, allowing them to determine a relative ratio of differentiated preosteoblasts to undifferentiated preosteoblasts from the exposure to TENG-ES, based on microscopic image analyses. However, this methodology presented flaws preventing an

assessment of the exact percentage of differentiated preosteoblasts, which would have yielded a more convincing result. In addition, the use of ALP is ineffective in providing a marker for the entire differentiation process, as it only shows the existence of early osteoblast differentiation.

Osteoblast attachment is yet another critical process in bone regeneration, with ALP used as an indicative biomarker to assess the presence of both early osteoblast differentiation as well as early bone matrix formation. Early bone matrix formation requires osteoblast attachment as it comprises the first step in the regeneration of bone tissue following the differentiation of preosteoblasts into mature osteoblasts. Tian et al. noted a higher concentration of ALP around the osteoblasts in the extracellular matrix, which they attributed to the ES therapy (Figure 2d). In addition, the staining of the seeded preosteoblasts with phalloidin and DAPI resulted in fluorescence microscopy images displaying an ≈45% increase in cell attachment and 78% increase in cellular spreading following 1 h of ES.[175] It is thought that ES influences the cellular alignment of the cells of interest due to the generation of local field potentials.

In the same study, osteoblast proliferation at the site of a fracture was investigated to garner an understanding of TENG-ES's regenerative potential. Here, the authors noted increased osteoblast proliferation levels correlated with TENG-ES exposure, corroborating the results from the MTT assay (Figure 2b). As shown in Figure 2b, after three and five days of the TENG-ES at the area of the bone fracture, cells proliferated 23.82% and 15.18% more than cells lacking exposure to ES. This is a significant increase in osteoblast proliferation, especially given the short time interval of ES stimulation. Bone tissue healing is an extremely long process that can take up to eight weeks, but it is hoped that through the use of TENG-ES, this timeline can be dramatically decreased, with the in vitro results showing promise for this potential future development.[175–177] These examples show promise in using TENG-ES as a means to not only promote healing of bone tissue, but also strengthen bone tissue in osteoporotic patients, whose bone integrity is compromised.[216]

The processes of osteoblast differentiation, attachment, and proliferation that promote bone tissue regeneration are also positively affected by the amount of cytosolic calcium ions, which was observed to be correspondingly upregulated by the introduction of TENG-ES. This ES was seen to activate the calcium ion signal transduction pathway in such a manner that it promoted the movement of calcium ions into the differentiated osteoblasts. As seen in Figure 2c, fluorescence imaging of bone tissue cells showed a significantly higher concentration of calcium ions with ES, compared to the control. This increase in the concentration of cytosolic calcium ions has been hypothesized to promote the cellular attachment, proliferation, and differentiation processes characteristic of bone tissue regeneration. However, the specific mechanisms behind these processes are still unknown.[175]

In summary, using TENG-ES to address bone fractures and bone-related diseases like osteoporosis has shown promising results via what are thought to be key mechanisms including promotion of osteoblast differentiation, attachment, and proliferation.

2.2. Wound Healing

Wounds are ubiquitously present in everyone's lives with wound healing representing a process that is critical to our survival, where disruption in this critical process can have deadly consequences, from infections, to scars, clots, and hemorrhage formation.[217,218] Various TENG devices have been developed to apply therapeutic ES to wound sites and have been shown to enhance the wound healing process in a number of ways.[178–180] The added benefit of employing TENG for ES is that those are microscaled and can be made to tailor specific areas depending on the size and location of the wound. This approach can ensure uniform ES to the affected wound site, minimizing patient discomfort.

The wound healing process of the skin, which is characterized by the repair of damage done to the dermis and epidermis, can be broken down into three stages: inflammatory, proliferative, and remodeling.[219,220] Since ES has not been shown to have much of an effect on the function of immune cells critical in the inflammatory response, researchers studying the effectiveness of TENG devices on wound healing have concentrated on monitoring the fibroblast migration, proliferation, and differentiation processes, characteristic to the proliferative and remodeling stages of the wound healing process.[221] Much like osteoblasts are known precursors to bone healing protocols, fibroblasts play a similar role for wound healing, breaking down the fibrin clot, rebuilding the extracellular matrix (ECM) with collagen, and promoting wound contraction. First, fibroblasts infiltrate the wound site, where they proliferate and interact with other cells including keratinocytes and mast cells, which further promote the wound healing process.[222] Subsequently, fibroblasts differentiate into myofibroblasts and build an ECM structure with collagen, while also secreting glycoproteins and cytokines that further upregulate vicinal fibroblasts within a positive feedback loop. The original fibrin-based ECM is subsequently replaced with a collagen-based ECM and the edges of the wound contract inward due to the actions of the fibroblasts.[223]

Before the fibroblasts are able to reconstruct the ECM, their migration to the wound site is necessary. In a study conducted by Hu et al., TENG-ES was applied to fibroblasts in vitro, where the two genes related to the migration of fibroblasts were observed to be significantly upregulated,[178,224] suggesting that TENG-ES promoted the migration of fibroblasts to the wound site. In addition, a significantly higher concentration of fibroblasts was found at the wound site when exposed to TENG-ES, compared to the control (Figure 2e).[178]

The two most important processes within the proliferative and remodeling phases of the wound healing process are fibroblast proliferation and differentiation, considering fibroblast proliferation directly drives the collagen-based ECM reconstruction of the wound, while differentiation of fibroblasts into myofibroblasts promotes the inflammatory response necessary for the recruitment of molecules and cells critical to wound healing and wound contraction.[225] It is speculated therefore, that in order to promote wound healing, TENG-ES must positively influence these two processes. In Figure 2f, Hu et al. showed that TENG-ES significantly upregulated fibroblast proliferation at the wound site,[178] although limited direct evidence

of fibroblast differentiation into myofibroblasts was presented, despite the determination of the existence of the wound contraction process, a process largely controlled by myofibroblast function.[225] Considering the role in supporting fibroblast migration, proliferation, and differentiation, TENG-ES seems to positively affect the wound healing process.

Although ES does have a positive effect on wound healing-associated migration, proliferation, and differentiation of fibroblasts, utilizing the correct current intensity to optimize therapeutic interventions is of paramount importance. Through the use of a TENG-coupled rheostat, Hu et al. were able to apply variable amounts of current to the wound site. When only 2 μA were applied to the wound site, there was virtually no effect on fibroblast proliferation, but when a 100 μA current was administered, proliferation of fibroblasts was inhibited.[178] The researchers speculated that this was likely associated with heat stroke[226,227] as peak promotion of fibroblast proliferation occurred at 50 μA of current, with a promoting rate of 53.8 ± 2.66% after just two days of TENG-ES application.[178]

Wound healing is associated with a concomitant inflammatory response in which growth factors are highly involved.[222] Growth factors trigger the inflammatory response by interacting with fibroblasts and other cells, to promote angiogenesis and cell recruitment. Through continuous TENG-ES, increased concentrations of growth factors were noted at the wound site. These growth factors upregulated proliferating cell nuclear antigen, the marker gene for fibroblast proliferation, and enhanced the fibroblast proliferation process significantly, suggesting that TENG-ES promoted the proliferation of fibroblasts by increasing growth factor concentrations at the wound site.[178]

Although continuous TENG-ES is necessary for the promotion of the wound healing process, it is important to address the possible side effects that continuous ES could have on surrounding cells, especially since previous ES wound healing technologies have shown a propensity to damage surrounding tissue after prolonged use,[226,227] with associated heat oftentimes being the culprit of the damage. Fortunately, as stated earlier, owing to TENG's low current consumption, little to no damaging heat was produced during the study. In addition, TENG produces its electricity through the natural means of the triboelectric effect, thus not holding a large amount of charge localized in one area, which could lead to detrimental biological effects.[228] However, damaging cells through heat created by current is not the only potentially detrimental side effect of TENG-ES for wound healing, and other potential side effects need to be determined. In a study conducted by Li et al., the potential side effects of TENG-ES were studied in which TENG-ES did not induce deformation in the actin cytoskeleton, which performs a vital role in the contraction of a wound, and there were no toxicity effects detected.[180] Seemingly, TENG-ES has no perceivable negative side effects on the wound healing process and surrounding cells.

The final process that is carried out in wound healing is the remodeling of the skin tissue characterized by the epithelialization of the epidermis. In a related study, as shown in Figure 2g, Long et al. utilized a TENG band to apply therapeutic TENG-ES to wounds in a rat model, in which the PTFE layer slides back and forth in relation to the Cu layer, thus generating electricity from the rats' breathing and bodily motions. This electricity was then applied to the wound, and the endogenous electrical field that was created as a result of TENG-ES from the band was able to effectively promote the healing process of the rats' wounds.[179] However, at the moment, wound healing through TENG-ES has only been tested on rats, and loose skinned animals like rats heal their wounds mainly through contraction, whereas humans heal their wounds predominantly through re-epithelialization.[229,230] Although the aforementioned TENG-ES wound healing technologies seems effective on rats,[178–180] there are stark differences in the wound healing processes between rats and humans, which puts into question whether or not TENG-ES would be as effective on humans. Regardless, the effectiveness of TENG-ES on human acute skin wounds should be studied as TENG-ES could prove to be an effective therapy capable of revolutionizing the field.

TENG-ES of acute skin wounds, overall, seems to have a variety of positive effects including enhancing fibroblast migration to the wound site, fibroblast proliferation, and differentiation, as well as enhancing the concentration of growth factors critical to the cellular recruitment function of the inflammatory response. Ultimately, TENG-ES has been shown to promote nearly every aspect of the wound healing process, making it a promising future therapy for acute skin wounds via the means of targeted IOB bioelectronics. However, in order to solidify this statement, more research needs to be conducted applying TENG-ES to human skin or human skin-like models.

2.3. Hair Growth

Alopecia, or hair loss, is a condition that affects over 50 million people in the US alone and is due to a number of causes including lack of growth factors and/or a defect in the hair growth cycle. This condition leads to localized, dispersed, or even universal hair loss, which can be both temporary or chronic.[231] There are a number of current treatments for alopecia, virtually all of which target hair growth on the scalp, and which range from topical treatments to surgical procedures, though they all present downsides, including limited efficacy, and undesired side effects such as infection and scarring.[232,233] Owing to their flexible and malleable architectural design, TENGs can be constructed in mesh-like structures able to supply therapeutic ES as well as contain suitable spaces to let nascent hair grow unimpeded.

Hair growth is partly dependent on the nutrition supplied by the blood vessels to hair follicles in which hair growth begins. This hair growth cycle occurs in three stages: anagen, catagen, and telogen.[234] Anagen is characterized as the growing phase in which the cells at the root of the hair are actively dividing, and forcing other hair cells out of the follicle to eventually create the hair shaft that becomes visible.[234,235] Anagen normally occurs for three to five years at a time at the scalp, and is characterized by the growth of the hair shaft as it emerges from the hair follicle embedded within the skin of the scalp and becomes visible. Subsequently, catagen occurs and hair growth stops while the "club hair" forms around the root of the hair follicle, essentially cutting off the hair from the blood supply.[236] Finally, in telogen, there is little to no cell division at the follicular level,

with the hair follicle and club hair both halted in growth, at which point the hair is shed, hair shaft is lost, and only the hair follicle is left behind.[237,238] Here the cells composing the hair follicle actively divide, and the transition from telogen to anagen is made, thus completing the hair growth cycle. Certain non-immune linked forms of alopecia such as male pattern androgenetic alopecia and telogen effluvium, essentially disrupt the hair growth cycle specifically in the critical telogen–anagen transition, resulting in shaftless hair follicles—leading to what is more commonly referred to as baldness.[239,240] In order to treat certain specific types of alopecia (nonimmune related) and promote hair growth, TENG therapy must show an ability to promote telogen to anagen hair follicle transition.

In order to determine whether or not TENG-ES of hirsute skin can facilitate the above, Yao et al. treated rats with hair removal cream leaving only hair follicles, to simulate the physiological state of hairs at the telogen stage. Differing electric field strengths were utilized with 3 V cm^{-1} as the optimal electric field strength for hair regeneration, inducing an influx of calcium into the root hair. This created a calcium gradient within the cytosol of the tip of the hair, a critical step for hair growth and cellular proliferation.[181]

The TENG device was also compared to current devices and treatments of hair growth, since the latter represent commonly used therapeutic solutions. In the study conducted by Yao et al., TENG-ES was compared to two other treatments: minoxidil (MNX), vitamin D_3 (VD_3), and normal saline (NS) as a control. The treatments and control were applied to four regions on the backs of the rats' torsos, and after three weeks of the study, it was concluded that TENG-ES was the most effective treatment, as its treated region displayed the longest and densest hair. The hair shaft length after TENG-ES application was ≈15.4 mm, whereas the three other experimental conditions resulted in hair shaft lengths of significantly lower length (8.7 mm for MNX, 6.9 mm for VD_3, and 3.4 mm for NS).[181]

These are promising results, but in order to truly treat alopecia, any TENG-ES therapy must be able to transition hair follicles from the telogen to the anagen phase. The authors were able to track the relative amount of hair follicles in anagen and telogen by staining the rats' skin with hematoxylin and eosin. Based on this staining, TENG-ES was shown to result in the transition of the hair follicles from telogen to anagen within the first week of treatment, whereas the other treatments resulted in the hair follicles remaining in telogen for the entire three weeks of treatment.[181]

Another factor critical to regular hair growth and regeneration is hair follicle proliferation.[234] The hair follicle proliferation percentage is calculated using the hematoxylin and eosin stains, and, in concordance with other results, TENG-ES was associated with the highest hair follicle proliferation percentage (96% after three weeks of treatment versus 68% proliferation in other treatments).[181] This seemed to suggest that TENG-ES is a promising technology for hair growth and regeneration.

Growth factors play a critical role in hair growth, thus it is essential that their relation with TENG-ES be studied. Two growth factors particularly key to the hair growth process are keratinocyte growth factor (KGF), which regulates hair follicle proliferation and differentiation, and vascular endothelial growth factor (VEGF), which regulates hair follicle growth and transition between stages.[235–237] The concentration of growth factors can be deduced by fluorescence imaging, in which fluorescence and growth factor concentration are directly correlated. For TENG-ES, the fluorescence intensities were particularly high at the follicular epithelium, but more importantly the fluorescence intensities, and thus the growth factor concentrations, steadily increased over the anagen phase, and slightly decreased over the catagen phase.[181] Nevertheless, the growth factor concentrations were at a significantly higher level than the control groups, indicating that TENG-ES was effective at upregulating KGF and VEGF.

Having shown that TENG-ES promotes hair growth, researchers set out to determine if it could be applied to rats with hair keratin disorder, a genetic disease that results in hair not being able to penetrate the epidermis because of a lack of growth factors. Likely owing to the fact that TENG-ES seems to promote the production of growth factors, marked improvements were seen in mice models with this genetic disorder. As shown in Figure 2h, TENG-ES seemed to promote the entire hair growth cycle, starting at telogen, transitioning into anagen by the third day, and persisting until the hairs transform into the catagen stage by day 12. Finally, a regression back to the telogen phase by day 15 was observed. While TENG-ES showed these promising results, other treatments stimulated hair follicles to enter the anagen stage even though here the anagen stage was short lived as the hair quickly transitioned into the catagen phase.[181] Consequently, TENG-ES seems to be able to promote hair growth by helping hair follicles transition from the telogen phase to the anagen phase, as well as enhance hair growth via an increase in anagen phase duration.

The main problem associated with certain types of alopecia, including telogen effluvium, is that the hair follicles are unable to transition from the telogen to the anagen phase, and thus are unable to grow. TENG-ES has a number of positive effects on the hair growth and regeneration processes including enhanced growth factor production, hair follicle proliferation, and inducing the transition of hair follicles from the telogen to anagen phase. Overall, however, considering the intrinsic differences between rat and human skin, studies with human skin and hair must be conducted to assess if TENG-ES maintains its apparent efficacy in humans.

2.4. Outlook

Regenerative medicine will be critical in treating the health problems of the next generation, and the recent advent of TENG positions itself as an ideal candidate for supplying therapeutic ES shown to promote processes critical to tissue regeneration. At the moment, in the field of regenerative medicine, TENG-ES devices have only been utilized to address bone and wound healing as well as hair growth but this will soon change as researchers make new developments.

The processes that are characteristic of all forms of tissue regeneration are cellular migration, proliferation, and differentiation, in which the only difference between these processes in bone and wound healing is that the cells that catalyze these processes in bone healing are osteoblasts whereas the corresponding cells in wound healing are fibroblasts. Hair growth is

a slightly different process as hair grows in a different manner compared to bone and skin. Nonetheless, cellular migration, proliferation, and differentiation also occurs in the process of hair growth. TENG-ES has not only been shown to promote the above, but also seems to promote other processes critical to bone and wound healing, as well as hair growth, including leading to an increase of growth factors and calcium ions.

Not only is TENG extremely well suited for regenerative medicine applications in view of its self-powered and bioconformability profile, it also has been shown that TENG-ES has little to no negative side effects on the surrounding ES-exposed cells. Despite the numerous positive effects of TENG-ES on the bone and wound healing processes, there is little direct evidence explaining precisely how this ES promotes osteoblast and fibroblast differentiation. For this reason, more research into directly proving the causative relationship between osteoblast and fibroblast differentiation and ES ought to be be conducted.

3. Neural Engineering

The nervous system acts as a centralized coordinator of a large number of functions within the human body thus being able to fully address abnormalities associated with its function is of critical importance for the well-being and livelihood of many people. There are ≈600 diseases associated with the nervous system, including severely impactful diseases such as motor neuron disease, Parkinson's disease, and strokes, which unfortunately often lack effective treatments and have associated high mortality rates.[241] Through various neural engineering techniques, researchers are able to develop, repair, and enhance nervous system structures, paving the way for the eventual cure or treatment of a number of neurological diseases.[242]

The nervous system communicates by way of electric potentials traveling through neural structures, until the elicited action potential eventually makes its way to either the brain to transmit sensory information, or to the muscles and organs depending on whether or not the electrical impulse runs through afferent or efferent neurons.[241,242] Thus, one way in which clinicians treat neurological diseases is through ES of particular neurons, consequently controlling the muscles, or functions associated with that particular neuron.[243,244] This ES essentially simulates the body's natural electrical impulses that flow through its neurons, making ES of nerves an effective tool in the field of neural engineering.

With the recent discovery of the TENG, a consistent supply of ES can be applied to nerves without the need for a separate power source as TENG generates its own electricity from passive biomechanical movements. TENG technology is especially suited for ES of nerves considering its characteristic low current creates minimal heat and minimizes nerve damage, a major problem associated with ES of nerves and nervous tissue. In addition, the exponential current waveform characteristic of the TENG is found to be the most efficient waveform to elicit nerve stimulation,[245] overall positioning TENG as an optimal candidate for direct nerve stimulation.

Recently, TENG-ES has been applied to a number of fields pertaining to neural engineering including the modulation of motor function,[182–186] neuronal cell differentiation,[187,188] weight control,[189] and bladder control[190,191] in such a way that it is able to intervene in these conditions via means of electrical interaction with the nervous system.

3.1. Modulation of Motor Function

Utilizing external ES can be beneficial in therapeutic applications as ES can effectively mimic the electrical impulses passing through the nerves of the human body. TENG-based neural interfacing of a particular nerve to control specific motor functions can potentially be utilized to treat various diseases and conditions. For this reason, TENG-based neural interfacing with a particular nerve has been studied in the hopes to restore muscle function in patients with peripheral nerve injury. However, since current research in this field is still in its infant stage, a large portion of research has focused on the treatment of foot drop via TENG-ES of the sciatic nerve, albeit simplistic, a linear and low-barrier research approach in attempting to prove TENG's efficacy in restoring lost or hindered function due to peripheral nerve damage.[182–186]

Neural interfacing is achieved through the combination of a stimulator, the TENG, and a neural interface, in this case a flexible sling interface that wraps around the nerve to ensure efficient and safe nerve stimulation. The neural interface can either interact with the central nervous system (CNS), composed of the brain and spinal cord, or the peripheral nervous system (PNS), composed of all the peripheral nerves within the rest of the nervous system. However, due to the stark anatomical differences between the two nervous systems, the mode of neural interfacing utilized must be compatible with the anatomical features of that particular neural structure. Currently, a majority of the studies regarding TENG-based neural interfacing are focused on PNS neural interfacing through the use of a flexible neural sling that wraps around the nerve of interest.[246] This is a generally safe mode of neural interfacing as it essentially stimulates that entire section of the nerve so there is a healthy balance between invasiveness and selectivity. On the other hand, other modes of neural interfacing such as intraneural multichannel microelectrodes offer optimal selectivity in neural fiber activation at the expense of a high degree of invasiveness and potential glial scarring.[247] However, Lee et al. developed a novel TENG device capable of attaining a high degree of selectivity without a corresponding increase in invasiveness. Using an array structure of neural electrodes, each individual pixel in the array could be individually activated to electrically stimulate the nerve of interest.[184] A major hurdle preventing effective neural interfacing with the CNS is that electrical signals tend to spread out within brain tissue, thus without a proper mode of application, neural interfacing with the CNS presents issues of low selectivity, and could lead to major neural damage in the brain.[248–250] Consequently, current studies are generally focused on neural interfacing with the PNS. It is conceivable to see, however, how such a microscaled technology as TENGs could be applied to the CNS upon development of proper neural interfacing mechanisms adapted to the anatomy of the CNS.

As mentioned, the bulk of TENG-based neural interfacing research is based on the treatment of foot drop via neural interfacing of a section of the sciatic nerve.[182–186] Normal foot motion is characterized by dorsiflexion and plantar flexion of the muscles in the foot during each phase of gait. However in patients with foot drop, certain motions such as excessive foot inversion and toe flexion yield the typical phenotypic result associated with the dropping of the forefoot. Thus, in order to treat foot drop, the TENG-based neural interfacing system must be able to prevent these detrimental motions of excessive foot inversion and toe flexion, as well as control the flexion of various muscles within the foot.[251] Only a particular set of nerves needs to be stimulated in each phase of gait. In order to achieve this, a flexible sling neural interface is utilized as its selectiveness is sufficient enough to stimulate only the desired nerves, thus enabling certain ankle motions, while avoiding undesired ones.

The way in which the flexible sling neural interface is able to achieve this level of selectiveness is through its unique structure. As shown in **Figure 3**a, Lee et al., devised a study in which the flexible sling interface was wrapped around the sciatic nerve with six electrodes on its central bridge, and two more ring electrodes surrounding the nerve on a neighboring bridge.[183] This bridge system enables the flexible sling interface to wrap around the nerve with optimal surface level contact that does not apply too much pressure, a factor that could potentially damage the nerve. In addition, the flexible nature of the sling interface allows it to integrate with a variety of sizes of nerves, making it an effective tool for TENG-ES neural interfacing.[182,183,185] The flexible sling interface is used in conjunction with the stacked TENG shown in Figure 3b. The stacked TENG generates an electrical current, which is then passed through the flexible neural interface in order to stimulate a section of the sciatic nerve affecting the movement of a particular muscle.

Due to the unique structure and the sheer number of electrodes on the flexible sling interface, this device was able to transmit the TENG-ES to stimulate the nerve of choice in two configurations: transverse and longitudinal polar. It was found that the transverse configuration could effectively function at only 0.4 mA while the longitudinal polar configuration could effectively function only at a much higher current of 2.4 mA.[183] The higher current associated with the longitudinal polar configuration generates more heat, which can have detrimental effects on the nerve, as well as delaminate the electrodes in the flexible sling interface. In addition, the transverse configuration yielded compound muscle action potentials (CMAPs) with a significantly higher amplitude than those of the longitudinal polar configuration. Thus, the transverse configuration is shown to be both the safer and more effective option for the application of TENG-ES to the sciatic nerve, for the treatment of foot drop.

In order to test the selectivity of the flexible sling interface, the CMAPs of the gastrocnemius medialis (GM) and tibialis anterior (TA) muscles were measured in response to TENG-ES of a specific portion of the sciatic nerve. As shown in Figure 3c, the TA muscles were more effectively stimulated compared to the GM muscle. Thus, the researchers determined that the existing system did not have a high enough degree of selectivity. In order to increase the selectivity of the system and test whether or not the TENG system was capable of generating enough electricity to induce full muscle contraction, the researchers wrapped a pair of Pt/Ir wires around a section of the sciatic nerve interfacing with the flexible neural sling interface. With the addition of the Pt/Ir wires, the TA muscle underwent full contraction and completed the dorsiflexion movement necessary in treating foot drop.[183] Thus, the TENG device seemed able to generate enough charge to control the contraction of the TA muscle when implemented with a flexible neural interface and a mode of increasing the selectivity of the system.

Neural interfacing with peripheral nerves through ES is a delicate process that can have a number of unwanted side effects. It is critical to test whether or not this neural interfacing has any effect on the nerves' other functions and processes, including their hemodynamics profile. Functional photoacoustic microscopy (fPAM) was utilized to determine the effect of TENG-ES on the sciatic nerve's hemodynamics. As shown in Figure 3d, fPAM images show no change in the blood flow within the sciatic nerve before and after the implantation of the flexible sling interface. Indeed, TENG-ES neural interfacing with the sciatic nerve seemed to indicate no detrimental effect on the hemodynamics of the sciatic nerve.[183]

Through the combination of the TENG, used as a stimulator, and a flexible sling interface, used as a neural interface, complete contraction of the TA muscle was achieved by the researchers, effectively counteracting foot drop. The use of TENGs in the modulation of motor function through neural interfacing is a relatively new field, and although at the moment one of the only applications of TENGs in neural interfacing is the treatment of foot drop, many new applications beyond this are likely to emerge in the coming years.

3.2. Neuronal Cell Differentiation

Neurons are cells that function as transmitters of information between the brain and the various parts of the human body, allowing amongst other things, the human body to optimize its interaction with the external environment it is found in, all while maintaining homeostasis. Neurogenesis generally occurs in the developmental stages of embryos. However, it is also a crucial process throughout the lifetimes of humans, and neuronal cell differentiation is a critical process contributing to the correct functioning of the nervous system.[252,253]

Neuronal cell differentiation is the process by which a neuronal cell is derived from another cell, whether this cell be a stem cell or another type of cell depends on the process by which the neural differentiation is conducted. The most well-known process is stem cell differentiation, in which unspecialized stem cells are known to be able to differentiate into a number of cell types. Neural stem cell differentiation is the process by which unspecialized stem cells differentiate into neuronal cells, including neurons, astrocytes, oligodendrocytes, or other types of neuronal cells, through the introduction of specific physicochemical factors into the microenvironment of the stem cells.[252] In addition to this process, direct cell conversion also exists, which is a much more recently discovered, and seemingly complex process by which fully differentiated mature

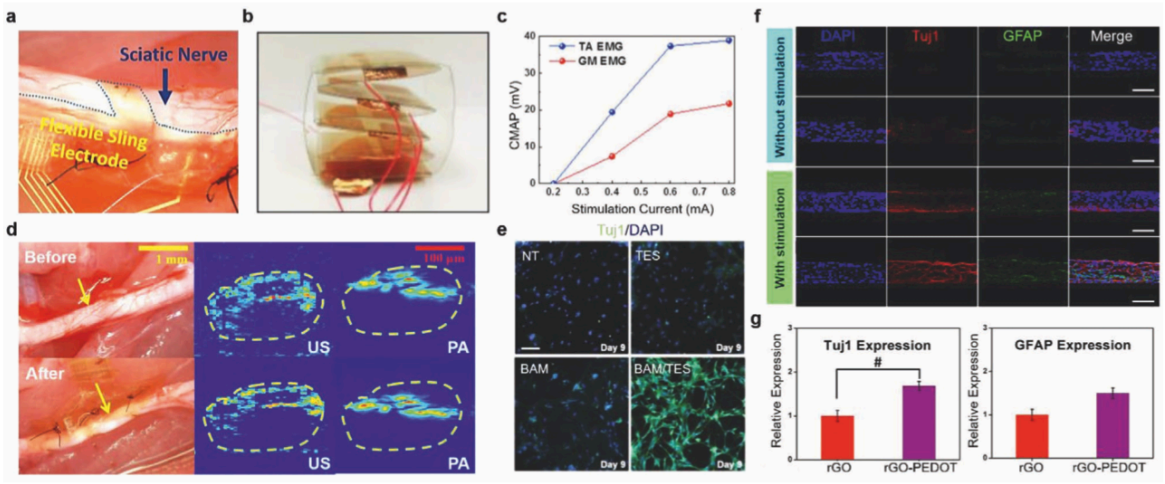

Figure 3. TENG-ES therapeutic devices for neural interfacing and neuronal cell differentiation. a) Implanted flexible sling electrode on rat sciatic nerve. b) Layered TENG device composed of Cu and PDMS triboelectric layers. b) Reproduced with permission.[182] Copyright 2018, IOPscience. c) TA and GM EMG signals. d) Photos of sciatic nerve before and after implantation of sling electrode in addition to photoacoustic measurements to assess hemodynamics. a,c,d) Reproduced with permission.[183] Copyright 2017, Elsevier. e) Expression of Tuj1 gene after 9 days of culture with various forms of stimulation (scale bar: 100 µm). Reproduced with permission.[188] Copyright 2016, Wiley-VCH. f) Immunostaining with DAP1, Tuj1, and GFAP with and without TENG-ES (scale bars: 100 µm). g) qPCR analysis of cell expression levels of Tuj1 and GFAP with and without hybridization of rGO and PEDOT microfibers. f,g) Reproduced with permission.[187] Copyright 2016, American Chemical Society.

cells are converted into specialized cell types, e.g., neuronal cells.[253] Direct cell conversion is a unique process capable of converting virtually any cell type into the desired cell type through a differentiation process that does not include a pluripotent state. This background is of relevance as TENG-ES has been studied to assess its effects on neural cell differentiation, covered below.

3.2.1. Stem Cell Differentiation

In several studies researching the effectiveness of TENG-ES on stem cell differentiation into neuronal cells, mesenchymal stem cells (MSC) were utilized as an easily sourced starting cell line, which could be isolated relatively easily. MSCs do not immediately differentiate into neuronal cells as they require external factors to induce differentiation, such as growth factors, ECM components, and even electrical signals from the environment.[254–258] Thus, the application of TENG-ES to assess MSC differentiation was studied.

Using a suitable neural scaffold, such as poly(3,4-ethylenedioxythiophene), or PEDOT, is a known method with which to aid the process of stem cell differentiation. PEDOT, specifically, is the most promising scaffold used in this sense, up to now.[259,260] However, PEDOT presents biocompatibility issues as it has trouble degrading in vitro. In order to address this issue, the carboxylic acid portion of the graphene oxide nanosheets (rGO) can be incorporated into the PEDOT structure. This hybridization between the rGO–PEDOT microfibers was utilized in a study conducted by Guo et al., and it allowed the researchers to develop a neural scaffold that was both biocompatible and highly conductive, due to the presence of rGO microfibers and PEDOT nanoparticle, respectively.[187] The crosslinking nature of the interaction between the rGO microfibers and the PEDOT nanoparticles allowed for increased protein adsorption, which accelerated the process of stem cell differentiation.[187,261] By itself, the rGO–PEDOT hybrid neural scaffold supports stem cell differentiation into neuronal cells, but it does not necessarily accelerate the process. Thus, an external factor must be introduced into the system in order to accelerate stem cell differentiation into neuronal cells.

TENG-ES was utilized as this external promoting factor since ES has been shown to have a significant effect on the process of stem cell differentiation into neuronal cells.[262–264] In order to determine how TENG-ES affects the process of stem cell differentiation, Guo et al. studied four experimental groups: two control groups of rGO and 15% rGO–PEDOT microfibers without exposure to TENG-ES, and two stimulation groups of rGO and 15% rGO–PEDOT microfibers with exposure to TENG-ES. As shown in Figure 3f, through the DAPI stained images, after 21 days of treatment the ES groups showed a much larger distribution and density of cells.[187] In order to determine how many of these cells were neuronal cells, the groups were also stained to visualize the existence of two neural markers (Tuj1 for neuronal cells and GFAP for glial cells). The stimulation groups showed a much larger degree of Tuj1 expression, however, more noticeably, the 15% rGO–PEDOT groups yielded a significantly higher degree of Tuj1 expression compared to its unhybridized counterpart. This shows that the hybridization of rGO microfibers and PEDOT nanoparticles serves as an excellent scaffold to support neural stem cell differentiation when combined with TENG-ES therapy, due to the highly conductive nature of the PEDOT nanoparticles. As can be seen by Figure 3g, the combination of the 15% rGO–PEDOT neural scaffold with TENG-ES served as the most effective tool for stem cell differentiation into

neuronal cells, as it resulted in the highest expression of neural marker cells such as Tuj1 and GFAP.

The use of an rGO–PEDOT neural scaffold induces stem cell differentiation into neuronal cells due to the conductive nature of the PEDOT nanoparticles and the biocompatible nature of the rGO microfibers. However, the implementation of this hybridized neural scaffold with TENG-ES is shown to be the most effective therapeutic application to accelerate stem cell differentiation into neuronal cells. This research is encouraging as it can seemingly lead to developments in IOB bioelectronic technology capable of inducing nerve regeneration. Utilizing TENG for ES in this case is of added benefit given the capability to organize the architecture of the device in such a manner that could be used to uniformly stimulate batches of stem cells for specific differentiation pathways.

3.2.2. Direct Cell Conversion

Direct cell conversion is a process in which any mature cell is converted into a specific cell type. The process occurs through the introduced expression of gene sets which code for cell type-specific transcription factors. For neural engineering applications, these cell type-specific transcription factors enhance the production of neuronal cell proteins, which subsequently promote the process of converting the original mature cell into a neuronal cell.[188,253]

Direct cell conversion is able to convert any cell type into the desired cell type. However, some cell types such as fibroblasts, are easier to transform.[253] Thus, to test whether or not TENG-ES promotes this process of direct cell conversion into neuronal cells, mouse fibroblasts were used. The process of direct cell conversion to neuronal cells requires the introduction of neuronal genes into the sample. Normally the process of direct cell conversion would occur at a slow rate, but through the use of TENG-ES this process can be sped up and rendered more efficient.[188]

In this study conducted by Jin et al., TENG-ES was found to closely mimic innate natural electric cues that control and stimulate the process of direct cell conversion, allowing TENG-ES to promote the direct differentiation process. In order to determine the efficiency of TENG-ES's ability to induce direct cell conversion of fibroblasts to neuronal cells, the fibroblasts were separated into two separate cultures with and without exposure to TENG-ES, and subsequently stained for neuronal marker class III beta-tubulin (Tuj1) starting on the ninth day of culture. Figure 3e shows the increased concentration of Tuj1 in the TENG-ES group compared to the other control groups. It was on this ninth day of the application of TENG-ES to the system that the cells that were originally fibroblasts started to take a more elongated shape, similar to that of a neuron. The conversion efficiency, which was calculated as the percentage ratio of Tuj1 positive cells to total cells, was 8.85%, compared to a mere 0.13% in the group lacking exposure to TENG-ES. In addition, during the 12th–14th days the conversion efficiency of the TENG-ES group was 14.17% whereas the control group had a conversion efficiency of only 6.41%.[188] This significant increase in the conversion efficiency correlates to an increase in the amount of neural-like cells within the sample, with significant indication that TENG-ES promotes direct cell conversion of fibroblasts into neuronal cells.

In addition, the continued use of TENG-ES through days 14–18 yielded induced neuronal cells with a more complex neural morphology. Following the maturation of the cells until the 30th day yielded neuronal cells with highly mature neural phenotype markers, evidence of synaptic connections. Throughout this entire process, the group of cells that were subjected to TENG-ES yielded significantly higher conversion efficiency rates and more evidence of neuronal cell morphologies.

3.3. Weight Control

One of the most crippling health-related problems that the modern world faces is obesity, a disease affecting millions of people around the world caused by a complex interplay between genetic susceptibility and nutritional, physiological, social, and environmental factors. Obesity is a major contributing factor to a number of chronic diseases such as diabetes, cardiovascular disease, and cancer.[265,266] Weight loss programs and diets are an ≈$11 BN industry that would benefit immensely from a technology capable of providing long term solutions.[267,268] Such a technology is described here as a TENG device capable of applying ES to the vagus nerve, reducing appetite and subsequent caloric intake. The flexibility of the TENG device can be altered through careful material and working mode selection to be adapted to being best suited for single nerve ES, a specific benefit of using TENG for ES in weight control.

The vagus nerve is a critical part of the nervous system that serves as a signal bridge between the brain and the thorax and abdomen. Its two branches, known as the posterior and anterior vagal trunks, form in the thorax and continue into the abdomen, and are critical in innervating the muscles of the digestive tract.[269–271] The vagus nerve is part of the autonomic nervous system, and thus cannot be controlled in the same manner as motor nerves. ES of the vagus nerve can have a number of effects as it controls the function of the heart, lungs, and digestive organs. However, ES of a portion of the vagus nerve, or vagus nerve stimulation (VNS), near the abdomen, has been shown to result in decreased appetite and weight loss. Excessive caloric intake is a critical factor in weight gain and obesity considering that once the body has received enough calories, the additional caloric intake is converted into fat to be stored. In concordance with this pivotal concept in treating obesity, TENG-ES was applied to the posterior and anterior vagal trunks of the vagus nerve in an attempt to decrease appetite and caloric intake, thus effectively tackling obesity.

In order to test the effects that TENG-ES of the vagus nerve has on weight control, Yao et al. developed a TENG device which was implanted into rats separated into four groups: the VNS group, which underwent TENG implantation and its attachment to the vagus nerve through leads; the sham group, which underwent TENG implantation without TENG connection to the vagus nerve; the laparotomy group, which underwent surgery but no TENG was implanted into the rats; and finally the Intact group, rats without any modifications.[189] Since these groups were devised to test the effectiveness of TENG-ES of the vagus nerve

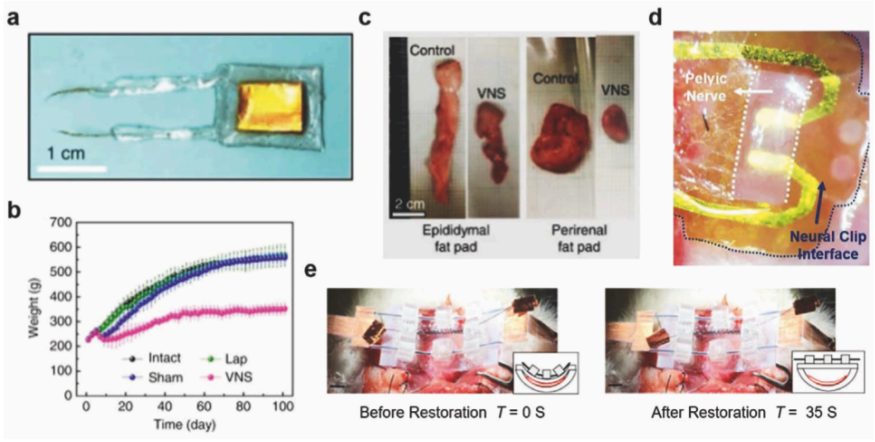

Figure 4. TENG-ES therapeutic devices for weight and bladder control. a) Implantable TENG-ES device applied to vagus nerve packaged in a multilayer film composed of PDMS, ecoflex, and polyimide. b) Average body weight of rats exposed to different conditions. c) Images of the epididymal and perirenal fat pads of rats with and without exposure to TENG-ES of the vagus nerve. a–c) Reproduced under the terms of the CC-BY Creative Commons Attribution 4.0 International License (https://creativecommons.org/licenses/by/4.0).[189] Copyright 2018, The Authors, published by Springer Nature. d) Neural clip interface attached to pelvic nerve 16 days after implantation. Reproduced with permission.[190] Copyright 2019, Elsevier. e) TENG bladder control device before and after restoration phase. Reproduced with permission.[191] Copyright 2018, American Chemical Society.

on weight control, the VNS group served as the experimental group and the three other groups served as the control groups. As can be seen in **Figure 4**a, the TENG device used to apply the VNS is packaged so that it can be implanted onto the rats' stomach wall. Since the TENG generates electricity from biomechanical movements, it only applies VNS when the stomach is undergoing peristalsis. In addition, the two Au leads wrapped around the anterior and posterior vagal trunks, through which the ES is applied to the vagus nerve, can also be seen. With the packaged TENG generating electricity from the passive movements of the stomach wall, it was able to supply enough electrical power for VNS to induce satiation and help with weight loss.

There was a significant difference between the weight of the VNS and that of the control groups throughout the length of the study. As can be seen by Figure 4b, throughout the first week of the study, all of the groups exhibited virtually identical weights due to the fact that the implantation of the TENG occurred on the seventh day. This demonstrates that the rats were under the same experimental conditions, and that the only factor contributing to the weight loss was TENG-ES. After implantation of the TENG device, the VNS group and the sham group exhibited a period of weight loss likely due to decreased food intake from the surgery, however throughout the length of the study the sham group regained weight to join the two other control groups, whereas the VNS group remained consistently at a lower weight. This shows that the effects of the implantation of the TENG have a temporary weight loss effect, as one would normally see in a postoperative course. By the end of the 100-day study, the three control groups exhibited an average weight of about 535 g while the VNS group exhibited a significantly lower average weight of 350 g, with the VNS group consuming approximately two thirds of the caloric intake compared to the control groups.[189] Consequently, TENG-ES does not induce weight loss by directly eliminating fat, but rather it reduces the body's caloric intake by tricking the rats into a false sense of satiation. Thus, the researchers believe that TENG-ES of the vagus nerve decreases the user's desire to eat resulting in a decreased caloric intake, and therefore, weight loss.

After the 100-day study, the anatomical adipose tissue consisting of both the epididymal and perirenal fat pads was extracted from the rats for direct comparison. As can be seen by Figure 4c, the size of both the epididymal fat pad and the perirenal fat pad were significantly smaller for the VNS group compared to the control groups. In order to effectively compare the adipose tissue weight between the control and VNS groups, the ratio between the epididymal fat pad and the total weight (EBR) was taken. The VNS group displayed an EBR of 1.14% whereas the control groups displayed an EBR of 1.7%. Thus, through TENG-ES of the vagus nerve, rats in the study were able to achieve a weight-loss ratio of 38%. There is always a possibility that ES of the vagus nerve can have adverse effects on the subjects of the study. In order to test TENG-ES's safety when applied to the vagus nerve, imaging and blood analyses were conducted. First, imaging analyses were conducted to determine whether or not the TENG device moved around within the body of the subject or if it remained in place throughout the 100 days of the study. 3D X-Ray images were created from CT scans of the rats after implantation of the TENG in order to examine device migration when rats exhibit normal daily activity. Throughout the entire length of the study, the TENG remained firmly in place and did not exhibit any movement, thus no adverse physical effects were shown in the rats due to TENG device implantation. In addition, there were no abnormal nerve cell morphology changes or inflammation in the vagus nerve, showing that the leads connecting the TENG device and the vagus nerve did not negatively impact the vagus nerve. Furthermore, in order to test whether or not TENG-ES of the vagus nerve had any other potential side effects, blood and chemical analyses were conducted. The blood testing results suggest that there are no adverse effects of TENG-ES of the vagus nerve on the blood contents, thus the device is hemocompatible. In

addition, the chemical tests showed similar results in that all of the organs retained original function.[189]

Essentially, TENG-ES of the vagus nerve resulted in decreased appetite in the subject, leading to decreased caloric intake and eventual weight loss. However, once the TENG device is implanted, its effect cannot be halted unless it is surgically removed from the subject. Thus, in an attempt to optimize the device, some sort of switch would need to be integrated into the system to allow on/off administration of the therapy, i.e., based on the user's weight gain (or fluctuations). In addition, current research on TENG-ES of the vagus nerve for weight loss is restricted to rat studies, thus in order for this device to be eventually utilized by humans, there needs to be a transition to the clinical field.

3.4. Bladder Control

Neurogenic bladder dysfunction affects the quality of life of a bulk of the population.[272,273] A number of treatments, ranging from medications to surgical interventions, have been developed with the hope of treating this condition.[274–278] However, due to the fact that neurogenic bladder dysfunction can arise from a number of conditions, including Parkinson's Disease, stroke, brain injury, and multiple sclerosis, developing a universal treatment for this condition remains a challenge.[279] Neurogenic bladder dysfunction has differing results which can range from an overactive bladder, to difficulty passing urine. A universal treatment for neurogenic bladder dysfunction must therefore be able to control numerous aspects of bladder function.

Bladder control is governed by the muscles comprising the bladder wall, namely the detrusor muscles. Action potentials travel down the pelvic nerve from the CNS, and stimulate the contraction of the detrusor muscles comprising the bladder walls, which induces micturition.[280,281] The pelvic nerve is the main parasympathetic nerve that runs through the lower urinary tract, and it controls many functions in this area as well as innervates a number of muscles. It has been shown that through pelvic nerve ES, certain muscles controlling bladder function can be activated, thus enabling researchers to control bladder function.[282,283] Currently, the main approach to treating bladder dysfunction is utilizing catheters. However, this approach has many shortcomings including the obvious downside that the individual must undergo frequent catheter changes.[284] In finding new technologies for treating neurogenic bladder dysfunction, two approaches can be used to control bladder function, namely activating the nerves controlling the detrusor muscles that are correlated with bladder function, or simply activating those muscles directly.

Through TENG-ES of the pelvic nerve, control over the nerves directing bladder function can be attained. In order to do so, Lee et al. integrated a TENG device and flexible neural clip into a unified system. In order to simplify the experimental setup, and to limit the amount of experimental variables to consider, the researchers tapped the TENG device with their hands at various frequencies in order to generate electricity. This electricity was then utilized to activate the pelvic nerve through ES, via a flexible neural clip.[190] As can be seen in Figure 4d the neural clip wraps around the pelvic nerve in such a way that it has optimal physical interactions with the nerve and effectively transmits ES without damaging the nerve itself. With this valuable information generated by the TENG, and given the capabilities to stimulate the pelvic nerve by the flexible neural clip, the system was able to control bladder function. There were two main factors that contributed to bladder function when it came to TENG-ES of the pelvic nerve, which were thoroughly investigated to determine their optimal combination: stimulation frequency, and the number of stimulation sessions. When testing the effect of stimulation frequency on bladder modulation, different beats per minute (BPM) of 25, 50, 100, and 150 were applied to the pelvic nerve while bladder pressure and micturition were measured. It was found that at 25 and 50 BPM there were changes in bladder pressure, though there was no micturition at 25 BPM, and a moderate amount at 50 BPM.[190] On the other hand, at 100 and 150 BPM, there were significant pressure changes alongside the occurrence of micturition. When testing for the effect of the number of stimulation pulses on bladder modulation, different numbers of pulses were applied with a constant BPM of 50. Although as previously stated, 50 BPM was not as effective as the 100 or 150 BPM frequencies, it was still a safer alternative and yielded moderate amounts of micturition. The results showed that one pulse did not supply enough energy for micturition to occur whereas two or more pulses supplied more than enough energy for the occurrence of micturition.[190,285] Thus, through a careful balance of stimulation frequency and the number of stimulation pulses TENG-ES can be utilized to control bladder function and the occurrence of micturition, through stimulation of the pelvic nerve. This experimental setup relied upon hand tapping to generate electricity through the TENG's characteristic contact-separation working mechanisms, however in the future this system could become unified through the implantation of the TENG device onto the walls of the bladder. This would allow for the TENG to not only apply therapeutic ES to the pelvic nerve to induce micturition, like the experiment conducted by Lee et al., but it would also allow for the TENG device to measure the fluid volume within the patient's bladder from the amount of electricity that is produced by the TENG device.

Instead of stimulating the nerve that controls the muscles that control bladder function, the nerve can be completely bypassed, with direct ES of the muscles that control bladder function. In a study conducted by Hassani et al., a sponge-based TENG device, which both generates electrical energy from the movements of the bladder wall and also senses how much fluid is inside the bladder, is incorporated with an actuator that directly stimulates the detrusor muscle.[191] Due to the fact that patients with neurogenic bladder dysfunction oftentimes have dysfunctional peripheral nerves as well as detrusor muscles, the TENG device is essentially replacing the function of the peripheral nerves in detecting the fluid volume of the bladder, and the actuator is enhancing the function of the detrusor muscles by direct activation via TENG-ES.

This system comprises the sponge-based TENG and the actuator, and works in two cycles: compression and reformation. Compression is the first step in which the springs within the actuator compress the bladder through the use of the electrical energy generated by the TENG device. In much a similar way in which the muscles involved in peristalsis push food through the digestive tract, the actuator contracts the detrusor

muscles which push urine out of the bladder. After this compression phase, a reformation phase must occur, in which the springs within the actuator are brought back to their original states (Figure 4e).[191] It was found that through this system of compression and reformation, a voiding percentage of 60% was achieved, making this approach a much more efficient solution than current catheter use. In addition, this use of a compression–reformation actuator results in this system being able to be adapted to a number of bladder sizes, making it a more universal solution to neurogenic bladder dysfunction.

Neurogenic bladder dysfunction is caused by underlying neurological damage to the nerves that carry information to and from the bladder and the CNS, composed of the brain and the spinal cord. Due to this damage in these nerves, the pelvic nerves and detrusor muscles are not able to receive a stimulus from the CNS directing them to induce micturition.[286] Thus, intervening directly onto one of those biological structures, via TENG-ES, can permit bladder function treatment. Although the effects that such TENG-ES can have on the pelvic nerve and surrounding tissue in the long run are still unknown, more focused research into the long-term effects of TENG-ES of the pelvic nerve and the detrusor muscles can be conducted to provide further insight on the clinical implementation of these solutions.

3.5. Outlook

Being able to treat the hundreds of neurological diseases that plague the world's population is of critical importance to improve affected patients' quality of life. The recent technological innovation of the TENG has become an incredibly useful tool in treating some of these diseases and conditions, with several positive attributes brought about by ES. However, there is still much to understand about these neurological diseases, thus, for TENGs to be applied to more of these diseases and conditions, we must learn more about the mechanisms behind them.

At the moment TENG-ES has only been used for simple neural interfacing with easily accessible nerves controlling single-function associated activities, such as bladder function and satiation. New methods of TENG-ES need to be developed, such as deep brain stimulation, for example, in order to treat more complex neurological diseases such as Parkinson's Disease. Furthermore, virtually all of the research in TENG-ES of parts of the nervous system, comprises the PNS rather than the CNS. Thus, although it is a much more complex process, TENG-ES of components of the CNS must be studied as this can prove to be an area of research with immense potential rewards.

Since neural engineering involves the manipulation of the nervous system, which controls the entire human body, its scope can be very broad, as seen by the TENG's application to the modulation of motor function, neuronal cell differentiation, weight control, and bladder control. However, despite neuronal cell differentiation, all of these applications of the TENG are relatively similar in that they involve ES of a nerve in order to control a particular bodily function. The progress in neural interfacing technology has advanced a lot in the past years with the development of flexible electrodes capable of mapping small sections of the nerves of interest,[287–291] thus this TENG-based neural interfacing technology may play a large role in the personalized healthcare industry in the future.

However, the potential applications of TENG devices do not stop there, as beyond their various applications in providing therapeutic electrical stimulation, TENG devices can also power therapeutic neuroprosthetics such as bionic limbs, cochlear implants, and bionic eyes, among others.[292,293] This could revolutionize the entire industry of human–machine interfacing as the TENG could be the bridge between the user and the prosthetic by generating electricity to power these neuroprosthetics from the energy associated with the biomechanical movements of the user, thus forming a self-sufficient system.

Scientists have constructed a considerably accurate understanding of the PNS consisting of all of the afferent and efferent nerves feeding information to and from the brain, however, as of now we still do not completely understand the full complexity of all brain functions.[294] More fundamental research into this field of study can open up new avenues in which TENG-ES can be of use via the means of targeted IOB bioelectronics.

4. Rehabilitation Engineering

Rehabilitation engineering is the broad field of study related to the application of engineering principles to treat ambulatory or motility disabilities that people live with on a daily basis. Millions of people around the world live with chronic conditions, such as arthritis, which greatly hinder their quality of life, and the current number of people suffering from arthritis is expected to increase by 49% by 2040.[295] Consequently, researchers are diligently exploring various treatments for arthritis through rehabilitative engineering techniques, as well as other ailments. Current studies have utilized ES for rehabilitative purposes to essentially stimulate the existing electric impulses flowing through the nervous system, as this ES has shown to be beneficial in rehabilitating both muscle and cardiac tissue after distress.

The recent discovery of the TENG provides an efficient, bioconformable, and self-sustainable source of ES, which can not only be used to generate electricity from biomechanical movements, but can also be used as a sensor to deduce the size and type of biomechanical movement. This sensing information can be invaluable for patients with chronic conditions as this information is vital in knowing the nature and progress of their debilitating conditions, as well as providing potential solutions to treatment courses.[296] In recent years TENG technology has been applied in rehabilitative capacities, mostly for applications in muscle rehabilitation, as well as cardiac rehabilitation, which are detailed below.

4.1. Muscle Rehabilitation

There are a number of ways in which loss of muscular function can occur, including stroke, spinal cord injury, multiple sclerosis, and even chronic venous insufficiency.[297–301] For many of the affected individuals, a long and laborious process involving constant physical rehabilitation is necessary to slowly gain back

some, if any, of the muscular function that was lost. Recovery of muscular function can be achieved more rapidly through TENG-ES, considering the now well established positive therapeutic influence of ES on neuromuscular rehabilitation.[192–194]

The key to muscle contraction is at the synapse, or the site in which information traveling through the motor neuron is transmitted to the muscle fibers. An action potential containing information pertaining to the contraction of a particular muscle fiber travels through the motor neuron until it reaches the synapse, at which point acetylcholine is released into the synaptic cleft.[302,303] This increased concentration of acetylcholine in the synaptic cleft induces an action potential along the surface of the muscle fiber. This action potential travels through a series of tubules to penetrate deep within the muscle itself, reaching the sarcoplasmic reticulum where calcium ion release occurs. Calcium ions are the driving force behind muscle contraction as they cause a sliding motion involving troponin, tropomyosin fibers, and myosin, yielding the characteristic contractile motion of muscle fibers. TENG-ES can induce muscle contraction as the ES essentially mimics the action potential traveling through the motor neuron and into the muscle fiber itself.

There are two ways in which TENG-ES, which has a characteristically low current and power, can effectively stimulate muscles, which have a relatively high electric potential threshold, to the point of contraction: targeted ES directly to the motor neurons that innervate and control the contraction and relaxation of muscle cells,[192] or generalized ES with increased power and current to sites where motor neurons are known to be found.[193] Through the use of a multichannel electrode, researchers were able to effectively map out the location of these motor neurons with which to accurately apply TENG-ES directly to the sites in which the motor neurons are located.[192] On the other hand, researchers were also able to increase the current and power generated by the TENG by integrating it with a diode, creating the diode-amplified TENG (D-TENG).[193] TENG devices, specifically, are extremely well suited to consistently yield high voltage, low current outputs, which are extremely important and best suited for muscle stimulation and muscle rehabilitation applications.

4.1.1. Multichannel Electrode

Electrical muscle stimulation is an established therapeutic option for muscle recovery, however its integration with TENGs is a novel development. Normally, muscles require mA-level ES in order to be activated and undergo contraction. TENGs normally reach low currents (around 35 μA), and need tailored modification in order to effectively allow for targeted muscle contraction through TENG-ES.[192,193]

The most efficient way in which TENG-ES is applied to the human body is through electrodes.[304] Since the motor neurons that control the muscle require a much higher current in order to transmit an action potential, applying TENG-ES directly to the motor neuron would mean that a 35 μA current would likely be enough to initiate an action potential within the motor neuron. Wang et al. developed a multiple-channel intramuscular electrode capable of mapping the scattered motor neurons distributed within the muscle tissue, thus allowing TENG-ES to be applied directly toward the motor neurons themselves.[192]

The rat tibialis anterior (TA) muscle was studied to see if TENG-ES coupled with the multichannel electrode could induce muscle contraction as well as map out the motor neurons within the muscle itself. As shown in **Figure 5**a, the anaesthetized rats were subjected to TENG-ES of the TA muscle and the resulting force of the motion was measured. Due to the multichannel nature of the electrode, multiple varying combinations of ES in different locations of the TA muscle, which were named e1 to e6 on the frontside and e1′ to e6′ on the backside, were applied to map out the location of the motor neurons. As shown in Figure 5b,c, during frontside TENG-ES, the only location which resulted in muscle contraction was e2, whereas for backside TENG-ES this location was e5′.[192] This shows that the e2 and e5′ locations were closest to motor neurons and consequently were sites in which TENG-ES was able to effectively contract the TA muscle.

Even though inducing muscle contraction does not fully regain muscles capabilities linked to clinical events such as spinal cord injury, multiple sclerosis, and other conditions, it is a step in the right direction toward independent muscle activity rehabilitation. In addition, continuous use of TENG-ES in this manner could eventually result in complete muscle function recovery as it essentially allows the user to regain control over certain movements. This research has proven that TENG-ES can induce muscle contraction without the need to perform rehabilitative muscular therapy.

4.1.2. Diode-Amplified TENGs

Another way in which researchers bypassed the intrinsic problem preventing the TENG from contracting a targeted muscle, was by directly increasing the current and power produced by the TENG. In this manner, the current could be increased to the mA threshold necessary to directly stimulate most muscles into contracting.

Wang et al. increased a TENG device's current and power output by incorporating a diode, or a semiconductor device, which allows for current to flow only in one direction, into the TENG device. This new TENG device, called a diode-amplified TENG (D-TENG), is characterized by its significantly higher current and power outputs. This increased current output however, was still not sufficiently high to create damage to nearby cells, making the D-TENG a safe therapeutic option.[193] The implementation of the diode into the TENG device amplifies the current and power of the device as the diode is integrated with a switch, thus the generated charge is accumulated at the diode and then released in shorter, higher current pulses. As a result of these shorter current pulses, the frequency of the ES is increased to a level which is very similar to the resonance frequency of the motor neurons that innervate the muscle tissue. Thus, the increased frequency resulting from the shorter current pulses characteristic of the D-TENG increases the activity of the motor neurons as well as directly inducing muscle contractions.

As shown in Figure 5d, D-TENG-ES resulted in muscle contraction in virtually every location at which ES was applied, due to the increased current and power generated by introducing a diode into the structure of the TENG device.[193] These results

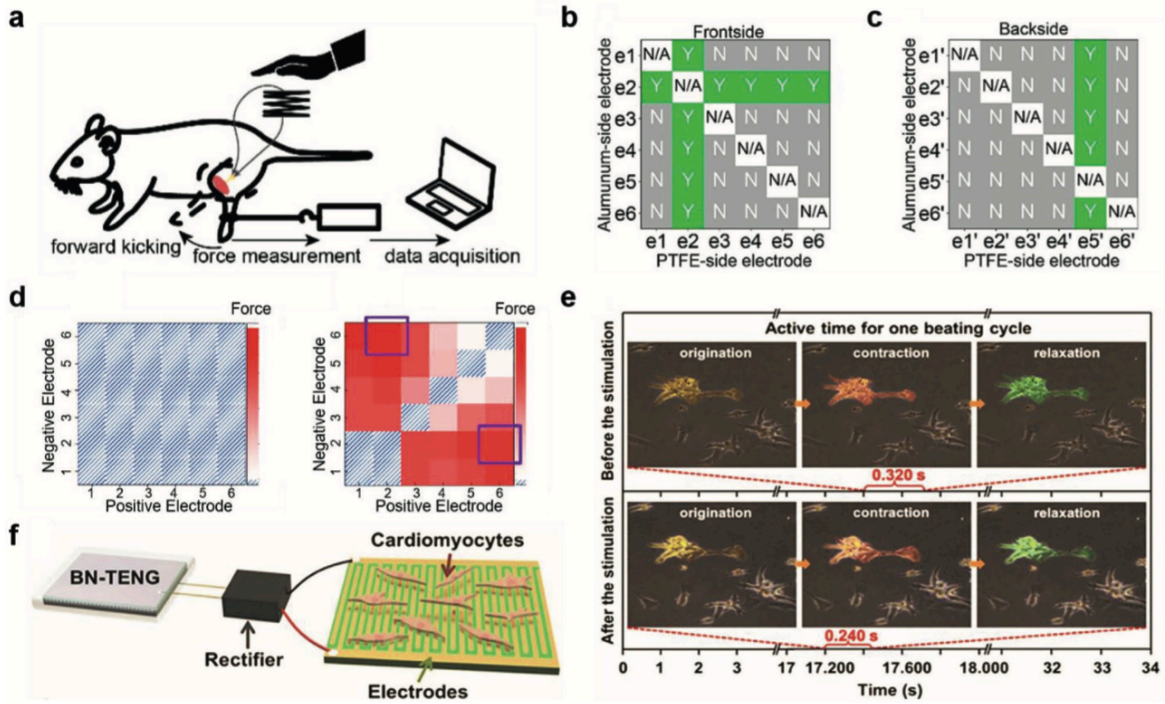

Figure 5. TENG-ES devices for muscular and cardiac therapy. a) In vivo testing setup for TENG-ES of TA muscle with TENG device composed of multiple layers of PTFE and Al. b,c) Stimulation capability matrix of the frontside (b) and reverse side (c) electrodes. a–c) Reproduced with permission.[192] Copyright 2019, American Chemical Society. d) Direct TENG-ES of TA muscle with and without diode in which red squares correlate to high muscle contraction force. Reproduced with permission.[193] Copyright 2019, Elsevier. e) Beating rates of cardiomyocyte clusters with and without TENG-ES. f) Schematic diagram of in vitro TENG-ES of cardiomyocyte clusters with TENG device encapsulated in a biodegradable silk fibroin film. e,f) Reproduced with permission.[195] Copyright 2018, Wiley-VCH.

strongly differ from the results of the previously described multichannel electrode TENG system as the former system was only able to induce TA muscle contraction in one or two specific locations, whereas the increased current and power of the D-TENG allowed virtually every single location in which ES was applied to yield TA muscle contraction. Indeed, when using D-TENG-ES, the highest force recorded for the kicking motion of the TA muscle was 0.24 N, which is significant considering it was measured from the TA muscle of a rat. Consequently, efficient contraction of the TA muscle was established through the application of D-TENG-ES. However, much like the multichannel electrode TENG system, the D-TENG is currently only capable of inducing muscle contraction in a healthy organism. It remains to be confirmed whether or not the D-TENG will be able to induce complete muscle function rehabilitation. More research into applying the D-TENG to diseased or injured muscle models would be helpful to assess TENG's eventual application toward muscular rehabilitative efforts.

4.2. Cardiac Rehabilitation

The heart supplies all of the tissues of the body with oxygen- and nutrient-filled blood through its regular beating. Said beating is brought about by the cardiomyocytes which make up the heart muscle.[305,306] Sometimes cardiomyocytes are either not functional or do not beat in unison, resulting in electrophysiological anomalies including bradycardia, various arrhythmias, and tachycardia.[307] In order to treat these widespread conditions, the cardiomyocytes, which drive the pumping of the heart, may require some form of rehabilitation. This can be achieved through ES, as cardiomyocytes interact with each other and function as a whole, through electrical connections known as gap junctions.[308] A TENG-ES device was developed in this sense to help treat bradycardia and various arrhythmias, by essentially rehabilitating the existing cardiomyocytes making up the heart muscle in a process known as cardioversion. TENG-ES devices are specifically suited for this role given their microscaled nature, the consistency of their output, their high resistance to cyclic stress, and their comfortability.

Cardiomyocytes are the functional units that make up the heart muscle. Through effective intracellular communication they are able to induce a regular and powerful beating motion to power the pumping of the heart.[309–311] Since cardiomyocytes are constantly contracting and relaxing, they are structurally different from most muscle cells, as they are more resistant to fatigue. Cardiomyocytes are similar to normal muscle cells in their general structure composed of functional units called sarcomeres, which give muscle cells their characteristic striated appearance. These sarcomeres are also present in skeletal

muscle cells, and function in the same manner. However, what sets cardiomyocytes apart from skeletal muscle cells is how electrical signals flow through them and their overall system connectivity. Morphologically, this is manifested in the form of intercalated disks composed of gap junctions, desmosomes, and adherens junctions allowing electrical signals to pass between cardiomyocytes' junctions, in addition to T-tubules which provide a more effective route for calcium ion flow to all the interconnected cardiomyocytes. The combination of the intercalated disks and T-tubules creates a unified system capable of providing continuous and rhythmic contractions of heart muscle tissue.

In order to function correctly, an implantable TENG device needs to be rendered biodegradable since this ES therapy does not require permanent administration. Jiang et al. developed a TENG device in which silk fibroin (SF) was used as the encapsulation layer due to its triboelectric properties, as well as its interactions with methanol which render it more resistant to body fluids.[195] In order to prove the increased resistivity of the methanol-treated SF (M-SF) in comparison to the untreated SF (U-SF), both were implanted near the heart of rats. After 21 days, the U-SF encapsulated TENG device was mostly dissolved by the rats' bodily fluids and only two small pieces remained. On the other hand, the M-SF encapsulated TENG device remained undissolved until the 42nd day. This stark difference in dissolving rates based on the treatment of the encapsulation layer with methanol, allows for the creation of specific degradation rates for the TENG device depending on the required duration of ES therapy. In addition, the degradation of the SF encapsulated TENG resulted in no observable inflammation or granulocyte formation, suggesting biocompatibility of the TENG device.

In order to evaluate the effect of TENG-ES therapy on cardiomyocyte rehabilitation, in vitro studies were conducted with primary cardiomyocytes seeded onto the surface of the TENG device's electrodes. Without ES, the five cardiomyocyte clusters (C1–C5) beat slowly with a long pause between beats, however when TENG-ES was applied to the cardiomyocyte clusters, the beating rates increased significantly, with the individual beating cycle for C1 reduced from 1.382 to 0.606 s.[195] In addition, the beating rates of C2 and C3 were almost nine times faster when provided with TENG-ES. As can be seen in Figure 5e the average time for one beating cycle before ES was 0.320 s, whereas that of the cardiomyocyte clusters after TENG-ES was only 0.240 s, indicating increased beating rates of cardiomyocyte clusters as a direct result of TENG-ES. Another factor to consider in addition to the beating rates of the cardiomyocyte clusters, is the dispersion of these beats. The coefficient of variation for the cardiomyocyte clusters not exposed to ES, was 0.81, which was ≈2.6× higher than the coefficient of variation after TENG-ES. Thus, the beating rates among the different cardiomyocyte clusters appeared more uniform after exposure to TENG-ES. Since cardiomyocytes communicate with each other through electrical interconnections made through gap junctions, the TENG-ES effectively provided each cluster of cardiomyocytes with electrical impulses directing their quicker and more unified contractions.

Although this TENG device appears to be an optimal candidate for cardiac therapy, especially in the cases of treating various temporary arrhythmias, the TENG device's ability to function normally in the hostile environment within the human body must be improved as oftentimes these implantable TENG systems rapidly lose efficiency due to body fluid infiltration into the electrodes. In addition, as shown by Figure 5f, the current state of the art in TENG-ES devices designed for cardiac therapy is not yet applied in vivo and is mostly utilized to perform therapeutic ES on cardiomyocytes in vitro due to the adverse conditions within the human body.[195] Thus, more research into the implantability and proper encapsulation of the TENG must be conducted before the TENG can be universally applied for cardiac therapies, especially in the form of IOB bioelectronic devices.

4.3. Outlook

Rehabilitative engineering technologies are of vital importance as they improve the quality of life of millions of people around the world suffering from various conditions and diseases. The recent advent of the TENG allows for a continuous and bioconformable form of ES that can be utilized in the field of rehabilitative engineering, even though it has so far mostly been applied to muscle rehabilitation and cardiac rehabilitation. Regardless, there are limitations to the current research conducted in these two subfields of rehabilitative engineering.

Current research pertaining to muscle rehabilitation only shows an ability of researchers to induce muscle contraction in healthy rats, thus the TENG's ability to rehabilitate damaged or malfunctioning muscles is not proven. However, inducing muscle contraction through TENG-ES is the first step toward creating a TENG-based rehabilitative system for patients with muscular disabilities. More research into the multichannel electrode TENG system and the D-TENG's abilities to induce muscle contraction must be conducted to help develop an effective TENG-based muscle rehabilitation technology.

In regards to cardiac rehabilitation, current research has only proven rehabilitation of malfunctioning cardiomyocytes in vitro, however this TENG-ES system is yet to be applied to cardiomyocytes in vivo. Moreover, TENG-ES has only been shown to improve the communication between healthy cardiomyocytes to improve irregular beating patterns. In addition to transitioning research on cardiomyocyte rehabilitation from in vitro to in vivo studies, research in the development of a TENG-based system capable of healing or inducing the proliferation of cardiomyocytes must be conducted. In the future, TENG devices could be used to aid with overall cardiac rehabilitation after myocardial infarctions, which would be a monumental development in the field of rehabilitative engineering.

5. Pharmaceutical Engineering

The pharmaceutical industry is the main contributing force behind the treatment and development of cures for diseases that affect people around the world. Drugs capable of treating diseases from rabies to smallpox have been developed and delivered to people around the world in such an effective manner that these diseases have been fundamentally contained or even eradicated. However, new diseases are always emerging

including the recent severe acute respiratory syndrome novel coronavirus 2 (SARS-CoV-2) and its associated pandemic coronavirus disease 2019 (COVID-19). The development of new vaccines and drugs is critical to stop this spread of novel diseases.[312] A critical factor in pharmaceutical engineering is drug administration. There are numerous different ways in which drugs can be administered: orally, intravenously, in nebulized form, and transdermally.[313] This transdermal approach for drug administration is becoming more popular as it provides a noninvasive, yet effective form of drug administration that bypasses oral degradation.[314]

In this sense, TENG-ES can be used to power various transdermal drug delivery systems. TENG is especially suited for powering drug delivery systems because not only does it induce the absorption of drug molecules, but it increases the permeability of the skin to drug molecules through the process of iontophoresis, increasing the rate at which the drug molecules are transferred across the dermal layers.[197] The main forms of transdermal drug delivery in which TENG-ES is utilized are microfluidic, transdermal patch, and microneedle drug delivery systems.[196–201] In addition, the main application of TENG-based drug delivery systems in cancer treatments is also addressed.[202]

5.1. Drug Delivery

The development of drugs to treat widespread diseases is the primary reason for which the average life expectancy and quality of life has been increasing in recent years.[315] The use of drugs to treat infections and diseases dates back to 3000 B.C., with Egyptians treating simple infections, and has evolved into modern day solutions such as biotherapeutics which include cell therapies. There are numerous ways in which drugs can be administered to the human body and within topical application, transdermal drug administration can include using normal topical application, microfluidic drug delivery,[196,199–201] needleless patch drug delivery systems,[197] or microneedle-based drug delivery systems.[198]

5.1.1. Microfluidic Drug Delivery

Transdermal drug delivery systems have been shown to yield promising results in drug delivery especially through the use of microtubes and combinatory approaches including the use of electrowetting techniques and microfluidic systems.[316,317] However, a portable and dependable power supply is needed to overcome the aforementioned powering limitations.[318] With the recent development of the TENG, existing drug delivery systems can attain a portable and dependable power supply with which to deliver drugs to the patient transdermally, specifically enhanced by TENG-ES devices' self-reliance and closed-loop system approach. Microfluidic systems are a cornerstone of modern drug delivery as they allow for efficient and predictable drug delivery.[316,317] However, in order to drive the movement of drug-containing microdroplets, microfluidic systems necessitate some form of actuation which can be provided by pneumatic micropumps, electroosmotic channels, or via electrostatic actuation. TENG is an optimal candidate to provide this actuation in the form of ES due to its biocompatibility and efficient conversion of biomechanical movements into electrical energy. There are two main ways in which microfluidic drug delivery systems can be facilitated as microdroplets can move through microtubes via: 1) actuation or via 2) electrowetting of water droplets.

When employing microtube-based microfluidic drug delivery systems, oftentimes the form of actuation of the microdroplets through the microtubes, is gas pressurization, as conducted by Song et al. for instance. As shown in **Figure 6**a, the microtube-based drug delivery device was composed of a reservoir in which drug molecules were stored in solution and a microtube extended out from the reservoir in addition to the connections to the TENG device.[196] The TENG could generate the gas pressure gradient needed by catalyzing the water splitting process, generating oxygen and hydrogen gas. This gas accumulated in a reservoir and pushed drug filled microdroplets through a microtube which could administer the drug molecules to virtually any part of the human body. The drug filled microdroplets could be administered through microtubes as long as 640 mm. In order to visualize the drug molecules as they are being administered into biological tissue, they were fluorescently stained and injected into a porcine eye through the TENG-based microtube drug delivery system. As can be seen in Figure 6b, these fluorescently stained particles filled the anterior chamber of the eye as expected. The rate of drug delivery was directly correlated with the electrical energy produced by the TENG, as this electrical energy was used to power the electrolysis reactions. This TENG-based microtube drug delivery system was able to administer ≈5.3–40 μL of drug filled microdroplets per minute, based on the amount of biomechanical movement stimulating the TENG device directly. In order to visualize this drug delivery into porcine skin, in a related study Ouyang et al. doped the porcine skin with FLU (6-carboxyfluorescein), and as shown in Figure 6c, the optimal drug delivery occurred when TENG-ES was introduced to the drug delivery system.[197] For many drug delivery applications, a rate of drug administration of 5.3–40 μL of drug filled nanoparticles per minute is sufficient, making such a TENG-based microtube drug delivery system an efficient and bioconformable form of drug delivery. As can be seen in Figure 6d, Ouyang et al. developed a transdermal drug delivery system powered by a radially arrayed TENG, which generates electricity through the rotary motion of the rotator in relation to the PTFE and stator layers.

Microfluidic drug delivery systems that rely on the electrowetting technique to transport drug-filled microdroplets are generally made up of a hydrophobic substrate as an encapsulation layer, the drug infused water microdroplets, and some type of actuator.[198] In order to test the effectiveness of the TENG device as an ES-based actuator for this electrowetting-based microfluidic drug delivery system, Kapton was used as the hydrophobic substrate, and Ag nanoparticles were used to mimic drug molecules infused within the water microdroplets that travel along the surface of the Kapton film. The electric field applied to the water microdroplets changes the contact angle they exhibit with the Kapton film, and this change in contact angle yields movement in the microdroplet due to Coulomb forces. This working mechanism allows the Ag nanoparticle infused microdroplets to move horizontally and vertically, allowing the use of this system anywhere on the human body. Since the water droplet is so small, once it reaches

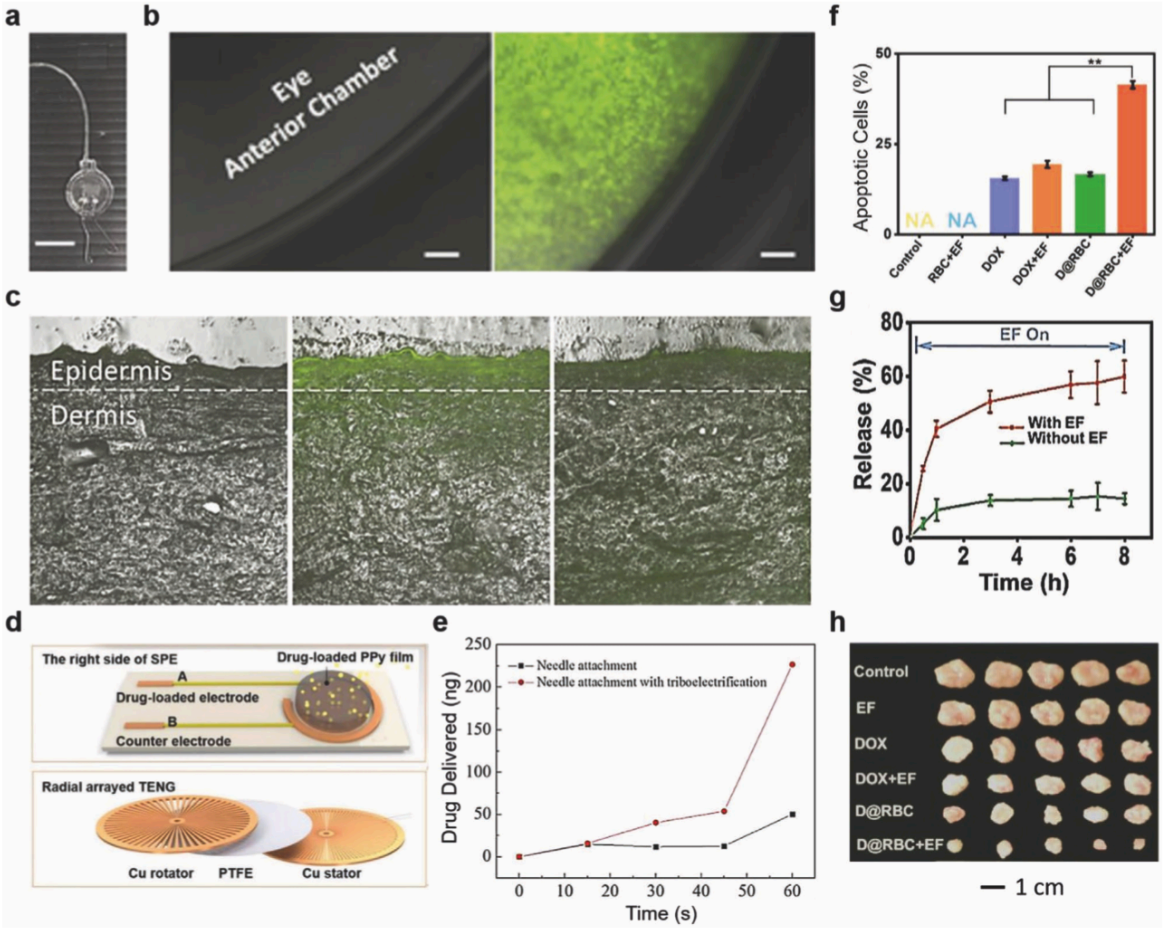

Figure 6. TENG-ES therapeutic devices for drug delivery and cancer therapy. a) Photograph of implantable drug delivery system which is attached to a rotary TENG composed of Cu and PTFE triboelectric layers (scale bar: 10 mm). b) Fluorescence microscopy images of delivery of fluorescent microparticles to anterior chamber of eye with TENG-based microfluidic drug delivery system (scale bars: 200 µm). a,b) Reproduced with permission.[196] Copyright 2017, Wiley-VCH. c) Fluorescence microscopy images of drugs delivered to porcine skin with TENG-based microfluidic drug delivery system. d) Structural design of radially array TENG in addition to transdermal drug delivery system. c,d) Reproduced with permission.[197] Copyright 2019, Elsevier. e) Amount of drug delivered into gelatin without TENG-ES of microneedle drug delivery system. Reproduced with permission.[198] Copyright 2018, Royal Society of Chemistry. f) Proportion of apoptotic cells after 2 days of treatment under various conditions. g) Release kinetics of drug delivery system with and without MTENG-ES. h) Images of harvested tumors exposed to different conditions. f–h) Reproduced with permission.[202] Copyright 2019, Wiley-VCH.

its target location, it does not take long for the water to volatilize, leaving the Ag nanoparticles behind which in this experiment mimicked drug particles. For example, a water droplet with a volume of only 100 nL, volatilized within only 2 min, a property which can be manipulated by researchers depending on the application. One of the main factors to take into account for this microfluidic drug delivery system was the concentration of Ag nanoparticles within each water microdroplet. There was a big drop off in driving distance when the concentration of Ag nanoparticles reached 100 mg mL^{-1}, however when the concentration was less than 50 mg mL^{-1} there was virtually no difference, and the system exhibited its maximum driving distance. There are several issues with integrating this microfluidic drug delivery system with the human body, but it remains an efficient form of delivering drugs with the help of TENG-ES.

Microfluidic drug delivery systems, whether they rely on microtubes or the electrowetting technique, are an excellent form of drug delivery as they are highly efficient as well as controllable. The introduction of the TENG into these microfluidic drug delivery systems renders these systems more bioconformable as well as self-dependent. However, further research needs to be conducted applying this TENG-based drug delivery technology to human skin models.

5.1.2. Transdermal Patch Drug Delivery

The most common form of transdermal drug delivery is through the use of a medicated patch that delivers drugs to the bloodstream through the patient's skin, once said patch is

exposed to a controllable stimulus.[319] In the study conducted by Ouyang et al., the patch was composed of responsive polymers, exogenous in nature, such that when they were exposed to a particular exogenous stimulus such as light, ultrasound, or an electric field, they altered their shape and released the loaded payload of drugs.[197,320] In order to introduce an exogenous stimulus to trigger the system's drug delivery capabilities, a miniaturized supplier of an exogenous stimulus must be utilized so as to protect the portability and efficiency of the drug delivery system. The TENG was utilized as the supplier of ES needed to excite the electric-responsive drug carriers that make up the patch. However, not only did the TENG device induce drug delivery by stimulating the polymers within the patch to release the loaded drug molecules, but the electric field generated by the TENG device also increased the rate at which the drug molecules crossed the skin through iontophoresis.[197]

In order to test the effectiveness of this new TENG-based drug delivery system, the experiment was compared to the most common drug delivery system which derives electric stimulus from a potentiostat. Dexamethasone sodium phosphate ($DEX\text{-}P^-$) was loaded onto the patch portion of both of the systems and the systems ran for 10 min. Porcine skin was used, and the amount of $DEX\text{-}P^-$ that was administered across the skin was measured through high-performance liquid chromatography. The amount of $DEX\text{-}P^-$ released in the TENG drug delivery system was 30.7 ng cm^{-2}, significantly higher than the 5.7 ng cm^{-2} of the drug released by the traditional drug delivery system after 10 min of operation. The TENG drug delivery system is such an efficient drug delivery system that the ES and electric field produced by the TENG created voltage differences across the surface of the skin, increasing its permeability and enhancing the small particles' movement. This voltage difference also induces the movement of drug molecules across the skin through the processes of electrophoresis and electroosmosis.[197,321] A blank control consisting of the patch without a TENG or any sort of device to introduce a stimulus was also tested, and yielded no $DEX\text{-}P^-$ molecules movement.[197] These results indicate that the TENG-ES of the patch induces the release of drugs within the patch as well as increases the rate of movement of the drug molecules across the skin through iontophoresis.

The TENG drug delivery system is an optimal and promising candidate for transdermal drug delivery. However, this current system has only been tested to the porcine skin model, thus testing on human skin must occur before TENG-ES for drug delivery can be converted into a commercial product.

5.1.3. Microneedle Drug Delivery

Transdermal drug delivery methods have been a focus of a lot of drug delivery research lately as they are painless and do not lead to drug degradation. Microneedles effectively create small holes in the skin through which drugs can pass through into the tissue.[322,323] The use of microneedles is often looked at in conjunction with the technique of electrophoresis, in which the permeability of the lipid bilayer is increased due to the existence of high voltage electric pulses.[324]

Microneedle-based drug delivery devices require drug-embedded microneedles to puncture the skin and allow for drugs to pass. TENG-ES can be used to generate electric pulses which induce electrophoresis across the lipid bilayer of the skin. In a particular study, microneedles were inserted into porcine skin, successfully penetrating the skin and dissolving.[198] In order to deduce the drug-administration capabilities of the TENG-ES based microneedle system, the microneedles were inserted into a transparent gelatin hydrogel derived from bovine skin. As can be seen in Figure 6e, after 60 min of TENG-ES microneedle drug administration, ≈220 ng of the drug were administered, while the control without the added electric stimulus from the TENG only administered 50 ng. This significant difference in the amount of drug molecules administered by the TENG-ES based microneedle drug delivery system is due to the fact that the microneedles are negatively charged, thus the drug diffusion is enhanced by the TENG-ES. Microneedle-based drug delivery is an exciting and revolutionary concept in the world of drug delivery, however current research is limited to hydrogel and porcine-based tests whereas this integrated system needs to be adapted to the human skin model in order to demonstrate its capabilities to deliver significantly impactful solutions.

5.2. Cancer Therapy

A very specific application of drug delivery is for the treatment of cancer. In order to treat many different forms of cancer, patients generally undergo chemotherapy treatment which consists of exposing the body to a high concentration of drugs, such as doxorubicin (DOX), that target fast-growing cells.[325]

Delivering DOX to cancerous cells utilizing red blood cells as drug carriers is the most effective approach, as the latter are perfectly biocompatible, have long half-lives, and have flexible structures, which allow them to permeate to cancerous sites.[326,327] Accordingly, red blood cells were the main drug carrier for the introduction of DOX into cancerous cells in the study conducted by Zhao et al. In order to create a controllable drug delivery system, a magnetic TENG (MTENG) was developed as the ES generated by the MTENG can induce DOX delivery from red blood cells to cancerous cells. As shown in Figure 6g, ≈40% of the DOX was released from the red blood cells after 1 h of MTENG-ES, whereas only 14% of the DOX was released in the red blood cells not exposed to ES.[192] In addition, when the MTENG system was temporarily hindered from generating ES, both groups of red blood cells released the same amount of DOX. This specific technique can be utilized by clinicians to control the amount of DOX that needs to be released to different parts of the body. When the MTENG drug delivery mechanism was introduced into a 3D multicellular spheroids (MCTS) environment, its effects on tumor development were studied through the combined use of TUNEL (terminal deoxynucleotidyl transferase-mediated dUTP nick-end labeling) assays and DAPI staining, allowing researchers to visualize the tumor size within the MCTS environment, as well as monitor to the number of cancerous cells undergoing apoptosis.

All of the groups in which DOX was introduced, induced some degree of apoptosis within the tumor cells, thus

significantly reducing the size of the extracted tumor (Figure 6f). The most successful of these groups in achieving decreased tumor size as well as increased apoptosis among tumor cells was the DOX-loaded red blood cells, whose drug delivery mechanisms were enhanced by MTENG-ES as shown by Figure 6h.[192] ES provided by the MTENG increased the rate at which DOX was administered to cancerous cells, and provided a controllable mechanism for drug delivery to ensure increased DOX concentrations exclusively at tumor sites. This approach can be an effective mechanism for tumor growth suppression, and can potentially provide a mechanism for delivering drugs to cancer patients in the future. Although TENG-based DOX drug delivery is shown to effectively hinder the proliferation of cancerous cells, this system can only be applied to DOX-sensitive tumors. Subsequently, different TENG-ES based drug delivery systems need to be developed in accordance with other drugs and cancer types.

5.3. Outlook

Drug delivery systems are needed to effectively deliver drugs to the required site of action. The development of TENG-ES is a monumental advancement in the field of drug delivery as it is especially apt at transdermal drug delivery, a mode of drug delivery that is becoming increasingly popular, due to its association with iontophoresis. TENG-ES based transdermal drug delivery systems, although effective, are still in their infant stages of development. With their proven application to human skin models, these TENG-ES based drug delivery systems could soon become leaders in drug delivery, integrated in targeted IOB bioelectronics.

6. Summary and Future Outlook

We have compiled the recent advances and developments in TENG use for the application of therapeutic ES. The field has rapidly grown in the last few years, and the above review should be testament to the wide-ranging potential of TENG-ES in constituting a novel technology platform in many medical fields. Compared to other novel microscaled energy harvesting technologies, such as piezoelectric nanogenerators (PENGs), TENGs have demonstrated the best suitability in the ES field given their adequate high voltage, low current generation capabilities as well as different working mechanisms that are able to harness the energy of a variety of biomechanical movements.

As mentioned, TENG will not only enable the replacement of what will seem antiquated external power sources, but by its inherent connectability predisposition, coupled with the emergence of the 5G network and IoT, will enable a holistic approach to IOB medtech. Such characteristics yield TENG systems capable of offering a connected, yet self-contained diagnostic, preventative, and therapeutic solution. Green chemistry and sustainability are becoming of ubiquitous importance in all industrial fields.[328] The miniaturized, low-cost, and easily manufacturable materials employed to manufacture TENG devices provide a solid foundation for inexpensive and ecofriendly IOB therapeutic solutions.

Efforts, however, also need to be focused at identifying objective and potential drawbacks of using TENGs as IOB devices, using ES for therapeutic application, and specifically at using TENG-ES. For instance, for the former, the use of rare metals, which are often used in TENG, and their use for the first time within IOB TENG devices needs to be closely monitored for cytotoxicity and tissue combability. Moreover, the small size of such devices mean that they could be easily displaced, and that the formation of hard fibrotic foreign-body response tissue around them might prevent TENGs from working effectively. On the second point, ES itself needs to be further investigated as it could lead to localized heat-shock, prolonged localized inflammation, as well as ES-related discomfort or pain. Finally, specifically for TENG-ES, there could be potential issues with TENG-ES IOB displacement to electrophysiologically sensitive areas such as areas near the heart, and for which adverse TENG-ES activity could lead to severe cardiovascular events.

Furthermore, we invite researchers to develop specific TENG-ES therapeutic protocols with which to test and validate optimized ES parameters for specific treatment applications, such as voltage and current outputs. A standardized approach within the TENG industry as well as the TENG-ES industry will be required to jettison this technology into the medical device industry and help develop commercially sound medical devices.

A stark difference that was highlighted recurrently in the review is the conformable shape and adherence to both internal and external human topography provided by TENG devices, and how this key aspect will bode well for the development of minimally invasive IOB medtech applications. The capability to both seamlessly fit into and onto the human body, as well as harness biomechanical movements to provide therapeutic ES in a self-sustainable manner, will propel TENG developments in areas that current medtech solutions do not allow. For instance, within the field of neural engineering alone, TENG devices can be utilized as preventative, rehabilitative, as well as therapeutic technologies (**Table 1**) for deleterious neural diseases such as Parkinson's Disease. For late-stage Parkinson's Disease patients, many resort to deep brain stimulation, which involves the implantation of leads into a specific portion of the brain through which carefully measured electrical stimulation is applied.[353–355] While this procedure is very invasive and requires surgery, it has shown to greatly enhance the quality of life of late-stage Parkinson's Disease patients, and TENG could be an excellent candidate for the energy generation of this device. Although this represents an ambitious task due to the density of neural connections found in the brain, TENG-ES's versatility could offer a potential treatment for Parkinson's disease through deep brain stimulation.

Within the field of regenerative medicine, TENG devices could potentially be utilized in conjunction with stem cell therapies in order to treat internal tissue wounds rather than surface level skin wounds. TENG-ES has already proved to enhance the differentiation of stem cells into neuronal cells given certain conditions, thus this same technology could be applied to stem cells with differentiation pathways into cells critical in the tissue regeneration and reconstruction processes, such as fibroblasts and endothelial cells. This approach could enhance the efficacy of current stem cell therapies for tissue regeneration applications as the electric field generated by the TENG device

Table 1. A summary of nascent ES therapies particularly suited to TENG-ES therapy.

Bioengineering fields	Types	Applications	Ref
Regenerative medicine	Preventative	Prevent sweating in patients with hyperhidrosis	[333–335]
		Prevent muscular atrophy in patients with diabetes	[336]
	Rehabilitative	Heal scar tissue	[337–339]
		Regenerate alveolar bone in periodontal disease	[340]
	Treatment	Use with stem cell therapies for internal wounds	[341–343]
		Regenerate lost or amputated limbs or appendages	[348]
Neural engineering	Preventative	Prevent development of Parkinson's Disease	[345–347]
		Prevent and reduce seizures due to epilepsy	[348]
	Rehabilitative	Motoneuron therapy for spinal cord injury	[349–351]
		Regeneration of neural tissue and connections	[352]
	Treatment	Deep brain stimulation for Parkinson's Disease	[353–355]
		Stimulation of tibial nerve for fecal incontinence	[356]
Rehabilitation engineering	Preventative	Prevent muscle weakness in critically ill patients	[357]
		Prevent venous thromboembolism	[358,359]
	Rehabilitative	Rebuild muscle mass and function	[360]
		Rehabilitate function in pulmonary diseases	[361]
	Treatment	Spinal realignment in scoliosis patients	[362,363]
		Enhance function in chronic kidney diseases	[364]
Pharmaceutical engineering	Preventative	Prevent corneal neuropathic pain	[365]
		Prevent auditory neuron degeneration	[366,367]
	Rehabilitative	Peripheral nerve regeneration	[368,369]
		Rehabilitate function in COVID-19 patients	[370,371]
	Treatment	Treatment of osteoporosis	[372]
		Treatment of various retinal diseases	[373,374]

could both enhance the differentiation of the stem cells and recruit cells critical to the regeneration process to the site of the wound.[341–343] Furthermore, this same system could be applied to the regeneration of scar tissue to a healthy state since stem cells are utilized in several tissue regeneration applications similar to scar tissue healing.[337–339] An approach that could prove to be useful in the future is the implementation of a hydrogel-based TENG device for therapeutic ES, since existing regenerative medicine applications rely on the application of hydrogel-based biomaterials.[329–331] However, this concept poses numerous problems, which require innovative solutions, such as the fact that hydrogel has a small compressive strength, and can break easily when under stress from a large pressing force.[332]

TENG-ES has also shown remarkable promise in rehabilitating musculoskeletal function in patients with impaired activity via tailored ES both at the muscle tissue level as well as at the neuromuscular junction. This TENG technology could be utilized for applications as simple as rebuilding muscle mass after treatment in an intensive care unit[360] to aiding in the process of spinal realignment in scoliosis patients.[362,363] Cardiac rehabilitation and cardiac tissue regeneration also have potential effective therapies to be gained via the use of TENG-ES, as discussed earlier. Finally, transdermal drug delivery methodologies, which can be enhanced by self-powered and autonomous TENG-ES, have been shown to pave the way for bespoke therapies in a number of fields, including cancer therapy. Existing studies can be expanded upon to include a TENG-based drug delivery system for the prevention of corneal neuropathic pain[365] and the treatment of various retinal diseases[373,374] since a TENG device for drug delivery to the eye has already been reported.

By delving into a number of medical applications and through a series of nifty engineering solutions, TENG-ES showcases a plethora of intelligent and forward-looking therapeutic solutions at the preventative, rehabilitative, and therapeutic level (Table 1). Despite a number of pain points that have yet to be addressed in depth (large scale manufacturing processes, economics, and introduction into industry), we have highlighted the benefits of such a promising technology, capable of eventually disrupting the medical device industry as well as enhancing the existing technologies comprising the body area network. Further research into a number of other fields such as rehabilitation and pharmaceutical engineering among others will provide a number of opportunities for TENG-ES therapy, further developing the medical device industry. We expect that specific unmet clinical needs best suited to ES, which could benefit from TENG-ES, include Parkinson's disease, Alzheimer's disease, motor neuron disorders, cerebral palsy, as well as highly fastidious conditions such as restless leg syndrome and clinical "tics," and invite applicative research in this field.

Acknowledgements

G.Conta and A.L. contributed equally to this work. The authors acknowledge the Henry Samueli School of Engineering & Applied Science and the Department of Bioengineering at the University of California, Los Angeles for the startup support.

Conflict of Interest

The authors declare no conflict of interest.

Keywords

bioelectronics, electrical stimulation, personalized healthcare, regenerative therapy, triboelectric nanogenerators

Received: November 2, 2020
Revised: December 3, 2020
Published online:

[1] F. Firouzi, A. M. Rahmani, K. Mankodiya, M. Badaroglu, G. V. Merrett, P. Wong, B. Farahani, *Future Gener. Comput. Syst.* **2018**, *78*, 583.
[2] A. Kelati, H. Tenhunen, in *Proc. of the 2018 IEEE/ACM Int. Conf. on Connected Health: Applications, Systems and Engineering Technologies*, IEEE, Piscataway, NJ, USA **2018**, pp. 7–8.
[3] E. Mirtaheri, C. Z. Li, *Electrochem. Soc. Interface* **2019**, *28*, 71.
[4] G. Misra, V. Kumar, A. Agarwal, K. Agarwal, *Am. J. Electr. Electron. Eng.* **2016**, *4*, 23.
[5] J. Kim, A. S. Campbell, B. E. F. de Ávila, J. Wang, *Nat. Biotechnol.* **2019**, *37*, 389.
[6] A. J. Bandodkar, J. Wang, *Trends Biotechnol.* **2014**, *32*, 363.
[7] M. Stoppa, A. Chiolerio, *Sensors* **2014**, *14*, 11957.
[8] M. Tamsin, *Int. J. Sci.* **2015**, *13*, 697.
[9] M. A. P. Mahmud, N. Huda, S. H. Farjana, M. Asadnia, C. Lang, *Adv. Energy Mater.* **2018**, *8*, 1701210.
[10] F. Rattay, *Neuroscience* **1999**, *89*, 335.
[11] J. B. Ranck, *Brain Res.* **1975**, *98*, 417.
[12] R. Imberti, A. Amatu, *Eur. J. Histochem.* **2010**, 54.
[13] M. Doblaré, J. M. García, M. J. Gómez, *Eng. Fract. Mech.* **2004**, *71*, 1809.
[14] M. S. Ghiasi, J. Chen, A. Vaziri, E. K. Rodriguez, A. Nazarian, *Bone Rep.* **2017**, *6*, 87.
[15] F. A. Sabet, A. Raeisi Najafi, E. Hamed, I. Jasiuk, *Interface Focus* **2016**, *6*, 20150055.
[16] I. Pastar, O. Stojadinovic, N. C. Yin, H. Ramirez, A. G. Nusbaum, A. Sawaya, S. B. Patel, L. Khalid, R. R. Isseroff, M. Tomic-Canic, *Adv. Wound Care* **2014**, *3*, 445.
[17] M. J. Portou, D. Baker, D. Abraham, J. Tsui, *Vasc. Pharm.* **2015**, *71*, 31.
[18] A. Tremblay, E. Doucet, *Obes. Rev.* **2000**, *1*, 27.
[19] R. S. Ahima, *J. Clin. Invest.* **2011**, *121*, 2076.
[20] F. Assimacopoulos-Jeannet, B. Jeanrenaud, *Clin. Endocrin. Metab.* **1976**, *5*, 337.
[21] S. Ramachandrappa, I. S. Farooqi, *J. Clin. Invest.* **2011**, *121*, 2080.
[22] S. F. Altekruse, C. L. Kosary, M. Krapcho, N. Neyman, R. Aminou, W. Waldron, J. Ruhl, N. Howlader, Z. Tatalovich, H. Cho, A. Mariotto, M. P. Eisner, D. R. Lewis, K. Cronin, H. S. Chen, E. J. Feuer, D. G. Stinchcomb, B. K. Edwards, *SEER Cancer Statistics Review 1975–2007* **2010**.
[23] S. Deandrea, M. Montanari, L. Moja, G. Apolone, *Ann. Oncol.* **2008**, *19*, 1985.
[24] M. H. J. van den Beuken-van Everdingen, J. M. de Rijke, A. G. Kessels, H. C. Schouten, M. van Kleef, J. Patijn, *Ann. Oncol.* **2007**, *18*, 1437.
[25] N. J. Karagan, *Psychol. Bull.* **1979**, *86*, 250.
[26] W. M. Snow, J. E. Anderson, L. S. Jakobson, *Neurosci. Biobehav. Rev.* **2013**, *37*, 743.
[27] I. E. C. Verhaart, A. Aartsma-Rus, *Nat. Rev. Neurol* **2019**, *15*, 373.
[28] J. M. Peake, O. Neubauer, P. A. Della Gatta, K. Nosaka, *J. Appl. Physiol.* **2016**, *122*, 559.
[29] M. D. Neher, S. Weckbach, M. A. Flierl, M. S. Huber-Lang, P. F. Stahel, *J. Biomed. Sci.* **2011**, *18*, 90.
[30] D. A. Ibrahim, A. Swenson, A. Sassoon, N. D. Fernando, *Clin. Orthop. Relat. Res.* **2017**, *475*, 560.
[31] P. M. Ramos, H. A. Miot, *An. Bras. Dermatol.* **2015**, *90*, 529.
[32] M. Gupta, V. Mysore, *J. Cutan. Aesthet. Surg.* **2016**, *9*, 3.
[33] H. M. Almohanna, A. A. Ahmed, J. P. Tsatalis, A. Tosti, *Dermatol. Ther.* **2019**, *9*, 51.
[34] G. Fabbrocini, M. Cantelli, A. Masarà, M. C. Annunziata, C. Marasca, S. Cacciapuoti, *Int. J. Womens Dermatol.* **2018**, *4*, 203.
[35] M. Zarei, T. C. Wikramanayake, L. Falto-Aizpurua, L. A. Schachner, J. J. Jimenez, *Lasers Med. Sci.* **2016**, *31*, 363.
[36] H. H. Grape, A. Dedering, A. F. Jonasson, *Neurourol. Urodyn.* **2009**, *28*, 395.
[37] X. Li, L. Liao, *Int. Urol. Nephrol.* **2016**, *48*, 919.
[38] A. M. Suskind, *Curr. Bladder Dysfunct. Rep.* **2017**, *12*, 42.
[39] G. Arkan, A. Beser, V. Ozturk, *J. Neurosci. Nurs.* **2018**, *50*, 42.
[40] P. Wolfgang, S. Helmut, US2939952A, **1960**.
[41] M. Gerritsen, J. A. Lutterman, J. A. Jansen, *J. Biomed. Mater. Res.* **2000**, *53*, 702.
[42] L. C. Kloth, *Adv. Wound Care* **2014**, *3*, 81.
[43] B. Mollon, V. da Silva, J. W. Busse, T. A. Einhorn, M. Bhandari, *J. Bone Joint Surg. Am.* **2008**, *90*, 2322.
[44] G. Victoria, B. Petrisor, B. Drew, D. Dick, *Indian J. Orthop.* **2009**, *43*, 117.
[45] M. Griffin, A. Bayat, *Eplasty* **2011**, *11*, e34.
[46] H. Vandenburgh, *US20040043010A1*, **2004**.
[47] A. E. Snellings, W. M. Grill, *BJU Int.* **2012**, *110*, 136.
[48] S. Vukicevic, H. Oppermann, D. Verbanac, M. Jankolija, I. Popek, J. Curak, J. Brkljacic, M. Pauk, I. Erjavec, I. Francetic, I. Dumic-Cule, M. Jelic, D. Durdevic, T. Vlahovic, R. Novak, V. Kufner, T. Bordukalo Niksic, M. Kozlovic, Z. Banic Tomisic, J. Bubic-Spoljar, I. Bastalic, S. Vikic-Topic, M. Peric, M. Pecina, L. Grgurevic, *Int. Orthop.* **2014**, *38*, 635.
[49] D. Bourbeau, A. Bolon, G. Creasey, W. Dai, B. Fertig, J. French, T. Jeji, A. Kaiser, R. Kouznetsov, A. Rabchevsky, B. G. Santacruz, J. Sun, K. B. Thor, T. Wheeler, J. Wierbicky, *Spinal Cord.* **2020**, *58*, 1.
[50] J. D'Argent, *Obes. Surg.* **2002**, *12*, S21.
[51] M. Mizrahi, A. Ben Ya'acov, Y. Ilan, *World J. Gastroenterol.* **2012**, *18*, 2309.
[52] K. Bielefeldt, *Auton. Neurosci.* **2017**, *202*, 40.
[53] M. R. van Balken, H. Vergunst, B. L. H. Bemelmans, *J. Urol.* **2004**, *172*, 846.
[54] F. Stewart, L. F. Gameiro, R. E. Dib, M. O. Gameiro, A. Kapoor, J. L. Amaro, *Cochrane Database Syst. Rev.* **2016**, *12*, CD010098.
[55] S. Reddy, L. He, S. Ramakrishana, *Biomed. Signal Proces.* **2018**, *41*, 255.
[56] C. D. Wahlstrand, R. M. Skime, *US7555345B2*, **2009**.
[57] A. Tooker, T. E. Madsen, A. Yorita, A. Crowell, K. G. Shah, S. Felix, H. S. Mayberg, S. Pannu, D. G. Rainnie, V. Tolosa, in *2013 35th Annual Int. Conf. of the IEEE Engineering in Medicine and Biology Society (EMBC)*, IEEE, Piscataway, NJ, USA **2013**, pp. 5159–5162.
[58] A. C. Richards Grayson, R. Scheidt Shawgo, Y. Li, M. J. Cima, *Adv. Drug Delivery Rev.* **2004**, *56*, 173.
[59] D. Svirskis, J. Travas-Sejdic, A. Rodgers, S. Garg, *J. Controlled Release* **2010**, *146*, 6.

[60] S. Z. Razzacki, P. K. Thwar, M. Yang, V. M. Ugaz, M. A. Burns, *Adv. Drug Delivery Rev.* **2004**, *56*, 185.
[61] A. A. Entezami, B. Massoumi, *Iran. Polym. J.* **2006**, *15*, 13.
[62] Y. Cho, R. Shi, A. Ivanisevic, R. B. Borgens, *Nanotechnology* **2009**, *20*, 275102.
[63] M. R. Prausnitz, *Adv. Drug Delivery Rev.* **1996**, *18*, 395.
[64] X. Kong, S. N. Gozani, *US9675801B2*, **2017**.
[65] S. Murdan, *J. Controlled Release* **2003**, *92*, 1.
[66] J. Qu, Y. Liang, M. Shi, B. Guo, Y. Gao, Z. Yin, *Int. J. Biol. Macromol.* **2019**, *140*, 255.
[67] A. Hurlow, M. I. Bennett, K. A. Robb, M. I. Johnson, K. H. Simpson, S. G. Oxberry, *Cochrane Database Syst. Rev.* **2012**, *2012*, CD006276.
[68] P. Egor, C. Rohit, C. Jillian, T. Timothy, T. Julie, B. Kyle, G. Mantu, *J. Urol.* **2017**, *197*, e662.
[69] T. J. Smith, G. Marineo, *Am. J. Hosp. Palliative Care* **2018**, *35*, 812.
[70] M. R. Borges, N. M. L. de Oliveira, I. B. S. Antonelli, M. B. Silva, E. Crema, L. F. R. M. Fernandes, *Pain Manag.* **2020**, *10*, 235.
[71] R. D. Searle, M. I. Bennett, M. I. Johnson, S. Callin, H. Radford, *J. Pain Symptom Manag.* **2009**, *37*, 424.
[72] S. K. An, J. U. Lim, C. H. Kim, S. H. Kim, C. S. Mun, *US20170209693A1*, **2017**.
[73] J. Li, C. Guo, Z. Wang, K. Gao, X. Shi, J. Liu, *Clin. Transl. Med.* **2016**, *5*, 5.
[74] S. Hamid, R. Hayek, *Eur. Spine J.* **2008**, *17*, 1256.
[75] M. Rath, A. H. Vette, S. Ramasubramaniam, K. Li, J. Burdick, V. R. Edgerton, Y. P. Gerasimenko, D. G. Sayenko, *J. Neurotrauma* **2018**, *35*, 2540.
[76] S. Ananthanarayan, K. A. Siek, in *2012 6th Int. Conf. on Pervasive Computing Technologies for Healthcare (PervasiveHealth) and Workshops*, IEEE, Piscataway, NJ, USA **2012**, pp. 236–240.
[77] T. Page, *Int. J. Technol. Diff.* **2015**, *6*, 12.
[78] Y. Gao, H. Li, Y. Luo, *Ind. Manag.* **2015**, *115*, 1704.
[79] R. W. Geib, P. J. Swink, A. J. Vorel, C. S. Shepard, A. N. Gurovich, G. N. Waite, *Biomed. Sci. Instrum.* **2015**, *51*, 69.
[80] G. L. Henriksen, D. R. Vissers, A. A. Chilenskas, *J. Power Sources* **1995**, *54*, 134.
[81] R. Osborne, M. A. Perkins, *Food Chem. Toxicol.* **1994**, *32*, 133.
[82] N. Bhogal, C. Grindon, R. Combes, M. Balls, *Trends Biotechnol.* **2005**, *23*, 299.
[83] Y. Otsubo, T. Nishijo, M. Miyazawa, K. Saito, H. Mizumachi, H. Sakaguchi, *Regul. Toxicol. Pharmacol.* **2017**, *88*, 118.
[84] Y. Yang, X. Yang, Y. Tan, Q. Yuan, *Nano Res.* **2017**, *10*, 1560.
[85] S. Choi, S. I. Han, D. Jung, H. J. Hwang, C. Lim, S. Bae, O. K. Park, C. M. Tschabrunn, M. Lee, S. Y. Bae, J. W. Yu, J. H. Ryu, S. W. Lee, K. Park, P. M. Kang, W. B. Lee, R. Nezafat, T. Hyeon, D. H. Kim, *Nat. Nanotechnol.* **2018**, *13*, 1048.
[86] Y. Khan, A. E. Ostfeld, C. M. Lochner, A. Pierre, A. C. Arias, *Adv. Mater.* **2016**, *28*, 4373.
[87] H. Kudo, T. Sawada, E. Kazawa, H. Yoshida, Y. Iwasaki, K. Mitsubayashi, *Biosens. Bioelectron.* **2006**, *22*, 558.
[88] T. Yang, X. Jiang, Y. Zhong, X. Zhao, S. Lin, J. Li, X. Li, J. Xu, Z. Li, H. Zhu, *ACS Sens.* **2017**, *2*, 967.
[89] T. Someya, Z. Bao, G. G. Malliaras, *Nature* **2016**, *540*, 379.
[90] S. Jung, J. Lee, T. Hyeon, M. Lee, D. H. Kim, *Adv. Mater.* **2014**, *26*, 6329.
[91] A. J. Bandodkar, J. Wang, *Electroanalysis* **2016**, *28*, 1188.
[92] C. Choi, Y. Lee, K. W. Cho, J. H. Koo, D. H. Kim, *Acc. Chem. Res.* **2019**, *52*, 73.
[93] L. Polsky, M. A. G. von Keyserlingk, *J. Dairy Sci.* **2017**, *100*, 8645.
[94] S. Ali, M. Rizwan, M. S. Arif, R. Ahmad, M. Hasanuzzaman, B. Ali, A. Hussain, *J. Plant Growth Regul.* **2020**, *39*, 456.
[95] S. C. Liu, M. Tomizuka, G. Ulsoy, *Struct. Control Health Monit.* **2006**, *13*, 946.
[96] R. L. Drury, *Front. Psychol.* **2014**, *5*, 853.
[97] Z. Lou, L. Li, L. Wang, G. Shen, *Small* **2017**, *13*, 1701791.
[98] F. Zahir-Jouzdani, J. D. Wolf, F. Atyabi, A. Bernkop-Schnürch, *Expert Opin. Drug Delivery* **2018**, *15*, 1007.
[99] X. Du, J. Zhou, J. Shi, B. Xu, *Chem. Rev.* **2015**, *115*, 13165.
[100] X. Li, A. T. L. Hong, N. Naskar, H. J. Chung, *Biomacromolecules* **2015**, *16*, 1525.
[101] A. M. V. Mohan, N. Kim, Y. Gu, A. J. Bandodkar, J. M. You, R. Kumar, J. F. Kurniawan, S. Xu, J. Wang, *Adv. Mater. Technol.* **2017**, *2*, 1600284.
[102] L. Han, L. Yan, M. Wang, K. Wang, L. Fang, J. Zhou, J. Fang, F. Ren, X. Lu, *Chem. Mater.* **2018**, *30*, 5561.
[103] H. J. Kim, E. C. Yim, J. H. Kim, S. J. Kim, J. Y. Park, I. K. Oh, *Nano Energy* **2017**, *33*, 130.
[104] Y. Yu, X. Wang, *Extreme Mech.* **2016**, *9*, 514.
[105] C. X. Lu, C. B. Han, G. Q. Gu, J. Chen, Z. W. Yang, T. Jiang, C. He, Z. L. Wang, *Adv. Eng. Mater.* **2017**, *19*, 1700275.
[106] X. Cheng, L. Miao, Y. Song, Z. Su, H. Chen, X. Chen, J. Zhang, H. Zhang, *Nano Energy* **2017**, *38*, 438.
[107] Y. Xie, S. Wang, L. Lin, Q. Jing, Z. H. Lin, S. Niu, Z. Wu, Z. L. Wang, *ACS Nano* **2013**, *7*, 7119.
[108] Q. Liang, Q. Zhang, X. Yan, X. Liao, L. Han, F. Yi, M. Ma, Y. Zhang, *Adv. Mater.* **2017**, *29*, 1604961.
[109] J. W. Lee, B. U. Ye, J. M. Baik, *APL Mater.* **2017**, *5*, 073802.
[110] A. Ahmed, I. Hassan, T. Jiang, K. Youssef, L. Liu, M. Hedaya, T. A. Yazid, J. Zu, Z. L. Wang, *Nanotechnology* **2017**, *28*, 185403.
[111] X. Xia, J. Chen, G. Liu, M. S. Javed, X. Wang, C. Hu, *Carbon* **2017**, *111*, 569.
[112] H. Shao, Z. Wen, P. Cheng, N. Sun, Q. Shen, C. Zhou, M. Peng, Y. Yang, X. Xie, X. Sun, *Nano Energy* **2017**, *39*, 608.
[113] Z. L. Wang, *Faraday Discuss.* **2015**, *176*, 447.
[114] F. R. Fan, L. Lin, G. Zhu, W. Wu, R. Zhang, Z. L. Wang, *Nano Lett.* **2012**, *12*, 3109.
[115] S. Pan, Z. Zhang, *Friction* **2019**, *7*, 2.
[116] J. M. Baik, J. P. Lee, *Sci. Technol. Adv. Mater.* **2019**, *20*, 927.
[117] C. A. Mizzi, A. Y. W. Lin, L. D. Marks, *Phys. Rev. Lett.* **2019**, *123*, 116103.
[118] J. Xiong, P. S. Lee, *Sci. Technol. Adv. Mater.* **2019**, *20*, 837.
[119] S. Wang, L. Lin, Z. L. Wang, *Nano Lett.* **2012**, *12*, 6339.
[120] W. Weng, J. Yang, Y. Zhang, Y. Li, S. Yang, L. Zhu, M. Zhu, *Adv. Mater.* **2020**, *32*, 1902301.
[121] N. Balke, P. Maksymovych, S. Jesse, I. I. Kravchenko, Q. Li, S. V. Kalinin, *ACS Nano* **2014**, *8*, 10229.
[122] Y. Jiang, L. Xu, K. Pan, T. Leng, Y. Li, L. Danoon, Z. Hu, *IET Microwave* **2019**, *13*, 99.
[123] W. C. Chuang, H. L. Lee, P. Z. Chang, Y. C. Hu, *Sensors* **2010**, *10*, 6149.
[124] X. Feng, Y. Zhang, L. Kang, L. Wang, C. Duan, K. Yin, J. Pang, K. Wang, *Front. Chem. Sci. Eng.* **2021**, *15*, 238.
[125] C. Chen, Z. Wen, J. Shi, X. Jian, P. Li, J. T. W. Yeow, X. Sun, *Nat. Commun.* **2020**, *11*, 4143.
[126] G. Liu, S. Xu, Y. Liu, Y. Gao, T. Tong, Y. Qi, C. Zhang, *Adv. Funct. Mater.* **2020**, *30*, 1909886.
[127] J. H. Bae, H. J. Oh, J. Song, D. K. Kim, B. J. Yeang, J. H. Ko, S. H. Kim, W. Lee, S. J. Lim, *Polymers* **2020**, *12*, 658.
[128] F. Yang, J. Guo, L. Zhao, W. Shang, Y. Gao, S. Zhang, G. Gu, B. Zhang, P. Cui, G. Cheng, Z. Du, *Nano Energy* **2020**, *67*, 104210.
[129] H. Wang, L. Xu, Y. Bai, Z. L. Wang, *Nat. Commun.* **2020**, *11*, 4203.
[130] H. Liu, Y. Feng, J. Shao, Y. Chen, Z. L. Wang, H. Li, X. Chen, Z. Bian, *Nano Energy* **2020**, *70*, 104499.
[131] J. Ding, W. Q. Tao, S. K. Fan, *Nano Energy* **2020**, *70*, 104473.
[132] I. W. Tcho, W. G. Kim, Y. K. Choi, *Nano Energy* **2020**, *70*, 104534.
[133] J. Liao, Y. Zou, D. Jiang, Z. Liu, X. Qu, Z. Li, R. Liu, Y. Fan, B. Shi, Z. Li, L. Zheng, *Nano Energy* **2020**, *69*, 104417.
[134] L. Liu, Q. Shi, C. Lee, *Nano Energy* **2020**, *76*, 105052.
[135] H. Wang, J. Zhu, T. He, Z. Zhang, C. Lee, *Nano Energy* **2020**, *78*, 105241.

[136] D. Vera Anaya, T. He, C. Lee, M. R. Yuce, *Nano Energy* **2020**, *72*, 104675.
[137] M. L. Seol, J. H. Woo, S. B. Jeon, D. Kim, S. J. Park, J. Hur, Y. K. Choi, *Nano Energy* **2015**, *14*, 201.
[138] C. Jin, D. S. Kia, M. Jones, S. Towfighian, *Nano Energy* **2016**, *27*, 68.
[139] S. Wang, L. Lin, Y. Xie, Q. Jing, S. Niu, Z. L. Wang, *Nano Lett.* **2013**, *13*, 2226.
[140] S. Niu, Y. Liu, S. Wang, L. Lin, Y. S. Zhou, Y. Hu, Z. L. Wang, *Adv. Mater.* **2013**, *25*, 6184.
[141] S. Niu, Y. Liu, S. Wang, L. Lin, Y. S. Zhou, Y. Hu, Z. L. Wang, *Adv. Funct. Mater.* **2014**, *24*, 3332.
[142] N. Kaur, J. Bahadur, V. Panwar, P. Singh, K. Rathi, K. Pal, *Sci. Rep.* **2016**, *6*, 38835.
[143] Y. Yang, H. Zhang, J. Chen, Q. Jing, Y. S. Zhou, X. Wen, Z. L. Wang, *ACS Nano* **2013**, *7*, 7342.
[144] Y. Yang, Y. S. Zhou, H. Zhang, Y. Liu, S. Lee, Z. L. Wang, *Adv. Mater.* **2013**, *25*, 6594.
[145] S. Wang, S. Niu, J. Yang, L. Lin, Z. L. Wang, *ACS Nano* **2014**, *8*, 12004.
[146] Y. Xie, S. Wang, S. Niu, L. Lin, Q. Jing, J. Yang, Z. Wu, Z. L. Wang, *Adv. Mater.* **2014**, *26*, 6599.
[147] S. Wang, Y. Xie, S. Niu, L. Lin, Z. L. Wang, *Adv. Mater.* **2014**, *26*, 2818.
[148] S. Niu, Y. Liu, X. Chen, S. Wang, Y. S. Zhou, L. Lin, Y. Xie, Z. L. Wang, *Nano Energy* **2015**, *12*, 760.
[149] C. Zhang, X. Lin, N. Zhang, Y. Lu, Z. Wu, G. Liu, S. Nie, *Nano Energy* **2019**, *66*, 104126.
[150] Y. C. Lai, J. Deng, S. L. Zhang, S. Niu, H. Guo, Z. L. Wang, *Adv. Funct. Mater.* **2017**, *27*, 1604462.
[151] F. Yi, L. Lin, S. Niu, P. K. Yang, Z. Wang, J. Chen, Y. Zhou, Y. Zi, J. Wang, Q. Liao, Y. Zhang, Z. L. Wang, *Adv. Funct. Mater.* **2015**, *25*, 3688.
[152] Y. Ma, Q. Zheng, Y. Liu, B. Shi, X. Xue, W. Ji, Z. Liu, Y. Jin, Y. Zou, Z. An, W. Zhang, X. Wang, W. Jiang, Z. Xu, Z. L. Wang, Z. Li, H. Zhang, *Nano Lett.* **2016**, *16*, 6042.
[153] P. K. Yang, Z. H. Lin, K. C. Pradel, L. Lin, X. Li, X. Wen, J. H. He, Z. L. Wang, *ACS Nano* **2015**, *9*, 901.
[154] H. Zhang, Y. Yang, T. C. Hou, Y. Su, C. Hu, Z. L. Wang, *Nano Energy* **2013**, *2*, 1019.
[155] P. K. Yang, L. Lin, F. Yi, X. Li, K. C. Pradel, Y. Zi, C. I. Wu, J. H. He, Y. Zhang, Z. L. Wang, *Adv. Mater.* **2015**, *27*, 3817.
[156] Q. Zheng, H. Zhang, B. Shi, X. Xue, Z. Liu, Y. Jin, Y. Ma, Y. Zou, X. Wang, Z. An, W. Tang, W. Zhang, F. Yang, Y. Liu, X. Lang, Z. Xu, Z. Li, Z. L. Wang, *ACS Nano* **2016**, *10*, 6510.
[157] G. T. Hwang, H. Park, J. H. Lee, S. Oh, K. I. Park, M. Byun, H. Park, G. Ahn, C. K. Jeong, K. No, H. Kwon, S. G. Lee, B. Joung, K. J. Lee, *Adv. Mater.* **2014**, *26*, 4880.
[158] K. Meng, J. Chen, X. Li, Y. Wu, W. Fan, Z. Zhou, Q. He, X. Wang, X. Fan, Y. Zhang, J. Yang, Z. L. Wang, *Adv. Funct. Mater.* **2019**, *29*, 1806388.
[159] Q. Zheng, Y. Zou, Y. Zhang, Z. Liu, B. Shi, X. Wang, Y. Jin, H. Ouyang, Z. Li, Z. L. Wang, *Sci. Adv.* **2016**, *2*, e1501478.
[160] R. Hinchet, S. W. Kim, *ACS Nano* **2015**, *9*, 7742.
[161] B. Shi, Q. Zheng, W. Jiang, L. Yan, X. Wang, H. Liu, Y. Yao, Z. Li, Z. L. Wang, *Adv. Mater.* **2016**, *28*, 846.
[162] Q. Zheng, Y. Jin, Z. Liu, H. Ouyang, H. Li, B. Shi, W. Jiang, H. Zhang, Z. Li, Z. L. Wang, *ACS Appl. Mater. Interfaces* **2016**, *8*, 26697.
[163] K. Y. Lee, H. J. Yoon, T. Jiang, X. Wen, W. Seung, S. W. Kim, Z. L. Wang, *Adv. Energy Mater.* **2016**, *6*, 1502566.
[164] J. Chun, J. W. Kim, W. Jung, C. Y. Kang, S. W. Kim, Z. L. Wang, J. M. Baik, *Energy Environ. Sci.* **2015**, *8*, 3006.
[165] K. N. Kim, J. Chun, J. W. Kim, K. Y. Lee, J. U. Park, S. W. Kim, Z. L. Wang, J. M. Baik, *ACS Nano* **2015**, *9*, 6394.
[166] L. Dhakar, S. Gudla, X. Shan, Z. Wang, F. E. H. Tay, C. H. Heng, C. Lee, *Sci. Rep.* **2016**, *6*, 22253.
[167] A. Ahmed, I. Hassan, T. Ibn-Mohammed, H. Mostafa, I. M. Reaney, L. S. C. Koh, J. Zu, Z. L. Wang, *Energy Environ. Sci.* **2017**, *10*, 653.
[168] K. Parida, G. Thangavel, G. Cai, X. Zhou, S. Park, J. Xiong, P. S. Lee, *Nat. Commun.* **2019**, *10*, 2158.
[169] X. Chen, Y. Song, H. Chen, J. Zhang, H. Zhang, *J. Mater. Chem. A* **2017**, *5*, 12361.
[170] H. Li, X. Fang, R. Li, B. Liu, H. Tang, X. Ding, Y. Xie, R. Zhou, G. Zhou, Y. Tang, *Nano Energy* **2020**, *78*, 105288.
[171] Y. Yu, Z. Li, Y. Wang, S. Gong, X. Wang, *Adv. Mater.* **2015**, *27*, 4938.
[172] Z. L. Wang, *Mater. Today* **2017**, *20*, 74.
[173] C. Han, C. Zhang, W. Tang, X. Li, Z. L. Wang, *Nano Res.* **2015**, *8*, 722.
[174] W. Tang, T. Jiang, F. R. Fan, A. F. Yu, C. Zhang, X. Cao, Z. L. Wang, *Adv. Funct. Mater.* **2015**, *25*, 3718.
[175] J. Tian, R. Shi, Z. Liu, H. Ouyang, M. Yu, C. Zhao, Y. Zou, D. Jiang, J. Zhang, Z. Li, *Nano Energy* **2019**, *59*, 705.
[176] F. C. Kao, P. Y. Chiu, T. T. Tsai, Z. H. Lin, *Sci. Technol. Adv. Mater.* **2019**, *20*, 1103.
[177] W. Tang, J. Tian, Q. Zheng, L. Yan, J. Wang, Z. Li, Z. L. Wang, *ACS Nano* **2015**, *9*, 7867.
[178] W. Hu, X. Wei, L. Zhu, D. Yin, A. Wei, X. Bi, T. Liu, G. Zhou, Y. Qiang, X. Sun, Z. Wen, Y. Pan, *Nano Energy* **2019**, *57*, 600.
[179] Y. Long, H. Wei, J. Li, G. Yao, B. Yu, D. Ni, A. L. Gibson, X. Lan, Y. Jiang, W. Cai, X. Wang, *ACS Nano* **2018**, *12*, 12533.
[180] Z. Li, H. Feng, Q. Zheng, H. Li, C. Zhao, H. Ouyang, S. Noreen, M. Yu, F. Su, R. Liu, L. Li, Z. L. Wang, Z. Li, *Nano Energy* **2018**, *54*, 390.
[181] G. Yao, D. Jiang, J. Li, L. Kang, S. Chen, Y. Long, Y. Wang, P. Huang, Y. Lin, W. Cai, X. Wang, *ACS Nano* **2019**, *13*, 12345.
[182] S. Lee, H. Wang, N. V. Thakor, S. C. Yen, C. Lee, *J. Phys. Conf. Ser.* **2018**, *1052*, 012007.
[183] S. Lee, H. Wang, Q. Shi, L. Dhakar, J. Wang, N. V. Thakor, S. C. Yen, C. Lee, *Nano Energy* **2017**, *33*, 1.
[184] S. Lee, H. Wang, J. Wang, Q. Shi, S. C. Yen, N. V. Thakor, C. Lee, *Nano Energy* **2018**, *50*, 148.
[185] S. Lee, H. Wang, Q. Shi, J. Wang, T. He, H. Wu, N. V. Thakor, S. C. Yen, C. Lee, in *2017 19th Int. Conf. on Solid-State Sensors, Actuators and Microsystems (TRANSDUCERS)*, IEEE, Piscataway, NJ, USA **2017**, pp. 1808–1811.
[186] J. Wang, T. He, C. Lee, *Nano Energy* **2019**, *65*, 104039.
[187] W. Guo, X. Zhang, X. Yu, S. Wang, J. Qiu, W. Tang, L. Li, H. Liu, Z. L. Wang, *ACS Nano* **2016**, *10*, 5086.
[188] Y. Jin, J. Seo, J. S. Lee, S. Shin, H. J. Park, S. Min, E. Cheong, T. Lee, S. W. Cho, *Adv. Mater.* **2016**, *28*, 7365.
[189] G. Yao, L. Kang, J. Li, Y. Long, H. Wei, C. A. Ferreira, J. J. Jeffery, Y. Lin, W. Cai, X. Wang, *Nat. Commun.* **2018**, *9*, 5349.
[190] S. Lee, H. Wang, W. Y. Xian Peh, T. He, S. C. Yen, N. V. Thakor, C. Lee, *Nano Energy* **2019**, *60*, 449.
[191] F. Arab Hassani, R. P. Mogan, G. G. L. Gammad, H. Wang, S. C. Yen, N. V. Thakor, C. Lee, *ACS Nano* **2018**, *12*, 3487.
[192] J. Wang, H. Wang, N. V. Thakor, C. Lee, *ACS Nano* **2019**, *13*, 3589.
[193] H. Wang, J. Wang, T. He, Z. Li, C. Lee, *Nano Energy* **2019**, *63*, 103844.
[194] J. Wang, H. Wang, T. He, B. He, N. V. Thakor, C. Lee, *Adv. Sci.* **2019**, *6*, 1900149.
[195] W. Jiang, H. Li, Z. Liu, Z. Li, J. Tian, B. Shi, Y. Zou, H. Ouyang, C. Zhao, L. Zhao, R. Sun, H. Zheng, Y. Fan, Z. L. Wang, Z. Li, *Adv. Mater.* **2018**, *30*, 1801895.
[196] P. Song, S. Kuang, N. Panwar, G. Yang, D. J. H. Tng, S. C. Tjin, W. J. Ng, M. B. A. Majid, G. Zhu, K. T. Yong, Z. L. Wang, *Adv. Mater.* **2017**, *29*, 1605668.
[197] Q. Ouyang, X. Feng, S. Kuang, N. Panwar, P. Song, C. Yang, G. Yang, X. Hemu, G. Zhang, H. S. Yoon, J. P. Tam, B. Liedberg, G. Zhu, K. T. Yong, Z. L. Wang, *Nano Energy* **2019**, *62*, 610.

[198] M. Bok, Y. Lee, D. Park, S. Shin, Z. J. Zhao, B. Hwang, S. H. Hwang, S. H. Jeon, J. Y. Jung, S. H. Park, J. Nah, E. Lim, J. H. Jeong, *Nanoscale* **2018**, *10*, 13502.
[199] J. Nie, Z. Ren, J. Shao, C. Deng, L. Xu, X. Chen, M. Li, Z. L. Wang, *ACS Nano* **2018**, *12*, 1491.
[200] J. Nie, Z. Ren, Y. Bai, J. Shao, T. Jiang, L. Xu, X. Chen, Z. L. Wang, *Adv. Mater. Technol.* **2019**, *4*, 1800300.
[201] L. Zheng, Y. Wu, X. Chen, A. Yu, L. Xu, Y. Liu, H. Li, Z. L. Wang, *Adv. Funct. Mater.* **2017**, *27*, 1606408.
[202] C. Zhao, H. Feng, L. Zhang, Z. Li, Y. Zou, P. Tan, H. Ouyang, D. Jiang, M. Yu, C. Wang, H. Li, L. Xu, W. Wei, Z. Li, *Adv. Funct. Mater.* **2019**, *29*, 1808640.
[203] J. Hunckler, A. de Mel, *J. Multidiscip. Healthcare* **2017**, *10*, 179.
[204] C. Mason, P. Dunnill, *Regener. Med.* **2008**, *3*, 1.
[205] V. Kontis, J. E. Bennett, C. D. Mathers, G. Li, K. Foreman, M. Ezzati, *Lancet* **2017**, *389*, 1323.
[206] A. Atala, *Rejuvenation Res.* **2004**, *7*, 15.
[207] E. Wang, M. Zhao, *Chin. J. Traumatol.* **2010**, *13*, 55.
[208] C. Chen, X. Bai, Y. Ding, I. S. Lee, *Biomater. Res.* **2019**, 23.
[209] N. Guzelsu, R. L. Regimbal, *J. Biomech.* **1990**, *23*, 661.
[210] E. Kawai, J. Nakanishi, N. Kumazawa, K. Ozawa, M. Denda, *Exp. Dermatol.* **2008**, *17*, 688.
[211] B. D. Bath, E. R. Scott, J. B. Phipps, H. S. White, *J. Pharm. Sci.* **2000**, *89*, 1537.
[212] C. J. Harland, T. D. Clark, R. J. Prance, *Meas. Sci. Technol.* **2001**, *13*, 163.
[213] T. D. Rachner, S. Khosla, L. C. Hofbauer, *Lancet* **2011**, *377*, 1276.
[214] A. Klibanski, L. Adams-Campbell, T. Bassford, S. N. Blair, S. D. Boden, K. Dickersin, D. R. Gifford, L. Glasse, S. R. Goldring, K. Hruska, S. R. Johnson, L. K. McCauley, W. E. Russell, *JAMA, J. Am. Med. Assoc.* **2001**, *285*, 2323.
[215] *Bone Health and Osteoporosis: A Report of the Surgeon General*, Office of the Surgeon General (US), Rockville, MD **2004**.
[216] J. Goldhahn, J. M. Féron, J. Kanis, S. Papapoulos, J. Y. Reginster, R. Rizzoli, W. Dere, B. Mitlak, Y. Tsouderos, S. Boonen, *Calcif. Tissue Int.* **2012**, *90*, 343.
[217] N. B. Menke, K. R. Ward, T. M. Witten, D. G. Bonchev, R. F. Diegelmann, *Clin. Dermatol.* **2007**, *25*, 19.
[218] Z. Kopecki, M. M. Luchetti, D. H. Adams, X. Strudwick, T. Mantamadiotis, A. Stoppacciaro, A. Gabrielli, R. G. Ramsay, A. J. Cowin, *J. Pathol.* **2007**, *211*, 351.
[219] L. Cañedo-Dorantes, M. Cañedo-Ayala, *Int. J. Inflam.* **2019**, 2019, 3706315.
[220] J. Li, J. Chen, R. Kirsner, *Clin. Dermatol.* **2007**, *25*, 9.
[221] P. M. Mountziaris, A. G. Mikos, *Tissue Eng., Part B* **2008**, *14*, 179.
[222] S. Barrientos, O. Stojadinovic, M. S. Golinko, H. Brem, M. Tomic-Canic, *Wound Repair Regener.* **2008**, *16*, 585.
[223] J. A. Sherratt, J. D. Murray, *Proc. Biol. Sci.* **1990**, *241*, 29.
[224] A. Guo, B. Song, B. Reid, Y. Gu, J. V. Forrester, C. A. B. Jahoda, M. Zhao, *J. Invest. Dermatol.* **2010**, *130*, 2320.
[225] M. Rouabhia, H. Park, S. Meng, H. Derbali, Z. Zhang, *PLoS One* **2013**, *8*, e71660.
[226] S. S. Welc, T. L. Clanton, S. M. Dineen, L. R. Leon, *J. Appl. Physiol.* **2013**, *115*, 1126.
[227] M. A. King, L. R. Leon, D. A. Morse, T. L. Clanton, *J. Appl. Physiol.* **2016**, *122*, 296.
[228] Y. Zhu, B. Yang, J. Liu, X. Wang, L. Wang, X. Chen, C. Yang, *Sci. Rep.* **2016**, *6*, 22233.
[229] W. A. Dorsett-Martin, *Wound Repair Regener.* **2004**, *12*, 591.
[230] K. P. Wilhelm, D. Wilhelm, S. Bielfeldt, *Skin Res. Technol.* **2017**, *23*, 3.
[231] P. Landge, *Bull. Pharm. Med. Sci.* **2015**, *3*, 3201.
[232] L. Falto-Aizpurua, S. Choudhary, A. Tosti, *Expert Opin. Emerging Drugs* **2014**, *19*, 545.
[233] V. M. Meidan, E. Touitou, *Drugs* **2001**, *61*, 53.
[234] D. Peus, M. R. Pittelkow, *Dermatol. Clin.* **1996**, *14*, 559.
[235] N. J. Hawkshaw, J. A. Hardman, M. Alam, F. Jimenez, R. Paus, *J. Dermatol.* **2020**, *182*, e169.
[236] A. M. Park, S. Khan, J. Rawnsley, *Facial Plast. Surg. Clin. North Am.* **2018**, *26*, 415.
[237] N. J. Hawkshaw, J. A. Hardman, M. Alam, F. Jimenez, R. Paus, *J. Dermatol.* **2020**, *182*, 1184.
[238] P. Wu, Y. Zhang, Y. Xing, W. Xu, H. Guo, F. Deng, X. Ma, Y. Li, *Cell Commun. Signaling* **2019**, *17*, 16.
[239] R. Sinclair, *BMJ* **1998**, *317*, 865.
[240] S. Harrison, R. Sinclair, *Clin. Exp. Dermatol.* **2002**, *27*, 389.
[241] D. Silberberg, N. P. Anand, K. Michels, R. N. Kalaria, *Nature* **2015**, *527*, S151.
[242] J. Lee, J. Jang, Y. K. Song, *Biomed. Eng. Lett.* **2016**, *6*, 205.
[243] E. L. Graczyk, B. P. Delhaye, M. A. Schiefer, S. J. Bensmaia, D. J. Tyler, *J. Neural Eng.* **2018**, *15*, 046002.
[244] J. Charthad, T. C. Chang, Z. Liu, A. Sawaby, M. J. Weber, S. Baker, F. Gore, S. A. Felt, A. Arbabian, *IEEE Trans. Biomed. Circuits Syst.* **2018**, *12*, 257.
[245] S. Jezernik, M. Morari, *IEEE Trans. Biomed. Eng.* **2005**, *52*, 740.
[246] M. Pisanello, F. Pisano, M. Hyun, E. Maglie, A. Balena, M. De Vittorio, B. L. Sabatini, F. Pisanello, *Front. Neurosci.* **2019**, *13*, 82.
[247] A. A. Jiman, D. C. Ratze, E. J. Welle, P. R. Patel, J. M. Richie, E. C. Bottorff, J. P. Seymour, C. A. Chestek, T. M. Bruns, *Sci. Rep.* **2020**, *10*, 15501.
[248] X. Navarro, T. B. Kreuger, N. Lago, S. Micera, T. Stieglitz, P. Dario, *J. Peripher. Nerv. Syst.* **2005**, *10*, 229.
[249] R. Sahyouni, A. Mahmoodi, J. W. Chen, D. T. Chang, O. Moshtaghi, H. R. Djalilian, H. W. Lin, *Neurosurg. Rev.* **2019**, *42*, 227.
[250] C. Mora Lopez, *IEEE Solid-State Circuits Mag.* **2019**, *11*, 43.
[251] L. Miller, A. McFadyen, A. C. Lord, R. Hunter, L. Paul, D. Rafferty, R. Bowers, P. Mattison, *Arch. Phys. Med. Rehabil.* **2017**, *98*, 1435.
[252] M. S. Vieira, A. K. Santos, R. Vasconcellos, V. A. M. Goulart, R. C. Parreira, A. H. Kihara, H. Ulrich, R. R. Resende, *Biotechnol. Adv.* **2018**, *36*, 1946.
[253] U. Pfisterer, F. Ek, S. Lang, S. Soneji, R. Olsson, M. Parmar, *Sci. Rep.* **2016**, *6*, 38290.
[254] N. Wagenaar, C. G. M. de Theije, L. S. de Vries, F. Groenendaal, M. J. N. L. Benders, C. H. A. Nijboer, *Pediatr. Res.* **2018**, *83*, 372.
[255] D. Benayahu, Y. Wiesenfeld, R. Sapir-Koren, *J. Cell. Physiol.* **2019**, *234*, 12133.
[256] B. L. Larson, S. N. Yu, H. Park, B. T. Estes, F. T. Moutos, C. J. Bloomquist, P. B. Wu, J. F. Welter, R. Langer, F. Guilak, L. E. Freed, *J. Tissue Eng. Regener. Med.* **2019**, *13*, 1453.
[257] S. Liu, R. Yang, N. Yin, Y. L. Wang, F. Faiola, *Ecotoxicol. Environ. Saf.* **2019**, *169*, 564.
[258] E. M. Lotz, M. B. Berger, B. D. Boyan, Z. Schwartz, *Bone* **2020**, *134*, 115260.
[259] S. Wang, S. Guan, W. Li, D. Ge, J. Xu, C. Sun, T. Liu, X. Ma, *Mat. Sci. Eng., C* **2018**, *93*, 890.
[260] S. Wang, S. Guan, J. Xu, W. Li, D. Ge, C. Sun, T. Liu, X. Ma, *Biomater. Sci.* **2017**, *5*, 2024.
[261] T. Aydin, C. Gurcan, H. Taheri, A. Yilmazer, in *Cell Biology and Translational Medicine*, Vol. *3* (Ed: K. Turksen), Stem Cells, Bio-Materials and Tissue Engineering, Springer International Publishing, Cham, Switzerland **2018**, pp. 129–142.
[262] J. Du, G. Zhen, H. Chen, S. Zhang, L. Qing, X. Yang, G. Lee, H. Q. Mao, X. Jia, *Biomaterials* **2018**, *181*, 347.
[263] W. Zhu, T. Ye, S. J. Lee, H. Cui, S. Miao, X. Zhou, D. Shuai, L. G. Zhang, *Nanomedicine* **2018**, *14*, 2485.
[264] S. M. Damaraju, Y. Shen, E. Elele, B. Khusid, A. Eshghinejad, J. Li, M. Jaffe, T. L. Arinzeh, *Biomaterials* **2017**, *149*, 51.
[265] M. Włodarczyk, G. Nowicka, *Int. J. Mol. Sci.* **2019**, *20*, 1146.
[266] G. Campanella, M. J. Gunter, S. Polidoro, V. Krogh, D. Palli, S. Panico, C. Sacerdote, R. Tumino, G. Fiorito,

S. Guarrera, L. Iacoviello, I. A. Bergdahl, B. Melin, P. Lenner, T. M. C. M. de Kok, P. Georgiadis, J. C. S. Kleinjans, S. A. Kyrtopoulos, H. B. Bueno-de-Mesquita, K. A. Lillycrop, A. M. May, N. C. Onland-Moret, R. Murray, E. Riboli, M. Verschuren, E. Lund, N. Mode, T. M. Sandanger, V. Fiano, M. Trevisan, G. Matullo, P. Froguel, P. Elliott, P. Vineis, M. Chadeau-Hyam, *Int. J. Obes.* **2018**, *42*, 2022.
[267] L. K. Brahe, A. Astrup, L. H. Larsen, *Adv. Nutr.* **2016**, *7*, 90.
[268] J. B. Cohen, K. M. Gadde, *Curr. Hypertens. Rep.* **2019**, *21*, 16.
[269] R. L. Johnson, C. G. Wilson, *J. Inflammation Res.* **2018**, 11.
[270] K. N. Browning, S. Verheijden, G. E. Boeckxstaens, *Gastroenterology* **2017**, *152*, 730.
[271] S. C. Cork, *J. Neuroendocrinol.* **2018**, *30*, e12643.
[272] L. 't Hoen, H. Ecclestone, B. F. M. Blok, G. Karsenty, V. Phé, R. Bossier, J. Groen, D. Castro-Diaz, B. P. Fernández, G. D. Popolo, S. Musco, J. Pannek, T. M. Kessler, T. Gross, M. P. Schneider, R. Hamid, *Neurourol. Urodyn.* **2017**, *36*, 1685.
[273] L. Martinez, L. Neshatian, R. Khavari, *Curr. Bladder Dysfunct. Rep.* **2016**, *11*, 334.
[274] C. Sager, M. Sanmartino, C. Burek, Y. R. Gomez, M. V. Patiño, S. Weller, J. Ruiz, F. L. Imizcoz, C. Tessi, T. Szklarz, J. P. Corbetta, *J. Pediatr. Urol.* **2020**, *16*, P655.E1.
[275] R. L. Coolen, J. Groen, B. F. M. Blok, *Med. Devices* **2019**, *12*, 337.
[276] K. E. Andersson, *Expert Opin. Investig. Drugs* **2019**, *28*, 749.
[277] L. Xu, C. Fu, Q. Zhang, F. Xiong, L. Peng, Z. Liang, L. Chen, C. He, Q. Wei, *BMJ Open* **2020**, *10*, e034582.
[278] S. C. Knüpfer, S. A. Schneider, M. M. Averhoff, C. M. Naumann, G. Deuschl, K. P. Jünemann, M. F. Hamann, *BMC Urol.* **2016**, *16*, 55.
[279] B. A. Allio, A. C. Peterson, *Transl. Androl. Urol.* **2016**, *5*, 31.
[280] R. Pewowaruk, D. Rutkowski, D. Hernando, B. B. Kumapayi, W. Bushman, A. Roldán-Alzate, *PLoS One* **2020**, *15*, e0238404.
[281] D. L. Corona-Quintanilla, R. López-Juárez, P. Pacheco, M. I. Romero-Ortega, F. Castelán, M. Martínez-Gómez, *Neurourol. Urodyn.* **2020**, *39*, 116.
[282] M. T. Sanford, A. M. Suskind, *Transl. Androl. Urol.* **2015**, *5*, 117.
[283] Y. T. Lin, T. H. Hsieh, S. C. Chen, C. H. Lai, T. S. Kuo, C. P. Chen, C. W. Lin, S. T. Young, C. W. Peng, *J. Formosan Med. Assoc.* **2016**, *115*, 703.
[284] J. J. E. Adriaansen, F. W. A. van Asbeck, M. Tepper, W. X. Faber, J. M. A. Visser-Meily, L. M. O. de Kort, M. W. M. Post, *J. Spinal Cord Med.* **2017**, *40*, 43.
[285] S. Lee, H. Wang, W. Y. X. Peh, N. V. Thakor, S. C. Yen, C. Lee, in *2019 9th Int. IEEE/EMBS Conf. on Neural Engineering (NER)*, IEEE, Piscataway, NJ, USA **2019**, pp. 706–709.
[286] J. N. Panicker, *Semin. Neurol.* **2020**, *40*, 569.
[287] J. Wang, H. Wang, C. Lee, *Adv. Biosyst.* **2019**, *3*, 1800281.
[288] H. Wang, J. Wang, X. Y. Thow, S. Lee, W. Y. X. Peh, K. A. Ng, T. He, N. V. Thakor, C. Lee, *Front. Comput. Neurosci.* **2020**, *14*, 50.
[289] Z. Xiang, S. Sheshadri, S.-H. Lee, J. Wang, N. Xue, N. V. Thakor, S.-C. Yen, C. Lee, *Adv. Sci.* **2016**, *3*, 1500386.
[290] Z. Xiang, S.-C. Yen, S. Sheshadri, J. Wang, S. Lee, Y.-H. Liu, L.-D. Liao, N. V. Thakor, C. Lee, *Adv. Mater.* **2016**, *28*, 4472.
[291] J. Wang, X. Y. Thow, H. Wang, S. Lee, K. Voges, N. V. Thakor, S.-C. Yen, C. Lee, *Adv. Healthcare Mater.* **2018**, *7*, 1700987.
[292] H. Wang, T. Wu, Q. Zeng, C. Lee, *Micromachines* **2020**, *11*, 865.
[293] Z. Xiang, J. Liu, C. Lee, *Microsyst. Nanoeng.* **2016**, *2*, 16012.
[294] A. Dietrich, in *Mobile Brain-Body Imaging and the Neuroscience of Art, Innovation and Creativity* (Eds: J. L. Contreras-Vidal, D. Robleto, J. G. Cruz-Garza, J. M. Azorín, C. S. Nam), Springer International Publishing, Cham, Switzerland **2019**, pp. 23–28.
[295] J. M. Hootman, C. G. Helmick, K. E. Barbour, K. A. Theis, M. A. Boring, *Arthritis Rheumatol.* **2016**, *68*, 1582.
[296] S. Lin, W. Yu, B. Wang, Y. Zhao, K. En, J. Zhu, X. Cheng, C. Zhou, H. Lin, Z. Wang, H. Hojaiji, C. Yeung, C. Milla, R. W. Davis, S. Emaminejad, *Proc. Natl. Acad. Sci. USA* **2020**, *117*, 19017.
[297] J. A. Faulkner, L. M. Larkin, D. R. Claflin, S. V. Brooks, *Clin. Exper. Pharmacol. Physiol.* **2007**, *34*, 1091.
[298] T. Mima, K. Toma, B. Koshy, M. Hallett, *Stroke* **2001**, *32*, 2597.
[299] A. Jayaraman, C. M. Gregory, M. Bowden, J. E. Stevens, P. Shah, A. L. Behrman, K. Vandenborne, *Spinal Cord* **2006**, *44*, 680.
[300] A. V. Ng, R. G. Miller, D. Gelinas, J. A. Kent-Braun, *Muscle Nerve* **2004**, *29*, 843.
[301] F. T. Padberg, M. V. Johnston, S. A. Sisto, *J. Vasc. Surgery* **2004**, *39*, 79.
[302] B. Swynghedauw, *Physiol. Rev.* **1986**, *66*, 710.
[303] T. J. Patel, R. L. Lieber, *Exercise Sport Sci. Rev.* **1997**, *25*, 321???364.
[304] W. Li, J. Sun, M. Chen, *Nano Energy* **2014**, *3*, 95.
[305] R. K. Li, Z. Q. Jia, R. D. Weisel, D. A. G. Mickle, J. Zhang, M. K. Mohabeer, V. Rao, J. Ivanov, *Ann. Thorac. Surg.* **1996**, *62*, 654.
[306] M. J. Foglia, K. D. Poss, *Development* **2016**, *143*, 5.
[307] C. E. Clancy, M. Tateyama, R. S. Kass, *J. Clin. Invest.* **2002**, *110*, 1251.
[308] R.-M. Marisol, G.-D. David, H. Bettina, P. H. Michael, S.-S. Jordi, *Circ. Res.* **1999**, *85*, 280.
[309] B. S. Pasumarthi Kishore, J. Field Loren, *Circ. Res.* **2002**, *90*, 1044.
[310] S. Guatimosim, M. J. Amaya, M. T. Guerra, C. J. Aguiar, A. M. Goes, N. L. Gómez-Viquez, M. A. Rodrigues, D. A. Gomes, J. Martins-Cruz, W. J. Lederer, M. F. Leite, *Cell Calcium* **2008**, *44*, 230.
[311] G. Gilbert, K. Demydenko, E. Dries, R. D. Puertas, X. Jin, K. Sipido, H. L. Roderick, *Cold Spring Harb. Perspect. Biol.* **2019**, a035428.
[312] S. Li, Y. Wang, J. Xue, N. Zhao, T. Zhu, *Int. J. Environ. Res. Public Health* **2020**, *17*, 2032.
[313] E. Touitou, *Expert Opin. Biol. Ther.* **2002**, *2*, 723.
[314] M. R. Prausnitz, R. Langer, *Nat. Biotechnol.* **2008**, *26*, 1261.
[315] P. Grootendorst, E. Piérard, M. Shim, *Expert Rev. Pharmacoecon. Outcomes Res.* **2009**, *9*, 353.
[316] R. Riahi, A. Tamayol, S. A. M. Shaegh, A. M. Ghaemmaghami, M. R. Dokmeci, A. Khademhosseini, *Curr. Opin. Chem. Eng.* **2015**, *7*, 101.
[317] S. T. Sanjay, W. Zhou, M. Dou, H. Tavakoli, L. Ma, F. Xu, X. Li, *Adv. Drug Delivery Rev.* **2018**, *128*, 3.
[318] C. Zylberberg, S. Matosevic, *Drug Delivery* **2016**, *23*, 3319.
[319] I. Ale, J. M. Lachapelle, H. I. Maibach, *Adv. Ther.* **2009**, *26*, 920.
[320] M. B. Brown, G. P. Martin, S. A. Jones, F. K. Akomeah, *Drug Delivery* **2006**, *13*, 175.
[321] Y. N. Kalia, A. Naik, J. Garrison, R. H. Guy, *Adv. Drug Delivery Rev.* **2004**, *56*, 619.
[322] M. R. Prausnitz, *Adv. Drug Delivery Rev.* **2004**, *56*, 581.
[323] S. Henry, *J. Pharm. Sci.* **1998**, *87*, 922.
[324] H. Chen, H. Zhu, J. Zheng, D. Mou, J. Wan, J. Zhang, T. Shi, Y. Zhao, H. Xu, X. Yang, *J. Controlled Release* **2009**, *139*, 63.
[325] T. A. Ahles, J. C. Root, *Annu. Rev. Clin. Psychol.* **2018**, *14*, 425.
[326] A. Lucas, D. Lam, P. Cabrales, *Drug Delivery* **2019**, *26*, 433.
[327] A. Jiang, B. Song, X. Ji, F. Peng, H. Wang, Y. Su, Y. He, *Nano Res.* **2018**, *11*, 2285.
[328] A. Peace, A. Ramirez, M. L. M. Broeren, N. Coleman, I. Chaput, T. Rydberg, G. N. Sauvion, *Sustainable Prod. Consumption* **2018**, *13*, 93.
[329] K. Parida, V. Kumar, W. Jiangxin, V. Bhavanasi, R. Bendi, P. S. Lee, *Adv. Mater.* **2017**, *29*, 1702181.
[330] W. Xu, L.-B. Huang, M.-C. Wong, L. Chen, G. Bai, J. Hao, *Adv. Energy Mater.* **2017**, *7*, 1601529.
[331] X. Pu, M. Liu, X. Chen, J. Sun, C. Du, Y. Zhang, J. Zhai, W. Hu, Z. L. Wang, *Sci. Adv.* **2017**, *3*, e1700015.
[332] C. Yang, Z. Suo, *Nat. Rev. Mater.* **2018**, *3*, 125.
[333] M. Q. H. Leow, H. L. Tey, *Indian J. Dermatol. Venereol. Leprol.* **2017**, *83*, 387.
[334] S. Gregoriou, P. Sidiropoulou, G. Kontochristopoulos, D. Rigopoulos, *Clin. Cosmet. Investig. Dermatol.* **2019**, *12*, 733.

[335] E. Ghandali, S. M. Hosseini, H. R. Moghimi, K. Khademi-Kalantari, S. T. Moghadam, A. A. Baghban, S. M. Mortazavi, *J. Bodyw. Mov. Ther.* **2020**, *24*, 57.
[336] Z. Su, A. Robinson, L. Hu, J. D. Klein, F. Hassounah, M. Li, H. Wang, H. Cai, X. H. Wang, *PLoS One* **2015**, *10*, e0134511.
[337] K. M. C. Oliveira, J. H. Barker, E. Berezikov, L. Pindur, S. Kynigopoulos, M. Eischen-Loges, Z. Han, M. B. Bhavsar, D. Henrich, L. Leppik, *Sci. Rep.* **2019**, *9*, 11433.
[338] J. M. Grasman, M. D. Williams, C. G. Razis, M. Bonzanni, A. S. Golding, D. M. Cairns, M. Levin, D. L. Kaplan, *ACS Biomater. Sci. Eng.* **2019**, *5*, 5327.
[339] X. F. Wang, M. L. Li, Q. Q. Fang, W. Y. Zhao, D. Lou, Y. Y. Hu, J. Chen, X. Z. Wang, W. Q. Tan, *Bioact. Mater.* **2021**, *6*, 230.
[340] D. Kaynak, R. Meffert, M. Günhan, O. Günhan, *J. Periodontol.* **2005**, *76*, 2194.
[341] L. Leppik, H. Zhihua, S. Mobini, V. Thottakkattumana Parameswaran, M. Eischen-Loges, A. Slavici, J. Helbing, L. Pindur, K. M. C. Oliveira, M. B. Bhavsar, L. Hudak, D. Henrich, J. H. Barker, *Sci. Rep.* **2018**, *8*, 6307.
[342] S. Mobini, L. Leppik, V. T. Parameswaran, J. H. Barker, *PeerJ* **2017**, *5*, e2821.
[343] M. Dodel, N. Hemmati Nejad, S. H. Bahrami, M. Soleimani, L. Mohammadi Amirabad, H. Hanaee-Ahvaz, A. Atashi, *Biologicals* **2017**, *46*, 99.
[344] L. P. Leppik, D. Froemel, A. Slavici, Z. N. Ovadia, L. Hudak, D. Henrich, I. Marzi, J. H. Barker, *Sci. Rep.* **2015**, *5*, 18353.
[345] M. G. Cunningham, G. Yadollahikhales, G. Vitaliano, C. van Horne, *BMC Psychiatry* **2016**, *16*, 399.
[346] X. Chen, C. Zhang, Y. Li, P. Huang, Q. Lv, W. Yu, S. Chen, B. Sun, Z. Wang, *bioRxiv* **2017**, 203406.
[347] C. Vitale, M. Amboni, R. Erro, M. Picillo, M. T. Pellecchia, P. Barone, L. Trojano, G. Santangelo, *Expert Rev. Neurother.* **2019**, *19*, 495.
[348] A. Berényi, M. Belluscio, D. Mao, G. Buzsáki, *Science* **2012**, *337*, 735.
[349] Y. T. Zhang, H. Jin, J. H. Wang, L. Y. Wen, Y. Yang, J. W. Ruan, S. X. Zhang, E. A. Ling, Y. Ding, Y. S. Zeng, *Neural Plast.* **2017**, 7351238.
[350] K. L. Bunday, M. A. Urbin, M. A. Perez, *Brain Stimul.* **2018**, *11*, 1083.
[351] R. Vastano, M. A. Perez, *J. Neurophysiol.* **2019**, *123*, 454.
[352] W. Mock, J. Erickson, T. Cameron, C. Chavez, *US20060161219A1*, **2006**.
[353] N. C. Swann, C. de Hemptinne, M. C. Thompson, S. Miocinovic, A. M. Miller, R. Gilron, J. L. Ostrem, H. J. Chizeck, P. A. Starr, *J. Neural Eng.* **2018**, *15*, 046006.
[354] M. L. Hacker, M. R. DeLong, M. Turchan, L. E. Heusinkveld, J. L. Ostrem, A. L. Molinari, A. D. Currie, P. E. Konrad, T. L. Davis, F. T. Phibbs, P. Hedera, K. R. Cannard, L. T. Drye, A. L. Sternberg, D. M. Shade, J. Tonascia, D. Charles, *Neurology* **2018**, *91*, e463.
[355] P. E. Mosley, S. Paliwal, K. Robinson, T. Coyne, P. Silburn, M. Tittgemeyer, K. E. Stephan, A. Perry, M. Breakspear, *Brain* **2020**, *143*, 2235.
[356] C. H. Knowles, E. J. Horrocks, S. A. Bremner, N. Stevens, C. Norton, P. R. O'Connell, S. Eldridge, CONFIDeNT Study Group, *Lancet* **2015**, *386*, 1640.
[357] K. Rahemtulla, *Master Thesis*, University of Alberta, Edmonton, AB, Canada **2019**.
[358] S. Hajibandeh, S. Hajibandeh, G. A. Antoniou, J. R. Scurr, F. Torella, *Cochrane Database Syst. Rev.* **2017**, *11*, CD011764.
[359] N. A. Maffiuletti, M. Roig, E. Karatzanos, S. Nanas, *BMC Med.* **2013**, *11*, 137.
[360] W. Gruther, F. Kainberger, V. Fialka-Moser, T. Paternostro-Sluga, M. Quittan, C. Spiss, R. Crevenna, *J. Rehabil. Med.* **2010**, *42*, 593.
[361] I. Vivodtzev, Y. Lacasse, F. Maltais, *J. Cardiopulm. Rehabil. Prev.* **2008**, *28*, 79.
[362] D. H. Kim, W. G. Yoo, *J. Phys. Ther. Sci.* **2018**, *30*, 1124.
[363] E. J. Ko, I. Y. Sung, G. J. Yun, J. A. Kang, J. Kim, G. E. Kim, *Disabil. Rehabil.* **2018**, *40*, 192.
[364] R. S. Roxo, V. B. Xavier, L. A. Miorin, A. O. Magalhães, Y. A. D. S. Sens, V. L. D. S. Alves, *J. Bras. Nefrol.* **2016**, *38*, 344.
[365] R. R. Sayegh, J. A. Sweet, J. P. Miller, S. M. Hayek, *Cornea* **2016**, *35*, 576.
[366] V. Scheper, I. Seidel-Effenberg, T. Lenarz, T. Stöver, G. Paasche, *Brain Sci* **2020**, *10*, 559.
[367] V. Scheper, A. Hoffmann, M. M. Gepp, A. Schulz, A. Hamm, C. Pannier, P. Hubka, T. Lenarz, J. Schwieger, *Front. Cell. Neurosci.* **2019**, *13*, 177.
[368] O. S. Manoukian, M. R. Arul, S. Rudraiah, I. Kalajzic, S. G. Kumbar, *J. Controlled Release* **2019**, *296*, 54.
[369] O. S. Manoukian, J. T. Baker, S. Rudraiah, M. R. Arul, A. T. Vella, A. J. Domb, S. G. Kumbar, *J. Controlled Release* **2020**, *317*, 78.
[370] K. Nakamura, H. Nakano, H. Naraba, M. Mochizuki, H. Hashimoto, *Crit. Care* **2020**, *24*, 342.
[371] R. Itani, M. Tobaiqy, A. Al Faraj, *Theranostics* **2020**, *10*, 5932.
[372] K. Gulati, S. Maher, S. Chandrasekaran, D. M. Findlay, D. Losic, *J. Mater. Chem. B* **2016**, *4*, 371.
[373] N. A. Sharif, *Neural Regener. Res.* **2018**, *13*, 1145.
[374] H. Kaji, N. Nagai, M. Nishizawa, T. Abe, *Adv. Drug Delivery Rev.* **2018**, *128*, 148.

II. Future of soft bioelectronics: integration in everyday wear

This section is summarized in the following in print article which we have written, and which follows next page:

***Libanori A**, Chen G, Zhao X, Zhao Y, Chen J. Smart textiles for personalised healthcare. *Nature Electronics* (manuscript accepted, in print)

Smart Textiles for Personalised Healthcare

Alberto Libanori[1,2], Guorui Chen[1,2], Xun Zhao[1], Yihao Zhou[1], Jun Chen[1,*]

[1]Department of Bioengineering, University of California, Los Angeles, Los Angeles, CA 90095, USA

[2]These authors contributed equally to this work.

[*]Correspondence to: jun.chen@ucla.edu (J. Chen)

Abstract

Incorporating sensing and therapeutic capabilities into everyday textiles holds the potential to be a powerful approach to help advance personalised healthcare solutions. The creation of such smart textiles has been driven by the fabrication of various miniaturised platform technologies, and has led to the construction of compact, autonomous, and interconnected functional textiles. Here we review the development of smart textiles for application in personalised healthcare. We examine their different platform technologies, fabrication strategies and the range of clinical scenarios in which they are used. We also explore the current commercial and regulatory landscapes, and consider issues of data management. Finally, we highlight key steps required to transition these technological platforms to commercial application, including suggestions to help foster collaboration.

Main Body

Introduction

Diagnostic, therapeutic, and post-care rehabilitative solutions to the global population vary in accessibility, quality, and clinical outcome[1-3], with centralised, one-size-fits-all healthcare models having proved to be inefficient in providing accessible, affordable, and quality healthcare[4]. Personalised healthcare has the potential to improve healthcare outcomes[5-7], but adoption remains a considerable challenge. Wearable devices could help decentralise healthcare access, but their application is limited by device bulkiness, power supply restrictions, ergonomic comfort limitations, and variations in quality and durability[8]; even discreet skin-adhering stretchable devices exhibit limitations, including skin breathability issues and the need for adhesives[9].

Incorporating sensing and therapeutic capabilities into everyday wear could be used as a pervasive approach to deliver bespoke healthcare services to a wide population, without the drawbacks of other wearable solutions[10]. Wearable bioelectronics were first introduced in the 1990s[11-13] and have now developed into a sophisticated range of technologies that can be integrated into textiles[14]. Such smart textiles — which can sense, react, and interact with a range of ambient stimuli (including mechanical, thermal, chemical, radiant, magnetic, and sound) and do not require electrical components to interact with external stimuli[15-19] — remain an underexploited asset in healthcare provision.

Smart textiles can provide insight into a person's physiological state[20] and can be used for *in situ* clinical monitoring[21] and intervention[22]. Such textiles could provide medical and economic benefits that range from disease prevention, improved clinical outcome and quality of life, to enhanced productivity, reduced healthcare burden, and decreased healthcare costs[23]. Data mining capabilities stemming from a large-scale roll out of smart textiles could also provide long-term, data-driven benefits[24].

Hardware and software limitations — as well as industrial issues of manufacturing and scalability, network integration, and user-readiness — have hampered the use of smart textiles within personalised healthcare. However, developments in miniaturised and low power consumption technologies, and their successful incorporation into textiles, mean that versatile smart textile healthcare platforms with suitable wearability profiles[25], are now available. The expansion of 5G networks, and the permeation of the Internet of Things (IoT), moreover mean that data relaying and interventional turnaround speed limitations are being addressed[26]. Furthermore, the existence of technologically savvy, wearable-adopting sections of society suggest that this is an optimal time for the expansion of smart textiles in personalised healthcare[27-29].

In this Review, we examine the development of smart textiles for personalised healthcare, consider different platform technologies employed, fabrication strategies, and explore diagnostic and therapeutic applications of smart textiles. We also examine the current commercial and regulatory landscapes, and assess issues of data management. Finally, we highlight key challenges in academia and industry that need to be addressed to realise the full potential of smart textiles.

Platform Technologies Employed in Smart Textiles

Textile sensors have been developed to help diagnose and prevent disease[21]. Drug-impregnated[18] and antimicrobial materials have also been used in wound management and infection prevention.

Since the introduction of smart textile use as a healthcare interface[30-35], many signal-to-function associative smart textile platform technologies have been developed (Figure 1). Diagnosis and therapy in smart textiles rely on certain miniaturised platform technologies which should be covered.

Electroluminescent Platforms

Light reflection and refraction provide useful biometric diagnostic information when interacting with tissues[36], whilst on a therapeutic front, light-emitting smart textiles have also shown many applications[37-41].

Piezoresistive Platforms

Piezoresistive semiconductors change electrical resistivity when exposed to mechanical stress. This mechanism has been harnessed for highly sensitive biomechanical sensing[42]. Chemical interactions[43] and temperature changes[44] have also been exploited for personalised biomolecular analysis and body temperature monitoring.

Thermoelectric Platforms

Thermoelectric generators can convert heat changes into electricity using the thermoelectric effect[45]. These textile thermoelectric generators have been explored to leverage body heat and generate electricity for healthcare applications[46].

Photovoltaic Platforms

Solar cells can convert sunlight directly into electricity[47]. Integrating photovoltaic technologies within textiles has provided powering capabilities for diagnostic and therapeutic devices within personalised healthcare settings[48].

Electrographic Platforms

Electrographic platforms can help in the diagnosis of heart and neurological conditions[49]. Their textile integration has been shown to provide highly flexible, comfortable, and long-lasting personalised healthcare platforms[50].

Capacitive Platforms

Textile capacitors exploit capacitance changes brought about by human motion[51]. In view of their high sensitivity, fast response time, and high stability, they have been frequently used in diagnostic devices[52]. Textile supercapacitors can moreover serve as an energy storage unit to power biomedical sensors or therapeutic devices[53].

Electromagnetic Platforms

Electromagnetic generators (EMGs) have been explored to convert human motion into electricity[54] and have been frequently used to harvest biomechanical energy[55].

Transistor Platforms

Transistors represent one of the building blocks of healthcare electronics[56]. Fibre/textile-based organic field-effect transistors and electrochemical transistors have been widely used for biomarker sensing[57], vital signs monitoring[58] and biomolecular analysis[59]. Moreover, fibre/textile transistors can be used to construct on-body circuits[60] to acquire data, and compute clinical interventions directly *in situ*.

Piezoelectric Platforms

Piezoelectric nanogenerators (PENG) rely on the piezoelectric effect to generate electricity and detect biomechanical motion *via* mechanical deformation[61]. Fibre-based PENGs possess high pressure sensitivity[62] and their easy implementation and self-powering capabilities have made them a more modern smart textile platform technology used in healthcare applications (sensing[63], electrical stimulation[64], and energy harvesting[65]).

Electrochemical Platforms

Electrochemical platforms have been explored to rely on the conversion of chemical energy to electricity, *via* known redox reactions[66]. Such platforms have shown the ability to leverage on ordinary perspiration, harnessing it as a renewable biofuel[67], as well as a bioanalytically relevant metabolite source for clinical insight.

Triboelectric Platforms

Triboelectric nanogenerators (TENG) convert mechanical motions into electricity, using contact electrification and electrostatic induction coupling[68-70]. TENGs effectively convert biomechanical movements to high voltage and low current signals[71]. Such performance, and a vast array of available biocompatible triboelectric materials,

have led to TENGs integration in smart healthcare textiles for use in diagnostic[72], therapeutic[73] and power supplying applications[74-76].

Magnetoelastic Platforms

Very recently, mechanically induced giant magnetoelastic effect in soft system has been discovered and developed in stand-alone systems, namely, magnetoelastic generators (MEGs)[77]. This technology has shown promise in vital sign monitoring and diagnosis, as well as in biomechanical energy harvesting for healthcare device powering.

Smart Textile Fabrication Strategies

An ever-growing number and variety of functional materials, fabrication technologies, and architectures have been utilised in smart textiles, with material classes chosen depending on desired functionality (Figure 2a). Diagnostic and therapeutic abilities of smart textiles rely on a range of functionalised materials.

Functional materials

Electrically conducting materials have been traditionally used as smart textile electrodes, in the form of metals (e.g., Ag, Cu, Ti, Au, Ni)[78], conducting polymers (poly(3,4-ethylenedioxythiophene) polystyrene sulfonate (PEDOT: PSS))[79], and certain carbon-based materials (carbon nanotubes, graphene)[80]. Metal textile fibre solutions provide high conductivity (~10^5 S cm^{-1}) capabilities, while polymers and carbon materials have been developed to introduce easier fabrication and overall fibre flexibility[81]. Having the capability to interact with the external environment is essential to smart textiles, and semiconducting or conducting functional materials have been employed to this end. Semiconducting functional materials influenced by mechanical (polyvinylidene difluoride, (PVDF))[82], thermal (carbon nanotubes (CNTs))[83], optical (metal-organic frameworks (MOFs))[84], and electromagnetic (MXenes)[27] activities have been integrated as a powerful tool to use in smart textile development. A detailed list of functional materials is provided in Table 1.

Fabrication technologies

Developing scalable and batch consistent smart textiles requires sturdy fabrication solutions. Various fabrication strategies have been developed (Figure 2b), with spinning[85], coating[86], printing[87] and thermal drawing[88] remaining the most prominent. Spinning can produce stand-alone functional fibres, or can be used to functionalise traditional textile/fibre substrates, and has been tested for large-scale manufacturing[89,90]. By manipulating the initial fabrication process, continuous fibres of varying diameters can be parallelly fabricated from a single or multiple functional materials. Wet spinning[91], dry spinning[92], melt spinning[93], and electrospinning[94] have all been used in smart textile fabrication using a range of functional materials. On another front, functional materials can be also transferred onto textile substrates using coating. Coating processes are usually employed to form functional layers on materials' surfaces. By controlling the coating thickness and the coating area, desired changes in active layer morphology can be produced based on desired functionality[95]. Widely adopted coating methods include spray coating[96], dipcoating[97], and electrochemical coating[98], providing a low-cost, convenient, and effective way to fabricate smart textiles. Printing[99], including 3D printing[87], has also been used in smart textile fabrication, with functional material inks both deposited locally on textiles, and extruded as 3D structures. This fabrication technique has already been implemented at industrial level given its predisposition to large-scale, autonomous, and low-cost processes. Screen printing[100] and inkjet printing[101], have also been used before. Thermal drawing, an industrial approach for producing fibres in a simple and scalable way[102], has also been employed in smart textile fabrication. This technique enables targeted functional materials to be positioned in a prepared model known as "preform"[103]. Here assembly of various shapes and structures can be used to form complex fibre electronics, while allowing simultaneous extrusion of multiple material fibres that can produce fibre electronics within a one-body design. Thermally drawn fibres can moreover be further miniaturised to the nanoscale[104], helping optimise smart textile solutions.

Smart textile architectures

Fibre architecture can provide clothing with flexibility, breathability, wear and tear resistance, and material integration. Such properties are normally provided by traditional fibres used alone, or mixed in different fabric forms, and through weaving architecture design. In addition to the above, smart textiles for personalised

healthcare must provide diagnostic or therapeutic capabilities. The presence of functional materials and knowledge of varying physicochemical processes (as detailed in platform technologies), provides a myriad of microscaled mechanisms of actions which can be engineered to provide personalised healthcare solutions, at the fibre-level, at the textile level, or in both mechanisms in parallel. Various versatile textile architectures exist within smart textiles.

Firstly, at the fibre-level: *ex novo* fibres can be developed using novel functional materials; existing traditional textile material fibres can be endowed with smart textile qualities; and *ex novo* fibres can be designed with specific multi-material internal architectures to provide diagnostic or therapeutic modes of action. Secondly, and on a macro and fabric-level scale: existing traditional textiles can be upgraded with smart qualities *via* applicative processes, and; pre-determined fibre organisation and weaving can be used to bring about specific therapeutic or diagnostic modes of action.

In the first approach, functional materials: can be either directly fabricated as fibres using techniques such as wet/dry spinning[105] or thermal-drawing[103], or; can be applied to modify conventional fibre surfaces *via* means of additive processes[106]. Specific architectural structures can be subsequently applied to functionalised fibres in various configurations;, such as coaxial, twisted, or parallel (Figure 2c)[107]. These fabrication approaches can allow for extremely complex smart textile solutions, employing multiple functional materials. For instance, in a TENG-based coaxial structure[108], one electrode layer, a pair of triboelectric layers, another electrode layer, and a final encapsulation layer, can be assembled in sequential fashion. Whilst in a twisting configuration, an electrode layer can be used as a second fibre and wound together with a triboelectric fibre at specific intertwined angles[76]. A twisted configuration provides constituting active materials with better interactions upon which external interfacing, such as photo-reactivity and chemical reactivity, can occur[109], a methodology well-suited to smart textiles comprising solar cells and biosensors[110].

In the second approach, functional materials are embedded: onto traditional textile substrates using the above fabrication technologies, as well as lamination[111]; or *in situ* chemical treatment processes[112]. These techniques are used to upgrade traditional textiles and provide smart textile qualities, resulting in an easier-to-access, cost-

effective, and scalable solution, that is widely used in the research community. In a Parkinson's disease evaluation smart textile solution, a PEDOT:PSS coated fabric (triboelectric layer 1), a Polytetrafluoroethylene (PTFE) film (triboelectric layer 2) and an Al film (electrode) were stacked to devise a textile TENG used for walking mornitoring[113]. Challenges in uniform layer deposition, and the formation of thin and defective functional layers on rugged textile surfaces, can however limit the electronic performance of smart textiles conceived this way[114]. Moreover, the additive functional materials can compromise the flexibility, conformity, and air permeability of the textile substrates[30].

As discussed, in the second approach: fibre-organisation can determine application. Indeed, the various types of fibres described above can furthermore be arranged in woven, knitted, nonwoven, and sewing structures to develop energy-producing[75], diagnostic[72] and therapeutic applications[22] (Figure 2d). Engineered smart fibres have been developed to mimic desired traditional textile properties including breathability and flexibility, but considering their multicomponent nature, can show a higher sensitivity to damage from wear-and-tear, mechanical deformation, friction, and the effects of the elements[30]. Smart textiles degrade more readily, meaning that maintaining thin, uniform, and durable functional layers on constantly mobile fibre surfaces, remains a challenge requiring focused research efforts[115]. On this front, we invite colleagues to consider interdisciplinary research that leverages on computational modelling, and on expertise from the clothing industry, to help develop body-wide smart textiles which are optimised for various non-linear parts of the body.

Smart Diagnostic Textiles

Diagnostic smart textile solutions have boomed in recent years[116-118], providing continuous monitoring of biophysical[119], biochemical[120], and environmental factors[121]. Textile-based wearable generators which harvest passive on-body energy sources to power smart textile diagnosis have also been developed. Here, we review important studies in smart textile-based sensors for healthcare monitoring relying on physical sensing and chemical sensing, each detailing use of smart textile generators for powering biosensors.

Textile Physical Sensors

Textile physical sensors convert physically stimulating inputs from physiological activities into information rich electrical signals, used to deduce physiological information[122]. Biomechanical sensors represent the most advanced physical sensor category used in textiles, and are found in the form of triboelectric[71], piezoelectric[63], resistive[42], or capacitive[51] pressure, or strain sensors. Such sensors can be used for broad biomechanical vital signal monitoring (heart rate, respiratory, and ambulatory sensing). TENGs have emerged as particularly useful in this field, providing functional and attractive smart textile solutions such as flower-shaped textile TENGs, used in pulse rate monitoring, and sleep apnoea diagnosis (Figure 3a and 3b)[20]. Recently, MEGs were developed for biomechanical-to-electrical signals conversion by combining the giant magnetoelastic effect with electromagnetic induction (Figure 3c)[77]. A textile MEG was fabricated by weaving 1D soft fibres with conductive yarns (Figure 3d)[122], converting arterial pulse into electrical signals even with heavy perspiration or underwater, without encapsulation (Figure 3e). TENG arrays have also been developed as knitted smart textile sensors tracking chest expansions-retraction respiratory cycles[123], simultaneously gathering breathing and heart rate information. Further to classic biomonitoring, biomechanical smart textile sensors can provide insight into neurological diseases[124,125] using motion tracking. Large scale sensing textiles have been fabricated using knitted nanocomposite-based piezoresistive fibres (Figure 3f) [126], and existing solutions such as tactile sensitive smart textile socks can be repurposed for early-stage detection of neurological diseases, by tracking pressure distribution. Integration of such sensing capabilities with machine learning based movement analysis could help with the diagnosis of neurological conditions such as dystonia, Parkinson's disease, epilepsy, and Alzheimer's disease[127].

Textile electrodes used to detect bioelectrical signals (electrocardiograms (ECG), electroencephalograms (EEG), and electromyograms (EMG)) have also been studied[49,50,128], possessing good wearing comfort, without causing skin irritation normally associated with conventional gel electrodes. Conductive flexible artificial silk textile patches made of PEDOT were developed for at home and clinical use[129], with a design which enabled simple skin-conformable positioning for continuous EMG monitoring (Figure 3g).

Textile physical sensors can moreover include optical properties, able to both detect and produce light[130], and have been used to monitor physiological parameters including sweat metabolites[131], heart rate[132], blood

pressure[133] and oxygen saturation[134]. In a recent example, fabrics embedded with light-emitting diode fibres and photo-detecting p-i-n diode fibres were developed to measure heart rate[132]. On another front, textile-embedded thermally sensitive resistors have also been used to detect resistance-correlated temperature changes[44] and help continuous and non-invasive body temperature monitoring. Using this type of smart clothing could help prevent thermally related clinical conditions including hyper- and hypothermia, but also help in extreme sport activity, as well as help monitor the emergence of wound infections, and fever[135]. Reduced graphene oxide-coated yarns[136] knitted into textile form, have shown suitability here. These solutions are already starting to come to market. Siren Sock™, a smart textile sock with thermal sensors, was developed to help alert patients and doctors on the presence of leg inflammation as a sign of ulcer formation in diabetes[137].

Textile Chemical Sensors

In addition to textile physical sensors, various textile chemical sensors have been developed[138], with electrochemical sensors used on body fluid metabolite (e.g., glucose and D-lactate concentrations) and electrolyte (e.g., Na^+, K^+, Ca^{2+} ions) analysis[139,140]. Specifically, multi-walled CNT twisted fibre electrochemical sensor have emerged strongly given their ability to detect multiple disease biomarkers *in vivo*[21]. Textile chemical sensors can monitor healthcare parameters directly from the epidermis (sweat-based), and upon contact with other fluids (even urine)[59]. An example worth mentioning includes an electrochemical textile developed by weaving a broad range of sensing fibre units (Figure 3h)[140]. These sensing units (fabricated by coating chemically-active materials onto CNT fibre substrates), proved effective in monitoring various parameters, including glucose, [Na^+], [K^+], [Ca^{2+}], and pH, showing continuous performance despite repeated mechanical stress.

Furthermore, certain textile sensors which detect humidity can also be used in personalised healthcare[141], detecting breathing rate[142], and monitoring healthcare-relevant environmental conditions[143]. In an example, a smart textile sensor for humidity detection was developed by coating a MIL-96(Al) MOF layer onto a fabric electrode[144]. This MOF-based textile humidity sensor specifically detected water vapour concentration even with the presence of several other compounds. On a chemical front, smart textiles have also been developed to directly diagnose physiological status using redox reactions between the textile itself and bodily secretions[66]. Textile

biofuel cells consisting of lactate oxidase-modified CNT bioanodes and Ag_2O/Ag-based biocathodes have been engineered to use the enzymatic oxidation of transpired lactate. This solution was able to produce voltage signals proportionate to lactate concentration[145], setting an example of a distinctly new type of smart textile analyte detection platform.

Smart Textiles for Diagnostic Device Powering

Portable power supplies such as batteries present limitations including limited lifespan, bulky nature, and environmental and health hazards[146]. Smart textiles can produce energy from several passive activities, used to power third party healthcare diagnostic devices[147] (Figure 3i). Harvesting passive energy sources can lead to uncontrollable power output linked to unstable (environmental) energy inputs[30], and smart textile solutions have been developed to address this[148]. A photo-rechargeable textile was developed to form a self-charging power unit[149], including a solar energy-harvesting component, and a rechargeable flexible textile battery component (Figure 3j). With the increasing light intensity, this energy textile could generate an improved stable output to power on-body biosensors.

Smart Therapeutic Textiles

Besides diagnosis, personalised healthcare also includes access to specific therapeutic solutions, which considers patient safety margins and personal life factors[150]. Smart textiles featuring therapeutic functions can interact with the human body for continuous and one-time therapeutic solutions, adjusting treatments according to a person's evolving health profile[151]. Smart textiles for personalised therapy are expected to offer an alternative to traditional one-size-fits-all therapeutic approaches, although their development is still early. A few specific areas have however started seeing an increase in smart textile therapeutic applications, including smart textile use for third party therapeutic device powering. We highlight these smart therapeutic textile fields below:

Assistive Technology

Assistive technology allows disabled, ill, and/or elderly patients to regain access to activities which are essential to leading an independent life[152]. Considering the growing elder population, developing upgraded everyday wear for various smart and assistive functions is critical. Smart textiles have been engineered to this end, with textile-based and mobility-assisting exoskeletal support[153], textile hearing aids, and textile prostheses[154] developed as smart textile assistive technology applications. Communication for speech impaired patients has also benefited from smart textile use with smart textile gloves developed for sign-to-speech translation[155] (Figure 4a). This assistive application helped with by converting American Sign Language into voice messages (Figure 4b). In addition to these therapeutic academic examples, commercially developed Palarum® Smart Socks were shown to help prevent patient falls using electrical rehabilitative therapy[156], with fabric pressure sensors measuring real time changes in movement and pressure, ensuring a quick response to balance problems (Figure 4c). Considering the large portion of the population expected to need assistive technologies by 2030[152], smart textiles are being exploited as a potential therapeutic platform to help address this need.

Thermotherapy

Thermotherapy is widely used in the treatment of musculoskeletal injuries, soft tissue injuries, and body aches[157]. Active smart textiles with integrated joule heating and thermoelectricity have been developed to help[158]. A textile thermotherapy system for instance was developed by combining a woven Kevlar fibre with copper–nickel nanowires, and reduced graphene oxide dispersed PDMS[159]. This textile thermotherapy system showed effective joule heating and reflected therapeutic infrared radiation back onto the patient's skin. In another example, a more sophisticated self-controllable joule heating solution was developed as a $Ti_3C_2T_x$ MXene textile (a two-dimensional transition metal comprising carbides and/or nitrides). This MXene textile was able to perform low-voltage thermotherapy used to not only help with a therapeutic effect, but also kill bacteria surrounding a wound (Figure 4d)[158].

Drug Delivery

Drug delivery enhanced by wearable devices provides a non-invasive, convenient, and highly controllable solution for drug dosing and improved administration time adherence, crucial elements of personalised healthcare

treatments[160-162]. Considering the large portions of the population requiring daily drug administration, smart textiles can be used to conform to the skin for a long period of time without pain or irritation and enable long-term and personalised administration of drugs without third party or doctor intervention[163]. Smart textile wound dressings have been developed for intelligent drug delivery with tailored dosage and administration times (Figure 4e). In an example, interwoven drug release fibres which formed a core electrical heater, were covered by a layer of thermoresponsive hydrogel drug carriers loaded with antibiotics and vascular endothelial growth factors[22]. Their use was shown to improve the healing rate of diabetic wounds (Figure 4f). Considering the prevalence of diabetes, this solution can open a new avenue of therapeutic smart textile solutions for diabetes and its effects.

Electrical Stimulation

Electrical stimulation has been shown as a promising therapy in the fields of chronic wound treatment, muscular dystrophy, tissue damage, and neuromodulation[164], and is emerging as a stand-alone personalised healthcare field. Smart textiles for electrical stimulation, such as a self-powered textile TENGs[73] and e-sleeves[165], show good wearing comfort and can provide personalised, continuous electrotherapy. Such a therapeutic approach using TENG smart textiles has been used to help accelerate wound healing[166] (Figure 4g and 4h).

Third Party Therapeutic Device Powering

Smart textiles have also been developed to harvest ambient (environment) energy with which to continuously power therapeutic devices. To this end, a textile system was developed using smart textile powered supply modules, display modules, and information input modules[167]. Here, photovoltaic smart textiles were used for energy harvesting, whilst zinc-ion battery fibres were used for energy storing (Figure 4i), even if with limited energy conversion efficiency. Improved energy conversion and storage efficiency are active research areas, as is harnessing new energy transduction mechanisms. Radiofrequencies for instance represent an ideal energy source for electricity generation using smart textiles. Recently, researcher fabricated a flexible rectenna on a polymer substrate[168], shown to be able to harvest Wi-Fi band electromagnetic radiation. Such a platform technology could be further developed into textile form, providing an environmentally friendly, and pervasive energy solution to

sustainably drive healthcare devices. A thorough summary of typical research-based smart textiles for personalised healthcare (both therapeutic and diagnostic) is provided in Table 2.

Smart Healthcare Textiles in Industry

The medical smart textiles market is expected to exceed $2 billion by 2027[169]. Bringing a smart textile personalised healthcare solution to the market, however, requires developing economically viable, technically sturdy and scientifically accurate solutions which are recognised as useful by the medical community, and accepted by the public.

To date, most smart textiles enabled personalised healthcare solutions, have focused on diagnosis or biomonitoring. Many fitness-focused examples have been developed, but we have not included them in this healthcare-focused review. On a smaller scale, smart textile therapeutic products have also been launched in specific fields. A summary of commercially available smart textiles for personalised healthcare is shown in Table 3.

Within diagnosis, there has been major focus on vital sign monitoring, where many companies have developed clothing equivalents (vests) as stand-alone smart textile solutions. Vital signs monitoring companies for consumer use include Canada's Carre Technologies Inc.'s Hexoskin[170], which also employs actigraphy for step counting and gait monitoring, and Israeli company HealthWatch, whose product focuses on heart electrophysiology monitoring[171]. Earlier stage commercial products have also focused on posture ⊥health, such as MIT spin-out Nextiles, which uses conductive and piezoresistive based smart textiles for gait and grip monitoring, to optimise posture and training protocols for athletes[172]. Theragnostic (both therapeutic and diagnostic) vest smart textile solutions have also been developed commercially. Japan's Xenoma developed wearable body suits and clothing which can be tailored to motion tracking, electrical stimulation, biomonitoring and physical therapy[173], whilst Canada's Myant Inc. developed its Skiin product for biomonitoring and thermotherapy applications.[174]

Smart socks solutions have also, perhaps surprisingly, been a key target of both diagnostic and theragnostic commercial focus. Companies such as Palarum®[156], Siren[137], Texisense[175] and Sensoria Health[176] have developed

solutions to provide assistive therapy, inflammation monitoring, posture monitoring and Parkinson's disease management, respectively. Impractically however, these vest and sock solutions include rather large modular (detachable) components for data storage and/or data relay to a remote device, highlighting how industry still hasn't fully addressed the bulky nature of these components. Moreover, although some of these options can carry out data analysis directly *in situ*, their level of complexity is still not clear.

Certain business-to-business smart textile healthcare solutions have also been launched commercially and seem to include a service component. French company Bioserenity[177], focused on smart textiles for clinical trial use, has developed products Cardioskin (ECG monitoring) and Neuronaute (EEG monitoring). These solutions are offered as part of a data analytics service-based model, rather than stand-alone smart textiles use for personalised healthcare.

Although major commercial efforts have been placed to help developing function-specific products, certain companies focused on platform smart textile fabrication. Dupont™ for instance has demonstrated large scale ability to print metallic conductive inks on flexible polymeric films, and produce light and stretchable conductive fibres that can be applied on any textile. They are offering therapeutic and monitoring/diagnostic applications in healthcare through their Intexar™ product line[178]. Nipponic Toray Industries' biomonitoring "hitoe" fabric[179], also seem to have addressed scalability. By filling nanofibre spaces with conductive polymeric material, their solution apparently provides long term wearability and washability resistance, though it is unclear what their commercialisation strategy is.

Despite international efforts in commercialising smart textile solutions for personalised healthcare, the product focus remains limited, especially in the therapeutic space. Beyond this, miniaturisation and smart textile integration of data process and relay solutions seem to remain largely unaddressed by industry, as too is unfortunately the expansion into disease-specific solutions. To our knowledge moreover, global pharmaceutical companies and medical device companies haven't yet started to develop smart textile solutions for personalised healthcare, and novel players are defining the industry.

Regulatory Considerations

The desire to push smart textiles in the fields of wellbeing and healthcare is strong, but regulatory restrictions need to be considered. The American Association of Textile Chemists and Colourists (AATCC)[180], the American Society for Testing and Materials (ASTM)[16], the Institute of Printed Circuits (IPC)[181], and the International Organisation for Standards-International Electrotechnical Commission (ISO IEC)[182], have all started to establish nomenclature and testing references for either e-textiles or smart textiles. However, from a medical use perspective, clinical regulation is also necessary. Within a clinical and regulatory setting, smart textiles can be largely considered as medical devices, with pathways for authorised use depending on regional regulatory agencies' approval. To our knowledge, to date, the only clinically approved smart textiles include the Food and Drug Administration (FDA) 510(k)-cleared Nanowear's SimpleSense[183], a heart rate monitoring textile[184], and HealthWatch's MasterCaution®, a vital sign monitor, which also holds a CE mark. Interestingly SimpleSense was regulated by the FDA as a "radiofrequency physiological signal transmitter and receiver"[185], whilst MasterCaution® received "telephone electrocardiograph transmitter and receiver"[186] nomenclature, suggesting an unplanned and *ad hoc* classification for these smart textile healthcare solutions, rather than a dedicated regulatory framework. Consequently, it is important to establish broader and more far-reaching specific regulatory approval committees and pathways in smart textiles. To achieve this, initiatives to promote discussions between scientists, clinicians, regulators, and industrial parties are necessary to unify efforts and translate smart textiles into clinically effective, approved solutions. We encourage translational research scientists to educate themselves on regulatory processes pertaining to medical devices, by partaking in FDA[187], European Medicines Agency[188], Pharmaceuticals and Medical Devices Agency[189], National Medical Products Administration[190] and other regulatory agencies meetings and workshops, highlighted in the above references. Beyond regulatory bodies, government-level initiatives have been established in this direction. The European Commission's CONTEXT initiative[191] was developed as a European network to foster research and innovation efforts on advanced smart textiles, and has a dedicated Healthcare and Medicine working group which reports to the European Commission, which we invite readers to consult. This type of set up should be embraced by regulatory bodies to set up cross-disciplinary roundtables and help establish future regulatory frameworks, which are key to developing medically

approved smart textiles for personalised healthcare. Moreover, from a payer perspective, in large, privatised healthcare markets such as the United States, specific regulatory reimbursement codes must be devised, whilst state health systems should set up committees to establish reimbursement schemes and integration of such smart textile-based personalised healthcare devices.

Computing Capabilities

Computing capabilities are essential to the advancement of smart textiles for personalised healthcare. Data management – including data acquisition, analysis, transmission, and storage – represents an essential component of smart textiles' correct functioning[117]. Data analysis expectations can range from implementing simple signal-to-function association, to carrying out sophisticated computational data flow processes[12]. Heart rate monitoring can for instance involve tracking pulses in a simple (binary) on/off manner[123] or involve in depth ECG monitoring with multi-lead positioning[35], with insights into heart electrophysiology. Data analysis in ultra-violet exposure monitoring[192] can in another way, be carried out using linear association to track sun (over)exposure. Varying levels of data management complexity can therefore be relayed when using smart textiles.

Some wearable devices can act independently of data analytics, such as (homeostatically-inspired) closed-loop solutions that self-regulate using analyte-induced physicochemical reactions[193], though most wearable solutions follow a pattern of data acquisition, analysis and clinical intervention (diagnostic or therapeutic)[20], governed and established by a third-party powered and modular decision-making unit (DMU) component[126]. For smart textiles, such components are usually wirelessly connected to a nearby computational device (smartphones, tablets) for data management, or third-party, cloud-based relays for remote monitoring. Efforts are now in place to transition data management onto the textile devices themselves, for *in situ* computing[194]. Besides hardware innovation, which, as seen previously, has still to catch up in commercially available products, integrating machine learning algorithms will also be required to help smart textile adapt to aging and evolving patient health[195], and to integrate health changes, e.g., pre- and post-diabetic changes, stroke or musculoskeletal injuries' implications.

Autonomous Textile Body-Area Networks

Developing autonomous, independent, and smart-textile embedded data management capabilities represents a great opportunity to deliver fully-fledged personalised healthcare solutions. To this end we wish to propose a new concept and use of Autonomous Textile Body Area Networks (ATBANs) as a practical smart textile-based solution. Smart textiles used in personalised healthcare rely on three core functionalities: energy provision[196], data management (acquisition, analysis, transmission and storage)[195], and clinical intervention (diagnostic or therapeutic)[20], with at least one of these functionalities dependent on outside intervention. Fortunately, recent technological advancements in materials science, nanoelectronics, and miniaturisation capabilities[197], have freed smart textiles from this external dependence, integrating key functionalities directly within the textiles themselves. From an interconnectability perspective, moreover, the growing presence of 5G infrastructure can now integrate smart textiles into the IoT *via* continuous wireless external communication[26]. By leveraging these capabilities, ATBANs can provide a fully closed loop personalised healthcare solution which include diagnostic technologies, therapeutic platforms, powering technologies, communication relays, and DMU computational capabilities. All these components can be fully integrated in an intelligent system supported by a cooperative, self-adaptive and intelligent node-based network[194] (Figure 5a).

To explain the potential of ATBAN for specific clinical conditions, a closed loop configuration for diabetic patients could be imagined. Such a system could include a smart textile with glucose-monitoring nodes, therapeutic insulin-delivery nodes, and energy harvesting nodes, working together to ensure intelligent and self-adaptive glucose level control. The presence of communication nodes could continuously communicate glucose level data through the users' smart phones, or remote cloud systems, sending alerts in case of hyper- or hypo-glycaemic states. In parallel, smart textiles could also save and index data into the patient's clinical record, allowing archiving and remote clinician monitoring/intervention.

With the emergence of translational research, moreover, developing ATBANs could expand implementation capabilities and reach, in clinical trials, introducing scalable and autonomous dosage, monitoring, and follow-up, with enrolled patients. This approach would *de facto* remove the need for costly and centralised facilities. ATBANs would thus provide personalised healthcare solutions that are independent and self-sufficient

energetically, in data management, and clinical intervention capabilities, shifting healthcare from the bench to the bedside. We have seen examples of this in Bioserenity's business model, as described earlier[177].

A versatile and modular ATBAN that can be fine-tuned to integrate specific functionalities, depending on personal patient clinical profile, could provide a clinical platform of interest, and could be systematically upgraded alongside technological advancements, incorporating increasingly complex and autonomous computational nodes, and software updates. ATBANs present very many advantages, including the capability to deliver timely, patient-specific, independent, and intelligent clinical monitoring, as well as autonomous computation and clinical interventions directly *in situ,* removing patient burden linked to traveling to the clinic. Such technologies will help democratise access to quality healthcare globally, providing a novel way to help thrust personalised healthcare into an optimised and cost-effective era (Figure 5b).

Developing ATBANs also presents significant limitations of using highly engineered textiles. Pushbacks to ATBANs' use also include user adoption[198]. To address these, developing smart textile wearables with detachable components could help remove water-damage risks and simplify user interaction. We invite multidisciplinary collaboration to optimise hardware, software, and device-to-device communications within ATBANS (Figure 5c).

Outlook

The future development of smart textiles requires consideration of key areas in academia and industry. In academia this should include material innovation, device structures, reliability and stability, functional integration, and performance standardisation. In industry this should include product standardisation, value chain creation, manufacturing and clinical integration.

Academic considerations: The use of novel raw materials and the development of novel composites will be important in addressing issues of washability, performance, and resistance (Figure 6a). Materials such as hybrid composites with programmable functionalities are promising in this regard[199] and should be explored further. Non-biocompatible or physiologically inadequate materials should be avoided, and focus should instead be placed

on developing corrosion-resistance self-healing textiles[200]. Furthermore, the use of rare, or expensive materials is unlikely to lead to industrially scalable solutions, and viable alternatives should be sought.

Smart textile devices often integrate functional materials with harsher mechanical properties. Miniaturisation of fibres (at the nanoscale), and coating with mechanically soft materials could help address this. Furthermore, heterogeneous functional layer deposition issues[201], which arise during fabrication, could be addressed using interface engineering to allow stable interfacial bonding and reduce the occurrence of fibre crack/delamination (Figure 6b)[202]. Moreover, advice from textile experts, including recognised fashion institutes of textile and technology, should be sought on comfort enhancing weaving techniques, rather than developing technologies afresh. Focus should also be placed on alternative weaving architectures and thread thickness to define novel healthcare functions, such as three-dimensional weaving structures. These are expected to deliver overall better healthcare applications[203], producing structural properties with inherent flexibility, robustness, porosity, and softness[30].

Smart textiles should offer breathability, washability, robustness, thermal stability, and air/moisture permeability (Figure 6c), which are all current weak points. Thus, focus should be placed on protection from oxidation, humidity, and mechanical deformation. Well-sealed textile sensors using polymer encapsulation (covering curvilinear surfaces) can provide a solution to this end[72]. Exploring ultrahydrophobicity could also help provide exciting solutions.

Developing efficient processing techniques to integrate multiple textile healthcare devices with a comfortable design will be an essential step toward fabricating complex smart textiles and ATBANs (Figure 6d). Digital sewing machines hold promise, as recently demonstrated with the fabrication of a fully integrated textile system consisting of textile display, keyboard, and power supply components[167]. Researchers should focus on scalable and automated processes relying on existing, low-barrier fabrication technologies.

Establishing objective performance comparison between smart textiles solutions is currently extremely challenging due to the heterogeneity of academic solutions developed. To allow effective and true comparison between academically devised smart textile healthcare solutions, we invite academics to research and, insofar as

possible, imitate textile testing methods based on ISO standards (such as ISO/TC 38/SC 24 testing standards)[204]. For personalised healthcare smart textiles, previous (similar) work and example testing conditions should be mimicked, and a comparative analysis given within the manuscript, rather than creating *ex novo* testing conditions. Editors and peer-reviewers should consider making this aspect a prerequisite to publishing articles related to smart textile solutions for personalised healthcare.

Industrial considerations. Growing efforts are being placed on standardising certain aspects of the smart textile industry, beginning with the nomenclature and differentiation between e-textiles, smart textiles, and wearable bioelectronics. Providing clarity and guidelines will be essential. Alongside infrastructural issues, which arise with novel hardware-heavy industry, broader and more abstract standardisation considerations must be addressed. For instance, regulatory consensus on the clinical testing, validation, approval, and medical device clearance guidelines, will need to be developed (Figure 6e).

Even though the traditional textile industry is mature and established, a well-defined value chain is still absent in smart textiles. Transitioning from small scale, *ad hoc*, academic focus, to industry, requires adaptation. High raw material costs, rarity and toxicity, as well as the need for a highly trained workforce skillset, also limit scaling up. Medical grade manufacturing standards requirements in healthcare also add a layer of complexity to smart textile production for clinical use. Initiatives have emerged to help on this front. The European Commission has set up the SmartX European Smart Textiles Accelerator to specifically help with academia–industry bridging and smart textile value chain creation[205], including a specific medical division. This initiative is dedicated to small and medium-sized enterprises smart textile solution development, and we encourage researchers and start-ups to initiate conversations with such bodies.

To address scaling up manufacturing issues[206], we suggest both a top-down scaling approach, and a bottom-up scaling approach. Diagnostic, large roll out, generalised smart textiles solutions could benefit from a top-down manufacturing strategy solution. Here, economies of scale factors, including lower raw material cost and provision, uniform design production, adaptation to existing machinery, and mirroring of established protocols would prevail and be applied in continuous manufacturing mode. Cheaper semiconductive functional materials

(phyisicochemically sensitive PTFE or PVDF) and monolithic platform technologies (PENG, MEG) would also provide easier scalability. Fabrication strategies such as spinning, demonstrated at scale[89], could be used to develop standardised clothing apparel with pre-set sensing areas (chest for heart and respiratory rate, integrated glove for oxygen saturation detection, and multi-position sensorial bodies for motion traction), possessing embedded metal conducting threads for plugging into data-relying units or nodes. These could be developed at scale and replace hospital gowns and be easily recycled. Owing to the material selection, these solutions would also be the most well suited to washability and long-term comfort for everyday use.

A bottom-up scaling approach for therapeutic or highly functionalised solutions, would be conversely driven by the specificity of the therapeutic function desired. Bottom-up scaling, requiring more technical expertise and raw material variety, could be carried out using batch manufacturing. Drug-delivering smart textiles such as thermoresponsive hydrogel drug carriers[22], could hold platform scaling up potential, with varying drugs being loaded onto the smart textile at parallel batch steps, to produce a portfolio of drug-releasing smart textiles. Insulin-releasing, wound healing, and post-operative surgery management smart textiles could all be a part of this more sophisticated bottom-up approach.

Ensuring scientific and clinical effectiveness recognition by the medical community is essential to smart textile adoption. Considering the substantial electrical engineering and material science focus of these devices, this could present alienation problems. Training clinicians (and patients) to appreciate the working modes of smart textiles will require dedicated focus. Optimised user interface, network integration and accessibility should also be closely developed alongside clinicians.

Given the multi-disciplinary nature of smart textiles in personalised healthcare, cross-collaboration between material scientists, electrical engineers, clothing industry experts, regulatory bodies, clinicians, patients, user-interface developers, and government entities will be required to optimise future development and integration. We hope that this Review, and having access to the initiatives mentioned above, will help colleagues contribute to the establishment of the value chain for smart textiles use in personalised healthcare (Figure 6f).

Acknowledgements

This is an invited review article. The authors acknowledge the Henry Samueli School of Engineering & Applied Science and the Department of Bioengineering at the University of California, Los Angeles, for the start-up support. J.C. also acknowledges the 2020 Okawa Foundation Research Grant and 2021 Hellman Follows Fund.

Author information

Affiliations:

Department of Bioengineering, University of California, Los Angeles, Los Angeles, CA, USA

Alberto Libanori, Guorui Chen, Xun Zhao, Yihao Zhou, Jun Chen

Author contributions:

J.C. initialised and supervised the project. A.L., G.C., and J. C. have coordinated the data collection, analysis and writing of this review. X.Z. and Y.Z. helped with the figure design and made technical comments. A.L. and G.C. contributed equally to this work. All the authors contributed to discussion and revised the manuscript at all stages.

Competing interests:

The authors declare no competing interests.[1]

Additional information

Correspondence should be addressed to J.C.

References

1 Wang, C., Horby, P.W., Hayden, F.G. & Gao, G.F. A novel coronavirus outbreak of global health concern. *The Lancet* **395**, 470-473 (2020).
2 Schwalbe, N. & Wahl, B. Artificial intelligence and the future of global health. *The Lancet* **395**, 1579-1586 (2020).
3 Howitt, P. *et al.* Technologies for global health. *The Lancet* **380**, 507-535 (2012).
4 Kerr, E.A. & Hayward, R.A. Patient-centered performance management: Enhancing value for patients and

health care systems. *JAMA* **310**, 137-138 (2013).
5 Bierman, A.S. & Tinetti, M.E. Precision medicine to precision care: Managing multimorbidity. *The Lancet* **388**, 2721-2723 (2016).
6 Gray, J.A.M. The shift to personalised and population medicine. *The Lancet* **382**, 200-201 (2013).
7 Rose, N. Personalized medicine: Promises, problems and perils of a new paradigm for healthcare. *Procedia. Soc. Behav. Sci.* **77**, 341-352 (2013).
8 Sultan, N. Reflective thoughts on the potential and challenges of wearable technology for healthcare provision and medical education. *Int. J. Inf. Manag. Sci.* **35**, 521-526 (2015).
9 Ye, S., Feng, S., Huang, L. & Bian, S. Recent progress in wearable biosensors: From healthcare monitoring to sports analytics. *Biosensors* **10**, 205 (2020).
10 Rai, P. *et al. Smart healthcare textile sensor system for unhindered-pervasive health monitoring*. (SPIE, 2012).
11 Wang, S., Bai, Y. & Zhang, T. *Wearable bioelectronics*. (Elsevier, 2020).
12 Ray, T.R. *et al.* Bio-integrated wearable systems: A comprehensive review. *Chem. Rev.* **119**, 5461-5533 (2019).
13 Kim, J., Campbell, A.S., de Ávila, B.E.-F. & Wang, J. Wearable biosensors for healthcare monitoring. *Nat. Biotechnol.* **37**, 389-406 (2019).
14 Araromi, O.A. *et al.* Ultra-sensitive and resilient compliant strain gauges for soft machines. *Nature* **587**, 219-224 (2020).
15 Chen, G., Fang, Y., Zhao, X., Tat, T. & Chen, J. Textiles for learning tactile interactions. *Nat. Electron.* **4**, 175-176 (2021).
16 Astm d8248-20 standard terminology for smart textiles. *ASTM International* (2020).
17 Yu, L. *et al.* A tightly-bonded and flexible mesoporous zeolite-cotton hybrid hemostat. *Nat. Commun.* **10**, 1932 (2019).
18 Si, Y. *et al.* Daylight-driven rechargeable antibacterial and antiviral nanofibrous membranes for bioprotective applications. *Sci. Adv.* **4**, eaar5931 (2018).
19 Lee, D.T., Jamir, J. D., Peterson, G. W. & Parsons, G. N. Protective fabrics: Metal-organic framework textiles for rapid photocatalytic sulfur mustard simulant detoxification. *Matter* **2**, 404-415 (2020).
20 Meng, K. *et al.* A wireless textile-based sensor system for self-powered personalized health care. *Matter* **2**, 896-907 (2020).
21 Wang, L. *et al.* Functionalized helical fibre bundles of carbon nanotubes as electrochemical sensors for long-term in vivo monitoring of multiple disease biomarkers. *Nat. Biomed. Eng.* **4**, 159-171 (2020).
22 Mostafalu, P. *et al.* A textile dressing for temporal and dosage controlled drug delivery. *Adv. Funct. Mater.* **27**, 1702399 (2017).
23 Collins, F.S. & Varmus, H. A new initiative on precision medicine. *N. Engl. J. Med.* **372**, 793-795 (2015).
24 Shilo, S., Rossman, H. & Segal, E. Axes of a revolution: Challenges and promises of big data in healthcare. *Nat. Med.* **26**, 29-38 (2020).
25 Karim, N. *et al.* Scalable production of graphene-based wearable e-textiles. *ACS Nano* **11**, 12266-12275 (2017).
26 Ilderem, V. The technology underpinning 5G. *Nat. Electron.* **3**, 5-6 (2020).
27 Wang, Q.-W. *et al.* Multifunctional and water-resistant mxene-decorated polyester textiles with outstanding electromagnetic interference shielding and joule heating performances. *Adv. Funct. Mater.* **29**, 1806819 (2019).
28 Yetisen, A.K., Martinez-Hurtado, J. L., Ünal, B., Khademhosseini, A. & Butt, H. Wearables in medicine. *Adv. Mater.* **30**, 1706910 (2018).
29 Zhao, Z. *et al.* Machine-washable textile triboelectric nanogenerators for effective human respiratory monitoring through loom weaving of metallic yarns. *Adv. Mater.* **28**, 10267-10274 (2016).
30 Chen, G., Li, Y., Bick, M. & Chen, J. Smart textiles for electricity generation. *Chem. Rev.* **120**, 3668-3720 (2020).

31 Alberghini, M. *et al.* Sustainable polyethylene fabrics with engineered moisture transport for passive cooling. *Nat. Sustain.* **4**, 715–724 (2021).
32 Sundaram, S. *et al.* Learning the signatures of the human grasp using a scalable tactile glove. *Nature* **569**, 698-702 (2019).
33 Post, E.R., Orth, M., Russo, P.R. & Gershenfeld, N. E-broidery: Design and fabrication of textile-based computing. *IBM Syst. J.* **39**, 840-860 (2000).
34 Carpi, F. & Rossi, D.D. Electroactive polymer-based devices for e-textiles in biomedicine. *IEEE Trans. Inf. Technol. Biomed.* **9**, 295-318 (2005).
35 Catrysse, M. *et al.* Towards the integration of textile sensors in a wireless monitoring suit. *Sensors and Actuators A: Physical* **114**, 302-311 (2004).
36 Grillet, A. *et al.* Optical fiber sensors embedded into medical textiles for healthcare monitoring. *IEEE Sens. J.* **8**, 1215-1222 (2008).
37 Lyu, S., He, Y., Yao, Y., Zhang, M. & Wang, Y. Photothermal clothing for thermally preserving pipeline transportation of crude oil. *Adv. Funct. Mater.* **29**, 1900703 (2019).
38 Mordon, S. *et al.* The conventional protocol vs. A protocol including illumination with a fabric-based biophotonic device (the phosistos protocol) in photodynamic therapy for actinic keratosis: A randomized, controlled, noninferiority clinical study. *Br. J. Dermatol.* **182**, 76-84 (2020).
39 Shen, J., Chui, C. & Tao, X. Luminous fabric devices for wearable low-level light therapy. *Biomed. Opt. Express* **4**, 2925-2937 (2013).
40 Park, S. *et al.* One-step optogenetics with multifunctional flexible polymer fibers. *Nat. Neurosci.* **20**, 612-619 (2017).
41 Zhang, Z. *et al.* A colour-tunable, weavable fibre-shaped polymer light-emitting electrochemical cell. *Nat. Photonics* **9**, 233-238 (2015).
42 Liu, M. *et al.* Large-area all-textile pressure sensors for monitoring human motion and physiological signals. *Adv. Mater.* **29**, 1703700 (2017).
43 Cho, S.-Y. *et al.* Continuous meter-scale synthesis of weavable tunicate cellulose/carbon nanotube fibers for high-performance wearable sensors. *ACS Nano* **13**, 9332-9341 (2019).
44 Wu, R. *et al.* Silk composite electronic textile sensor for high space precision 2D combo temperature–pressure sensing. *Small* **15**, 1901558 (2019).
45 Ding, T. *et al.* Scalable thermoelectric fibers for multifunctional textile-electronics. *Nat. Commun.* **11**, 6006 (2020).
46 Sun, T. *et al.* Stretchable fabric generates electric power from woven thermoelectric fibers. *Nat. Commun.* **11**, 572 (2020).
47 Jeong, E.G., Jeon, Y., Cho, S.H. & Choi, K.C. Textile-based washable polymer solar cells for optoelectronic modules: Toward self-powered smart clothing. *Energy Environ. Sci.* **12**, 1878-1889 (2019).
48 Zhang, N. *et al.* A wearable all-solid photovoltaic textile. *Adv. Mater.* **28**, 263-269 (2016).
49 Matsuhisa, N. *et al.* Printable elastic conductors with a high conductivity for electronic textile applications. *Nat. Commun.* **6**, 7461 (2015).
50 Jin, H. *et al.* Enhancing the performance of stretchable conductors for e-textiles by controlled ink permeation. *Adv. Mater.* **29**, 1605848 (2017).
51 Lee, J. *et al.* Conductive fiber-based ultrasensitive textile pressure sensor for wearable electronics. *Adv. Mater.* **27**, 2433-2439 (2015).
52 Li, R. *et al.* Supercapacitive iontronic nanofabric sensing. *Adv. Mater.* **29**, 1700253 (2017).
53 Dalton, A.B. *et al.* Super-tough carbon-nanotube fibres. *Nature* **423**, 703-703 (2003).
54 Etches, J., Bond, I. & Mellor, P. *The manufacturing of magnetically-active fiber-reinforced composites for use in power generation*. (SPIE, 2004).
55 Lee, H. & Roh, J.-S. Wearable electromagnetic energy-harvesting textiles based on human walking. *Text. Res. J.* **89**, 2532-2541 (2019).
56 Li, H. *et al.* Chemical and biomolecule sensing with organic field-effect transistors. *Chem. Rev.* **119**, 3-35

(2019).
57 Kim, S.J. *et al.* A new architecture for fibrous organic transistors based on a double-stranded assembly of electrode microfibers for electronic textile applications. *Adv. Mater.* **31**, 1900564 (2019).
58 Shi, W., Guo, Y. & Liu, Y. When flexible organic field-effect transistors meet biomimetics: A prospective view of the internet of things. *Adv. Mater.* **32**, 1901493 (2020).
59 Yang, A. *et al.* Fabric organic electrochemical transistors for biosensors. *Adv. Mater.* **30**, 1800051 (2018).
60 Hamedi, M., Forchheimer, R. & Inganäs, O. Towards woven logic from organic electronic fibres. *Nat. Mater.* **6**, 357-362 (2007).
61 Egusa, S. *et al.* Multimaterial piezoelectric fibres. *Nat. Mater.* **9**, 643-648 (2010).
62 Qin, Y., Wang, X. & Wang, Z.L. Microfibre–nanowire hybrid structure for energy scavenging. *Nature* **451**, 809-813 (2008).
63 Su, Y. *et al.* Muscle fibers inspired high-performance piezoelectric textiles for wearable physiological monitoring. *Adv. Funct. Mater.* **31**, 2010962 (2021).
64 Azimi, B. *et al.* Electrospinning piezoelectric fibers for biocompatible devices. *Adv. Healthc. Mater.* **9**, 1901287 (2020).
65 Soin, N. *et al.* Novel "3-D spacer" all fibre piezoelectric textiles for energy harvesting applications. *Energy Environ. Sci.* **7**, 1670-1679 (2014).
66 Kwon, C.H. *et al.* High-power biofuel cell textiles from woven biscrolled carbon nanotube yarns. *Nat. Commun.* **5**, 3928 (2014).
67 Lv, J. *et al.* Sweat-based wearable energy harvesting-storage hybrid textile devices. *Energy Environ. Sci.* **11**, 3431-3442 (2018).
68 Fan, F.-R., Tian, Z.-Q. & Wang, Z.L. Flexible triboelectric generator. *Nano Energy* **1**, 328-334 (2012).
69 Chen, J. & Wang, Z.L. Reviving vibration energy harvesting and self-powered sensing by a triboelectric nanogenerator. *Joule* **1**, 480-521 (2017).
70 Zhou, Y., Deng, W., Xu, J. & Chen, J. Engineering materials at the nanoscale for triboelectric nanogenerators. *Cell. Rep. Phys. Sci.* **1**, 100142 (2020).
71 Chen, G., Au, C. & Chen, J. Textile triboelectric nanogenerators for wearable pulse wave monitoring. *Trends Biotechnol.* **39**, 1078-1092 (2021).
72 Zhou, Z. *et al.* Single-layered ultra-soft washable smart textiles for all-around ballistocardiograph, respiration, and posture monitoring during sleep. *Biosens. Bioelectron.* **155**, 112064 (2020).
73 He, T. *et al.* Self-sustainable wearable textile nano-energy nano-system (NENS) for next-generation healthcare applications. *Adv. Sci.* **6**, 1901437 (2019).
74 Jung, S., Lee, J., Hyeon, T., Lee, M. & Kim, D.-H. Fabric-based integrated energy devices for wearable activity monitors. *Adv. Mater.* **26**, 6329-6334 (2014).
75 Chen, C. *et al.* 3D double-faced interlock fabric triboelectric nanogenerator for bio-motion energy harvesting and as self-powered stretching and 3d tactile sensors. *Mater. Today* **32**, 84-93 (2020).
76 Zhong, J. *et al.* Fiber-based generator for wearable electronics and mobile medication. *ACS Nano* **8**, 6273-6280 (2014).
77 Zhou, Y. *et al.* Giant magnetoelastic effect in soft systems for bioelectronics. *Nat. Mater.* **20**, 1300 (2021).
78 Wu, Y., Mechael, S.S., Lerma, C., Carmichael, R.S. & Carmichael, T.B. Stretchable ultrasheer fabrics as semitransparent electrodes for wearable light-emitting e-textiles with changeable display patterns. *Matter* **2**, 882-895 (2020).
79 Ryan, J.D., Mengistie, D.A., Gabrielsson, R., Lund, A. & Müller, C. Machine-washable pedot:Pss dyed silk yarns for electronic textiles. *ACS Appl. Mater. Interfaces* **9**, 9045-9050 (2017).
80 Aboutalebi, S.H. *et al.* High-performance multifunctional graphene yarns: Toward wearable all-carbon energy storage textiles. *ACS Nano* **8**, 2456-2466 (2014).
81 Lund, A. *et al.* Conducting materials as building blocks for electronic textiles. *MRS Bull.* **46**, 491-501 (2021).
82 Ghosh, S.K. & Mandal, D. Synergistically enhanced piezoelectric output in highly aligned 1D polymer

nanofibers integrated all-fiber nanogenerator for wearable nano-tactile sensor. *Nano Energy* **53**, 245-257 (2018).
83 Zheng, Y. *et al.* Carbon nanotube yarn based thermoelectric textiles for harvesting thermal energy and powering electronics. *J. Mater. Chem. A* **8**, 2984-2994 (2020).
84 Nazari, M. *et al.* Metal-organic-framework-coated optical fibers as light-triggered drug delivery vehicles. *Adv. Funct. Mater.* **26**, 3244-3249 (2016).
85 Yan, J. *et al.* Transformation of oxide ceramic textiles from insulation to conduction at room temperature. *Sci. Adv.* **6**, eaay8538 (2020).
86 Park, M. *et al.* Highly stretchable electric circuits from a composite material of silver nanoparticles and elastomeric fibres. *Nat. Nanotechnol.* **7**, 803-809 (2012).
87 Chatterjee, K. & Ghosh, T.K. 3D printing of textiles: Potential roadmap to printing with fibers. *Adv. Mater.* **32**, 1902086 (2020).
88 Loke, G. *et al.* Digital electronics in fibres enable fabric-based machine-learning inference. *Nat. Commun.* **12**, 3317 (2021).
89 Duan, X. *et al.* Large-scale spinning approach to engineering knittable hydrogel fiber for soft robots. *ACS Nano* **14**, 14929-14938 (2020).
90 Huang, Y. *et al.* Large-scale spinning of silver nanofibers as flexible and reliable conductors. *Nano Lett.* **16**, 5846-5851 (2016).
91 Tang, Z. *et al.* Highly stretchable core–sheath fibers via wet-spinning for wearable strain sensors. *ACS Appl. Mater. Interfaces* **10**, 6624-6635 (2018).
92 Zhao, Y. *et al.* A moss-inspired electroless gold-coating strategy toward stretchable fiber conductors by dry spinning. *Adv. Electron. Mater.* **5**, 1800462 (2019).
93 Wang, Q. *et al.* Melt spinning of low-cost activated carbon fiber with a tunable pore structure for high-performance flexible supercapacitors. *ACS Appl. Energy Mater.* **3**, 9360-9368 (2020).
94 Nayeem, M.O.G. *et al.* All-nanofiber–based, ultrasensitive, gas-permeable mechanoacoustic sensors for continuous long-term heart monitoring. *Proc. Natl. Acad. Sci. U.S.A.* **117**, 7063-7070 (2020).
95 Allison, L., Hoxie, S. & Andrew, T.L. Towards seamlessly-integrated textile electronics: Methods to coat fabrics and fibers with conducting polymers for electronic applications. *Chem. Commun.* **53**, 7182-7193 (2017).
96 Samanta, A. & Bordes, R. Conductive textiles prepared by spray coating of water-based graphene dispersions. *RSC Adv.* **10**, 2396-2403 (2020).
97 Zheng, C. *et al.* Superhydrophobic and flame-retardant alginate fabrics prepared through a one-step dip-coating surface-treatment. *Cellulose* **28**, 5973-5984 (2021).
98 Park, Y., Park, M.-J. & Lee, J.-S. Reduced graphene oxide-based artificial synapse yarns for wearable textile device applications. *Adv. Funct. Mater.* **28**, 1804123 (2018).
99 Zhang, M. *et al.* Printable smart pattern for multifunctional energy-management e-textile. *Matter* **1**, 168-179 (2019).
100 Cao, R. *et al.* Screen-printed washable electronic textiles as self-powered touch/gesture tribo-sensors for intelligent human–machine interaction. *ACS Nano* **12**, 5190-5196 (2018).
101 Shahariar, H., Kim, I., Soewardiman, H. & Jur, J.S. Inkjet printing of reactive silver ink on textiles. *ACS Appl. Mater. Interfaces* **11**, 6208-6216 (2019).
102 Yan, W. *et al.* Thermally drawn advanced functional fibers: New frontier of flexible electronics. *Mater. Today* **35**, 168-194 (2020).
103 Loke, G., Yan, W., Khudiyev, T., Noel, G. & Fink, Y. Recent progress and perspectives of thermally drawn multimaterial fiber electronics. *Adv. Mater.* **32**, 1904911 (2020).
104 Wang, Z. *et al.* Designer patterned functional fibers via direct imprinting in thermal drawing. *Nat. Commun.* **11**, 3842 (2020).
105 Frutiger, A. *et al.* Capacitive soft strain sensors via multicore–shell fiber printing. *Adv. Mater.* **27**, 2440-2446 (2015).

106 Wang, Y. *et al.* 3D-printed all-fiber li-ion battery toward wearable energy storage. *Adv. Funct. Mater.* **27**, 1703140 (2017).
107 Zhang, X. *et al.* Recent advances in functional fiber electronics. *SusMat* **1**, 105-126 (2021).
108 Yu, X. *et al.* A coaxial triboelectric nanogenerator fiber for energy harvesting and sensing under deformation. *J. Mater. Chem. A* **5**, 6032-6037 (2017).
109 Li, R., Xiang, X., Tong, X., Zou, J. & Li, Q. Wearable double-twisted fibrous perovskite solar cell. *Adv. Mater.* **27**, 3831-3835 (2015).
110 Xu, X., Xie, S., Zhang, Y. & Peng, H. The rise of fiber electronics. *Angew. Chem. Int. Ed.* **58**, 13643-13653 (2019).
111 Park, J.W., Kwon, S., Kwon, J.H., Kim, C.Y. & Choi, K.C. Low-leakage fiber-based field-effect transistors with an al2o3–mgo nanolaminate as gate insulator. *ACS Appl. Electron. Mater.* **1**, 1400-1407 (2019).
112 Zhang, M.C. *et al.* Carbonized cotton fabric for high-performance wearable strain sensors. *Adv. Funct. Mater.* **27**, 1604795 (2017).
113 Zhu, M. *et al.* Self-powered and self-functional cotton sock using piezoelectric and triboelectric hybrid mechanism for healthcare and sports monitoring. *ACS Nano* **13**, 1940-1952 (2019).
114 Andrew, T.L. *et al.* Melding vapor-phase organic chemistry and textile manufacturing to produce wearable electronics. *Acc. Chem. Res.* **51**, 850-859 (2018).
115 Lee, J. *et al.* Stretchable and suturable fibre sensors for wireless monitoring of connective tissue strain. *Nat. Electron.* **4,** 291–301 (2021).
116 Tessarolo, M., Gualandi, I. & Fraboni, B. Recent progress in wearable fully textile chemical sensors. *Adv. Mater. Technol.* **3**, 1700310 (2018).
117 Coyle, S. *et al.* Biotex—biosensing textiles for personalised healthcare management. *IEEE Trans. Inf. Technol. Biomed.* **14**, 364-370 (2010).
118 Su, Y. *et al.* Muscle fibers inspired high-performance piezoelectric textiles for wearable physiological monitoring. *Adv. Funct. Mater.* **31**, 2010962 (2021).
119 Yang, Z. *et al.* Graphene textile strain sensor with negative resistance variation for human motion detection. *ACS Nano* **12**, 9134-9141 (2018).
120 Parrilla, M., Cánovas, R., Jeerapan, I., Andrade, F. J. & Wang, J. A textile-based stretchable multi-ion potentiometric sensor. *Adv. Healthc. Mater.* **5**, 996-1001 (2016).
121 Smith, M.K. & Mirica, K. A. Self-organized frameworks on textiles (soft): Conductive fabrics for simultaneous sensing, capture, and filtration of gases. *J. Am. Chem. Soc.* **139**, 16759-16767 (2017).
122 Zhao, X. *et al.* Soft fibers with magnetoelasticity for wearable electronics. *Nat. Commun.* **12**, 6755 (2021).
123 Fan, W. *et al.* Machine-knitted washable sensor array textile for precise epidermal physiological signal monitoring. *Sci. Adv.* **6**, eaay2840 (2020).
124 Mattay, V.S. *et al.* Neurophysiological correlates of age-related changes in human motor function. *Neurology* **58**, 630-635 (2002).
125 Ahn, S. *et al.* Wearable multimode sensors with amplified piezoelectricity due to the multi local strain using 3D textile structure for detecting human body signals. *Nano Energy* **74**, 104932 (2020).
126 Luo, Y. *et al.* Learning human–environment interactions using conformal tactile textiles. *Nat. Electron.* **4**, 193-201 (2021).
127 Varatharajan, R., Manogaran, G., Priyan, M.K. & Sundarasekar, R. Wearable sensor devices for early detection of alzheimer disease using dynamic time warping algorithm. *Clust. Comput.* **21**, 681-690 (2018).
128 Homayounfar, S.Z. *et al.* Multimodal smart eyewear for longitudinal eye movement tracking. *Matter* **3**, 1275-1293 (2020).
129 Jia, Z. *et al.* Bioinspired conductive silk microfiber integrated bioelectronic for diagnosis and wound healing in diabetes. *Adv. Funct. Mater.* **31,** 2010461 (2021).
130 Quandt, B.M. *et al.* Body-monitoring and health supervision by means of optical fiber-based sensing systems in medical textiles. *Adv. Healthc. Mater.* **4**, 330-355 (2015).

131 Morris, D. *et al.* Bio-sensing textile based patch with integrated optical detection system for sweat monitoring. *Sens. Actuators B Chem.* **139**, 231-236 (2009).
132 Rein, M. *et al.* Diode fibres for fabric-based optical communications. *Nature* **560**, 214-218 (2018).
133 Bennett, A. *et al.* Monitoring of vital bio-signs by analysis of speckle patterns in a fabric-integrated multimode optical fiber sensor. *Opt. Express* **28**, 20830-20844 (2020).
134 Krehel, M. *et al.* Development of a luminous textile for reflective pulse oximetry measurements. *Biomed. Opt. Express* **5**, 2537-2547 (2014).
135 Peng, Y. & Cui, Y. Advanced textiles for personal thermal management and energy. *Joule* **4**, 724-742 (2020).
136 Afroj, S. *et al.* Engineering graphene flakes for wearable textile sensors via highly scalable and ultrafast yarn dyeing technique. *ACS Nano* **13**, 3847-3857 (2019).
137 Temperature monitoring for better foot care. (2021); https://siren.care/
138 Shim, B.S., Chen, W., Doty, C., Xu, C. & Kotov, N.A. Smart electronic yarns and wearable fabrics for human biomonitoring made by carbon nanotube coating with polyelectrolytes. *Nano Lett.* **8**, 4151-4157 (2008).
139 He, W. *et al.* Integrated textile sensor patch for real-time and multiplex sweat analysis. *Sci. Adv.* **5**, eaax0649 (2019).
140 Wang, L. *et al.* Weaving sensing fibers into electrochemical fabric for real-time health monitoring. *Adv. Funct. Mater.* **28**, 1804456 (2018).
141 Jia, T. *et al.* Moisture sensitive smart yarns and textiles from self-balanced silk fiber muscles. *Adv. Funct. Mater.* **29**, 1808241 (2019).
142 Ma, L. *et al.* Full-textile wireless flexible humidity sensor for human physiological monitoring. *Adv. Funct. Mater.* **29**, 1904549 (2019).
143 Weremczuk, J., Tarapata, G. & Jachowicz, R. Humidity sensor printed on textile with use of ink-jet technology. *Procedia Eng.* **47**, 1366-1369 (2012).
144 Rauf, S. *et al.* Highly selective metal–organic framework textile humidity sensor. *ACS Appl. Mater. Interfaces* **12**, 29999-30006 (2020).
145 Jeerapan, I., Sempionatto, J.R., Pavinatto, A., You, J.-M. & Wang, J. Stretchable biofuel cells as wearable textile-based self-powered sensors. *J. Mater. Chem. A* **4**, 18342-18353 (2016).
146 Kang, D.H.P., Chen, M. & Ogunseitan, O.A. Potential environmental and human health impacts of rechargeable lithium batteries in electronic waste. *Environ. Sci. Technol.* **47**, 5495-5503 (2013).
147 Chen, J. *et al.* Micro-cable structured textile for simultaneously harvesting solar and mechanical energy. *Nat. Energy* **1**, 16138 (2016).
148 Cheng, H. *et al.* Textile electrodes woven by carbon nanotube–graphene hybrid fibers for flexible electrochemical capacitors. *Nanoscale* **5**, 3428-3434 (2013).
149 Zhang, N. *et al.* Photo-rechargeable fabrics as sustainable and robust power sources for wearable bioelectronics. *Matter* **2**, 1260-1269 (2020).
150 Davenport, M. *et al.* New and developing diagnostic technologies for urinary tract infections. *Nat. Rev. Urol.* **14**, 296-310 (2017).
151 Vargas, A.J. & Harris, C.C. Biomarker development in the precision medicine era: Lung cancer as a case study. *Nat. Rev. Cancer* **16**, 525-537 (2016).
152 Cook, A.M. & Polgar, J.M. *Assistive technologies-e-book: Principles and practice*. (Elsevier, 2014).
153 Awad, L.N. *et al.* A soft robotic exosuit improves walking in patients after stroke. *Sci. Transl. Med.* **9**, eaai9084 (2017).
154 Heim, F., Durand, B. & Chakfe, N. Textile heartvalve prosthesis: Manufacturing process and prototype performances. *Text. Res. J.* **78**, 1124-1131 (2008).
155 Zhou, Z. *et al.* Sign-to-speech translation using machine-learning-assisted stretchable sensor arrays. *Nat. Electron.* **3**, 571-578 (2020).
156 Palarum smart sock. (2021); https://palarum.org/

157 Choi, S. *et al.* Stretchable heater using ligand-exchanged silver nanowire nanocomposite for wearable articular thermotherapy. *ACS Nano* **9**, 6626-6633 (2015).
158 Zhao, X. *et al.* Smart $Ti_3C_2T_x$ mxene fabric with fast humidity response and joule heating for healthcare and medical therapy applications. *ACS Nano* **14**, 8793-8805 (2020).
159 Hazarika, A. *et al.* Woven kevlar fiber/polydimethylsiloxane/reduced graphene oxide composite-based personal thermal management with freestanding cu–ni core–shell nanowires. *Nano Lett.* **18**, 6731-6739 (2018).
160 Liang, K., Carmone, S., Brambilla, D. & Leroux, J.-C. 3D printing of a wearable personalized oral delivery device: A first-in-human study. *Sci. Adv.* **4**, eaat2544 (2018).
161 Amjadi, M., Sheykhansari, S., Nelson, B.J. & Sitti, M. Recent advances in wearable transdermal delivery systems. *Adv. Mater.* **30**, 1704530 (2018).
162 Joo, H. *et al.* Soft implantable drug delivery device integrated wirelessly with wearable devices to treat fatal seizures. *Sci. Adv.* **7**, eabd4639 (2021).
163 Lee, H. *et al.* Device-assisted transdermal drug delivery. *Adv. Drug Delivery Rev.* **127**, 35-45 (2018).
164 Xiao, X., Chen, G., Libanori, A. & Chen, J. Wearable triboelectric nanogenerators for therapeutics. *Trends Chem.* **3**, 279-290 (2021).
165 Liu, M. *et al.* Electronic textiles based wearable electrotherapy for pain relief. *Sens. Actuator A Phys.* **303**, 111701 (2020).
166 Jeong, S.-H. *et al.* Accelerated wound healing with an ionic patch assisted by a triboelectric nanogenerator. *Nano Energy* **79**, 105463 (2021).
167 Shi, X. *et al.* Large-area display textiles integrated with functional systems. *Nature* **591**, 240-245 (2021).
168 Zhang, X. *et al.* Two-dimensional MoS_2-enabled flexible rectenna for Wi-Fi-band wireless energy harvesting. *Nature* **566**, 368-372 (2019).
169 Medical smart textiles market by technology (textile sensors, wearable technology), by application (surgery, bio-monitoring, therapy, and wellness), by end-use (hospitals and clinics, medical academic and research center), and by region. (2021); https://www.emergenresearch.com/industry-report/medical-smart-textiles-market
170 Hexoskin. (2021); https://www.hexoskin.com/
171 The next generation in dressable smart sensing medical device garment. (2021); https://healthwatchtech.com/
172 Nextiles. (2021); https://www.nextiles.tech/
173 Xenoma. (2021); https://xenoma.com/
174 The skiin (2021); https://skiin.com/
175 Texis. (2021); https://www.texisense.com/
176 Sensoria health. (2021); https://www.sensoriahealth.com/products/
177 Bioserenity. (2021); https://www.bioserenity.com
178 Dupont. (2021); https://electronics-imaging.dupont.com/intexar
179 Hitoe. (2021); https://www.hitoe.toray
180 Evaluation procedure for electrical resistance of electronically-integrated textiles. *AATCC* (2020).
181 Ipc-8921 requirements for woven and knitted electronic textiles (e-textiles) integrated with conductive fibers, conductive yarns and/or wires. *IPC* (2019).
182 Textiles and textile products — smart (intelligent) textiles— definitions, categorisation, applications and standardization needs. *ISO* (2020).
183 Nanowear. (2021); https://www.nanowearinc.com/
184 510(k) premarket notification simplecg. (2016); https://www.accessdata.fda.gov/scripts/cdrh/cfdocs/cfpmn/pmn.cfm?ID=K161431
185 Code of federal regulations title 21. (2020); https://www.accessdata.fda.gov/scripts/cdrh/cfdocs/cfcfr/cfrsearch.cfm?fr=870.2910
186 510(k) premarket notification master caution device mcd. (2015);

https://www.accessdata.fda.gov/scripts/cdrh/cfdocs/cfPMN/pmn.cfm?ID=K142476
187 Workshops & conferences (medical devices). (2020); https://wayback.archive-it.org/7993/20201217211859/https://www.fda.gov/medical-devices/news-events-medical-devices/workshops-conferences-medical-devices
188 Multi-stakeholder workshop to support implementation of the medical devices regulation on drug-device combinations. (2020); https://www.ema.europa.eu/en/events/multi-stakeholder-workshop-support-implementation-medical-devices-regulation-drug-device
189 Pharmaceuticals and medical devices agency. (2021); https://www.pmda.go.jp/english/index.html
190 National medical products administration. (2021); http://english.nmpa.gov.cn/medicaldevices.html
191 European network to connect research and innovation efforts on advanced smart textiles. (2021); https://www.context-cost.eu/
192 Xu, X. *et al.* A real-time wearable uv-radiation monitor based on a high-performance p-CuZnS/n-TiO_2 photodetector. *Adv. Mater.* **30**, 1803165 (2018).
193 Chen, B. Z., Zhang, L. Q., Xia, Y. Y., Zhang, X. P. & Guo, X. D. A basal-bolus insulin regimen integrated microneedle patch for intraday postprandial glucose control. *Sci. Adv.* **6**, eaba7260 (2020).
194 Zhou, F. & Chai, Y. Near-sensor and in-sensor computing. *Nat. Electron.* **3**, 664-671 (2020).
195 Loke, G. *et al.* Computing fabrics. *Matter* **2**, 786-788 (2020).
196 Yin, L. *et al.* A self-sustainable wearable multi-modular e-textile bioenergy microgrid system. *Nat. Commun.* **12**, 1542 (2021).
197 Tian, X. *et al.* Wireless body sensor networks based on metamaterial textiles. *Nat. Electron.* **2**, 243-251 (2019).
198 Liu, S., Ma, K., Yang, B., Li, H. & Tao, X. Textile electronics for vr/ar applications. *Adv. Funct. Mater.* **31**, 2007254 (2021).
199 Tang, T.-C. *et al.* Materials design by synthetic biology. *Nat. Rev. Mater.* **6**, 332-350 (2021).
200 Kang, J., Tok, J.B.H. & Bao, Z. Self-healing soft electronics. *Nat. Electron.* **2**, 144-150 (2019).
201 Jur, J.S., Sweet III, W.J., Oldham, C.J. & Parsons, G.N. Atomic layer deposition of conductive coatings on cotton, paper, and synthetic fibers: Conductivity analysis and functional chemical sensing using "all-fiber" capacitors. *Adv. Funct. Mater.* **21**, 1993-2002 (2011).
202 Ma, H., Yip, H.-L., Huang, F. & Jen, A.K.-Y. Interface engineering for organic electronics. *Adv. Funct. Mater.* **20**, 1371-1388 (2010).
203 Dong, K. *et al.* Shape adaptable and highly resilient 3D braided triboelectric nanogenerators as e-textiles for power and sensing. *Nat. Commun.* **11**, 2868 (2020).
204 Standards by iso/tc 38/sc 24 conditioning atmospheres and physical tests for textile fabrics. (2021); https://www.iso.org/committee/48344/x/catalogue/
205 Smartx. (2021); https://www.smartx-europe.eu/
206 He, J. *et al.* Scalable production of high-performing woven lithium-ion fibre batteries. *Nature* **597**, 57-63 (2021).
207 Chen, L. *et al.* Textile-based capacitive sensor for physical rehabilitation via surface topological modification. *ACS Nano* **14**, 8191-8201 (2020).
208 Peng, Y. *et al.* Nanoporous polyethylene microfibres for large-scale radiative cooling fabric. *Nat. Sustain.* **1**, 105-112 (2018).
209 Kim, H. *et al.* Spirally wrapped carbon nanotube microelectrodes for fiber optoelectronic devices beyond geometrical limitations toward smart wearable e-textile applications. *ACS Nano* **14**, 17213-17223 (2020).

Figures and Captions

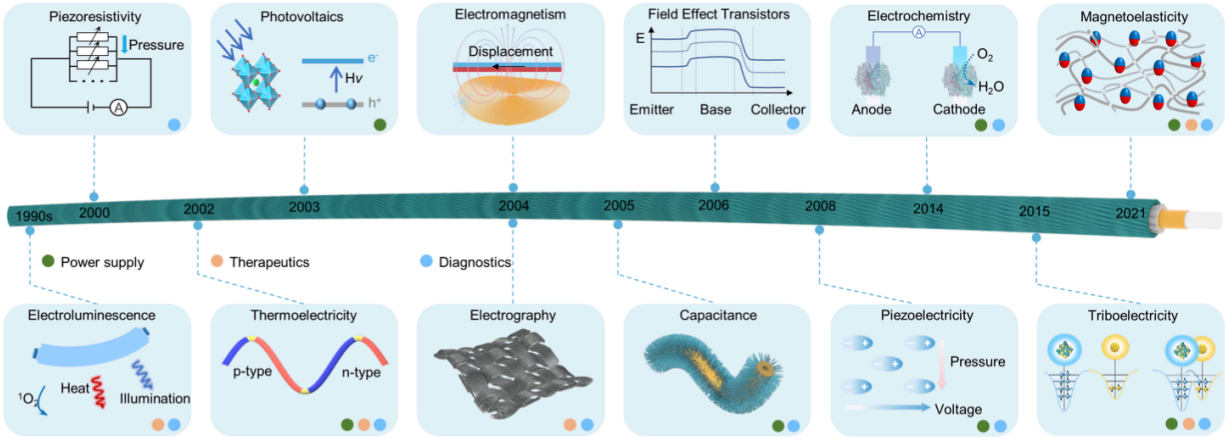

Fig.1 | Milestone research timeline of platform technologies for smart healthcare textiles. Embedding electronics into clothing began in the 1990s and was in turn applied to the field of healthcare. Nanoelectronics and material science platform technology developments saw the introduction of a plethora of diagnostic, therapeutic and energising applications. A timeline and summary of such technology platform developments and applications to the healthcare field is presented.

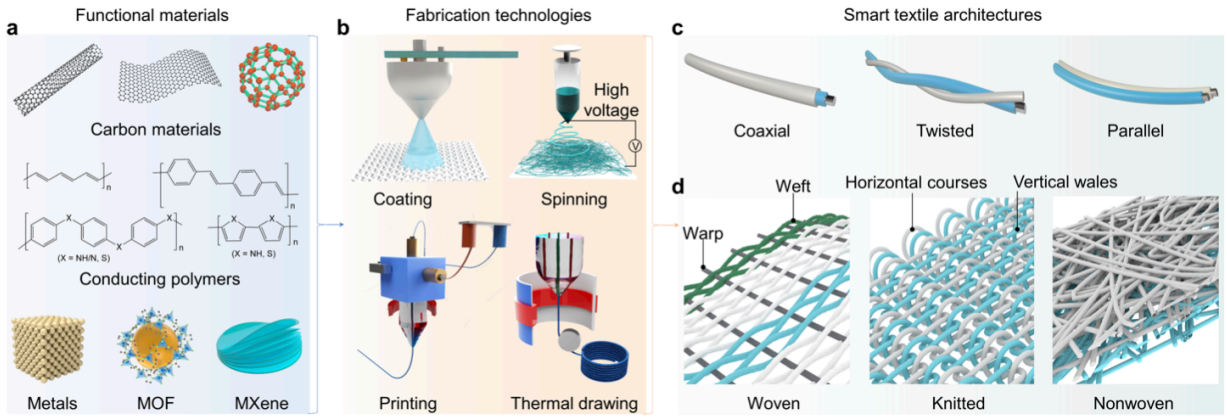

Fig. 2 | Fabrication strategies of smart healthcare textiles. a, Raw materials employed in smart textiles: Functional materials are embedded onto the as-fabricated textile substrates. **b,** Fabrication strategies employed for smart textiles: Functional materials can be directly fabricated within the fibres using techniques such as coating, spinning, printing and thermal drawing. **c,** Architectures used for smart textiles: Various fibre-level arrangements which help functionalise smart textiles. **d,** Textile-level structuring means yarns can be woven, knitted or integrated in nonwoven ways, and spun into large-scale smart textiles.

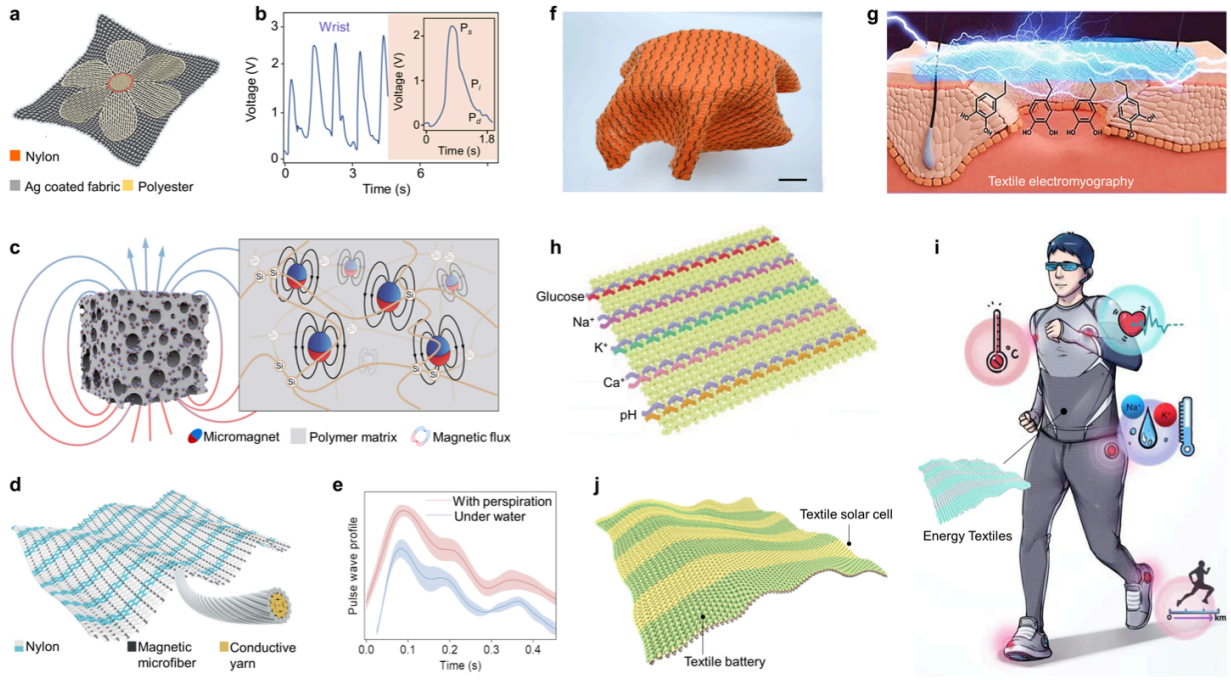

Fig. 3 | Smart diagnostic textiles. a, Schematic illustration of a flower-shaped textile sensor for wireless measurement of cardiovascular parameters. **b,** Acquired pulse waveforms as carried out on an elderly patient. **c,** Giant magnetoelastic effect in soft systems for biomechanical-to-electrical signals conversion. **d,** Textile MEG by weaving the 1D soft fibers with conductive yarns. **e,** Textile MEGs can accurately convert the arterial pulse wave into electrical signals under heavy perspiration or underwater without encapsulations. **f,** Photograph of the large-scale tactile sensing textile. Scale bar, 0.5 cm. **g,** A conductive flexible silk patch consisting of PEDOT serving as an epidermal sensor to monitor electromyogram signals. **h,** An electrochemical sensing textile for glucose, [Na^+], [K^+], [Ca^{2+}], and pH monitoring. **i.** Textile able to harvest renewable energy from the human body and its surroundings, providing a sustainable power source for diagnostic devices. **j,** A photo-rechargeable textile comprising a textile solar cell and a textile battery. Figures reproduced with permission from: **a, b,** ref.[20], Elsevier. **c,** ref.[77], Springer Nature Ltd. **d, e,** ref.[122], Springer Nature Ltd. **f,** ref.[126], Springer Nature Ltd. **g,** ref.[129], Wiley. **h,** ref.[140], Wiley. **i, j,** ref.[149], Elsevier.

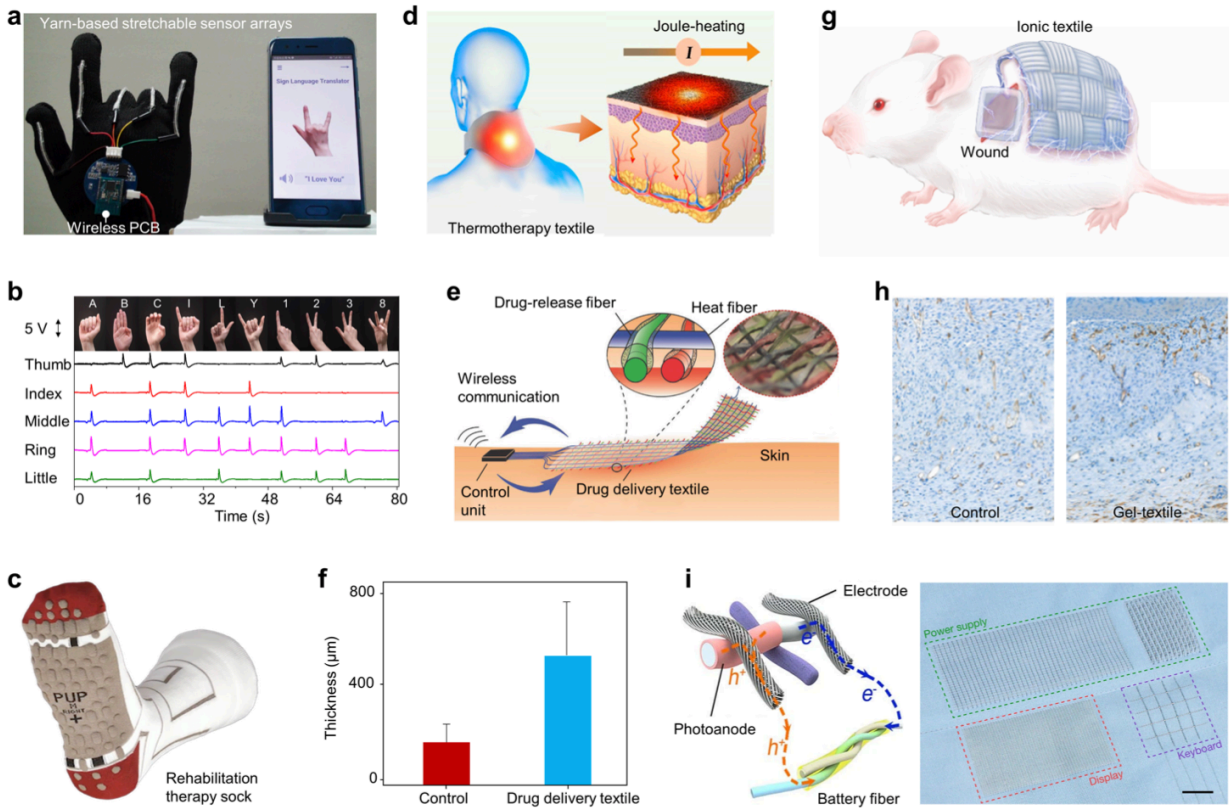

Fig. 4 | Smart therapeutic textiles. a, Smart glove as an assistive therapy for sign-to-speech translation and communication. **b,** Generated electrical signal patterns from American Sign Language hand gestures and their letter representation. **c,** Palarum® Smart Sock, a commercial product that can prevent patient falls, working as an effective assistive technology and enhanced rehabilitation therapy. **d,** A $Ti_3C_2T_x$ MXene textile featuring self-controllable joule heating for thermotherapy and killing bacteria surrounding a wound. **e,** A smart wound dressing textile for drug delivery with tailored dosage and medication time administration. **f,** A threefold increase in granulation tissue deposition in a wound bed with drug-releasing textile compared to controls. **g,** A TENG textile based on weaving of ionically conductive organogel fibres, able to generate electric field and accelerate wound healing. **h,** Immunostaining images of CD34 expression in the wound region after 14 days in control and Gel-textile TENG conditions. **i,** An integrated textile system consisting of power supply, display, and information input modules. Scale bar, 2 cm. Figures reproduced with permission from: **a, b,** ref.[155], Springer Nature Ltd. **c,** ref.[156]. **d,** ref.[159], ACS. **e, f,** ref.[22], Wiley. **g, h,** ref.[166], Elsevier. **i,** ref.[167], Springer Nature Ltd.

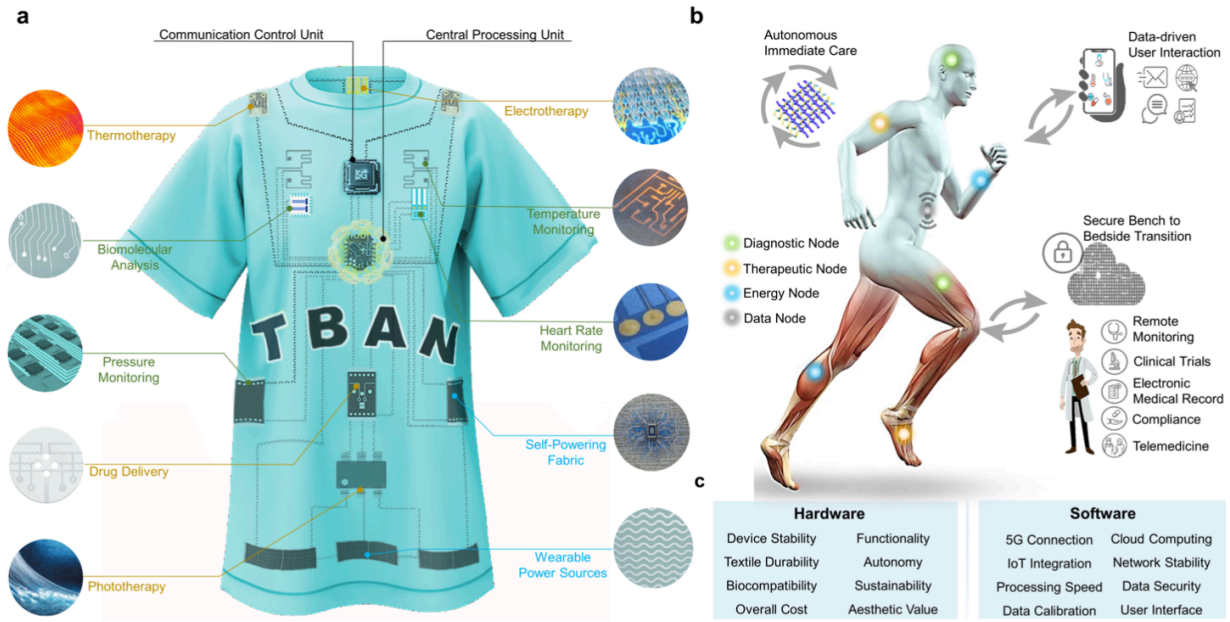

Fig. 5 | Autonomous Textile Body-Area Network for personalised healthcare. a, An Autonomous Textile Body-Area Network (ATBAN) t-shirt, enabling parallel monitoring of metabolites (biomolecular analysis), mobility (pressure monitoring), cardiovascular function (heart rate monitoring) and pyretic state (temperature monitoring). Drug delivery, phototherapeutic, electrotherapeutic and thermotherapeutic nodes ensure constant medical intervention capabilities when required, and as directed by the central processing unit node. Energy nodes supply constant power by harnessing passive energy sources, including to the communication control unit node used for integration with the IoT. **b,** Varying types of ATBAN personalised healthcare functionalities *via* diagnostic (green), therapeutic (yellow), energy (blue) and data processing (grey) nodes. These include autonomous *in* situ intervention, data-based user-driven intervention, and cloud-based integration within a plethora of remote translational research applications. **c,** Summary of key hardware and software focus points essential for optimal ATBAN development.

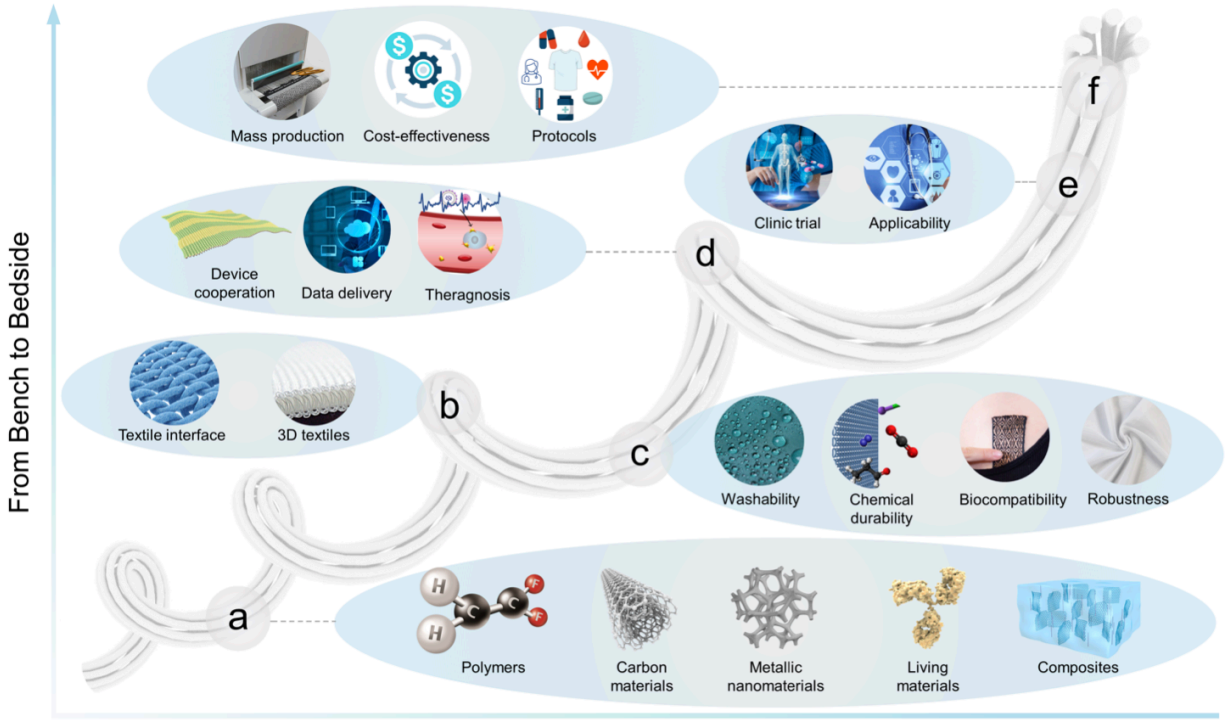

Fig. 6 | Evolutionary trends of smart healthcare textiles. The future evolutionary trends of smart healthcare textiles from bench to bedside. **a,** Fundamental material areas of focus in smart technologies. **b,** Optimised device design using advanced manufacturing techniques. **c,** Improving reliability of smart textiles for practical applications. **d,** Systematic level integration and optimisation of textile electronic components to improve healthcare outcomes. **e,** Applicative scenarios of smart healthcare textiles in clinical practise and translational research. **f,** Macroscopic considerations linked to scaling healthcare textiles at industrial level.

Table 1 | Functional Materials used in smart textiles

Materials for Smart Textiles	Functionality and Applications
Conductive Materials	
Metals[79] (~10^5 S cm^{-1}) e.g., Ag, Cu, Ti, Au Conducting polymers[80] (~10^{-3}–10^3 S cm^{-1}) e.g., PEDOT: PSS, Polyaniline Carbon materials[81] (~10–10^4 S cm^{-1}) e.g., CNT, Graphene	Fibre/textile electrode/ Textile circuits for connection and computing/ Electrography
Active Materials	
Electrochemically active materials, e.g., $LiMn_2O_4$, Ag_2O/Ag, CNT, Graphene, MOFs	Biochemical sensing textiles/ Energy storage textiles/ Drug delivery textiles
Mechanically active materials, e.g., PVDF, ZnO, PZT*, $BaTiO_3$, MXenes	Biomechanical sensing textiles Biomechanical energy harvesting textiles
Thermoactive materials, e.g., PEDOT:PSS, CNT, Sb_2Te_3-Bi_2Te_3	Temperature sensing textiles /Body heat energy harvesting textiles /Thermotherapy textiles
Photoactive materials, e.g., TiO_2, P3HT:PCBM*	Photovoltaic textiles/ Phototherapy textiles
Encapsulating Materials	
Natural materials, e. g., Silk, Cotton,	Waterproof layer for textile electronic components/Shielding layer for human skin
Synthetic materials, e.g., PDMS, EVA	Waterproof layer for textile electronic components/ Shielding layer for human skin

*PZT: Lead zirconate titanate; P3HT:PCBM: poly(3-hexylthiophene) and [6,6]-phenyl C61-butyric acid methylester

Table 2 | Typical research-based textile devices for personalized healthcare

Textile devices	Main mechanisms	Active materials	Healthcare application	Ref
Diagnostics				
Wireless textile-based sensor	Triboelectric effect	Polyester/Ag	Obstructive sleep apnoea-hypopnea syndrome diagnosis.	20
Textile MEGs	Magnetoelastic effect	Silicone rubber/magnets	Cardiovascular disease	122
Muscle fibres inspired piezoelectric textiles	Piezoelectric effect	$BaTiO_3$/PVDF	Pulse wave measurement	118
All-textile pressure sensors	Piezoresistive effect	CNT coated fabric	Pulse wave measurement	42
Textile-based capacitive sensor	Capacitive effect	Ni-coated fabrics	Physiological monitoring during rehabilitation exercises	207
Wearable textile sensors	Thermoresistive effect	Graphene flakes	Body temperature monitoring	136
Nanoporous polyethylene microfibres	Radiative cooling	Polyethylene	Personal thermal management	208
Photoplethysmogram bandage	Photoplethysmography	Spirally wrapped CNT	Heart-rate measurements	209
Electronic textile	Electrography	Ag flakes/elastomer	Electromyogram	49
Bioinspired conductive silk microfiber	Electrography	PEDOT/silk	Electrocardiograph and Electromyogram	129
Textile biofuel cell	Electrochemical reaction	Glucose oxidase/CNT	Sweat analysis	145
Single-ply sensing fibre	Electrochemical reaction	Multi-walled CNT	Venous blood analysis	21
Therapeutics				
Yarn-based stretchable sensor arrays	Triboelectric effect	PDMS/Polyester	Sign-to-speech translation	155
Smart $Ti_3C_2T_x$ MXene Fabric	Electrothermal effect	$Ti_3C_2T_x$ nanosheets	Moderately kill bacteria for wound healing	158
Mxene-decorated polyester textiles	Electrothermal effect	Ppy modified $Ti_3C_2T_x$ sheets	Thermotherapy	27
Large-area display textiles	Electroluminescence	ZnS phosphors	Assistive communication	167
Textile nano-energy nano-system	Triboelectric effect	Silicone rubber/nitrile coated textile	Muscle and nerve stimulation	73
Ionic patch	Triboelectric effect	Organogel/silicone rubber	Wound healing	166
Textile dressing	Electrothermal effect	PEGDA-Alg hydrogel	Drug delivery	22
MOF-coated optical fibres	Light triggered reaction	UiO-66 MOF	Drug delivery	84
Protective fabrics	Light triggered reaction	Al-porphyrin MOF	Sulphur mustard detoxification	19
Nanofibrous membranes	Light triggered reaction	Photobiocide treated PVA-co-PE nanofibrous	Antibacterial and antiviral	18

Table 3 | Commercialised Smart Textiles for Personalised Healthcare
A summary of the main commercial players in smart healthcare textiles whose products are primarily involved in delivering personalised healthcare.

Textile Product	Company	Healthcare Field	Clothing Solution	Platform Technology
Neurofabric™ [137]	Siren	Inflammation, Diabetes	Smart Socks	Thermoresistors*
Smart Socks [156]	Palarum®	Mobility, Physical Therapy	Smart Socks	Pressure Sensors*
Texisock [175]	Texisense	Mobility, Physical Therapy	Smart Socks	Pressure Sensors*
Sensoria® Smart Socks [176]	Sensoria Health	Neurological	Smart Socks	Pressure Sensors*
Heoskin [170]	Carre Technologies Inc.	Cardiovascular, Physical Therapy	Vest	Multiple*
MasterCaution® [171]	HealthWatch	Cardiovascular, Physical Therapy	Vest	Multiple*
SimpliECG [183]	Nanowear	Cardiovascular, Physical Therapy	Vest	Elastomeric*
Cardioskin [177]	Bioserenity	Cardiovascular	Vest	Electrodes
Neuronaute [177]	Bioserenity	Neurological	Vest and Cap	Electrodes
e-skin [173]	Xenoma	Mobility, Physical Therapy	Body Suit	Multiple*
Skiin [174]	Myant Inc.	Mobility, Physical Therapy, Thermotherapy	Body Suit	Multiple*
Nextiles Fabric [172]	Nextiles	Mobility, Physical Therapy	Fabric	Piezoresistor
Intexar™ [178]	DuPont™	Reproductive, Respiratory, Physical Therapy	Fabric	Conductive ink*
Hitoe [179]	Toray Industries	Reproductive, Respiratory, Physical Therapy	Fabric	Elastomeric*

*Information not clearly elucidated and deduced from published patents and /or publicly available information.